

THREE-PHASE DIODE RECTIFIERS
WITH LOW HARMONICS
Current Injection Methods

POWER ELECTRONICS AND POWER SYSTEMS

Predrag Pejović

Three-Phase Diode
Rectifiers with Low
Harmonics

Engineering and Economics

 Springer

THREE-PHASE DIODE RECTIFIERS WITH LOW HARMONICS

Current Injection Methods

Predrag Pejović
University of Belgrade



Predrag Pejović
University of Belgrade
Faculty of Electrical Engineering
11120 Belgrade
Serbia

Series Editors:

M. A. Pai, Professor Emeritus
Dept. of Electrical and Computer Engineering
University of Illinois at Urbana-Champaign
Urbana, IL 61801

Alex M. Stankovic, Professor
Dept. of Electrical & Computer Engineering, 440DA
Northeastern University
360 Huntington Ave.
Boston, MA 02115

Library of Congress Control Number: 2006932798

ISBN 978-0-387-29310-3 e-ISBN 978-0-387-32936-9

Printed on acid-free paper.

© 2007 Springer Science+Business Media, LLC

All rights reserved. This work may not be translated or copied in whole or in part without the written permission of the publisher (Springer Science+Business Media, LLC, 233 Spring Street, New York, NY 10013, USA), except for brief excerpts in connection with reviews or scholarly analysis. Use in connection with any form of information storage and retrieval, electronic adaptation, computer software, or by similar or dissimilar methodology now known or hereafter developed is forbidden. The use in this publication of trade names, trademarks, service marks and similar terms, even if they are not identified as such, is not to be taken as an expression of opinion as to whether or not they are subject to proprietary rights.

9 8 7 6 5 4 3 2 1

springer.com

Preface

This book presents a treatise of the current injection methods applied in three-phase diode bridge rectifiers to reduce the harmonic content of the input currents. The material presented in the book is a result of a decade of research in the area. Some of the results were published in a shorter form in a number of journals, and previously presented at several conferences. However, the book is not a collection of papers. Writing a book was an opportunity to present the results in a more readable form, with all of the necessary derivations and explanations. In addition, some of the results presented in the book were written several years after the research was done and the initial results were obtained, which provided some time to judge them and to make corrections. The book also contains some new results, never previously published, primarily in Chapter 13 that treats current injection versions of 12-pulse rectifiers, but new material can be found in other chapters of the book as well. A special chapter that deals with current injection devices is included in the book, and this important topic was previously only casually mentioned in the research papers. All of the results are presented in a uniform style that should provide an easier comparison of the methods. This book should be helpful for researchers in the area, as well as for the practicing engineers who are interested in applying the current injection methods.

The complex math that underlines current injection methods results in simple rectifiers, which consist of a moderate number of elements. Reduction of the input current harmonics is always obtained at a cost. Thus, unless there are regulations that limit the input current harmonics, devices that apply this reduction are infrequent. Current injection based rectifiers qualify as an attractive choice to meet the regulations and/or to resolve the

power quality problems since they are simple and robust. The rectifier topologies proposed and analyzed in this book meet the harmonic regulations and are readily waiting for the regulations to arrive.

The current injection methods have an oscillating history. To the best of my knowledge, the first ideas regarding current injection date back to 1954. Just after their invention, the methods had been forgotten until the late 1960s and the beginning of the 1970s. The next outburst of research results occurred in the mid-1980s, followed by several years of reduced activity. Finally, starting from the 1990s, the current injection methods have been continuously a topic of interest to researchers.

I wish to express my sincere thanks to many people who contributed to this book. The first is a colleague who initiated my research in the area. Next are many colleagues who contributed to my research through inspiring discussions. Then, there are students who asked many relevant questions and forced me to provide better explanations and to improve my arguments. Many thanks are due to a colleague who suggested I publish this book. Finally, the editorial staff significantly improved this book and deserves sincere appreciation for their efforts. An attempt to name all of these people would inevitably result in an incomplete list and would be unfair to those excluded. However, without all of these people, this book would not appear in its present form. I would also like to thank the IEEE and the IET for granting the copyright permissions.

Contents

Preface	v
Introduction	1
Three-Phase Diode Bridge Rectifier	7
Principles of Current Injection	23
Current Injection Devices	31
The Optimal Third-Harmonic Current Injection	73
Current Injection Networks for the Third-Harmonic Current Injection	91
The Optimal Current Injection	117
Current Injection Networks for the Optimal Current Injection	127
Operation of the Rectifier in the Discontinuous Conduction Mode	141
Recovery of the Current Injection Network Power Applying a Current-Loaded Resistance Emulator	165
Recovery of the Current Injection Network Power Applying a Voltage-Loaded Resistance Emulator	193
Current Injection Applying a Switching Current Injection Device	233

Rectifiers that Apply Square-Wave Current Injection	267
Conclusions	303
References	307
Index	311

Chapter 1

INTRODUCTION

1. MOTIVATION

This book makes available, in a single volume, fundamental results in the area of three-phase rectifiers with reduced harmonic distortion of the input currents based on current injection methods. The bulk of the material is available in references [6], [7], [10], [11], [24]–[40], and [51] which have the author as one of the co-authors. Some new results are included such as magnetic devices that integrate the current injection network inductor, and the application of delta-wye transformers to provide the current injection. Also included are the simulation method applied to analyze effects caused by higher order harmonics in the rectifier, the rectifiers that apply voltage-loaded resistance emulators, and square-wave current injection rectifiers. Thus an integrated approach on the subject is presented.

2. SCOPE OF THE BOOK

Power quality problems caused by significant increase of nonlinear loads initiated intensive research in the area of high power factor rectifiers, or more precisely, in the area of the rectifiers that provide low harmonic distortion of the input currents and high power factor. A recent review paper in this area, [50], focused only on three-phase rectifiers. Many approaches to improve performance of three-phase rectifiers are discussed there, including the current injection method.

Rectifiers that apply any kind of high-frequency switching are excluded from the scope of this book. References [35] and [36] discuss switching power converters utilized as resistance emulators. In references [25] and [28] complete power is processed by the switching converters.

The topic of this book is a class of three-phase current injection based rectifiers that provide current injection applying ripple of the diode bridge output terminal voltages. The network that provides the current injection is

connected in parallel to the load. The rectifiers that apply passive components, i.e., transformers, inductors, capacitors, and diodes, without controlled switching, are the main focus of the book, with the exception of Chapter 12, where three controlled switches are applied to realize a special type of current injection device. Three types of current injection are analyzed: the third-harmonic sinusoidal current injection, the optimal current injection, and the square-wave current injection. The third-harmonic current injection provides the input current THD of about 5%, but the current injection network is required to satisfy a resonant constraint. The optimal current injection provides sinusoidal input currents, in phase with corresponding phase voltages, but requires switching resistance emulators to recover power taken by the current injection network. The last group of rectifiers, that apply square-wave current injection, provides total harmonic distortion of the input currents of about 15%, but these types of rectifiers require the simplest circuitry, and do not require any resonant constraints to be satisfied. All three of these types of current injection are going to be analyzed, and various circuits that apply these techniques will be described.

3. CURRENT INJECTION METHODS: A BRIEF LITERATURE SURVEY

Current injection methods were first discussed in 1969 [5]. In [5], diode rectifiers were used, although it is mentioned that generalization of the results to thyristor-controlled rectifiers is possible. Further progress is reported in [1], where the current injection is extended to injection of the harmonics at higher order triples of the line frequency. Extension of the results to thyristor rectifiers is presented in [2]. In [3] and [4], the ripple at the rectifier DC side is utilized to generate the injected currents.

It appears that interest in the third harmonic current injection again started in 1992 [13], [18], and [41]. Reference [13] is closely related to the topic of this book. Papers [16], [18]–[21], [41]–[44] cover many topics, and most of the papers treat the double boost topology as a basic unit to control the waveform of the input currents. The results presented in this group of papers start from the rectifiers that apply resonant current injection device [16], [18], and [41], which can be considered an early stage of the development of the Minnesota rectifier. An improved version of the rectifier, with a magnetic current injection device based on a zigzag autotransformer, is presented in [20] and [42], and it is mentioned in [17]. A resonant version of the Minnesota rectifier is presented in [42] and [44], where application of the zero current quasiresonant switch in the boost converters is proposed.

Inverter version of the Minnesota interface is presented in [17], pp. 478–480, and in [21]. An important part of [21] is optimization of the injected current spectrum, where injection of the harmonics at the triple and at the sixth multiple of the line frequency is analyzed. This approach is extended in Chapter 7 of this book and the related papers, and all of the harmonic components at triples of the line frequency are included, resulting in purely sinusoidal waveforms of the input currents. Another important paper from this group is [19], in which a simple magnetic current injection device is analyzed. The paper is somewhat specific, since it only discusses the current injection device, but it was a very important reference for the results presented in Chapter 4 of this book. A simple magnetic current injection device is presented in [19], and reduction of parasitic inductance of the device neutral point applying an aluminum shield is proposed. Finally, a comparative evaluation of harmonic reduction techniques in three-phase rectifiers is presented in [43].

The rectifier proposed in [12] deserves special attention, since reference [12] was one of the papers that significantly influenced the research presented in this book. The rectifier proposed in [12] was simple and attractive. Some of the mathematical foundations of the paper needed to be clarified, which is done in [27], where the mathematical foundations of the method were discussed, and the rectifiers proposed in [12] and [13] were compared. Somewhat expanded results of [27] are presented in Chapters 5 and 6 of this book.

4. OVERVIEW OF THE BOOK

In this book, systematized results of [6], [7], [10], [11], and [24]–[39] are presented. In Chapter 2, basic results regarding three-phase diode bridge rectifiers are provided, and include spectra of the output terminal voltages, spectrum of the output voltage, and definitions of the diode state functions are frequently applied in the subsequent text. Waveforms of the input currents are presented, and their THD values are computed. Notches in the rectifier input voltages caused by discontinuities in the input currents are illustrated via experimental results. Current injection principles are presented in Chapter 3, where a current injection system consisting of a current injection network and a current injection device is introduced. Fundamental ideas behind the method are discussed, including the essential question of why the injected currents should have spectral components at triples of the line frequency. A common misunderstanding that the third-harmonic current injection is a sort of compensation for the third-harmonic component in the input currents is clarified.

In Chapter 4, magnetic current injection devices are analyzed. The volt-ampere rating of a magnetic device is defined, since this quantity is a measure to compare various constructions of the current injection devices. Various current injection devices are presented, and their performance is compared. Presented results indicate that in most applications it would be best to apply a current injection device based on a zigzag autotransformer. In Section 4.6, a novel magnetic device that integrates the current injection device and the inductor of the current injection network is proposed. This result has not been published previously. Application of a three-phase wye-wye connected transformer to adjust the voltage level and to provide current injection, as utilized in [13] and [15], is discussed next. Issues regarding the volt-ampere rating are clarified, and it is shown that the transformer can provide the current injection with negligible increase of the volt-ampere rating. Application of a delta-wye connected transformer to provide the current injection, utilized in [46], is discussed in Section 4.8, and it is shown that transformers of this type provide negligible inductance of the neutral point, as well as negligible stray flux, at the cost of somewhat increased volt-ampere rating.

The third-harmonic current injection is discussed in Chapters 5 and 6. Chapter 5 presents a theoretical study of the third-harmonic current injection, where amplitude and phase of the injected current are optimized to minimize the input current THD. Simple current injection networks are discussed in Chapter 6, where the current injection networks proposed in [12] and [13] are compared. The third of the current injection networks discussed in Chapter 6, proposed in [30], is analyzed in detail, and this current injection network is frequently utilized in the rectifiers that are analyzed in subsequent text.

The optimal current injection is the topic of Chapters 7 and 8. The optimal current injection provides ideal sinusoidal waveforms of the input currents, and it relies on injection of the currents containing spectral components at triples of the line frequency, i.e., the injected current is enriched by higher order harmonics. Basic principles of the optimal current injection are presented in Chapter 7. The author of this book has published some ideas about the optimal current injection in [25], [26], [28], [29], and [35], while the waveforms of the diode bridge load currents that provide purely sinusoidal input currents can also be found in [22], [45], [47], and [48]. Current injection networks that provide the optimal current injection are presented in Chapter 8, which also provides systematized and expanded results of [26] and [35].

Chapter 9 is somewhat specific, as it analyzes the discontinuous conduction mode in three-phase diode bridge rectifiers. The problem is mathematically complex and it resisted attempts at solution for a long time.

The first results regarding this problem are presented in [6], while the final results were published three years later, in [7]. A piecewise linear state space model of the rectifier is developed, normalization of variables is applied to generalize the results, and special mathematical techniques [51] are developed to solve the problem numerically. It is shown that the rectifier discontinuous conduction mode might be of practical interest, since it provides acceptable values of the input current THD and high efficiency applying simple and robust circuitry.

Passive resistance emulators are the topic of Chapters 10 and 11. In Chapter 10, a current-loaded passive resistance emulator is described. The rectifier structure was originally proposed in [32] and [34], and is described in more detail in Chapter 10. The rectifier provides automatic adjustment of the injected current amplitude to the load current. A novel simulation method to analyze dependence of the input current THD on the load current is presented in Chapter 10, which has not been published previously. Chapter 11 presents completely new results for the first time. The topic of this chapter is the voltage-loaded resistance emulator, which has an impressive performance in comparison to other topologies. The rectifier is simple, and requires only one resonant circuit and a small number of other components that are exposed to relatively low voltage and current stress. Although adjustment of the injected current amplitude to the load current is not as straightforward as it is in the rectifier in Chapter 10, even better results are obtained experimentally. The rectifier is analyzed both in the discontinuous and the continuous conduction modes, since both occur, depending on the load current.

Chapter 12 is a difficult one because all of the concepts developed for the rectifiers that apply magnetic current injection devices are adjusted to the switching current injection device proposed in this chapter. The switching current injection device is analyzed first, and it is shown that it provides an attractive opportunity to provide the same results as obtained applying magnetic current injection devices, but with three times lower amplitude of the injected current. On the other hand, the switching current injection device is more complex than the magnetic one, and its robustness is lower. In Chapter 12, it is shown that all of the results obtained applying the magnetic current injection devices could be achieved by the switching current injection device. The only difference is operation of the rectifier in the discontinuous conduction mode, which cannot be utilized in the case of the switching current injection device owing to high values of the input current THD. Unfortunately, this significantly reduces applicability of the voltage-loaded resistance emulator proposed in Chapter 11, but all other methods are directly applicable.

The rectifiers that apply square-wave current injection are analyzed in Chapter 13. In the first part of Chapter 13, the rectifier proposed in [14] is analyzed. It is shown that this rectifier can be treated as a special case of the one analyzed in Chapter 10, which applies the third-harmonic current injection and current-loaded passive resistance emulator. Thus, it is natural to analyze the square-wave current injection version of the rectifier analyzed in Chapter 11, which applies a voltage-loaded resistance emulator. This is the second rectifier analyzed in Chapter 13, and it has not been published previously.

Finally, the conclusions are presented at the end, where all of the results are summarized. In the book, experimental results are presented only for the most important concepts. Experimental verification of the auxiliary results can be found in the reference list, and they are cited where appropriate.

Chapter 2

THREE-PHASE DIODE BRIDGE RECTIFIER

The subject of this book is reduction of total harmonic distortion (THD) of input currents in three-phase diode bridge rectifiers. Besides the reduction of the input current THD, the methods proposed here result in improvement of the rectifier power factor (PF). To build a foundation to introduce the new methods, in this chapter a three-phase diode bridge rectifier is analyzed and relevant voltage waveforms are presented and their spectra derived. Also, logic functions that define states of the diodes in the three-phase diode bridge, termed diode state functions, are defined.

Let us consider a three-phase diode bridge rectifier as shown in Fig. 2-1. The rectifier consists of a three-phase diode bridge, comprising diodes D1 to D6. In the analysis, it is assumed that the impedances of the supply lines are low enough to be neglected, and that the load current I_{OUT} is constant in time. The results and the notation introduced in this chapter are used throughout the book.

First, let us assume that the rectifier is supplied by a balanced undistorted three-phase voltage system, specified by the phase voltages:

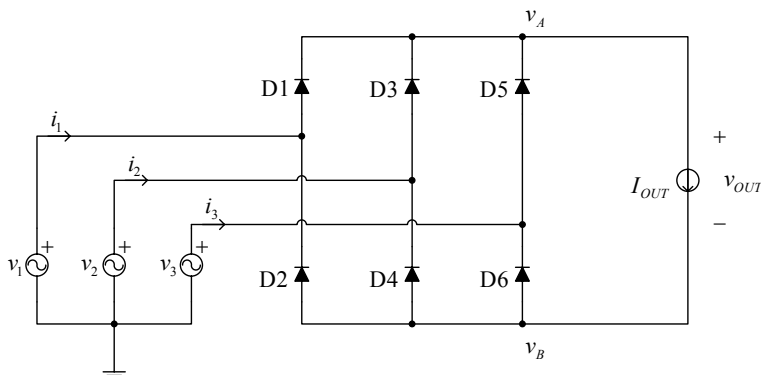


Figure 2-1. Three-phase diode bridge rectifier.

$$v_1 = V_m \cos(\omega_0 t), \quad (2.1)$$

$$v_2 = V_m \cos\left(\omega_0 t - \frac{2\pi}{3}\right), \quad (2.2)$$

and

$$v_3 = V_m \cos\left(\omega_0 t - \frac{4\pi}{3}\right). \quad (2.3)$$

The amplitude of the phase voltage V_m equals

$$V_m = V_{PRMS} \sqrt{2}, \quad (2.4)$$

where V_{PRMS} is the root-mean-square (RMS) value of the phase voltage. Waveforms of the input voltages are presented in Fig. 2-2.

Assuming that I_{OUT} is strictly greater than zero during the whole period, in each time point two diodes of the diode bridge conduct. The first conducting diode is from the group of odd-indexed diodes $\{D1, D3, D5\}$, and it is connected by its anode to the highest of the phase voltages at the time point considered. The second conducting diode is from the group of even-indexed diodes $\{D2, D4, D6\}$, and it is connected by its cathode to the lowest of the phase voltages. Since one phase voltage cannot be the highest and the lowest at the same time for the given set of phase voltages specified by (2.1), (2.2), and (2.3), two of the phases are connected to the load while one phase is unconnected in each point in time. This results in an input current equal to zero in the time interval when the phase voltage is neither maximal nor minimal. The gaps in the phase currents are the main reason for introducing the current injection methods, as they are analyzed in the next chapter.

The described operation of the diodes in the diode bridge results in a positive output terminal voltage equal to the maximum of the phase voltages, i.e.,

$$v_A = \max(v_1, v_2, v_3), \quad (2.5)$$

while the voltage of the negative output terminal equals the minimum of the phase voltages,

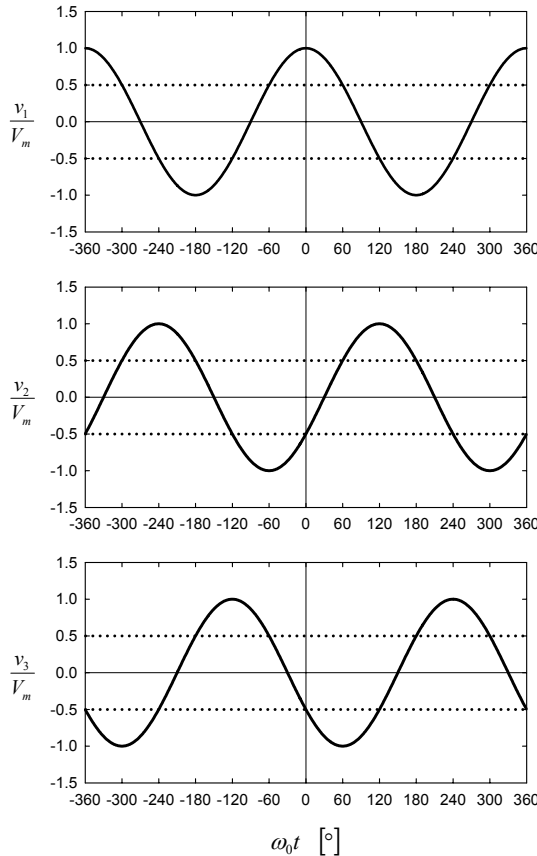


Figure 2-2. Waveforms of the input voltages.

$$v_B = \min(v_1, v_2, v_3). \quad (2.6)$$

Waveforms of the output terminal voltages specified by (2.5) and (2.6) are presented in Fig. 2-3. These waveforms are periodic, with the period equal to one third of the line period; thus their spectral components are located at triples of the line frequency. Fourier series expansion of the waveform of the positive output terminal leads to

$$v_A = \frac{3\sqrt{3}}{\pi} V_m \left(\frac{1}{2} + \sum_{n=1}^{+\infty} \frac{(-1)^{n+1}}{9n^2 - 1} \cos(3n\omega_0 t) \right), \quad (2.7)$$

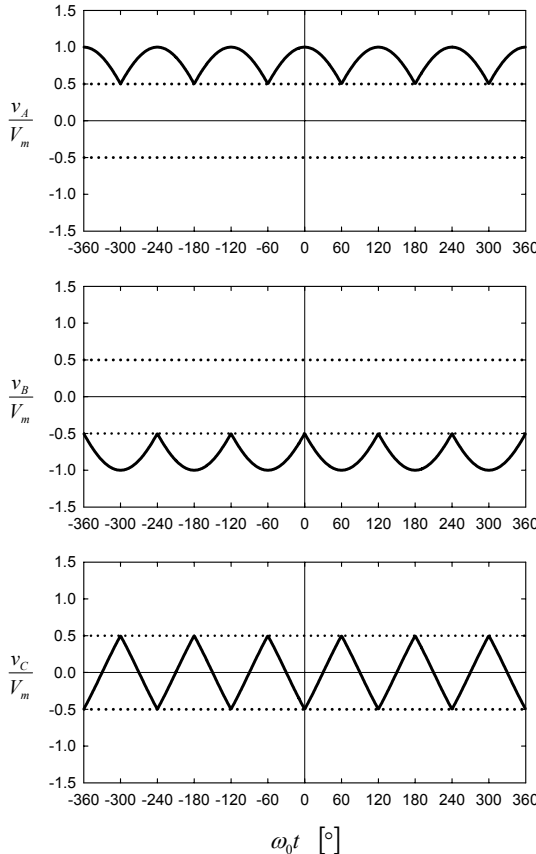


Figure 2-3. Waveforms of the output terminal v_A and v_B , and the waveform of v_C .

while the Fourier series expansion of the voltage of the negative input terminal results in

$$v_B = \frac{3\sqrt{3}}{\pi} V_m \left(-\frac{1}{2} + \sum_{n=1}^{+\infty} \frac{1}{9n^2 - 1} \cos(3n\omega_0 t) \right). \quad (2.8)$$

These Fourier series expansions are used frequently in analyses of various current injection methods. Some useful properties of the Fourier series expansions of the output terminal voltages should be underlined here. First, both Fourier series expansions contain spectral components at multiples of tripled line frequency, i.e., at triples of the line frequency. The corresponding spectral components of v_A and v_B at odd triples of the line frequency at

$3(2k-1)\omega_0$, where $k \in N$, are the same, having the same amplitudes and the same phases. On the other hand, the corresponding spectral components at even triples of the line frequency, at $6k\omega_0$, have the same amplitudes, but opposite phases. These properties are used in the design of current injection networks described in Chapters 6 and 8.

The diode bridge output voltage is given by

$$v_{OUT} = v_A - v_B, \quad (2.9)$$

and its waveform is presented in Fig. 2-4. The Fourier series expansion of the output voltage is

$$v_{OUT} = \frac{3\sqrt{3}}{\pi} V_m \left(1 - \sum_{k=1}^{+\infty} \frac{2}{36k^2 - 1} \cos(6k\omega_0 t) \right). \quad (2.10)$$

Since spectra of v_A and v_B have the same spectral components at odd triples of the line frequency, these spectral components cancel out in the spectrum of the output voltage. Thus, the spectrum of the output voltage contains spectral components only at sixth multiples of the line frequency. The DC component of the output voltage equals

$$V_{OUT} = \frac{3\sqrt{3}}{\pi} V_m \approx 1.65V_m \approx 2.34V_{PRMS}, \quad (2.11)$$

while the Fourier series expansion of the AC component of the output voltage is

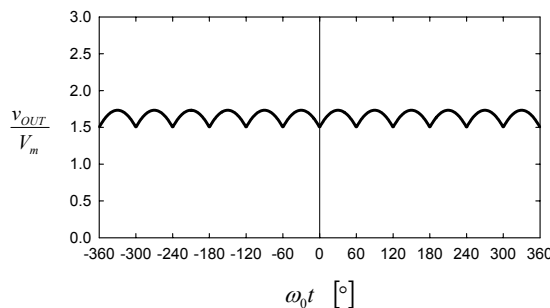


Figure 2-4. Waveform of the output voltage.

$$\hat{v}_{OUT} = -\frac{3\sqrt{3}}{\pi} V_m \sum_{k=1}^{+\infty} \frac{2}{36k^2 - 1} \cos(6k\omega_0 t). \quad (2.12)$$

Another waveform of interest in the analyses that follow is the waveform of “the remaining” voltage, v_C , i.e., the waveform obtained from segments of the phase voltages during the time intervals when they are neither maximal nor minimal. A node in the circuit of Fig. 2-1 where that voltage could be measured does not exist, in contrast to the waveforms of v_A and v_B that can be observed at the diode bridge output terminals. However, the waveform and the spectrum of v_C can be computed easily using the fact that the sum of the instantaneous values of the phase voltages equals zero,

$$v_1 + v_2 + v_3 = 0. \quad (2.13)$$

In each point in time, one of the phase voltages equals v_A , another one equals v_B , while the remaining one equals v_C . Thus, the output terminal voltages and “the remaining voltage” add up to zero. This gives the following expression for “the remaining voltage”:

$$v_C = -v_A - v_B, \quad (2.14)$$

and its spectrum is computed using spectra of v_A and v_B , given by (2.7) and (2.8), resulting in

$$v_C = -\frac{3\sqrt{3}}{\pi} V_m \sum_{k=1}^{+\infty} \frac{2}{(6k-3)^2 - 1} \cos((6k-3)\omega_0 t). \quad (2.15)$$

In the spectrum of “the remaining voltage” the spectral components are located at odd triples of the line frequency, since the spectral components of v_A and v_B at even triples of the line frequency cancel out.

Another voltage of interest is the average of the output terminal voltages, defined as

$$v_{AV} = \frac{1}{2}(v_A + v_B) = -\frac{1}{2}v_C. \quad (2.16)$$

Using the spectrum of v_C , given by (2.15), the spectrum of v_{AV} is obtained as

$$v_{AV} = \frac{3\sqrt{3}}{\pi} V_m \sum_{k=1}^{+\infty} \frac{1}{(6k-3)^2 - 1} \cos((6k-3)\omega_0 t). \quad (2.17)$$

The spectral components of v_{AV} are located at odd triples of the line frequency, the same as in the spectrum of v_C .

After the waveforms of the rectifier voltages are defined and their spectra derived, waveforms of the rectifier currents are analyzed. In the analysis of the rectifier currents, let us start from the states of the diodes. First, let us define the diode state functions d_k for $k \in \{1, 2, 3, 4, 5, 6\}$ such that $d_k = 1$ if the diode indexed with k conducts, and $d_k = 0$ if the diode is blocked. Values of the diode state functions are summarized in Table 2-1, while the waveforms of the diode state functions during two line periods are depicted in Fig. 2-5. From the data of Table 2-1 it can be concluded that the rectifier of Fig. 2-1 can be analyzed as a periodically switched linear circuit, since the states of the diodes are expressed as functions of the time variable. This significantly simplifies the analysis, as seen in Chapter 9, where the discontinuous conduction mode of the diode bridge is analyzed, though with significant mathematical difficulties, since the circuit cannot be treated as a periodically switched linear circuit.

After the diode state functions are defined, currents of the diodes can be expressed as

$$i_{Dk} = d_k(\omega_0 t) I_{OUT} \quad (2.18)$$

for $k \in \{1, 2, 3, 4, 5, 6\}$. All of the diode current waveforms have the same average value:

$$I_D = \frac{1}{3} I_{OUT}, \quad (2.19)$$

Table 2-1. Diode state functions.

Segment	$d_1(\omega_0 t)$	$d_2(\omega_0 t)$	$d_3(\omega_0 t)$	$d_4(\omega_0 t)$	$d_5(\omega_0 t)$	$d_6(\omega_0 t)$
$0 < \omega_0 t < 60^\circ$	1	0	0	0	0	1
$60^\circ < \omega_0 t < 120^\circ$	0	0	1	0	0	1
$120^\circ < \omega_0 t < 180^\circ$	0	1	1	0	0	0
$180^\circ < \omega_0 t < 240^\circ$	0	1	0	0	1	0
$240^\circ < \omega_0 t < 300^\circ$	0	0	0	1	1	0
$300^\circ < \omega_0 t < 360^\circ$	1	0	0	1	0	0

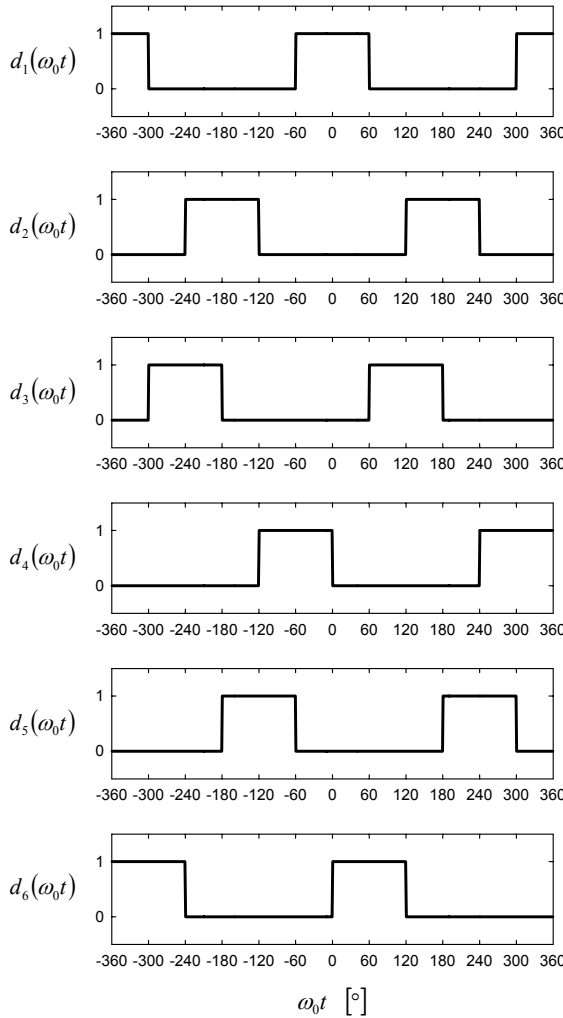


Figure 2-5. Waveforms of the diode state functions.

which is of interest for sizing the diodes. The maximum of the reverse voltage that the diodes are exposed to is equal to the maximum of the output voltage and equal to the line voltage amplitude,

$$V_{D\max} = V_m \sqrt{3} = V_{PRMS} \sqrt{6}. \quad (2.20)$$

Using the diode state functions, the rectifier input currents i_p , where

$p \in \{1, 2, 3\}$, can be expressed as

$$i_p = I_{OUT} (d_{2p-1}(\omega_0 t) - d_{2p}(\omega_0 t)). \quad (2.21)$$

Waveforms of the input currents are presented in Fig. 2-6. The input currents have the same RMS value, equal to

$$I_{RMS} = \frac{\sqrt{6}}{3} I_{OUT}. \quad (2.22)$$

The output power of the rectifier is

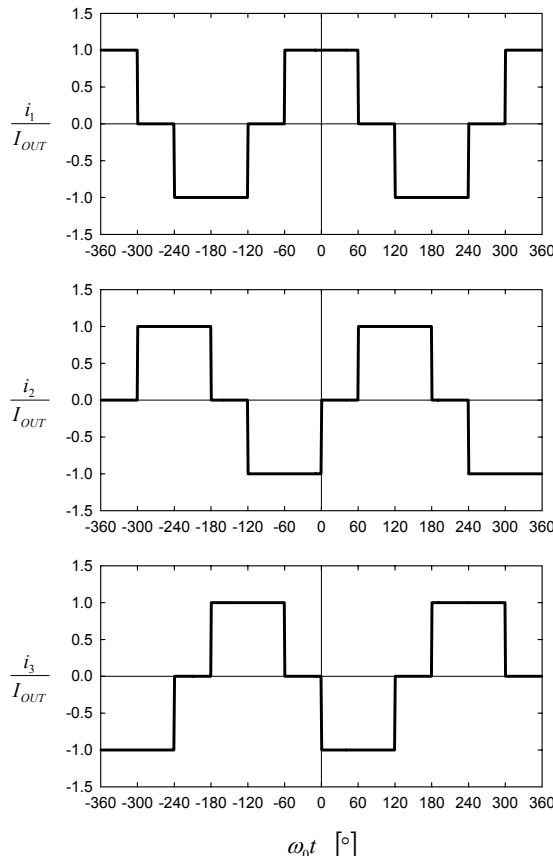


Figure 2-6. Waveforms of the input currents.

$$P_{OUT} = V_{OUT} I_{OUT} = \frac{3\sqrt{3}}{\pi} V_m I_{OUT} = P_{IN} \quad (2.23)$$

and it is the same as the input power P_{IN} , since losses in the rectifier diodes are neglected in the analysis and there are no other elements in the circuit of Fig. 2-1. The apparent power observed at the rectifier input is

$$S_{IN} = 3V_{PRMS} I_{RMS} = \sqrt{3}V_m I_{OUT}. \quad (2.24)$$

From the rectifier input power given by (2.23) and the rectifier apparent power given by (2.24), the power factor at the rectifier input is obtained as

$$PF = \frac{P_{IN}}{S_{IN}} = \frac{3}{\pi} = 0.9549. \quad (2.25)$$

This value for the power factor is reasonably good, and satisfies almost all of the power factor standards. It is significantly better than the power factor value of the rectifier with the capacitive filter connected at the output, which forces the rectifier to operate in the discontinuous conduction mode. The result is also good in comparison to single-phase rectifiers. Thus, the power factor value of (2.25) is not something to worry about. The parameter of the rectifier of Fig. 2-1 on which attention is focused is total harmonic distortion (THD) of the input currents.

To compute the THD values of the input currents, the RMS value of the input current fundamental harmonic is determined as

$$I_{1RMS} = \frac{\sqrt{6}}{\pi} I_{OUT}. \quad (2.26)$$

The fundamental harmonics of the input currents are displaced to the corresponding phase voltages for

$$\varphi_1 = 0, \quad (2.27)$$

which results in the displacement power factor (DPF):

$$DPF = \cos \varphi_1 = 1. \quad (2.28)$$

The THD of the input currents is determined applying

$$THD = \frac{\sqrt{I_{RMS}^2 - I_{1RMS}^2}}{I_{1RMS}}, \quad (2.29)$$

resulting in

$$THD = \frac{1}{3} \sqrt{\pi^2 - 9} = 31.08\%. \quad (2.30)$$

This THD value is considered relatively high, and its reduction is of interest in some applications. Efficient methods to reduce the THD value of the input currents in three-phase diode bridge rectifiers are the topic of this book.

Some standards limit amplitudes of particular harmonic components of the input currents. Thus, the spectrum of the input currents is a topic of interest. The input currents can be expressed by Fourier series expansions of the form

$$\begin{aligned} i(t) &= I_{DC} + \sum_{n=1}^{+\infty} (I_{C,n} \cos(n\omega_0 t) + I_{S,n} \sin(n\omega_0 t)) \\ &= I_{DC} + \sum_{n=1}^{+\infty} I_n \cos(n\omega_0 t - \varphi_n), \end{aligned} \quad (2.31)$$

where

$$I_{DC} = \frac{1}{2\pi} \int_{-\pi}^{\pi} i(t) d(\omega_0 t), \quad (2.32)$$

$$I_{C,n} = \frac{1}{\pi} \int_{-\pi}^{\pi} i(t) \cos(n\omega_0 t) d(\omega_0 t), \quad (2.33)$$

$$I_{S,n} = \frac{1}{\pi} \int_{-\pi}^{\pi} i(t) \sin(n\omega_0 t) d(\omega_0 t), \quad (2.34)$$

$$I_n = \sqrt{I_{C,n}^2 + I_{S,n}^2}, \quad (2.35)$$

and

$$\tan \varphi_n = \frac{I_{S,n}}{I_{C,n}}. \quad (2.36)$$

In the case of the input current of the first phase, specified by (2.21) for $p=1$, the harmonic components are

$$I_{1,DC} = 0, \quad (2.37)$$

$$I_{1,C,n} = \frac{2}{\pi n} \left(\sin \frac{2\pi n}{3} + \sin \frac{\pi n}{3} \right) I_{OUT}, \quad (2.38)$$

$$I_{1,S,n} = 0; \quad (2.39)$$

thus

$$I_{1,n} = \frac{2}{\pi n} \left| \sin \frac{2\pi n}{3} + \sin \frac{\pi n}{3} \right| I_{OUT} \quad (2.40)$$

and

$$\varphi_n = \frac{\pi}{2} \left(1 - \text{sgn} \left(\sin \frac{2\pi n}{3} + \sin \frac{\pi n}{3} \right) \right). \quad (2.41)$$

Waveforms of the input currents of the remaining two phases of the rectifier are displaced in phase for $2\pi/3$ in comparison to one to another, according to

$$i_1(\omega_0 t) = i_2 \left(\omega_0 t - \frac{2\pi}{3} \right) = i_3 \left(\omega_0 t + \frac{2\pi}{3} \right). \quad (2.42)$$

Thus, all of the input currents share the same amplitude spectrum but have different phase spectra, as can be derived by applying the time-displacement property for the Fourier series expansions in complex form.

To illustrate the operation of the diode bridge rectifier and to compare its real operation with the derived model, waveforms of an experimental rectifier are recorded and presented. The experimental rectifier operates with a phase voltage RMS value of $V_{PRMS} = 100$ V, corresponding to the input voltage amplitude of $V_m = 140$ V. The output current range is $0 < I_{OUT} < 10$ A, resulting in an output power of up to 2.5 kW. Experimentally recorded waveforms of the phase voltages, accompanied by the input currents, are presented in Fig. 2-7. From the waveforms, it can be concluded that the voltage system is balanced, but the voltages are slightly distorted in the form of two typical deviations: flattened sinusoid tops and notches. The flattened tops of the waveforms are caused primarily by single-phase rectifiers with capacitive filtering, typical for electronic equipment, and this type of distortion is not caused by the analyzed rectifier. However, the notches are caused by the nonzero line impedance and commutations in the diode bridge. This commutation effect can also be observed in a finite slope of the input current waveforms during the rising and falling edges, coinciding with the notches in the corresponding phase voltages.

Waveforms of the output voltage and the output current are presented in the bottom row of Fig. 2-7. The voltage waveform is different from the waveform presented in Fig. 2-4 around the minimums of the voltage, due to the notches in the phase voltages. Again, this effect is caused by nonzero impedance of the supply lines. In the output current waveform, the output current ripple at the sixth multiple of the line frequency can be observed. This ripple slightly affects the input current waveforms.

To illustrate dependence of the input voltage and the input current waveforms on the output current, and to determine limits of the accepted rectifier model, waveforms of the phase voltage and the input current are presented in Fig. 2-8 for $I_{OUT} = 4$ A, $I_{OUT} = 7$ A, and $I_{OUT} = 10$ A. The first effect to be observed is an increase in the duration of the notches at the phase voltage waveform by increases of the output current, caused by finite impedance of the supply lines. The second effect is increased output current ripple at $I_{OUT} = 10$ A, which is caused by saturation of the filter inductor core. Other than these two effects that are not captured by the accepted rectifier model, the rectifier behavior is within expected limits. In Table 2-2, dependence of the THD of the input voltage, THD of the input current, the input power, the apparent power at the rectifier input, and the rectifier power factor are presented. The voltage waveform is moderately distorted, which slightly increases the output current, due to the increased duration of the notches. The input current THD is slightly lower than predicted by (2.30), which is caused by the nonzero impedance of the supply lines. This

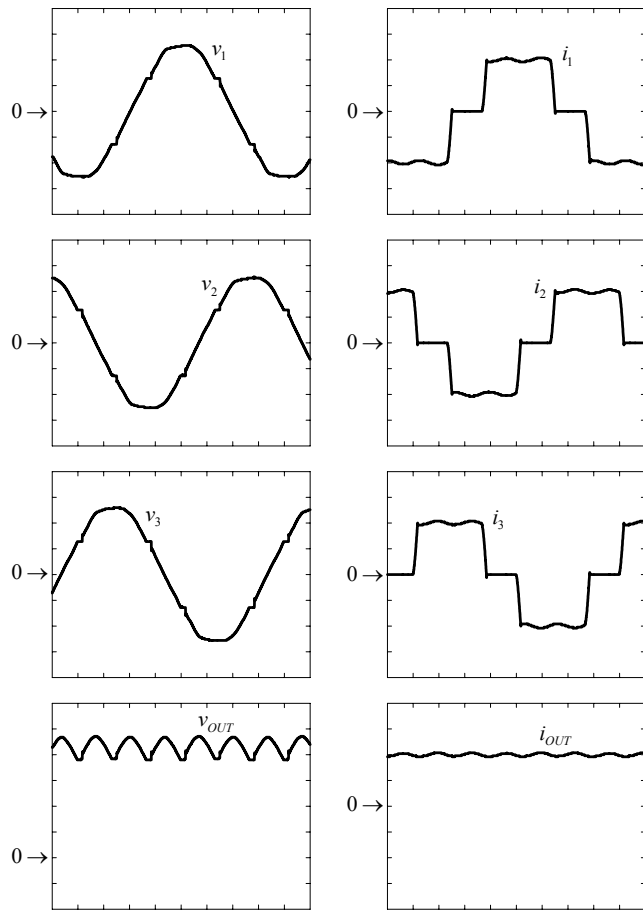


Figure 2-7. Experimentally recorded waveforms of the input voltages, the input currents, the output voltage, and the output current. Voltage scale = 50 V/div. Current scale = 5 A/div. Time scale = 2.5 ms/div.

impedance slightly smoothes the input current waveform during the diode state transitions, resulting in a lower THD. The power factor at the rectifier input is close to the expected value, given by (2.25).

From the experimental data it can be concluded that the rectifier model adequately describes the rectifier operation. However, the supply line

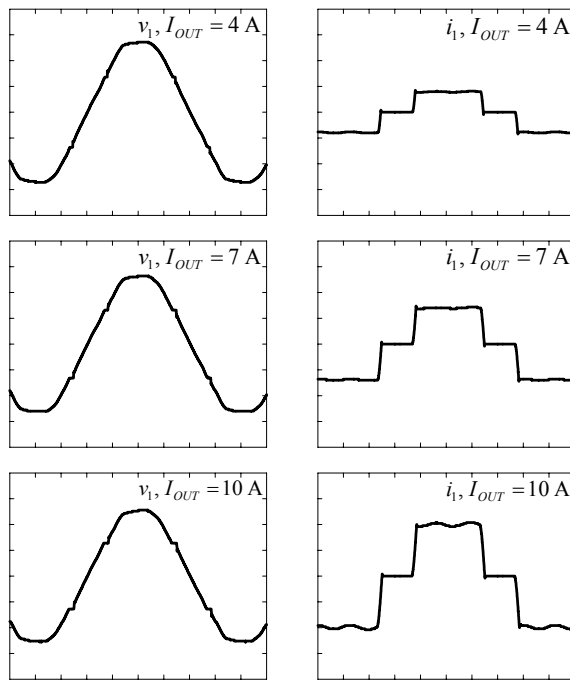


Figure 2-8. Experimentally recorded waveforms of the phase voltage and the input current for $I_{OUT} = 4 \text{ A}$, $I_{OUT} = 7 \text{ A}$, and $I_{OUT} = 10 \text{ A}$. Voltage scale = 50 V/div. Current scale = 5 A/div. Time scale = 2.5 ms/div.

Table 2-2. Dependence of the rectifier parameters on I_{OUT} .

I_{OUT}	$THD(v_1)$	$THD(i_1)$	P_{IN}	S_{IN}	PF
4 A	3.17 %	29.47 %	909.8 W	946.8 VA	0.9610
7 A	3.34 %	28.65 %	1544.3 W	1607.8 VA	0.9605
10 A	3.42 %	27.94 %	2121.0 W	2212.1 VA	0.9588

inductance and the output current ripple might slightly affect the rectifier operation, and these phenomena are not included in the rectifier model. Application of the current injection methods will remove the notches from the phase voltages and make the inductance of the supply lines irrelevant. Thus, the output current ripple will remain the only parasitic effect to be concerned about.

Chapter 3

PRINCIPLES OF CURRENT INJECTION

The three-phase diode bridge rectifier discussed in Chapter 2 suffers from relatively high total harmonic distortion (THD) of the input currents. Reduction of this distortion is the focus of this book, and the problem is approached by applying a general scheme as presented in Fig. 3-1. In comparison to the diode bridge rectifier shown in Fig. 2-1, in the circuit shown in Fig. 3-1 two units, a current injection network and a current injection device, are added. When these two units are analyzed together, they are connected to the three-phase diode bridge at all five of its terminals, providing a link between the diode bridge output and the input. The purpose of these two units is to shape the input currents and to reduce their THD values.

Let us assume that the rectifier is supplied by a symmetric undistorted three-phase voltage system,

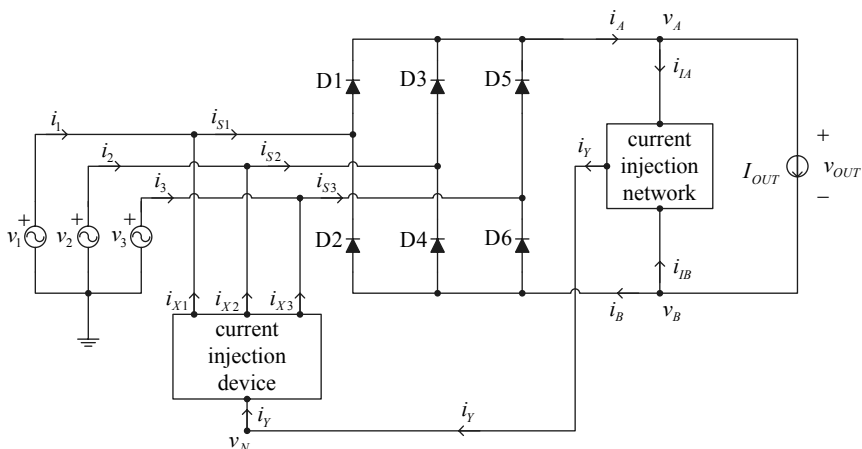


Figure 3-1. A three-phase diode bridge rectifier applying current injection.

$$v_p = V_m \cos\left(\omega_0 t - (p-1)\frac{2\pi}{3}\right) \quad (3.1)$$

for $p \in \{1, 2, 3\}$. Our ultimate goal is to achieve purely sinusoidal input currents in phase with the corresponding phase voltages,

$$i_p = I_m \cos\left(\omega_0 t - (p-1)\frac{2\pi}{3}\right). \quad (3.2)$$

In this case, each of the supply sources observes an equivalent resistive load

$$R_E = \frac{V_m}{I_m}. \quad (3.3)$$

Although the waveforms of (3.2) are our goal, waveforms close to that, with the THD on the order of several percent, will be acceptable.

To reduce the THD of the input currents, the main obstacles are the gaps in the input currents, present during the time intervals when the phase voltage of the considered phase is neither minimal nor maximal among the phase voltages, causing both of the diodes connected to that phase to be reverse biased. In terms of the diode state functions, these intervals are described by

$$d_{2p-1}(\omega_0 t) + d_{2p}(\omega_0 t) = 0 \quad (3.4)$$

for $p \in \{1, 2, 3\}$. Patching of the input currents in these time intervals with the injected current is the basic idea behind the current injection method.

Let us express the input currents of the rectifier shown in Fig. 3-1, applying the diode state functions defined in Chapter 2. In an expanded form, the input currents are

$$i_1(\omega_0 t) = d_1(\omega_0 t)i_A(\omega_0 t) - d_2(\omega_0 t)i_B(\omega_0 t) - i_{X1}(\omega_0 t), \quad (3.5)$$

$$i_2(\omega_0 t) = d_3(\omega_0 t)i_A(\omega_0 t) - d_4(\omega_0 t)i_B(\omega_0 t) - i_{X2}(\omega_0 t), \quad (3.6)$$

and

$$i_3(\omega_0 t) = d_5(\omega_0 t) i_A(\omega_0 t) - d_6(\omega_0 t) i_B(\omega_0 t) - i_{X3}(\omega_0 t). \quad (3.7)$$

A reasonable requirement to be imposed on the input currents is that they should have the same waveforms, except for the displacement for one third of the line period,

$$i_1(\omega_0 t) = i_2\left(\omega_0 t - \frac{2\pi}{3}\right) = i_3\left(\omega_0 t - \frac{4\pi}{3}\right), \quad (3.8)$$

which is referred to as “phase displacement constraint.” The same phase displacement relation holds for the diode state functions of the odd-indexed diodes in the diode bridge:

$$d_1(\omega_0 t) = d_3\left(\omega_0 t - \frac{2\pi}{3}\right) = d_5\left(\omega_0 t - \frac{4\pi}{3}\right), \quad (3.9)$$

as well as for the even-indexed diodes:

$$d_2(\omega_0 t) = d_4\left(\omega_0 t - \frac{2\pi}{3}\right) = d_6\left(\omega_0 t - \frac{4\pi}{3}\right). \quad (3.10)$$

One way to satisfy the phase displacement constraint (3.8), having the diode state functions satisfying the same constraint as specified by (3.9) and (3.10), is to provide the injected currents i_{X1} , i_{X2} , and i_{X3} satisfying

$$i_{X1}(\omega_0 t) = i_{X2}\left(\omega_0 t - \frac{2\pi}{3}\right) = i_{X3}\left(\omega_0 t - \frac{4\pi}{3}\right), \quad (3.11)$$

and the diode bridge load currents i_A and i_B periodic with the period equal to one third of the line period,

$$i_A(\omega_0 t) = i_A\left(\omega_0 t - \frac{2\pi}{3}\right) = i_A\left(\omega_0 t - \frac{4\pi}{3}\right) \quad (3.12)$$

and

$$i_B(\omega_0 t) = i_B\left(\omega_0 t - \frac{2\pi}{3}\right) = i_B\left(\omega_0 t - \frac{4\pi}{3}\right). \quad (3.13)$$

It should be noted here that the fundamental frequency of the waveforms of i_A and i_B that satisfies (3.12) and (3.13) is the triple of the line frequency, $3\omega_0$. For waveforms of the injected current i_{X1} , i_{X2} , and i_{X3} , only the phase displacement constraint is assumed, and the fundamental frequency of these currents can be the line frequency, like for the input currents i_1 , i_2 , and i_3 . On the other hand, the phase displacement constraint can be satisfied in a special case that the injected currents are the same:

$$i_{X1}(\omega_0 t) = i_{X2}(\omega_0 t) = i_{X3}(\omega_0 t) = i_X(\omega_0 t), \quad (3.14)$$

and in that case the injected currents have to be periodic with the fundamental frequency equal to the triple of the line frequency, $3\omega_0$. This directly follows from the phase displacement constraint

$$i_X(\omega_0 t) = i_X\left(\omega_0 t - \frac{2\pi}{3}\right) = i_X\left(\omega_0 t - \frac{4\pi}{3}\right). \quad (3.15)$$

Where the currents injected to the supply lines are the same, they are equal to one third of the current supplied to the current injection device,

$$i_X(\omega_0 t) = \frac{1}{3} i_Y(\omega_0 t). \quad (3.16)$$

Thus, the purpose of the current injection device in (3.14) is to divide the current supplied from the current injection network into three equal parts, and to inject them back to the supply lines. In this book, two methods of current injection are analyzed. The first one utilizes mutually equal injected currents, satisfying (3.14), and this method is analyzed in detail. The second method utilizes different injected currents, with the fundamental frequency equal to the line frequency, ω_0 . This method is analyzed in Chapter 12.

According to Kirchhoff's current law, the current supplied to the current injection device is equal to the difference of the currents that load the diode bridge,

$$i_Y(\omega_0 t) = i_A(\omega_0 t) - i_B(\omega_0 t). \quad (3.17)$$

The average of the current that loads the positive output terminal of the diode bridge is

$$I_A = \frac{3}{2\pi} \int_0^{2\pi/3} i_A(\omega_0 t) d(\omega_0 t), \quad (3.18)$$

while the average, i.e., the DC component, of the current that loads the negative output terminal of the diode bridge is

$$I_B = \frac{3}{2\pi} \int_0^{2\pi/3} i_B(\omega_0 t) d(\omega_0 t). \quad (3.19)$$

Assuming that the current injection network does not take any of the DC component of the diode bridge load currents, and assuming that the output current is free from AC ripple, the output current is equal to the DC components of the diode bridge load currents,

$$I_{OUT} = I_A = I_B; \quad (3.20)$$

thus these DC components have to be the same. In this case, the currents that the current injection network takes from the diode bridge output terminals are

$$i_{IA} = i_A - I_A = i_A - I_{OUT} \quad (3.21)$$

and

$$i_{IB} = I_B - i_B = I_{OUT} - i_B. \quad (3.22)$$

Since i_A and i_B are periodic at the triple of the line frequency, the same applies for i_{IA} and i_{IB} , according to (3.21) and (3.22). This is convenient since the diode bridge output terminal voltages v_A and v_B are periodic at the triple of the line frequency, as shown by (2.7) and (2.8). Thus, the source to synchronize i_{IA} and i_{IB} is readily available.

According to Kirchhoff's current law, the current that the current injection network supplies to the current injection device is

$$i_Y = i_{IA} + i_{IB}. \quad (3.23)$$

These relations are used frequently in subsequent analyses.

Another important issue is the effect of the current injection on average currents of the diodes in the three-phase diode bridge. Since the diode bridge load currents i_A and i_B are periodic with the triple of the line frequency, averages of the diode bridge currents are the same for all of the diodes, being

$$I_{D(2k-1)} = \frac{1}{3} I_A = \frac{1}{3} I_{OUT} \quad (3.24)$$

for the odd-indexed diodes, and

$$I_{D(2k)} = \frac{1}{3} I_B = \frac{1}{3} I_{OUT} \quad (3.25)$$

for even-indexed diodes. Thus, the average values of the diode currents remained the same as in the diode bridge rectifier without the current injection.

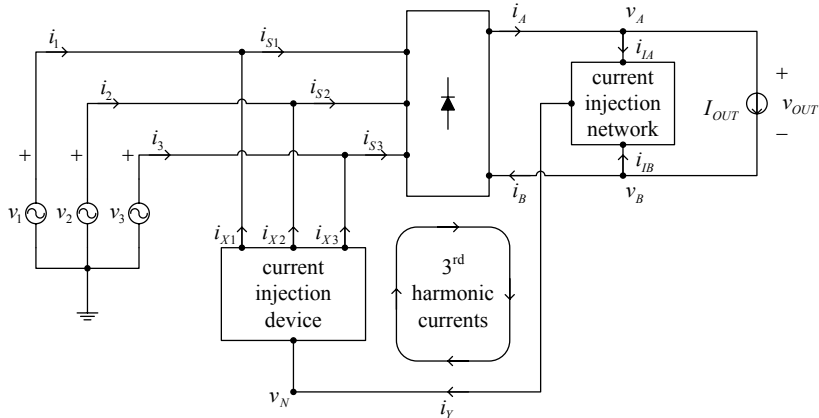


Figure 3-2. Flow of the third-harmonic currents.

A common misconception about the current injection is that it is a sort of compensation for the third-harmonic currents taken by the diode bridge rectifier. First of all, the diode rectifier bridge is a symmetric load, supplied by a symmetric three-wire system; thus harmonics at triples of the line frequency are absent from the input currents i_1 , i_2 , i_3 , both before and after the current injection is applied. The flow of the harmonic currents at the triple of the line frequency is shown in Fig. 3-2. The harmonic currents at the triple of the line frequency are taken from the rectifier output terminals by i_{IA} and i_{IB} , flowing through an asymmetric three-wire system consisting of

i_{IA} , i_{IB} , and i_Y . After the injected current i_Y is processed by the current injection device, the flow of the third-harmonic currents is located to a symmetric four-wire system consisting of i_{S1} , i_{S2} , i_{S3} , and i_Y . The flow is closed through the three-phase diode bridge, which is a nonlinear device. Thus, through the nonlinear processing in the diode bridge, the circular flow of the third-harmonic currents depicted in Fig. 3-2 improves the total harmonic distortion of the input currents. The input currents did not contain any of the third-harmonic components before or after the current injection was applied.

Issues discussed in the following chapters concern the waveforms of i_{IA} and i_{IB} convenient to be realized to minimize the input current THD, providing a high power factor at the same time, efficient realization of current injection devices, and the design of simple and reliable current injection networks to provide the required waveforms of i_{IA} and i_{IB} .

Chapter 4

CURRENT INJECTION DEVICES

Current injection devices, introduced in Fig. 3-1, are the subject of this chapter. The current injection device divides the current supplied by the current injection network into three equal parts and injects them back to the supply lines. In terms of electrical element characteristics, the current injection device in Fig. 3-1 is completely described by

$$i_{X1} = i_{X2} = i_{X3} = i_X = \frac{1}{3}i_Y \quad (4.1)$$

and

$$v_N = \frac{1}{3}(v_1 + v_2 + v_3) = 0. \quad (4.2)$$

Development of a current injection device as a magnetic element is discussed here. Several methods to build the current injection device are proposed and compared. Besides construction the current injection device as a separate component, it is shown that the current injection device can be incorporated in the transformer if it is applied at the rectifier input, and two transformer-based constructions of the current injection device are discussed. The main parameter to compare various forms of current injection devices is the volt-ampere rating of the required core. Thus, the volt-ampere rating is the first topic analyzed.

1. VOLT-AMPERE RATING

Volt-ampere rating of ferromagnetic cores is a parameter frequently observed in product specifications. The volt-ampere rating is given for specified frequencies of the voltages and currents, assuming that the waveforms are sinusoidal. The aim of the analysis presented in this section is to generalize the volt-ampere rating to situations in which the operating frequency differs from the assumed value, and when the voltage and current waveforms are not sinusoidal.

The concept of the volt-ampere rating is based on the fact that there are two main limiting factors for the power transferred through the ferromagnetic core: saturation of the core and maximum of the current that can pass through the core window without the device overheating. These two parameters are coupled, such that increase in the number of turns reduces the flux in the core, but the increased number of turns will increase the current effectively passing through the core window.

Let us define the volt-ampere rating of a single-phase core as

$$S_{T1} = \frac{\omega_0}{2\sqrt{2}} \Phi_{\max} \sum_{k=1}^{n_w} n_k I_{k RMS}. \quad (4.3)$$

In (4.3), ω_0 is the angular frequency of the voltages and currents at which the volt-ampere rating provided in data sheets is specified. The most common value of this parameter corresponds to the line frequency $f_0 = 50$ Hz or $f_0 = 60$ Hz, where $\omega_0 = 2\pi f_0$. The parameter Φ_{\max} is the maximum of the magnetic flux that the core can withstand without becoming saturated. Finally, the sum $\sum_{k=1}^{n_w} n_k I_{k RMS}$ represents the current load of the core window, where n_w is the number of transformer windings, n_k is the number of turns of the k th winding, and $I_{k RMS}$ is the RMS value of the current passing through the k th winding. Every core has a limit on the current load of its window,

$$\sum_{k=1}^{n_w} n_k I_{k RMS} \leq k_{FF} J_{\max} A_w, \quad (4.4)$$

where A_w is the window area; k_{FF} is the fill factor, i.e., ratio of the window area filled with copper to the whole window area, usually with a value somewhere around 0.5; and J_{\max} is the maximum RMS current density that the windings can withstand without getting overheated. The value of J_{\max} depends on the core size in a nonlinear fashion, being as high as 8 A/mm^2 for very small cores, rapidly decreasing with a core size to about 2 A/mm^2 , and slowly decreasing afterward. The exact value of J_{\max} for a considered core is found in the manufacturer's data sheets.

To apply the volt-ampere rating concept, two approximations should be accepted: the first is that Φ_{\max} is not dependent on the applied voltage frequency, and the second is that J_{\max} is not dependent of the frequency of the currents passing through the windings. As long as these assumptions hold, the volt-ampere rating concept can be applied.

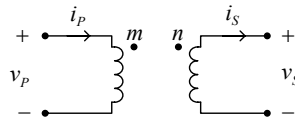


Figure 4-1. A single-phase transformer.

Let us consider a single-phase transformer, shown in Fig. 4-1, and assume that the transformer primary is supplied by a voltage source:

$$v_p = V_m \cos(\omega_0 t). \quad (4.5)$$

Assuming the transformer voltages and currents are adequately related by the ideal transformer model, being the model of perfect magnetic coupling and negligible magnetizing current, the voltage at the transformer secondary is

$$v_s = V_n \cos(\omega_0 t) = \frac{n}{m} V_m \cos(\omega_0 t). \quad (4.6)$$

Next, let us assume that the load connected at the transformer secondary takes sinusoidal current with the amplitude \$I_n\$, displaced in phase by a phase angle \$\varphi\$:

$$i_s = I_n \cos(\omega_0 t - \varphi). \quad (4.7)$$

The assumed ideal transformer model for the primary current gives

$$i_p = I_m \cos(\omega_0 t - \varphi) = \frac{n}{m} I_n \cos(\omega_0 t - \varphi). \quad (4.8)$$

After the currents of the transformer windings are determined, the current load of the transformer window can be computed. Since the transformer number of windings is \$n_w = 2\$, for the window current load we obtain

$$\sum_{k=1}^{n_w} n_k I_{k RMS} = m I_{m RMS} + n I_{n RMS} = 2m I_{m RMS} = \sqrt{2} m I_m. \quad (4.9)$$

To determine the maximum of the flux in the transformer core, let us express the primary voltage applying Faraday's law of electromagnetic induction,

$$v_P = m \frac{d\Phi}{dt}, \quad (4.10)$$

while the secondary voltage is given by

$$v_S = n \frac{d\Phi}{dt}. \quad (4.11)$$

Integrating the waveforms of (4.5) and (4.6), and assuming that the DC component of the core flux is equal to zero, both equations (4.10) and (4.11) for the maximum of the core flux provide the same result:

$$\Phi_{\max} = \frac{V_m}{m\omega_0} = \frac{V_n}{n\omega_0}. \quad (4.12)$$

Finally, for the transformer volt-ampere rating, applying (4.3) we obtain the expected result:

$$S_{T1} = \frac{\omega_0}{2\sqrt{2}} \frac{V_m}{m\omega_0} \sqrt{2} m I_m = V_{m RMS} I_{m RMS}. \quad (4.13)$$

Actually, this result is the origin of the formula (4.3), i.e., the formula is fitted to provide the result (4.13) at a rated frequency for sinusoidal waveforms of the voltages and currents. The formula is invented to generalize the core volt-ampere rating to the situations when the waveforms are not sinusoidal, and the frequency is not equal to the rated frequency. As mentioned previously, the generalized volt-ampere rating of (4.3) is applicable as long as it can be assumed that the core can withstand Φ_{\max} without getting saturated and without considerable increase of the core loss at higher frequencies, and as long as the core window can withstand the rated current density without the device overheating. Both parameters are frequency dependent; Φ_{\max} is primarily affected by an increase of the core loss at higher frequencies due to the core hysteresis and eddy currents, while the current density should be reduced at higher frequencies due to the skin and proximity effects. However, in a moderate frequency range, the volt-ampere rating concept provides reasonably accurate results. It is also worth underlining here that the result (4.13) states that transformer volt-ampere rating in the all-sinusoidal case is dependent on the transformer apparent power, not on the average power.

The volt-ampere rating concept can be generalized to three-phase transformers, and for a symmetrically loaded transformer the formula to compute the volt-ampere rating is

$$S_{T3} = \frac{3\omega_0}{2\sqrt{2}} \Phi_{\max} \sum_{k=1}^{n_w} n_k I_{k RMS}, \quad (4.14)$$

where the sum and n_w apply to one of the core limbs—any one, but only one. Equation (4.14) is obtained by a straightforward generalization of (4.3), assuming balanced operation of the transformer.

To compute the volt-ampere rating, formulas (4.3) and (4.14) can be simplified in some special cases. In practice, the most frequent is the case when the voltage across the windings is sinusoidal with angular frequency ω_0 , and the transformer has two windings. The voltage waveform and frequency fit the conditions when manufacturer's data apply; thus we do not have to worry about a derate for the transformer core. In the case of a single-phase transformer, depicted in Fig. 4-1, (4.3) reduces to

$$S_{T1} = \frac{\omega_0}{2\sqrt{2}} \left(\frac{V_{P RMS} \sqrt{2}}{m\omega_0} \right) (mI_{P RMS} + nI_{S RMS}). \quad (4.15)$$

Since

$$mi_P = ni_S, \quad (4.16)$$

we have

$$nI_{S RMS} = mI_{P RMS}; \quad (4.17)$$

thus

$$S_{T1} = V_{P RMS} I_{P RMS}. \quad (4.18)$$

Equation (4.15) can be generalized for the three-phase transformers to

$$S_{T3} = \frac{3}{2} (V_{P RMS} I_{P RMS} + V_{S RMS} I_{S RMS}). \quad (4.19)$$

It should be noted here that (4.17) does not apply for three-phase transformers in general, since their primary and secondary currents might

have different waveforms, as shown in Section 4.7. Thus, (4.19) is written in a form that is more general than (4.18), requiring waveforms of the transformer voltages and currents only to be symmetric.

To compute the volt-ampere rating, equations (4.18) and (4.19) apply for transformers with two windings per phase, supplied with the sinusoidal voltage with rated frequency. No assumptions are made regarding the current; thus waveforms and frequency of the winding currents may be considered arbitrary. However, when applying (4.18) and (4.19), we should be aware of their limitations caused by skin and proximity effects at higher frequencies, requiring some derate in the current density.

In the text that follows, application of (4.18) and (4.19) is referred to as “direct computation of the volt-ampere rating.” This method was applied in Chapter 12 of [9] to compute volt-ampere ratings for rectifier transformers. However, it had to be generalized to (4.3) and (4.14) to be applied to some special cases of interest in this book.

2. CURRENT INJECTION DEVICE APPLYING A THREE-PHASE TRANSFORMER WITH UNLOADED DELTA-CONNECTED SECONDARY WINDING

The simplest form of the current injection device to analyze is the one applying a wye-delta transformer with unloaded secondary. The schematic diagram for this current injection device is presented in Fig. 4-2. The unloaded secondary forces all three of the primary currents to be equal,

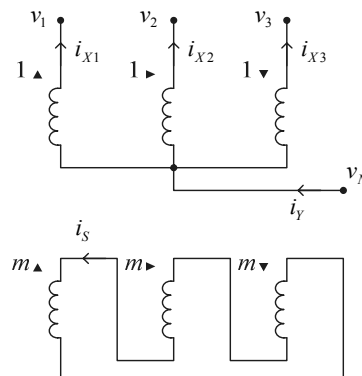


Figure 4-2. Current injection device obtained by applying a wye-delta transformer with unloaded secondary.

$$mi_S = i_{X1} = i_{X2} = i_{X3}, \quad (4.20)$$

thus

$$i_{X1} = i_{X2} = i_{X3} = i_X = \frac{1}{3}i_Y, \quad (4.21)$$

which satisfies the first requirement imposed on the current injection device, (4.1).

From the loop equation over the unloaded delta-connected secondary,

$$m(v_1 - v_N) + m(v_2 - v_N) + m(v_3 - v_N) = 0, \quad (4.22)$$

the second condition imposed on the current injection device, (4.2), is satisfied:

$$v_N = \frac{1}{3}(v_1 + v_2 + v_3) = 0. \quad (4.23)$$

Thus, the device depicted in Fig. 4-2 is really a current injection device. The volt-ampere rating of the device is directly obtained as

$$S_0 = 3 \frac{V_m}{\sqrt{2}} I_{X RMS} = \frac{V_m I_{Y RMS}}{\sqrt{2}}. \quad (4.24)$$

This realization of the current injection device is simple, the influence of parasitic effects is negligible, and it can even be obtained by applying three single-phase transformers. However, it is not efficient in terms of the required volt-ampere rating. The application area of the device in Fig. 4-2 is thus restricted to laboratory prototypes of the current injection based rectifiers, since required components are usually readily available.

3. CURRENT INJECTION DEVICE APPLYING A ZIGZAG AUTOTRANSFORMER

The second realization of the current injection device to be analyzed is based on application of a zigzag autotransformer. The circuit diagram of this form is shown in Fig. 4-3. This device is common in practice, and it is usually obtained by applying a three-phase transformer core, but it can also

be obtained by applying three single-phase transformers with the 1:1 turns ratio.

Under the constraint that reluctances of the transformer core are negligible, magnetomotive forces applied to each of the core limbs are equal to zero, resulting in the sum of the ampere-turns applied to the limb equal to zero. Applying this on the first limb of the transformer of Fig. 4-3, i_{X1} and i_{X2} are found to be equal,

$$i_{X1} = i_{X2} \quad (4.25)$$

The same equation over the second limb forces

$$i_{X2} = i_{X3}, \quad (4.26)$$

while applying the equation over the third limb forces

$$i_{X3} = i_{X1}. \quad (4.27)$$

Thus, from (4.25), (4.26), and (4.27)

$$i_{X1} = i_{X2} = i_{X3} = i_X = \frac{1}{3}i_Y, \quad (4.28)$$

which satisfies (4.1).

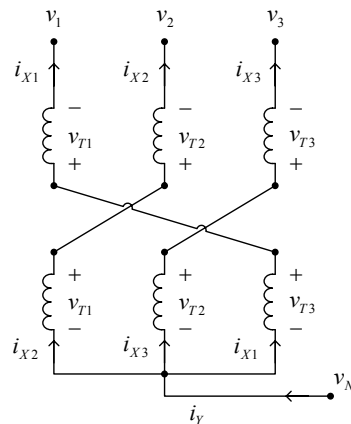


Figure 4-3. Current injection device obtained by applying a zigzag autotransformer.

To determine the voltage equation for the device in Fig. 4-3, let us start with the voltage from v_1 to v_N , which is

$$v_1 - v_N = v_{T3} - v_{T1}, \quad (4.29)$$

while

$$v_2 - v_N = v_{T1} - v_{T2}, \quad (4.30)$$

and

$$v_3 - v_N = v_{T2} - v_{T3}. \quad (4.31)$$

Adding (4.29), (4.30), and (4.31), we get

$$v_N = \frac{1}{3}(v_1 + v_2 + v_3) = 0, \quad (4.32)$$

which is the same as (4.2); thus both requirements for the current injection device are satisfied.

Voltages v_{T1} , v_{T2} , and v_{T3} across the windings cannot be uniquely determined from the system of linear equations comprising (4.29), (4.30), and (4.31), since the system is singular. However, taking an additional constraint

$$v_{T1} + v_{T2} + v_{T3} = 0, \quad (4.33)$$

the voltages can be uniquely determined as

$$v_{T1} = \frac{1}{3}(v_2 - v_1), \quad (4.34)$$

$$v_{T2} = \frac{1}{3}(v_3 - v_2), \quad (4.35)$$

and

$$v_{T3} = \frac{1}{3}(v_1 - v_3). \quad (4.36)$$

Root-mean-square values of the winding voltages are

$$V_{T1RMS} = V_{T2RMS} = V_{T3RMS} = V_{TRMS} = \frac{1}{\sqrt{6}} V_m, \quad (4.37)$$

resulting in the directly computed volt-ampere rating of the current injection device of Fig. 4-3,

$$S_1 = 3V_{TRMS}I_{XRMS} = \frac{V_m I_{YRMS}}{\sqrt{6}}. \quad (4.38)$$

This volt-ampere rating is significantly lower than the value of (4.24) obtained for the current injection device of Fig. 4-2,

$$S_1 = \frac{1}{\sqrt{3}} S_0 = 57.74\% S_0. \quad (4.39)$$

Hence the current injection device in Fig. 4-3 is a better choice for the rectifier design. Like the device in Fig. 4-2, it does not have significant parasitic effects, and it was the most frequently used realization during the research whose results are presented in this book.

4. CURRENT INJECTION DEVICE APPLYING TWO SINGLE-PHASE TRANSFORMERS

Another type of current injection device to be analyzed is somewhat specific, since it applies two single-phase transformers. This realization is proposed in [49], and it is applied in the rectifiers proposed in [45] and [46]. The current injection device is named “zero-sequence filter” in these references.

The current injection device realization that applies two single-phase transformers is shown in Fig. 4-4, and this is the only current injection device analyzed in this book that does not apply a three-phase ferromagnetic core. The transformers T1 and T2 are assumed to be adequately represented by ideal transformer models, i.e., they are assumed to have perfect coupling and negligible magnetizing currents. The first of the transformers, labeled T1, divides the injected current i_Y in the ratio 2:1, resulting in

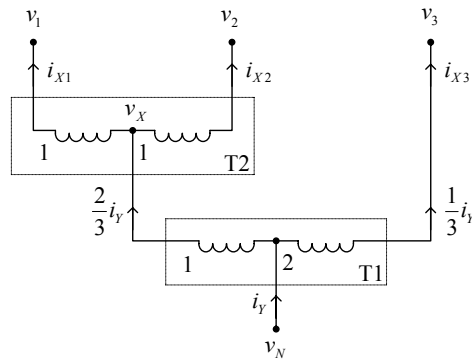


Figure 4-4. Current injection device obtained by applying two single-phase transformers.

$$i_{x3} = \frac{1}{3}i_Y, \quad (4.40)$$

which satisfies one third of the first current injection device requirement (4.1). The larger of the parts i_Y is divided to $(2/3)i_Y$, and is further divided by the second of the transformers, labeled T2, into two equal parts. Thus,

$$i_{x1} = i_{x2} = \frac{1}{3}i_Y, \quad (4.41)$$

which completely satisfies the first current injection device requirement.

The transformer T2 provides the middle-point voltage:

$$v_X = \frac{1}{2}(v_1 + v_2). \quad (4.42)$$

This voltage affects the neutral point voltage v_N , which according to the element characteristic of T1 is given by

$$v_N = \frac{2}{3}v_X + \frac{1}{3}v_3. \quad (4.43)$$

Substituting (4.42) in (4.43), the neutral point voltage is obtained as

$$v_N = \frac{1}{3}(v_1 + v_2 + v_3) = 0, \quad (4.44)$$

which satisfies the second current injection device criterion, (4.2).

The volt-ampere rating of T1 is directly computed as

$$S_{T1} = \frac{V_m I_{Y RMS}}{3\sqrt{2}} = \frac{1}{3} S_0 \approx 33.33\% S_0. \quad (4.45)$$

The computation is simple, since the voltage across the winding with the larger number of turns equals the phase voltage, and currents in the windings are as labeled in Fig. 4-4. The volt-ampere rating of T2 is directly computed, again, and the result is

$$S_{T2} = \frac{V_m I_{Y RMS}}{2\sqrt{6}} = \frac{1}{2\sqrt{3}} S_0 \approx 28.87\% S_0, \quad (4.46)$$

since the voltages across the transformer windings are equal to one half of the line-to-line voltage, and the currents of the windings are as labeled in Fig. 4-4. The sum of the volt-ampere ratings (4.45) and (4.46) is

$$S_{T1} + S_{T2} = \left(\frac{1}{3\sqrt{2}} + \frac{1}{2\sqrt{3}} \right) V_m I_{Y RMS} = \left(\frac{1}{3} + \frac{1}{2\sqrt{3}} \right) S_0 = 62.20\% S_0. \quad (4.47)$$

The result is slightly worse than given by (4.39), but better than (4.24). However, two additional facts should be kept in mind while making a design decision: first, single-phase cores are heavier and more expensive in comparison to the three-phase cores with the same volt-ampere rating; second, size and cost of a transformer are not linear functions of its volt-ampere rating, thus the addition of the volt-ampere ratings presented in (4.47) is used just as an illustration, and it should not be considered an exact measure.

This current injection device form might be useful in experiments, since the two single-phase transformers required to build the current injection device are readily available in almost all power electronics labs.

5. CURRENT INJECTION DEVICE APPLYING A THREE-PHASE INDUCTOR

Although the current injection device in Fig. 4-3 provided significant improvement in the volt-ampere rating of the core the device requires, further reduction of the volt-ampere rating is possible applying three-phase inductor as a current injection device, as proposed in [19]. Let us consider a three-phase inductor shown in Fig. 4-5. This inductor is different from three single-phase inductors, since it is wound around a three-phase ferromagnetic core. The core is depicted in Fig. 4-6, where spatial locations of its equivalent electric circuit parameters are indicated. In the analysis, it will be assumed that reluctances of the core limbs are the same, R_m , while the reluctance that characterizes flow of the magnetic flux outside the ferromagnetic core is R_{m0} .

The device in Fig. 4-5 has three windings that produce a magnetomotive force, and the electric equivalent of its magnetic circuit is presented in Fig. 4-7. The magnetomotive force sources are

$$F_k = -ni_{Xk}, \quad (4.48)$$

where $k \in \{1, 2, 3\}$. Assuming that

$$R_{m0} \rightarrow \infty, \quad (4.49)$$

magnetomotive force F_0 at the core ends is obtained as

$$F_0 = \frac{1}{3}(F_1 + F_2 + F_3). \quad (4.50)$$

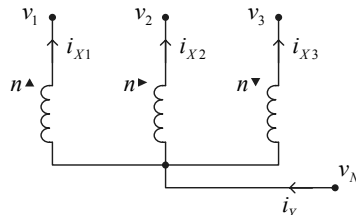


Figure 4-5. Current injection device obtained by applying a three-phase inductor.

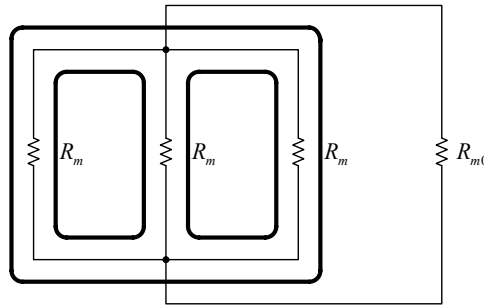


Figure 4-6. Magnetic circuit of a three-phase transformer core.

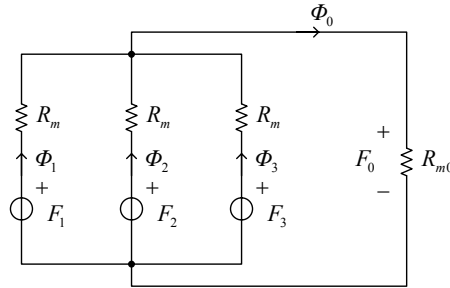


Figure 4-7. Magnetic circuit corresponding to the current injection device realized as a three-phase inductor.

Now, assuming that the reluctance of the ferromagnetic core is negligible,

$$R_m \rightarrow 0, \quad (4.51)$$

we obtain

$$F_1 = F_2 = F_3 = F_0. \quad (4.52)$$

This implies

$$i_{x1} = i_{x2} = i_{x3} = i_x = \frac{1}{3} i_y, \quad (4.53)$$

which satisfies requirement (4.1).

Since $R_{m0} \rightarrow \infty$,

$$\Phi_0 = 0, \quad (4.54)$$

resulting in

$$\Phi_1 + \Phi_2 + \Phi_3 = 0. \quad (4.55)$$

Voltages across the device windings are determined applying Faraday's law

$$v_k - v_N = n \frac{d\Phi_k}{dt}, \quad (4.56)$$

for $k \in \{1, 2, 3\}$. Differentiating (4.55) over time and multiplying by the number of turns, a voltage equation is obtained,

$$n \frac{d\Phi_1}{dt} + n \frac{d\Phi_2}{dt} + n \frac{d\Phi_3}{dt} = 0, \quad (4.57)$$

which according to (4.56) results in

$$v_N = \frac{1}{3}(v_1 + v_2 + v_3) = 0. \quad (4.58)$$

Equations (4.53) and (4.58), derived under the assumptions that $R_m \rightarrow 0$ and $R_{m0} \rightarrow \infty$, satisfy the requirements (4.1) and (4.2) imposed on the current injection device.

The volt-ampere rating of the current injection device in Fig. 4-5, under the assumptions that $R_m \rightarrow 0$ and $R_{m0} \rightarrow \infty$, can be computed directly, and the result is

$$S_2 = 3 \frac{V_m}{2\sqrt{2}} I_{X RMS} = \frac{V_m I_{Y RMS}}{2\sqrt{2}}. \quad (4.59)$$

Compared to the previously discussed current injection device realizations,

$$S_2 = \frac{1}{2} S_0 = 50\% S_0 = \frac{\sqrt{3}}{2} S_1 = 86.60\% S_1, \quad (4.60)$$

and some savings in the volt-ampere rating are obtained in comparison to the device in Fig. 4-3.

Unfortunately, the device in Fig. 4-5, although having a promising volt-ampere rating, suffers from significant parasitic effects, since the approximations $R_{m0} \rightarrow \infty$ and $R_m \rightarrow 0$ are not good enough to be accepted without doubt. This primarily applies for the approximation $R_{m0} \rightarrow \infty$, since finite values for R_{m0} cause significant parasitic inductance at the current injection device neutral point. To analyze the current injection device in Fig. 4-5 assuming finite values for R_m and R_{m0} , first let us compute the magnetomotive force F_0 at the ends of the core. This magnetomotive force causes leakage of the magnetic flux outside the ferromagnetic core. From the magnetic circuit depicted in Fig. 4-7, F_0 is obtained as

$$F_0 = \frac{R_{m0}}{R_m + 3R_{m0}} (F_1 + F_2 + F_3), \quad (4.61)$$

which reduces to (4.50) for $R_m \rightarrow 0$. The magnetic flux in each of the core limbs is given by

$$\Phi_k = \frac{F_k - F_0}{R_m}, \quad (4.62)$$

for $k \in \{1, 2, 3\}$. Voltages across the device windings are determined by applying Faraday's law, given by (4.56). Expanding (4.56) for $k \in \{1, 2, 3\}$, applying (4.48), (4.61), and (4.62), currents and voltages across the device are mutually related, providing the element characteristic in a matrix form

$$\begin{bmatrix} v_1 - v_N \\ v_2 - v_N \\ v_3 - v_N \end{bmatrix} = - \begin{bmatrix} L & -M & -M \\ -M & L & -M \\ -M & -M & L \end{bmatrix} \frac{d}{dt} \begin{bmatrix} i_{X1} \\ i_{X2} \\ i_{X3} \end{bmatrix}, \quad (4.63)$$

where L is given by

$$L = \frac{n^2}{R_m} \frac{R_m + 2R_{m0}}{R_m + 3R_{m0}}, \quad (4.64)$$

while M is

$$M = \frac{n^2}{R_m} \frac{R_{m0}}{R_m + 3R_{m0}}. \quad (4.65)$$

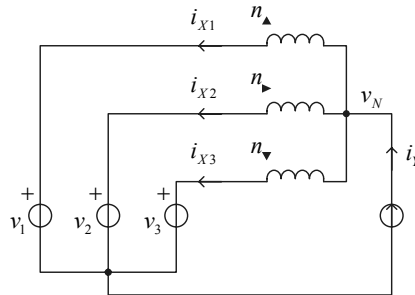


Figure 4-8. Circuit applied to test the current injection device.

To determine the behavior of the current injection device specified by (4.63) in a rectifier that applies current injection, consider the circuit in Fig. 4-8. The current injection device is supplied by a balanced undistorted three-phase voltage system v_1 , v_2 , and v_3 , specified by (2.1), (2.2), and (2.3). A current source i_Y is applied to represent the current injection network. Since the element characteristic of the current injection device given by (4.63) is linear, the superposition principle can be applied, computing response of the circuit i_{X1} , i_{X2} , and i_{X3} , as a sum of the responses on i_Y and v_1 , v_2 , v_3 taken separately.

Taking

$$i_Y = 0, \quad (4.66)$$

applying Kirchhoff's current law on the node with the voltage v_N , we obtain

$$i_{X1} + i_{X2} + i_{X3} = 0. \quad (4.67)$$

Applying (4.67) in (4.63), non-diagonal elements of the inductance matrix of (4.63) are eliminated, leaving

$$v_k = -(L + M) \frac{di_{Xk}}{dt} \quad (4.68)$$

for $k \in \{1, 2, 3\}$, and

$$v_N = 0. \quad (4.69)$$

Thus, in the considered case, the line voltages observe magnetizing inductance of the current injection device of

$$L_m = L + M = \frac{n^2}{R_m}, \quad (4.70)$$

which is expected since the device is designed as a three-phase inductor. For $R_m \rightarrow 0$, we have that $L_m \rightarrow \infty$. In practice, nonzero values of R_m do not significantly affect the performance of the current injection device, unless an air gap is applied in the inductor core.

It should be noted here that a finite value of the magnetizing inductance L_m causes magnetizing currents to flow through the current injection device. These currents do not obey the requirement (4.1) imposed on the current injection device; thus the magnetizing inductance should be kept reasonably high to provide low amplitudes of the magnetizing currents, in order to satisfy (4.1) approximately.

As the second case, let us analyze the situation when the phase voltages are turned off,

$$v_1 = v_2 = v_3 = 0. \quad (4.71)$$

Substituting (4.71) into (4.63), currents i_{X1} , i_{X2} , and i_{X3} of the current injection device are derived to be the same,

$$i_{X1} = i_{X2} = i_{X3} = i_X = \frac{1}{3}i_Y. \quad (4.72)$$

Thus dividing the injected current i_Y into three equal parts is performed successfully. However, the voltage of the neutral point of the current injection device, v_N , is no longer zero. Instead,

$$v_N = \frac{1}{3}(L - 2M) \frac{di_Y}{dt}. \quad (4.73)$$

This is the most important parasitic effect, and it should be studied in detail. According to (4.73), current source i_Y observes an inductance of the neutral point

$$L_n = \frac{L - 2M}{3} = \frac{n^2}{3(R_m + 3R_{m0})}, \quad (4.74)$$

which goes to zero as $R_{m0} \rightarrow \infty$. However, values of R_{m0} encountered in practice cause L_n to have significant value, in the order of 10 mH for the cores with the rated power of the order of several hundreds of watts. The inductance of the neutral point may be used as an element of the current injection network.

The finite value of the inductance of the neutral point affects the voltages across the current injection device windings, thus affecting the core flux, and finally affecting the device volt-ampere rating. To compute the device volt-ampere rating from the voltages and currents it is exposed to, let us consider the first limb of the three-phase core with the phase voltage

$$v_1 = V_m \cos(\omega_0 t), \quad (4.75)$$

applied at one end of the corresponding winding. Also, assume that the current to be injected is given by

$$i_Y = I_{Ym} \cos(3\omega_0 t), \quad (4.76)$$

resulting in the neutral point voltage

$$v_N = L_n \frac{di_Y}{dt} = -3\omega_0 L_n I_{Ym} \sin(3\omega_0 t) = -V_N \sin(3\omega_0 t). \quad (4.77)$$

Thus, the voltage across the winding of the first limb is

$$v_1 - v_N = V_m \cos(\omega_0 t) + V_N \sin(3\omega_0 t) = V_m (\cos(\omega_0 t) + a \sin(3\omega_0 t)), \quad (4.78)$$

where parameter a is the ratio of the amplitude of the voltage at the neutral point to the amplitude of the phase voltage,

$$a = \frac{V_N}{V_m}. \quad (4.79)$$

Integrating (4.78) over time and dividing by the number of turns, the maximum of the limb flux is obtained as

$$\Phi_{\max} = \frac{V_m}{n\omega_0} \max \left(\sin(\omega_0 t) - \frac{a}{3} \cos(3\omega_0 t) \right) = \frac{V_m}{n\omega_0} f(a), \quad (4.80)$$

where

$$f(a) = \max \left(\sin(\omega_0 t) - \frac{a}{3} \cos(3\omega_0 t) \right). \quad (4.81)$$

Thus, the volt-ampere rating of the current injection device of Fig. 4-5 can be expressed as

$$S_3 = S_2 f(a), \quad (4.82)$$

where S_2 is specified by (4.59), and the derate $f(a)$ is given by (4.81). Dependence of the volt-ampere rating on a is depicted in Fig. 4-9.

Now, let us consider a special case when

$$a_{EC} = \frac{3\sqrt{3}}{2\pi} \approx 0.827, \quad (4.83)$$

which corresponds to the situation of the maximal AC component of the voltage across the current injection network capacitors that enables application of electrolytic capacitors. This issue is discussed in detail in Chapter 6. The value of a given by (4.83) represents a maximum the current injection network is expected to be exposed to. In that case,

$$f(a_{EC}) \approx 1.1792, \quad (4.84)$$

and the corresponding volt-ampere rating of the current injection device is

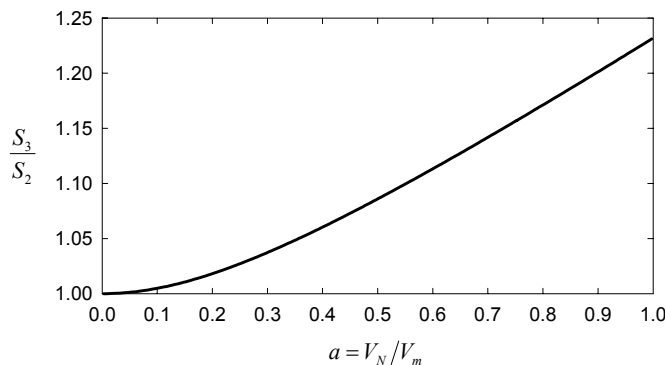


Figure 4-9. Dependence of the volt-ampere rating on a .

$$\frac{S_2 f(a_{EC})}{S_1} \approx 1.0212. \quad (4.85)$$

This means that for an increase of only 2% in the volt-ampere rating of the current injection device in comparison to the current injection device realized as a zigzag autotransformer, a current injection device with integrated inductor can be obtained.

Design of this type of current injection device might not be a straightforward procedure, since there are two criteria to determine the number of turns. The first criterion is based on the maximum of the core flux, and according to that criterion,

$$n \geq \frac{V_m}{\omega_0 \Phi_{\max}} f(a). \quad (4.86)$$

On the other hand, to provide the desired inductance of the neutral point, the number of turns should be

$$n = \sqrt{3(R_m + 3R_{m0})L_n}. \quad (4.87)$$

The best situation that might occur is that both of the equations (4.86) and (4.87) provide the same number of turns. However, this situation is highly unlikely to occur. If the number of turns provided by (4.87) is greater than the limiting value of (4.86), the designer should choose either to accept the value obtained by (4.87), reducing the maximum of the core flux, or to accept the lower limit of (4.86), which results in insufficient inductance of the neutral point. The remaining part of the inductance could be obtained by applying an additional inductor. On the other hand, the number of turns provided by (4.87) could be lower than the minimum value imposed by (4.86). This situation is frequently observed with the cores of the volt-ampere rating on the order of several hundreds of watts. To resolve this situation, the designer should either redesign the current injection network to allow a larger value of the inductance, or apply the technique described in the next section.

It should be noted here that a part of the text in this section, starting from (4.76), might not be clear on the first reading. This is natural, since full understanding of this part of the text requires some knowledge of the design of current injection networks, which is discussed in Chapter 6. This inconvenience is a result of an attempt to present the research results in a sequential order, having similar topics grouped, instead of a historical order that would cause a great deal of fragmentation and switching between different topics.

6. CONTROL OF THE NEUTRAL POINT INDUCTIVITY IN THE AUTOTRANSFORMER-BASED CURRENT INJECTION DEVICES

As shown in the previous section, the current injection device in Fig. 4-5 requires a ferromagnetic core with minimal volt-ampere rating, for the price of being followed by a parasitic inductance of the neutral point given by (4.74). It was suggested that the parasitic inductance may be utilized as a part of or instead of the inductor in the current injection network, and the volt-ampere rating in that case is given by (4.82). In the case where L_n is lower or equal to the inductance required by the current injection network, the device in Fig. 4-5 could be readily applied. However, experimental results show that actual values of L_n are frequently greater than needed, thus it would be convenient to have tools to provide L_n reduced. A method to reduce L_n is to place an air gap in the ferromagnetic core. This approach was tried, and the results indicated that placing the air gap greatly reduced L_n , but this effect was followed by significant reduction of L_m , given by (4.70), causing unacceptable reduction of the rectifier displacement power factor. Another approach to reduce L_n is proposed here, based on the fact that the current injection device built as a zigzag autotransformer with the turns ratio of 1:1, shown in Fig. 4-3, reduced L_n to zero. On the other hand, the current injection device obtained as a three-phase inductor can be treated as a special case of the current injection device based on the zigzag autotransformer, assuming the turns ratio 1:0. Based on these facts, it can be supposed that variation of the turns ratio of the zigzag autotransformer based current injection device might be a tool to control the inductance of the neutral point.

Let us consider the current injection device shown in Fig. 4-10. The device in Fig. 4-10 reduces to the device in Fig. 4-3 for $n = m$, and to the device in Fig. 4-5 for $n = 0$. Without making any assumptions about values of m and n , magnetomotive forces across the core limbs are

$$F_1 = ni_{X1} - mi_{X2}, \quad (4.88)$$

$$F_2 = ni_{X2} - mi_{X3}, \quad (4.89)$$

and

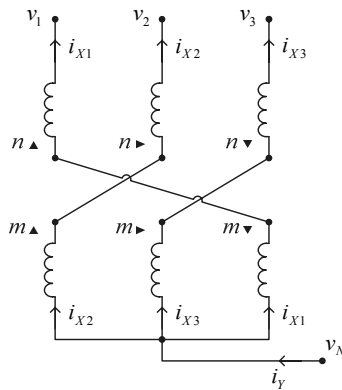


Figure 4-10. Current injection device based on an $n:m$ autotransformer.

$$F_3 = ni_{X3} - mi_{X1}. \quad (4.90)$$

Since the equivalent magnetic circuit for the device is presented in Fig. 4-7, the magnetomotive force across the core ends is

$$F_0 = \frac{R_{m0}}{R_m + 3R_{m0}} (F_1 + F_2 + F_3), \quad (4.91)$$

which is the same as given by (4.61), since the magnetic circuit is the same. In the same manner, magnetic fluxes of the core limbs are

$$\Phi_k = \frac{F_k - F_0}{R_m} \quad (4.92)$$

for $k \in \{1, 2, 3\}$.

Analyzing the magnetic circuit of Fig. 4-7, fluxes in the core limbs and the magnetomotive forces across the limbs can be mutually related, and the result can be presented in a matrix form as

$$\begin{bmatrix} \Phi_1 \\ \Phi_2 \\ \Phi_3 \end{bmatrix} = \begin{bmatrix} A_L & -A_M & -A_M \\ -A_M & A_L & -A_M \\ -A_M & -A_M & A_L \end{bmatrix} \begin{bmatrix} F_1 \\ F_2 \\ F_3 \end{bmatrix}, \quad (4.93)$$

where

$$A_L = \frac{1}{R_m} \frac{R_m + 2R_{m0}}{R_m + 3R_{m0}} \quad (4.94)$$

and

$$A_M = \frac{1}{R_m} \frac{R_{m0}}{R_m + 3R_{m0}}. \quad (4.95)$$

Rephrasing (4.88) to (4.90) in matrix form, the limb fluxes can be expressed in terms of the device currents as

$$\begin{bmatrix} \Phi_1 \\ \Phi_2 \\ \Phi_3 \end{bmatrix} = \begin{bmatrix} A_L & -A_M & -A_M \\ -A_M & A_L & -A_M \\ -A_M & -A_M & A_L \end{bmatrix} \begin{bmatrix} n & -m & 0 \\ 0 & n & -m \\ -m & 0 & n \end{bmatrix} \begin{bmatrix} i_{X1} \\ i_{X2} \\ i_{X3} \end{bmatrix}. \quad (4.96)$$

On the other hand, voltages across the device terminals are in terms of time derivatives of the limb fluxes expressed as

$$\begin{bmatrix} v_1 - v_N \\ v_2 - v_N \\ v_3 - v_N \end{bmatrix} = - \begin{bmatrix} n & 0 & -m \\ -m & n & 0 \\ 0 & -m & n \end{bmatrix} \frac{d}{dt} \begin{bmatrix} \Phi_1 \\ \Phi_2 \\ \Phi_3 \end{bmatrix}. \quad (4.97)$$

Finally, from (4.96) and (4.97), currents and voltages of the device are mutually related, and the element characteristic is obtained as

$$\begin{bmatrix} v_1 - v_N \\ v_2 - v_N \\ v_3 - v_N \end{bmatrix} = - \begin{bmatrix} L & -M & -M \\ -M & L & -M \\ -M & -M & L \end{bmatrix} \frac{d}{dt} \begin{bmatrix} i_{X1} \\ i_{X2} \\ i_{X3} \end{bmatrix}, \quad (4.98)$$

where

$$\begin{bmatrix} L & -M & -M \\ -M & L & -M \\ -M & -M & L \end{bmatrix} =$$

$$= \begin{bmatrix} n & 0 & -m \\ -m & n & 0 \\ 0 & -m & n \end{bmatrix} \begin{bmatrix} A_L & -A_M & -A_M \\ -A_M & A_L & -A_M \\ -A_M & -A_M & A_L \end{bmatrix} \begin{bmatrix} n & -m & 0 \\ 0 & n & -m \\ -m & 0 & n \end{bmatrix}. \quad (4.99)$$

Equating corresponding matrix elements on both sides of (4.99), inductances in the element characteristic of (4.98) are obtained as

$$L = A_L(m^2 + n^2) + 2A_Mmn \quad (4.100)$$

and

$$M = A_Lmn + A_M(m^2 - mn + n^2). \quad (4.101)$$

Applying the same analysis method as in Section 4.5, the magnetizing inductance of the device of Fig. 4-10 is obtained as

$$L_m = L + M = \frac{m^2 + n^2 + mn}{R_m}, \quad (4.102)$$

while the inductance of the neutral point is obtained as

$$L_n = \frac{L - 2M}{3} = \frac{(m-n)^2}{3(R_m + 3R_{m0})}. \quad (4.103)$$

Obviously, L_n can be controlled by the choice of m and n . For $n=m$ we obtain $L_n=0$ and $L_m=3n^2/R_m$, corresponding to the current injection device described in Section 4.3. On the other hand, for $n=0$ the value of L_n reduces to (4.74), corresponding to the device described in Section 4.5. Choosing the value of n somewhere in the range $0 < n < m$, the neutral point inductance can be reduced to any required value.

The design procedure for this type of current injection device is not straightforward. At first, a suitable core should be chosen, with the volt-ampere rating in a range from S_2 given by (4.59) to the value of S_1 given by (4.38). For the chosen core, parameters R_m and R_{m0} should be determined. They need to be determined experimentally, since they are not included in standard data sheets. Actually, it is sufficient to determine the value of $3(R_m + 3R_{m0})$, which can be done by only one impedance measurement having three test windings with the same number of turns placed on the core limbs. After the core parameters are determined, the

difference in the number of turns of the windings, defined as

$$p = m - n, \quad (4.104)$$

should be determined according to

$$p = \sqrt{3(R_m + 3R_{m0})L_n}. \quad (4.105)$$

The next task is to determine the number of turns m of the winding with the larger number of turns such that the core does not saturate. To determine the fluxes in the core limbs, it is convenient to analyze them as consisting of two components, a component at the line frequency caused by the phase voltages v_1 , v_2 , and v_3 , and a component at triple the line frequency caused by the injected current. Applying the superposition principle, the two components are computed separately, and then added to obtain fluxes in the core limbs.

To compute the flux components at the line frequency, let us consider the test circuit in Fig. 4-8, but applied to the current injection device in Fig. 4-10. To compute the first component of the fluxes, the current source i_Y should be turned off. In that case $v_N = 0$, and the fluxes are related to the phase voltages by

$$\begin{bmatrix} v_1 \\ v_2 \\ v_3 \end{bmatrix} = \begin{bmatrix} -n & 0 & m \\ m & -n & 0 \\ 0 & m & -n \end{bmatrix} \frac{d}{dt} \begin{bmatrix} \Phi_{1,1} \\ \Phi_{2,1} \\ \Phi_{3,1} \end{bmatrix}, \quad (4.106)$$

where $\Phi_{1,1}$, $\Phi_{2,1}$, and $\Phi_{3,1}$ are components of the limb fluxes at the line frequency. The matrix in (4.106) is nonsingular for $n \neq m$, and the time derivatives of the fluxes can be expressed in terms of the phase voltages. Waveforms of the fluxes in the core limbs are mutually shifted in phase for $2\pi/3$ and have the same maxima. Thus, it is enough to consider only one of the fluxes. The time derivative of the flux component in the first limb of the core is obtained from (4.106) as

$$\frac{d\Phi_{1,1}}{dt} = \frac{m\sqrt{3}\sin(\omega_0 t) - (m+2n)\cos(\omega_0 t)}{2(m^2 + mn + n^2)} V_m, \quad (4.107)$$

assuming phase voltages given by (2.1), (2.2), and (2.3).

To determine the components of the limb fluxes at triple the line frequency, let us set the voltage sources in the circuit in Fig. 4-8 to

$v_1 = v_2 = v_3 = 0$, and turn the current source i_Y on. According to (4.98), we obtain $i_{X1} = i_{X2} = i_{X3} = (1/3)i_Y$; thus fluxes in the core limbs are the same in this situation, without any phase shift. This results in

$$-v_N = m \frac{d\Phi_{1,3}}{dt} - n \frac{d\Phi_{1,3}}{dt}, \quad (4.108)$$

where $\Phi_{1,3}$ represents the component of the first limb flux at triple the line frequency. Substituting the actual value for v_N , given by (4.77), (4.108) transforms to

$$3\omega_0 L_n I_{Ym} \sin(3\omega_0 t) = a V_m \sin(3\omega_0 t) = (m - n) \frac{d\Phi_{1,3}}{dt}. \quad (4.109)$$

Thus, overall flux in the first limb is determined by

$$\frac{d\Phi_1}{dt} = V_m \left(\frac{m\sqrt{3} \sin(\omega_0 t) - (3m - 2p) \cos(\omega_0 t)}{2(3m^2 - 3mp + p^2)} + \frac{a}{p} \sin(3\omega_0 t) \right). \quad (4.110)$$

This results in the maximum of the limb flux given by

$$\Phi_{\max} = \frac{V_m}{\omega_0} g(m, p, a), \quad (4.111)$$

where

$$g(m, p, a) = \max \left(\frac{m\sqrt{3} \cos(\omega_0 t) + (3m - 2p) \sin(\omega_0 t)}{2(3m^2 - 3mp + p^2)} + \frac{a}{3p} \cos(3\omega_0 t) \right). \quad (4.112)$$

Since parameter a is determined by the current injection network design and is known prior to the design of the current injection device, and since parameter p is determined during the first phase of the current injection device design by (4.105), (4.111) and (4.112) are applied to determine m . It seems that the most convenient way to determine m is to create a short numeric procedure that computes the lowest value of m that satisfies

$$g(m, p, a) = \frac{\omega_0 \Phi_{limb \max}}{V_m}, \quad (4.113)$$

where $\Phi_{limb\ max}$ is taken from the core data sheet as the maximum of the flux in the core limb that does not saturate the core material.

Finally, actual volt-ampere rating of the core can be computed applying

$$S_4 = \frac{V_m I_{Y\ RMS}}{2\sqrt{2}} (2m - p) g(m, p, a), \quad (4.114)$$

and hopefully it fits the initial guess. However, it may happen that the windings for computed numbers of turns and required wire diameter cannot fit in the core window. This means that the initial guess about the core volt-ampere rating is too low. In that case, the procedure should be repeated with a larger core. Experience with the procedure is that it converges very fast, and that the most time-consuming part is the measurement of $3(R_m + 3R_{m0})$.

7. CURRENT INJECTION APPLYING WYE-WYE CONNECTED TRANSFORMER

In some cases, a transformer is applied at the rectifier input to adjust the rectifier input voltage to a required level. In these cases, the current injection can be provided directly, injecting the current to the neutral point of the transformer secondary. This approach is applied in [1], [2], [3], [4], [5], [13], and [15], where wye-wye connected transformers have been applied. In this section, the current injection in the secondary neutral point of the wye-wye connected transformer is analyzed to determine its suitability, limitations, and required volt-ampere rating of the transformer.

To begin, consider a transformer shown in Fig. 4-11, assuming that it is supplied by an undistorted balanced three-phase voltage system

$$v_p = \frac{n}{m} V_m \cos\left(\omega_0 t - (p-1)\frac{2\pi}{3}\right), \quad (4.115)$$

for $p \in \{1, 2, 3\}$. The transformer secondary is loaded by three phase currents i_{S1} , i_{S2} , and i_{S3} , being connected in four-wire fashion, enabling the flow of the injected current i_Y in the neutral conductor.

Magnetomotive forces applied on the core limbs are given by

$$F_k = ni_k - mi_{Sk}, \quad (4.116)$$

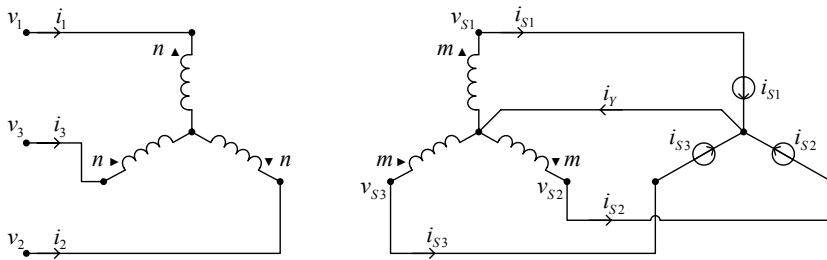


Figure 4-11. Current injection applying wye-wye transformer.

for $k \in \{1, 2, 3\}$. Now, let us take a crucial approximation that

$$R_{m0} \rightarrow \infty. \quad (4.117)$$

Consequences of this approximation have been discussed in Sections 4.5 and 4.6. In the case the approximation holds,

$$F_0 = \frac{1}{3}(F_1 + F_2 + F_3). \quad (4.118)$$

Taking another assumption,

$$R_m \rightarrow 0, \quad (4.119)$$

the requirement for finite fluxes in the core limbs results in

$$F_1 = F_2 = F_3 = F_0. \quad (4.120)$$

Thus, expanding (4.120) in three equations and substituting (4.118), magnetomotive forces should satisfy

$$\begin{bmatrix} 2 & -1 & -1 \\ -1 & 2 & -1 \\ -1 & -1 & 2 \end{bmatrix} \begin{bmatrix} F_1 \\ F_2 \\ F_3 \end{bmatrix} = \begin{bmatrix} 0 \\ 0 \\ 0 \end{bmatrix}, \quad (4.121)$$

which is a homogeneous system of linear equations expressed in a matrix form. Since the determinant of the system matrix is

$$\begin{vmatrix} 2 & -1 & -1 \\ -1 & 2 & -1 \\ -1 & -1 & 2 \end{vmatrix} = 0, \quad (4.122)$$

the system has a nontrivial solution. Expanding the magnetomotive forces to the level of constituent currents according to (4.116), the homogeneous system of (4.121) is transformed to

$$\begin{bmatrix} 2n & -n & -n \\ -n & 2n & -n \\ -n & -n & 2n \end{bmatrix} \begin{bmatrix} i_1 \\ i_2 \\ i_3 \end{bmatrix} = \begin{bmatrix} 2m & -m & -m \\ -m & 2m & -m \\ -m & -m & 2m \end{bmatrix} \begin{bmatrix} i_{S1} \\ i_{S2} \\ i_{S3} \end{bmatrix}, \quad (4.123)$$

or

$$\begin{bmatrix} 2 & -1 & -1 \\ -1 & 2 & -1 \\ -1 & -1 & 2 \end{bmatrix} \begin{bmatrix} i_1 \\ i_2 \\ i_3 \end{bmatrix} = \frac{m}{n} \begin{bmatrix} 2 & -1 & -1 \\ -1 & 2 & -1 \\ -1 & -1 & 2 \end{bmatrix} \begin{bmatrix} i_{S1} \\ i_{S2} \\ i_{S3} \end{bmatrix}. \quad (4.124)$$

Since the system matrix of (4.124) is singular according to (4.122), a unique solution of (4.124) does not exist. On the other hand, taking an additional constraint

$$i_1 + i_2 + i_3 = 0, \quad (4.125)$$

imposed by the three-wire connection at the transformer primary, a unique solution for the transformer input currents is obtained as

$$\begin{bmatrix} i_1 \\ i_2 \\ i_3 \end{bmatrix} = \frac{m}{3n} \begin{bmatrix} 2 & -1 & -1 \\ -1 & 2 & -1 \\ -1 & -1 & 2 \end{bmatrix} \begin{bmatrix} i_{S1} \\ i_{S2} \\ i_{S3} \end{bmatrix}. \quad (4.126)$$

The solution (4.126) could be rephrased to

$$i_k = \frac{m}{n} \left(i_{Sk} - \frac{1}{3} (i_{S1} + i_{S2} + i_{S3}) \right), \quad (4.127)$$

for $k \in \{1, 2, 3\}$. This shows that the same transformation of i_{S1} , i_{S2} , and i_{S3} is performed as if a current injection device has been applied.

To illustrate the transformer operation and to compute its volt-ampere rating, let us assume the transformer secondary currents i_{S1} , i_{S2} , and i_{S3} that correspond to the optimal third-harmonic current injection, which is discussed in the next chapter. In that case,

$$i_{Sk} = I_{OUT} \left(\left(1 + \frac{3}{4} \cos(3\omega_0 t) \right) d_{2k-1}(\omega_0 t) - \left(1 - \frac{3}{4} \cos(3\omega_0 t) \right) d_{2k}(\omega_0 t) \right) \quad (4.128)$$

for $k \in \{1, 2, 3\}$, where the diode state functions $d_n(\omega_0 t)$ are defined in Chapter 2, and shown in Fig. 2-5. Waveforms of i_{S1} , i_{S2} , and i_{S3} , defined by (4.128), are shown in Fig. 4-12. The RMS value of the currents i_{S1} , i_{S2} , and i_{S3} is

$$I_{S_{RMS}} = \frac{\sqrt{123}}{12} I_{OUT}. \quad (4.129)$$

Waveforms of the transformer primary currents, i_1 , i_2 , and i_3 are computed applying (4.126), and the resulting waveforms are presented in Fig. 4-13. The RMS value of the currents shown in Fig. 4-13 is

$$I_{P_{RMS}} = \frac{\sqrt{105}}{12} \frac{m}{n} I_{OUT}. \quad (4.130)$$

Finally, applying (4.19), the volt-ampere rating of the transformer is obtained as

$$S_{YY} = \frac{\sqrt{105} + \sqrt{123}}{8\sqrt{2}} V_m I_{OUT}. \quad (4.131)$$

Since the rectifier output power is

$$P_{OUT} = \frac{105\sqrt{3}}{32\pi} V_m I_{OUT}, \quad (4.132)$$

which is derived in Chapter 5, the transformer volt-ampere rating is expressed in terms of the rectifier output power as

$$\frac{S_{YY}}{P_{OUT}} = \frac{2\pi}{105} (\sqrt{82} + \sqrt{70}) \approx 104.25\%. \quad (4.133)$$

Next, let us compare the volt-ampere rating given by (4.133) to the volt-ampere rating of a transformer loaded with a rectifier without the current injection based shaping of the input currents, having the same output voltage and the output power as the previously considered current injection based rectifier. According to (2.22), RMS values of the secondary phase currents are

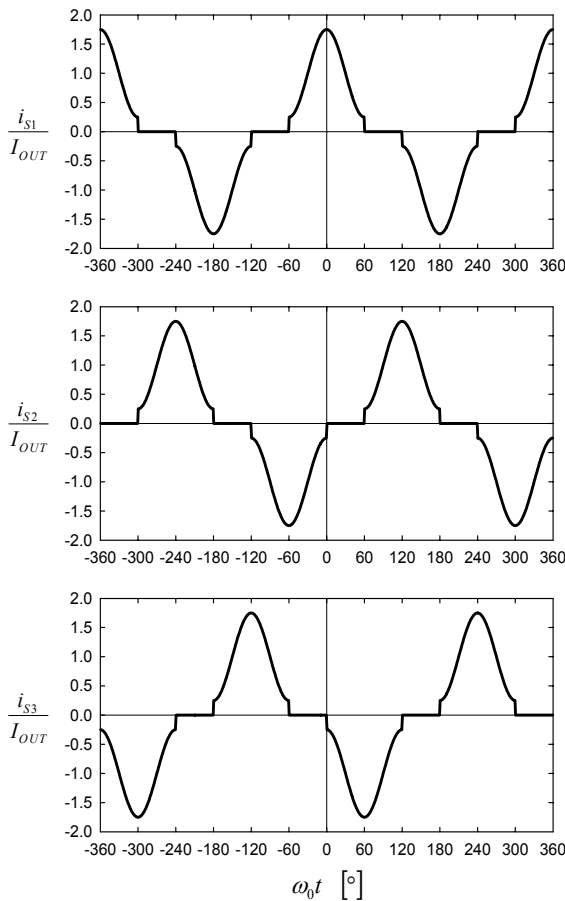


Figure 4-12. Waveforms of the transformer secondary currents, the optimal third-harmonic current injection.

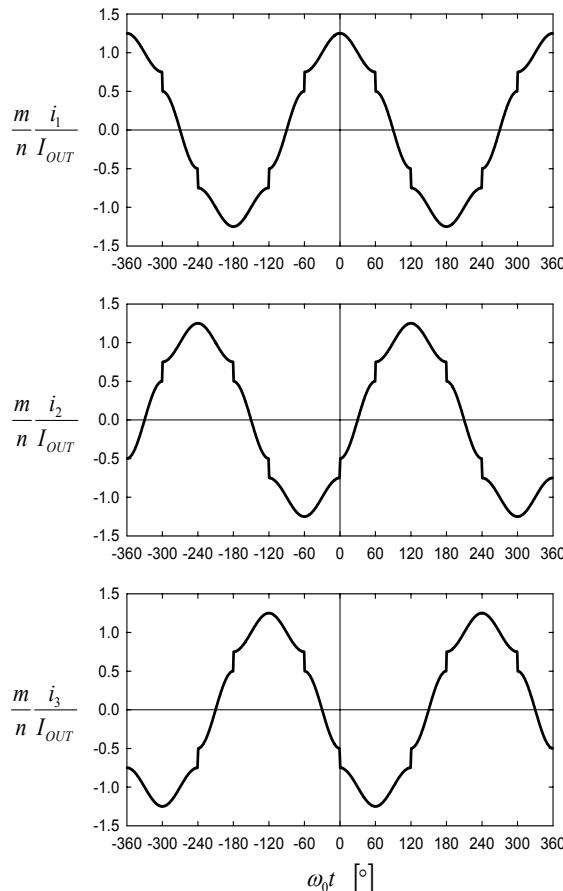


Figure 4-13. Waveforms of the transformer primary (i.e., input) currents, the optimal third-harmonic current injection, wye-wye transformer.

$$I_{S RMS} = \frac{\sqrt{6}}{3} I_{OUT}, \quad (4.134)$$

while the RMS values of the primary currents are

$$I_{P RMS} = \frac{\sqrt{6}}{3} \frac{m}{n} I_{OUT}. \quad (4.135)$$

Thus, applying (4.19), the transformer volt-ampere rating is

$$S_{T0} = \sqrt{3} V_m I_{OUT}. \quad (4.136)$$

Since the rectifier output power is given by (2.23) as

$$P_{OUT} = \frac{3\sqrt{3}}{\pi} V_m I_{OUT}, \quad (4.137)$$

the transformer volt-ampere rating is expressed in terms of the rectifier output power as

$$\frac{S_{T0}}{P_{OUT}} = \frac{\pi}{3} \approx 104.72\%. \quad (4.138)$$

This value is negligibly higher than the value given by (4.133), meaning that the current injection at the transformer secondary neutral point is provided at no cost, since the transformer does not have to be derated to provide the current injection. However, RMS values of the currents in the transformer windings are different in these two cases, and this is a fact that the designer should be aware of. The ratio of the volt-ampere rating of the transformer for the rectifier that applies current injection and the volt-ampere rating of the rectifier that does not apply the current injection is

$$\frac{S_{YY}}{S_{T0}} = \frac{2}{35} (\sqrt{82} + \sqrt{70}) \approx 99.55\%. \quad (4.139)$$

This fact, that the volt-ampere rating of the input transformer is lower if the current injection is applied than if it is not, opens an application area of the current injection method in cases when a transformer is required at the rectifier input, since the most expensive part of the current injection system, the current injection device, is not required.

The volt-ampere rating of the transformer is dependent on the waveforms of the voltages and the currents. Besides the previously analyzed case where the waveforms of the secondary currents specified by (4.128) result in the input currents corresponding to the optimal third-harmonic current injection, let us also analyze the case of the optimal current injection where higher order harmonics are included in the injected current in order to provide purely sinusoidal waveforms of the input currents. This type of current injection is analyzed in detail in Chapter 7.

The waveforms of the transformer secondary currents corresponding to the optimal current injection are shown in Fig. 4-14, having the RMS value

$$I_{S\text{ RMS}} = I_m \sqrt{1 - \frac{3\sqrt{3}}{4\pi}}. \quad (4.140)$$

Waveforms of the secondary currents, depicted in Fig. 4-14, result in the input currents

$$i_k = \frac{m}{n} I_m \cos\left(\omega_0 t - (k-1)\frac{2\pi}{3}\right), \quad (4.141)$$

for $k \in \{1, 2, 3\}$. RMS values of the primary currents are

$$I_{P\text{ RMS}} = \frac{m}{n\sqrt{2}} I_m, \quad (4.142)$$

thus, according to (4.19) the volt-ampere rating of the transformer is

$$S_{YY} = \frac{3}{4} \left(1 + \sqrt{2 - \frac{3\sqrt{3}}{2\pi}} \right) V_m I_m. \quad (4.143)$$

Assuming that the rectifier output power is equal to the input power, the output power is

$$P_{OUT} = \frac{3}{2} V_m I_m, \quad (4.144)$$

and the transformer volt-ampere rating expressed in terms of the rectifier output power is

$$\frac{S_{YY}}{P_{OUT}} = \frac{1}{2} \left(1 + \sqrt{2 - \frac{3\sqrt{3}}{2\pi}} \right) \approx 104.15\%, \quad (4.145)$$

which is even lower than the value given by (4.133), and thus lower than the value of (4.138). The ratio of the transformer volt-ampere rating in the case the optimal current injection is applied to the case that current injection is not applied is

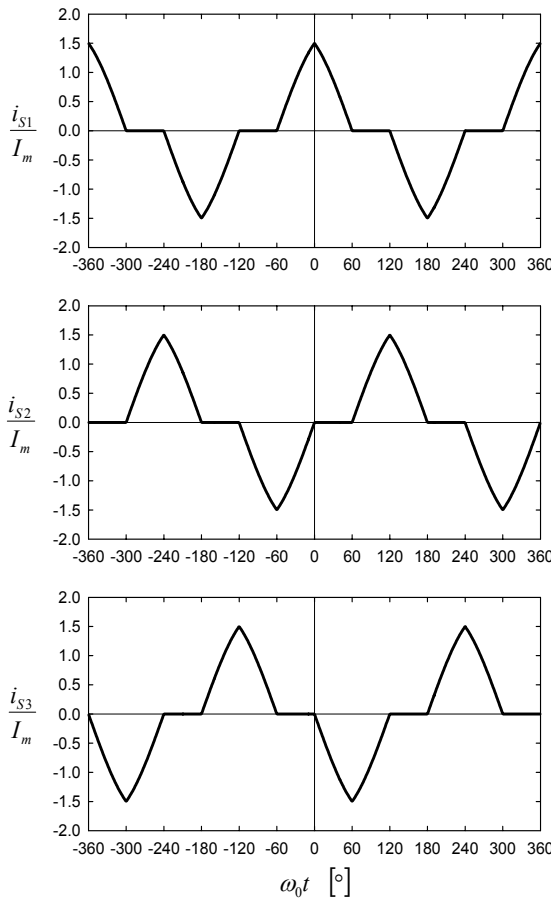


Figure 4-14. Waveforms of the transformer secondary currents, the optimal current injection.

$$\frac{S_{YY}}{S_{T0}} = \frac{3}{2\pi} \left(1 + \sqrt{2 - \frac{3\sqrt{3}}{2\pi}} \right) \approx 99.46\%. \quad (4.146)$$

Thus, the current injection device can be avoided at no cost if a transformer is applied at the rectifier input, again.

8. CURRENT INJECTION APPLYING DELTA-WYE CONNECTED TRANSFORMER

The current injection device analyzed in the previous section suffers from the same drawback as the current injection device analyzed in Section 4.5, which is the parasitic inductance of the neutral point. This effect is caused by a finite value of the ferromagnetic core reluctance R_{m0} , indicated in Fig. 4-6. To avoid this drawback, application of a delta-wye transformer is discussed here. This method of current injection can even be achieved applying three single-phase transformers. Previously, the current injection with delta-wye transformer has been applied in [46].

Let us consider the delta-wye transformer arrangement shown in Fig. 4-15. To provide the same amplitudes of the secondary voltages as achieved by the transformer analyzed in the previous section, the turns ratio is chosen to be $n\sqrt{3} : m$. According to the circuit diagram in Fig. 4-15, the rectifier input currents are given by

$$\begin{bmatrix} i_1 \\ i_2 \\ i_3 \end{bmatrix} = \frac{m}{n\sqrt{3}} \begin{bmatrix} 1 & -1 & 0 \\ 0 & 1 & -1 \\ -1 & 0 & 1 \end{bmatrix} \begin{bmatrix} i_{S1} \\ i_{S2} \\ i_{S3} \end{bmatrix}, \quad (4.147)$$

while the voltages at the transformer secondary are

$$\begin{bmatrix} v_{S1} \\ v_{S2} \\ v_{S3} \end{bmatrix} = \frac{m}{n\sqrt{3}} \begin{bmatrix} 1 & 0 & -1 \\ -1 & 1 & 0 \\ 0 & -1 & 1 \end{bmatrix} \begin{bmatrix} v_1 \\ v_2 \\ v_3 \end{bmatrix}. \quad (4.148)$$

Thus, in comparison to the previously analyzed case of the wye-wye transformer, the secondary voltages are delayed in phase for 30° , but retain the same amplitudes. This implies that the secondary currents will be delayed for 30° in phase in comparison to the wye-wye transformer case, but their RMS values will not be affected by this phase shift.

First, let us analyze the case of the optimal third-harmonic current injection. In that case, RMS values of the secondary currents are

$$I_{S\text{ RMS}} = \frac{\sqrt{123}}{12} I_{OUT}. \quad (4.149)$$

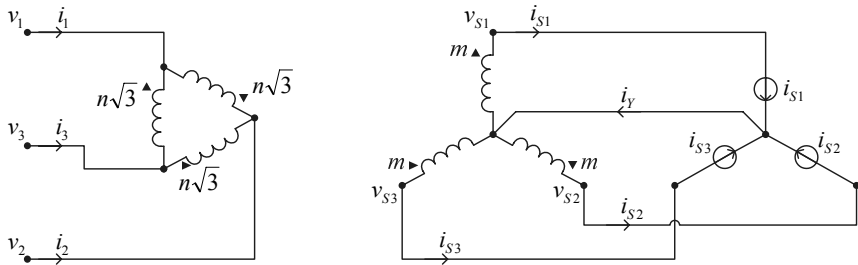


Figure 4-15. Current injection applying delta-wye transformer.

In the case of the delta-wye transformer, currents in the primary windings have the waveforms proportional to the currents of the secondary windings, thus their RMS values are

$$I_{P\text{ RMS}} = \frac{m}{n\sqrt{3}} \frac{\sqrt{123}}{12} I_{OUT}. \quad (4.150)$$

After the RMS values of the voltages and currents of the transformer windings are known, and since the voltage waveforms are sinusoidal, the transformer volt-ampere rating can be directly computed, which results in

$$S_{DY} = \frac{\sqrt{123}}{4\sqrt{2}} V_m I_{OUT}. \quad (4.151)$$

Since the output power of the rectifier is given by (4.132), the volt-ampere rating of the delta-wye transformer normalized to the rectifier output power is

$$\frac{S_{DY}}{P_{OUT}} = \frac{4\pi\sqrt{82}}{105} \approx 108.37\%, \quad (4.152)$$

which is somewhat higher than the value of (4.133) for the case of the wye-wye transformer, and higher than the value of (4.138) for the case in which the current injection is not applied. However, this increase in the volt-ampere rating is not significant, and it is well justified by the fact that parasitic inductance of the secondary neutral point and the leakage flux are completely removed.

The ratio of the delta-wye transformer volt-ampere rating and the transformer volt-ampere rating in the case the current injection is not applied

results in

$$\frac{S_{DY}}{S_{T_0}} = \frac{4\sqrt{82}}{35} \approx 103.49\%, \quad (4.153)$$

which illustrates that the current injection is provided with negligible increase of the transformer volt-ampere rating of about 3.5%, without any parasitic effects.

Transformation that maps the transformer secondary currents to the input currents, given by (4.147), for the delta-wye transformer is different than the transformation corresponding to the wye-wye transformer, given by (4.126). This affects the input current waveforms, and the waveforms obtained for the optimal third-harmonic current injection are presented in Fig. 4-16. The waveforms are obtained applying the secondary currents given by (4.128), depicted in Fig. 4-12, but delayed in phase for 30° according to the phase shift of the secondary voltages. The input current waveforms of Fig. 4-16 are different than the waveforms of Fig. 4-13 that correspond to the application of a wye-wye transformer or any other current injection device. However, values of the input current THD are the same in both of cases. This unexpected result can be explained in the frequency domain, where a detailed analysis shows that both of transformer configurations remove the zero-sequence components of the secondary currents. For positive-sequence components of the secondary currents, the wye-wye transformer does not introduce any phase shift, while the delta-wye transformer advances them for 30° in phase. On the other hand, the negative-sequence components of the secondary currents are delayed in phase for 30° by the delta-wye transformer, while the wye-wye transformer did not introduce any phase shift, again. However, amplitudes of the harmonic components of the input currents are the same in both of cases. Since a THD value is affected only by amplitudes of the spectral components, the THD values of the input currents are the same in both of cases, regardless of the phase shifting introduced by the delta-wye transformer.

In the case of the optimal current injection, applying the secondary currents shown in Fig. 4-14, but delayed in phase for 30° according to the phase delay of the secondary voltages in the delta-wye transformer case, RMS values of the secondary currents are

$$I_{S\text{ RMS}} = I_m \sqrt{1 - \frac{3\sqrt{3}}{4\pi}}, \quad (4.154)$$

while RMS values of the currents in the primary windings are

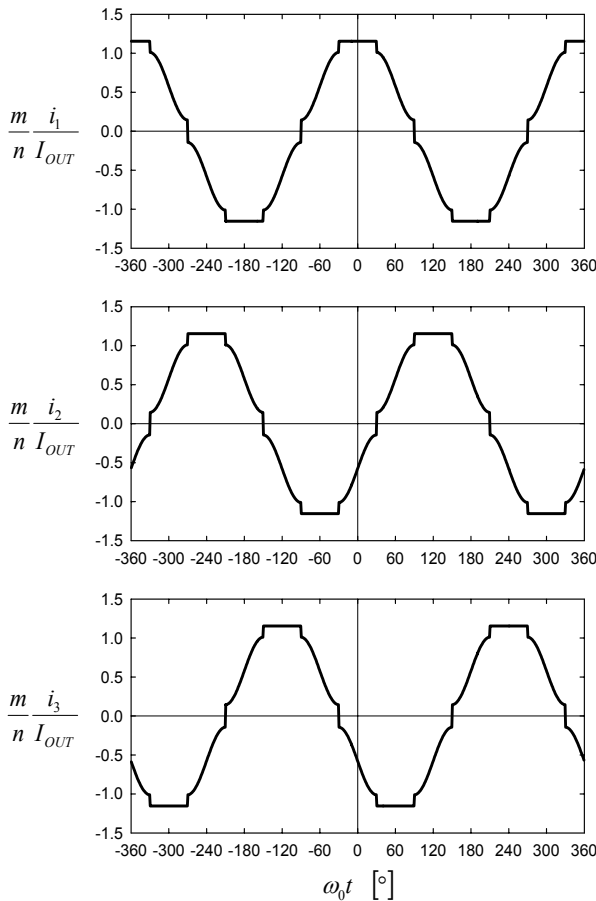


Figure 4-16. Waveforms of the input currents, the optimal third-harmonic current injection, delta-wye transformer.

$$I_{P\text{ RMS}} = \frac{m}{n\sqrt{3}} I_m \sqrt{1 - \frac{3\sqrt{3}}{4\pi}}, \quad (4.155)$$

which is the value of (4.154) scaled according to the transformer turns ratio. Voltages at the transformer windings are sinusoidal, with the RMS values of

$$V_{S\text{ RMS}} = \frac{V_m}{\sqrt{2}} \quad (4.156)$$

and

$$V_{P\text{ RMS}} = \frac{n\sqrt{3}}{m} \frac{V_m}{\sqrt{2}}. \quad (4.157)$$

Thus, applying (4.19) to compute the volt-ampere rating of the delta-wye transformer in this case,

$$S_{DY} = \frac{3}{\sqrt{2}} \sqrt{1 - \frac{3\sqrt{3}}{4\pi}} V_m I_m \quad (4.158)$$

is obtained. Since the input currents are purely sinusoidal, the output power of the rectifier is

$$P_{OUT} = \frac{3}{2} V_m I_m, \quad (4.159)$$

which is obtained as the input power, neglecting losses in the rectifier. Thus, the ratio of the transformer volt-ampere rating and the rectifier output power is

$$\frac{S_{DY}}{P_{OUT}} = \sqrt{2 - \frac{3\sqrt{3}}{2\pi}} \approx 108.30\%. \quad (4.160)$$

Again, the result is somewhat higher than for the wye-wye transformer. Compared to the transformer volt-ampere rating if the current injection is not applied, the volt-ampere rating of the delta-wye transformer is

$$\frac{S_{DY}}{S_{T_0}} = \frac{3}{\pi} \sqrt{2 - \frac{3\sqrt{3}}{2\pi}} \approx 103.42\%. \quad (4.161)$$

Thus, current injection is provided with a negligible increase of the transformer volt-ampere rating, while leakage flux and parasitic inductance of the secondary neutral point are avoided.

Comparing wye-wye and delta-wye transformer configurations applied in the rectifiers with current injection, it can be concluded that the delta-wye transformer requires somewhat higher volt-ampere rating of about 4%, but has the advantage that the stray flux is avoided, resulting in negligible inductance of the transformer secondary neutral point.

Chapter 5

THE OPTIMAL THIRD-HARMONIC CURRENT INJECTION

In this chapter, we focus on the third-harmonic current injection, and optimal amplitude and phase of the injected current are derived in order to minimize the input current total harmonic distortion (THD). The results systematized in this chapter were originally presented in [24] and [29].

The circuit being analyzed is shown in Fig. 5-1. Besides the voltage sources, the three-phase diode bridge, and the load, the circuit contains the current injection device, discussed in detail in Chapter 4, and the current injection network. The current injection network is represented by two current sources in the circuit diagram of Fig. 5-1, i_{IA} and i_{IB} .

Voltage v_A at the positive output terminal of the diode bridge is given by (2.5) and (2.7), and it is expanded in the Fourier series as

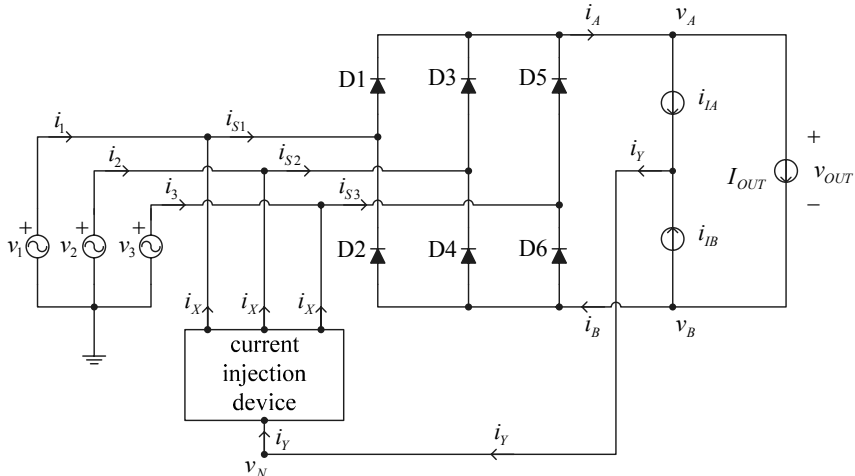


Figure 5-1. Equivalent circuit of the rectifier.

$$\begin{aligned} v_A &= \frac{3\sqrt{3}}{\pi} V_m \left(\frac{1}{2} + \sum_{n=1}^{+\infty} \frac{(-1)^{n+1}}{9n^2 - 1} \cos(3n\omega_0 t) \right) \\ &= V_{A,0} + \sum_{n=1}^{+\infty} V_{A,n} \cos(3n\omega_0 t) = V_{A,0} + \sum_{n=1}^{+\infty} v_{A,n}(\omega_0 t), \end{aligned} \quad (5.1)$$

where $V_{A,0}$ is the DC component of v_A , $V_{A,n}$ is the amplitude of the n th harmonic of v_A , and $v_{A,n}$ is the instantaneous value of the n th harmonic component of v_A . In the same manner, the voltage of the negative output terminal of the rectifier is expanded as

$$\begin{aligned} v_B &= \frac{3\sqrt{3}}{\pi} V_m \left(-\frac{1}{2} + \sum_{n=1}^{+\infty} \frac{1}{9n^2 - 1} \cos(3n\omega_0 t) \right) \\ &= V_{B,0} + \sum_{n=1}^{+\infty} V_{B,n} \cos(3n\omega_0 t) = V_{B,0} + \sum_{n=1}^{+\infty} v_{B,n}(\omega_0 t), \end{aligned} \quad (5.2)$$

applying the same notation as for v_A . It is important to note here that spectral components of v_A and v_B at odd triples of the line frequency are the same, having same amplitudes and phases,

$$V_{A,2k-1} = V_{B,2k-1} = \frac{3\sqrt{3}}{\pi} \frac{1}{9(2k-1)^2 - 1} V_m. \quad (5.3)$$

On the other hand, spectral components of v_A and v_B at even triples of the line frequency have the same amplitudes, but the opposite phases,

$$V_{A,2k} = -V_{B,2k} = -\frac{3\sqrt{3}}{\pi} \frac{1}{9(2k)^2 - 1} V_m. \quad (5.4)$$

These properties will be helpful in the analysis of the current injection network behavior for higher order harmonics, discussed in Chapter 6.

The current injection device is assumed to be characterized by

$$i_X = \frac{1}{3} i_Y \quad (5.5)$$

and

$$v_N = \frac{1}{3}(v_1 + v_2 + v_3) = 0. \quad (5.6)$$

Now, let us assume that currents i_{IA} and i_{IB} of the current injection network have the same waveform, containing only a spectral component located at the triple of the line frequency,

$$i_{IA} = i_{IB} = kI_{OUT} \cos(3\omega_0 t - \varphi). \quad (5.7)$$

Current i_A that loads the positive terminal of the rectifier diode bridge is given by

$$i_A = I_{OUT} + i_{IA}, \quad (5.8)$$

while current i_B that loads the negative output terminal is

$$i_B = I_{OUT} - i_{IB}. \quad (5.9)$$

In the analysis that follows, a continuous conduction mode of the rectifier bridge is assumed, requiring $i_A > 0$ and $i_B > 0$ during the whole period, which is achieved if

$$|k| < 1. \quad (5.10)$$

Current i_Y at the output of the current injection network is given by

$$i_Y = i_{IA} + i_{IB}, \quad (5.11)$$

according to Kirchhoff's current law.

Finally, current i_l at the first of the rectifier phases is given by

$$i_l = d_1 i_A - d_2 i_B - i_X \quad (5.12)$$

where the diode state functions d_1 and d_2 are as defined in Chapter 2, having the waveforms depicted in Fig. 2-5. The other two rectifier input currents have the same waveform as i_l , but delayed in phase for $2\pi/3$ in the case of i_2 , and for $4\pi/3$ in the case of i_3 . During one line period, for $-120^\circ < \omega_0 t < 240^\circ$, the input current i_l could be expressed as

$$\frac{i_1}{I_{OUT}} = \begin{cases} 1 + \frac{1}{3}k \cos(3\omega_0 t - \varphi) & \text{for } -60^\circ < \omega_0 t < 60^\circ \\ -\frac{2}{3}k \cos(3\omega_0 t - \varphi) & \text{for } 60^\circ < |\omega_0 t| < 120^\circ \\ -1 + \frac{1}{3}k \cos(3\omega_0 t - \varphi) & \text{for } 120^\circ < \omega_0 t < 240^\circ, \end{cases} \quad (5.13)$$

according to (5.7), (5.12), and Table 2-1. The waveform specified by (5.13) is for $k = 2/3$ and $\varphi = 30^\circ$ depicted in Fig. 5-2, in order to illustrate effects of current injection.

The next problem is to determine the THD of the waveform specified by (5.13) in an analytical form. First, let us compute the RMS value of the waveform, which results in

$$\frac{I_{RMS}}{I_{OUT}} = \frac{1}{3} \sqrt{k^2 + 6}. \quad (5.14)$$

Next, the RMS value of the fundamental harmonic of the waveform is obtained as

$$\frac{I_{1RMS}}{I_{OUT}} = \frac{1}{4\pi} \sqrt{\frac{3}{2} \left(k^2 (9 - 8(\cos \varphi)^2) + 16k \cos \varphi + 64 \right)}. \quad (5.15)$$

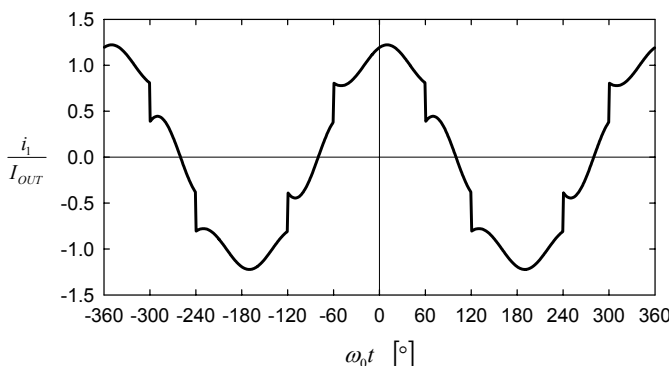


Figure 5-2. Waveform of the input current for $k = 2/3$ and $\varphi = 30^\circ$.

Phase displacement of the first harmonic of i_l in comparison to v_l is obtained as

$$\gamma_1 = -\arctan \frac{3k \sin \varphi}{8 + k \cos \varphi}. \quad (5.16)$$

Having the RMS values of the waveform and of its fundamental harmonic, the THD is computed according to

$$THD(k, \varphi) = \frac{\sqrt{I_{RMS}^2 - I_{1RMS}^2}}{I_{1RMS}}. \quad (5.17)$$

To minimize the THD, at first consider that φ is fixed, and equate the partial derivative of the THD with respect to k to zero,

$$\frac{\partial THD(k, \varphi)}{\partial k} = 0. \quad (5.18)$$

Solving (5.18), the optimal value of the injected current amplitude for a prespecified phase displacement φ of the injected current is obtained as

$$k_{opt}(\varphi) = \frac{48 \cos \varphi}{\sqrt{576(\cos \varphi)^4 + 624(\cos \varphi)^2 + 25 + 24(\cos \varphi)^2 + 5}}. \quad (5.19)$$

Dependence of k_{opt} on the phase displacement φ of the injected current is depicted in Fig. 5-3. The entire curve of the diagram in Fig. 5-3 is within the continuous conduction mode limits, $|k| < 1$; thus the assumption of the continuous conduction mode of the rectifier operation is valid. For $\varphi = \pm 90^\circ$ the optimal amplitude of the injected current is equal to zero; hence for these phase displacements of the injected current, the current injection cannot provide improvement of the input current THD. For $-180^\circ < \varphi < -90^\circ$ and for $90^\circ < \varphi < 180^\circ$ the optimal amplitudes of the injected current are negative, while for the phase angle range of $-90^\circ < \varphi < 90^\circ$ the optimal amplitudes of the injected current are positive.

In the case where the amplitude of the injected current has the optimal value specified by (5.19), the THD of the input current becomes only a function of the phase displacement of the injected current, φ ,

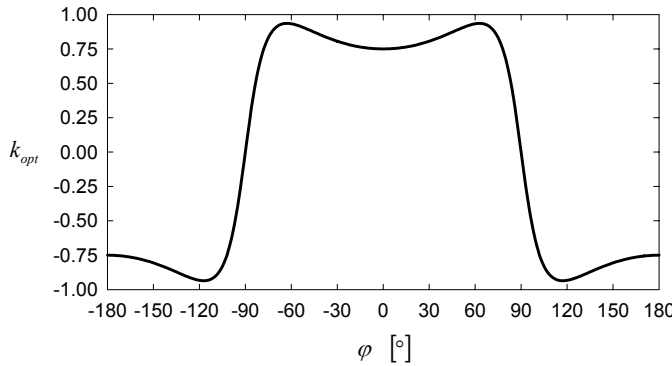


Figure 5-3. Optimal value of k as a function of φ . © [1999] IEEE.

$$THD(k_{opt}(\varphi), \varphi) = \frac{\sqrt{6(4\pi^2 - 45)(\cos \varphi)^2 + 5\pi^2 - 45 + (\pi^2 - 9)\sqrt{576(\cos \varphi)^4 + 624(\cos \varphi)^2 + 25}}}{3\sqrt{\sqrt{576(\cos \varphi)^4 + 624(\cos \varphi)^2 + 25} + 30(\cos \varphi)^2 + 5}}. \quad (5.20)$$

Dependence of the minimum of the input current THD on the phase displacement of the injected current is depicted in Fig. 5-4. For $k = k_{opt}(\varphi)$, the THD becomes a function of only one variable, φ , having the minimum at $\varphi = 0$. In that case,

$$k_{OPT} = k_{opt}(0) = \frac{3}{4} \quad (5.21)$$

and the corresponding value of the THD is

$$THD_{min} = THD\left(\frac{3}{4}, 0\right) = \sqrt{\frac{32\pi^2}{315} - 1} \approx 5.12\%. \quad (5.22)$$

This case, when $\varphi = 0$ and $k = 3/4$, is the optimal third-harmonic current injection that provides the minimum of the input current THD.

On the other hand, for $\varphi = \pm 90^\circ$, the optimal amplitude of the injected current is equal to zero, and the corresponding value of the THD is

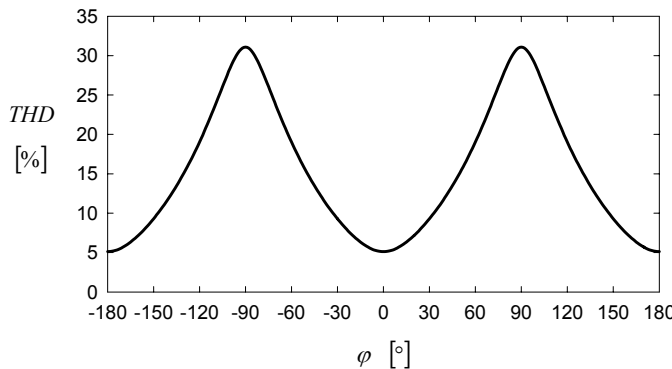


Figure 5-4. Minimum of the THD as a function of φ . © [1999] IEEE.

$$THD(0,0) = \frac{1}{3}\sqrt{\pi^2 - 9} \approx 31.08\%, \quad (5.23)$$

which is the same as (2.30).

The next issue to be discussed is the power taken by the current injection network. The harmonic components of v_A and v_B at the triple of the line frequency are the same, equal to

$$v_{A,3} = v_{B,3} = \frac{3\sqrt{3}}{8\pi} V_m \cos(3\omega_0 t). \quad (5.24)$$

Thus, the power taken by the current injection network from the diode bridge output terminals is

$$P_{INJ} = \frac{3\sqrt{3}}{8\pi} V_m I_{OUT} k \cos \varphi. \quad (5.25)$$

Since $v_N = 0$, this power cannot be restored at the current injection network output, and it has to be dissipated inside the current injection network. An alternative method is to apply the resistance emulation technique and to restore this power at an additional port of the current injection network, which is connected to the rectifier output, sometimes in series with the load (current loaded resistance emulator) and sometimes in parallel with the load (voltage loaded resistance emulator). These issues are discussed in detail in Chapters 10 and 11. In the case $\varphi = \pm 90^\circ$, the current injection network does

not take any power from the diode bridge output terminals, but in these cases the input current THD cannot be improved by applying current injection.

The rectifier in Fig. 5-1 provides the output power

$$P_{OUT} = V_{OUT} I_{OUT} = \frac{3\sqrt{3}}{\pi} V_m I_{OUT}. \quad (5.26)$$

The input power of the rectifier is the sum of the output power and the power taken by the current injection network,

$$P_{IN} = P_{OUT} + P_{INJ} = \frac{3\sqrt{3}}{\pi} \left(1 + \frac{k}{8} \cos \varphi \right) V_m I_{OUT}, \quad (5.27)$$

since losses in the diode bridge are neglected.

The rectifier power factor is defined as

$$PF = \frac{P_{IN}}{S_{IN}}, \quad (5.28)$$

where S_{IN} is the apparent power at the rectifier input, given by

$$S_{IN} = 3 \frac{V_m}{\sqrt{2}} \frac{I_{OUT}}{3} \sqrt{k^2 + 6}. \quad (5.29)$$

Finally, the rectifier power factor is

$$PF = \frac{3\sqrt{6}(8 + k \cos \varphi)}{8\pi\sqrt{6 + k^2}}. \quad (5.30)$$

Dependence of the rectifier power factor on phase displacement of the injected current is depicted in Fig. 5-5 for $k = k_{opt}(\varphi)$.

The displacement power factor is defined as

$$DPF = \cos \gamma_1, \quad (5.31)$$

and for the phase displacement of the input current fundamental harmonic given by (5.16), the dependence of the displacement power factor on φ is shown in Fig. 5-6. The displacement power factor is equal to one for $\varphi = 0^\circ$, for $\varphi = \pm 90^\circ$, and for $\varphi = \pm 180^\circ$, which is the same as $\varphi = 0^\circ$ since $k_{opt}(0) = -k_{opt}(\pm 180^\circ)$. The case $\varphi = \pm 90^\circ$ corresponds to the diode bridge rectifier without the current injection, analyzed in Chapter 2.

Assuming that the power taken by the current injection network is dissipated, the rectifier efficiency is equal to

$$\eta = \frac{P_{OUT}}{P_{OUT} + P_{INJ}}. \quad (5.32)$$

Substituting (5.25) and (5.26) in (5.32), the efficiency is obtained as

$$\eta(k, \varphi) = \frac{8}{8 + k \cos \varphi} \quad (5.33)$$

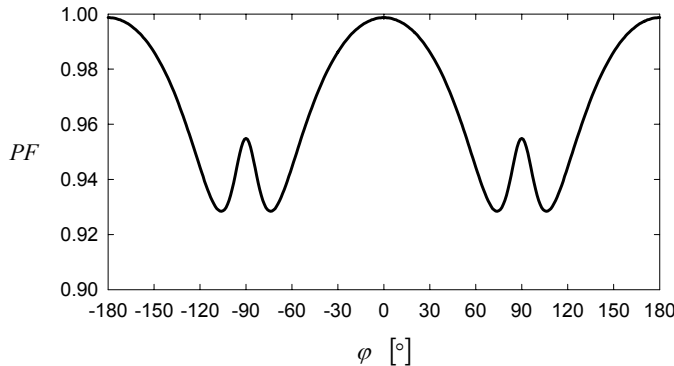


Figure 5-5. Power factor as a function of φ .

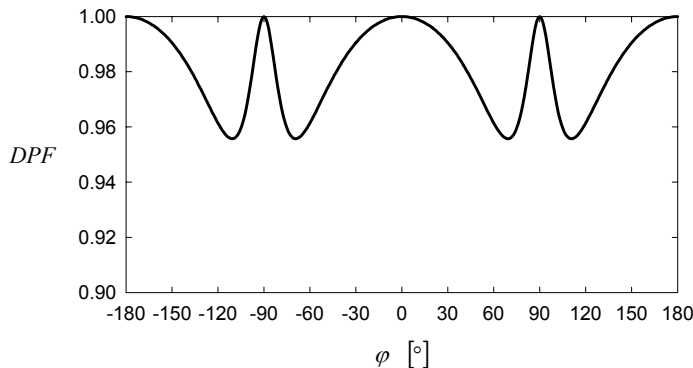


Figure 5-6. Displacement power factor as a function of φ . © [1999] IEEE.

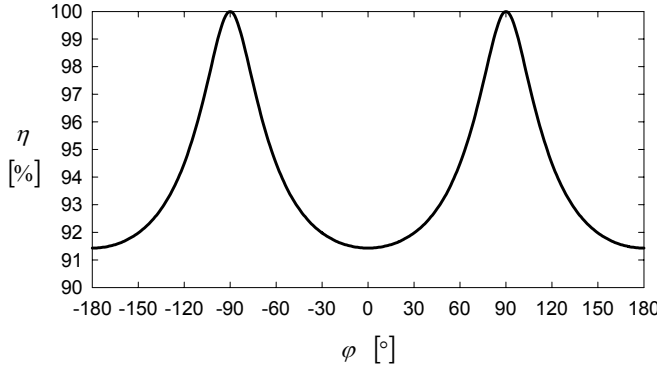


Figure 5-7. The rectifier efficiency as a function of φ . © [1999] IEEE.

for any value of φ and any k in the range $|k| < 1$ that guarantees continuous conduction mode of the rectifier. In a special case that $k = k_{opt}(\varphi)$, the rectifier efficiency becomes only a function of the injected current phase displacement, and it is given by

$$\eta(\varphi) = \eta(k_{opt}(\varphi), \varphi) = \frac{\sqrt{576(\cos \varphi)^4 + 624(\cos \varphi)^2 + 25} + 24(\cos \varphi)^2 + 5}{\sqrt{576(\cos \varphi)^4 + 624(\cos \varphi)^2 + 25} + 30(\cos \varphi)^2 + 5}. \quad (5.34)$$

The dependence of the efficiency on the phase displacement of the injected current is shown in Fig. 5-7.

From the application point of view, it would be interesting to relate the input current THD given by (5.20) and the rectifier efficiency given by (5.34). Since the parameter φ cannot be explicitly removed from (5.20) and (5.34) (that would result in a closed form relation between the THD and the efficiency), the relation is presented in graphical form, as depicted in Fig. 5-8. The curve presented in Fig. 5-8 shows that improvement of the input current THD can be obtained only at the price of the power taken by the current injection network. In the case of the optimal third-harmonic current injection, the THD of the input currents reaches a minimum of 5.12%, as given by (5.22), and the power taken by the current injection network reaches its maximum of

$$P_{INJ\max} = \frac{9\sqrt{3}}{32\pi} V_m I_{OUT} = \frac{3}{32} P_{OUT} = \frac{3}{35} P_{IN} \approx 8.57\% P_{IN}. \quad (5.35)$$

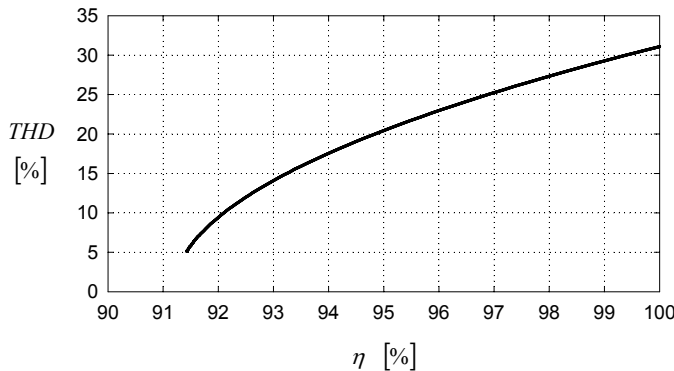


Figure 5-8. The input current THD as a function of efficiency.

In that case, the rectifier efficiency reaches a minimum of

$$\eta_{\min} = \frac{32}{35} = 91.43\%. \quad (5.36)$$

In the case of the optimal third-harmonic current injection, the input power of the rectifier is

$$P_{IN} = \frac{105\sqrt{3}}{32\pi} V_m I_{OUT}, \quad (5.37)$$

and the output power of the rectifier can be increased up to this value applying resistance emulation techniques.

To illustrate the optimal third-harmonic current injection, normalized waveforms of the diode bridge output terminal load currents, i_A and i_B , and the injected current i_Y are presented in Fig. 5-9. The waveforms are normalized to the value of the output current, as indicated on the vertical axes of the diagrams. All of the waveforms are periodic with the triple of the line frequency. Waveforms of i_A and i_B are always greater than zero, corresponding to the rectifier continuous conduction mode. The injected current, given by

$$i_Y = i_A - i_B, \quad (5.38)$$

is free from the DC component, and its spectral component at the triple of the line frequency is doubled in comparison to i_A and i_B .

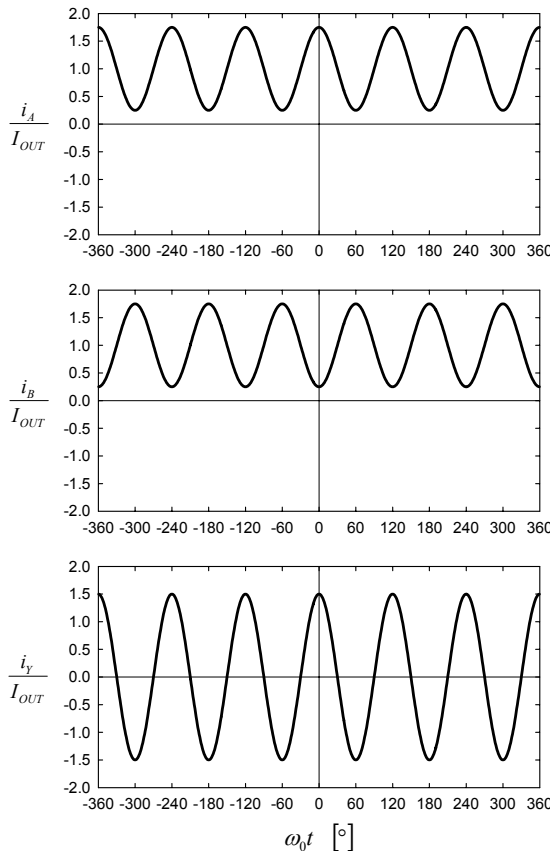


Figure 5-9. Waveforms of i_A , i_B , and i_Y .

In the first diagram in Fig. 5-10, the normalized waveform of the first of the diode bridge input currents is presented. The segment of the waveform when the current is positive corresponds to the conduction of D1, while the segment when the current is negative corresponds to the conduction of D2. The average of the diode currents, equal to one third of the output current, could be visualized. Gaps in the diode bridge input currents can also be observed. These gaps are going to be patched by current i_X that is being injected in each of the rectifier phases. The normalized waveform of i_X , the current injected in each of the rectifier phases, is presented in the second diagram of Fig. 5-10. The waveform is periodic at the triple of the line frequency, and it is equal to one third of i_Y . The rectifier input current is given by

$$i_1 = i_{S1} - i_X , \quad (5.39)$$

and its normalized waveform is presented in the third diagram of Fig. 5-10. The THD of this waveform is 5.12%, as given by (5.22).

To illustrate the power the current injection network takes from the diode bridge output terminals, in Fig. 5-11 waveforms of v_A , i_{IA} , and the power the current injection network takes from the positive output terminal, $v_A i_{IA}$, are presented. The power taken from the positive output terminal contains a considerable reactive component that originates from the cross product between the DC component of v_A and the fundamental harmonic of i_{IA} . The same set of waveforms corresponding to the negative output terminal, v_B , i_{IB} , and $v_B i_{IB}$, is presented in Fig. 5-12.

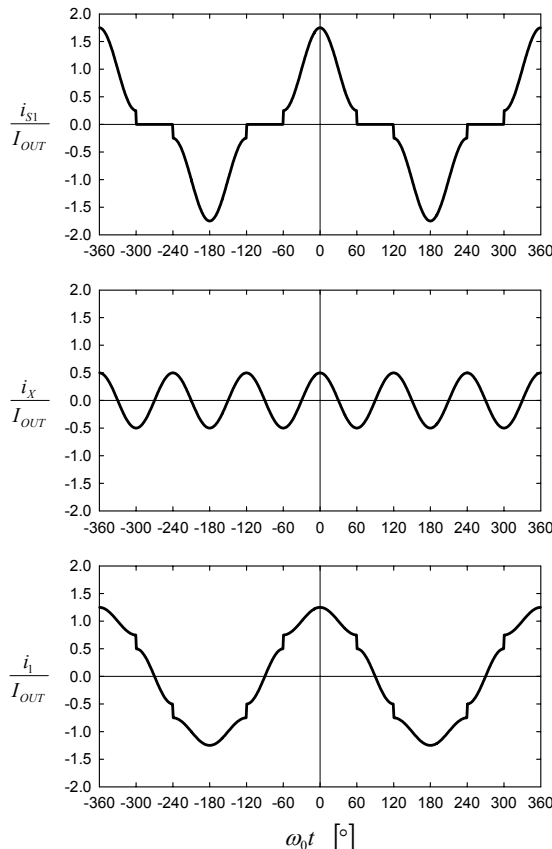


Figure 5-10. Waveforms of i_{S1} , i_X , and i_1 .

The only difference between Fig. 5-11 and Fig. 5-12 is that the waveforms of Fig. 5-12 are shifted in phase for $\pi/3$, i.e., one half of the period, in comparison to the waveforms of Fig. 5-11. This results in the waveform of the power the current injection network takes from the diode bridge output terminals, specified by

$$P_{INJ} = v_A i_{IA} + v_B i_{IB}, \quad (5.40)$$

presented in Fig. 5-13. The waveform in Fig. 5-13 is presented in the same scale as the power waveforms in Figs. 5-11 and 5-12 to illustrate that the reactive component is considerably reduced by adding $v_A i_{IA}$ and $v_B i_{IB}$. the average of the power the current injection network takes from the diode bridge output terminals is as specified by (5.35).

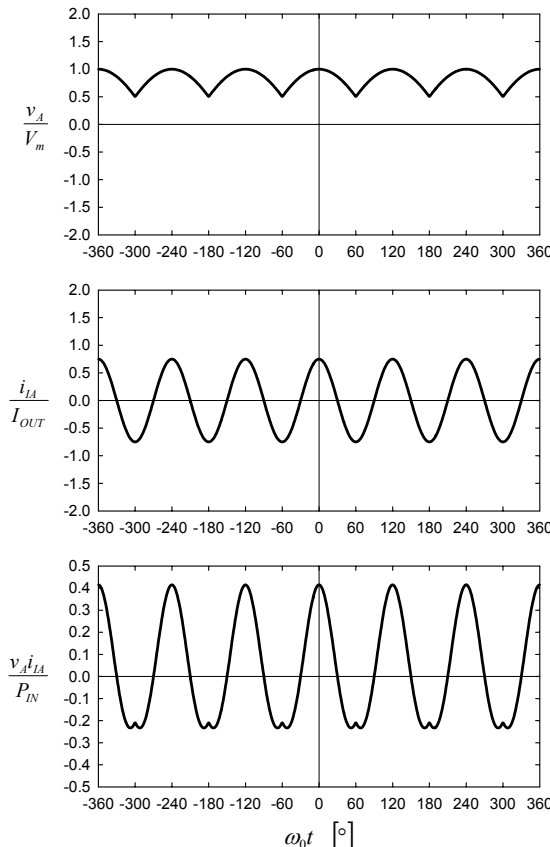


Figure 5-11. Waveforms of v_A , i_{IA} , and $v_A i_{IA}$.

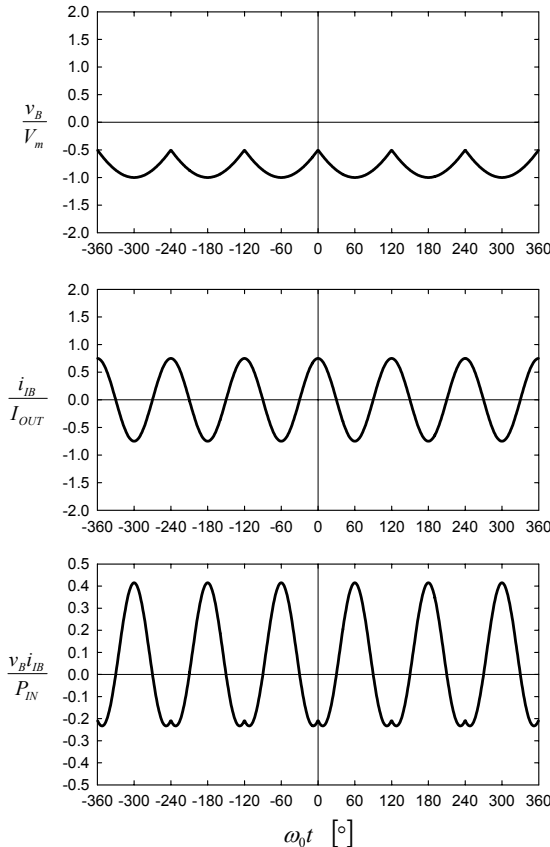


Figure 5-12. Waveforms of v_B , i_{IB} , and $v_B i_{IB}$.

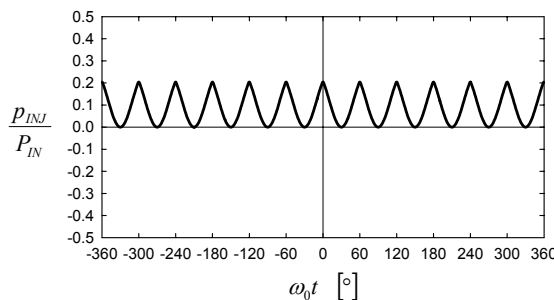


Figure 5-13. Waveform of the power the current injection network takes from the diode bridge output terminals, p_{INJ} .

Since some harmonic standards limit amplitudes of particular harmonic components of input currents, amplitude spectra of the input currents in the case of the optimal third-harmonic current injection should be derived. In the case of the optimal third-harmonic current injection, the input current of the first phase is obtained from (5.13) for $k = 3/4$ and $\varphi = 0$ as

$$\frac{i_1}{I_{OUT}} = \begin{cases} 1 + \frac{1}{4} \cos(3\omega_0 t), & \text{for } -\frac{\pi}{3} < \omega_0 t < \frac{\pi}{3} \\ -\frac{1}{2} \cos(3\omega_0 t), & \text{for } -\frac{2\pi}{3} < \omega_0 t < -\frac{\pi}{3} \text{ and } \frac{\pi}{3} < \omega_0 t < \frac{2\pi}{3} \\ -1 + \frac{1}{4} \cos(3\omega_0 t), & \text{for } -\pi < \omega_0 t < -\frac{2\pi}{3} \text{ and } \frac{2\pi}{3} < \omega_0 t < \pi \end{cases} . \quad (5.41)$$

Applying formulae (2.31) to (2.36) for the input current waveform of the first phase of the rectifier, specified by (5.41), the input current amplitude spectrum is obtained as

$$I_{1,n} = \frac{1}{2\pi n} \frac{n^2 - 36}{n^2 - 9} \left| \sin \frac{2\pi n}{3} + \sin \frac{\pi n}{3} \right| I_{OUT}, \quad (5.42)$$

for $n \neq 3$, and $I_{1,3} = 0$. The amplitude spectrum of (5.42) contains nonzero spectral components only for odd values of n that are not a multiple of three, i.e., the amplitude spectrum of i_1 can be represented as

$$I_{1,n} = \begin{cases} \frac{\sqrt{3}}{2\pi n} \left| \frac{n^2 - 36}{n^2 - 9} \right| I_{OUT}, & \text{for } n = 6k - 5 \text{ or } n = 6k - 1 \\ 0, & \text{otherwise} \end{cases} \quad (5.43)$$

where $k \in N$. The waveforms of the remaining two of the input currents are displaced in time for one third of the period; thus they share the same amplitude spectrum as i_1 .

To compare the input current amplitude spectra in the case of the optimal third-harmonic current injection and the case in which the current injection is not applied, relative size of the harmonics is presented in the bar chart of Fig. 5-14, where the amplitudes are normalized to the amplitude of the fundamental harmonic for the case in which the current injection is not applied. To generate the data, it was assumed that both rectifiers were supplied with the same voltages, as well as loaded with the same output

currents. The diagram indicates that the optimal third-harmonic current injection resulted in an increase of the amplitude of the fundamental harmonic for the factor $35/32 = 1.09375$. This corresponds to the power taken by the current injection network which increased the input power, since the output power is assumed to be the same in both cases. On the other hand, the optimal third-harmonic current injection reduced the higher order harmonics for the factor

$$\frac{I_n|_{inj}}{I_n|_{no\ inj}} = \left| \frac{n^2 - 36}{4n^2 - 36} \right|, \quad (5.44)$$

where *inj* refers to the case of the optimal third-harmonic current injection, and *no inj* corresponds to the case in which the current injection is not applied. According to (5.44), since

$$\lim_{n \rightarrow \infty} \frac{I_n|_{inj}}{I_n|_{no\ inj}} = \lim_{n \rightarrow \infty} \frac{n^2 - 36}{4n^2 - 36} = \frac{1}{4}, \quad (5.45)$$

it can be concluded that the optimal third-harmonic current injection reduces amplitudes of the high order harmonics approximately four times.

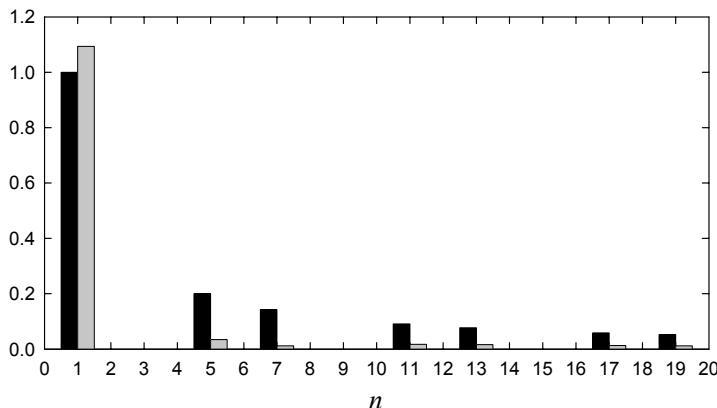


Figure 5-14. Normalized amplitude spectra of the input currents; black bars: current injection is not applied; gray bars: the optimal third-harmonic current injection.

Chapter 6

CURRENT INJECTION NETWORKS FOR THE THIRD-HARMONIC CURRENT INJECTION

The third-harmonic current injection is analyzed in Chapter 5, and conditions for the optimal third-harmonic current injection are derived. To minimize the total harmonic distortion (THD) of the input currents, the injected current should be in phase with the harmonic component of the rectifier output terminal voltages at the triple of the line frequency, and the amplitude of the third-harmonic current the current injection network takes from the rectifier output terminals should be equal to $3/4$ of the output current. The next task is to invent a current injection network that provides the required injected current. The current injection network should be as simple as possible and inexpensive. The popularity of the third-harmonic current injection has grown after simple current injection networks were proposed in [13] (in 1992) and [12] (in 1994). These two current injection networks are described and analyzed in this chapter for historical reasons. After analyzing advantages and drawbacks of these two current injection networks, a novel current injection network is proposed, combining the advantages of the current injection network [12] with the advantages of the current injection network [13], and providing additional improvement in the input current THD. The novel current injection network was originally proposed in [30]. After [30] appeared, it seems that there were no further improvements in the current injection network design, except in the area of resistance emulation. The current injection network of [30] is applied in the third-harmonic current injection based rectifiers that apply passive resistance emulation, presented in [32], [34], and [39].

The current injection networks that are analyzed in this chapter are labeled A for the current injection network of [13], B for the network of [12], and C for the network of [30].

1. CURRENT INJECTION NETWORK A

The first of the current injection networks to be analyzed in this chapter is the current injection network proposed in [13], termed here current injection

network A. A somewhat generalized form of the current injection network of [13] is shown in Fig. 6-1. The generalization is made in order to include losses in the current injection device modeled by $(1-a)R$ resistor in the current injection network model, making the current injection network model solely responsible for the amplitude and the phase of the injected current.

Resistors $2aR$ are [13] intentionally included in the current injection network to provide a means to control the amplitude of the injected current. A part of resistance of the resistors $2aR$ is parasitic resistance of the current injection network elements. The remaining part is the resistance of added resistors. The resistance parameter a is within the limits

$$0 \leq a \leq 1. \quad (6.1)$$

At odd triples of the line frequency, spectral components of the output terminal voltages v_A and v_B have the same waveforms,

$$v_{A,2k-1} = v_{B,2k-1}, \quad (6.2)$$

according to (5.1) and (5.2). Thus, the circuit of Fig. 6-1 can be represented by an equivalent circuit shown in Fig. 6-2. The circuit of Fig. 6-2 is a series resonant circuit, having the phase resonance at

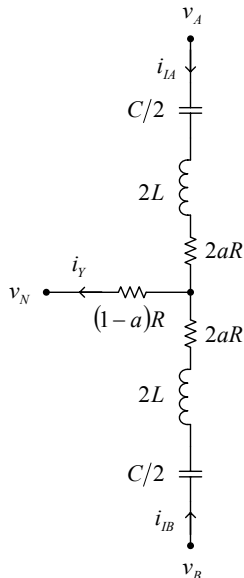


Figure 6-1. Current injection network A. © [1999] IEEE.

$$\omega_R = \frac{1}{\sqrt{LC}} . \quad (6.3)$$

To provide the injected current in phase with spectral components of v_A and v_B at the triple of the line frequency, phase resonance of the circuit of Fig. 6-2 should be placed at the triple of the line frequency,

$$\omega_R = 3\omega_0 . \quad (6.4)$$

Let us define the Q -factor of the current injection network as a Q -factor of the circuit shown in Fig. 6-2,

$$Q = \frac{1}{R} \sqrt{\frac{L}{C}} . \quad (6.5)$$

Thus, impedance that relates spectral components of the rectifier output terminal voltages to corresponding currents taken from these terminals, according to the equivalent circuit of Fig. 6-2, is

$$\begin{aligned} Z(j\omega) &= \frac{V_{A,2k-1}}{I_{IA,2k-1}} = \frac{V_{B,2k-1}}{I_{IB,2k-1}} = 2 \left(R + j\omega L + \frac{1}{j\omega C} \right) \\ &= 2R \left(1 + jQ \left(\frac{\omega}{\omega_R} - \frac{\omega_R}{\omega} \right) \right), \end{aligned} \quad (6.6)$$

which at odd triples of the line frequency where the equivalent circuit of Fig. 6-2 is valid, for $\omega = 3(2k-1)\omega_0$, reduces to

$$Z(j3(2k-1)\omega_0) = 2R \left(1 + jQ \left(2k-1 - \frac{1}{2k-1} \right) \right). \quad (6.7)$$

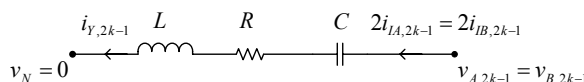


Figure 6-2. Equivalent circuit of the current injection network at odd triples of the line frequency. © [1999] IEEE.

In particular, at the triple of the line frequency, for $k=1$, the impedance of the current injection network becomes purely resistive,

$$Z(3j\omega_0) = 2R . \quad (6.8)$$

This impedance controls the amplitude of the injected current, and according to the requirements of the optimal third-harmonic current injection specified by (5.21), it should be

$$Z(3j\omega_0) = \frac{V_{A,1}}{(3/4)I_{OUT}} = \frac{\sqrt{3}}{2\pi} \frac{V_m}{I_{OUT}} . \quad (6.9)$$

From (6.8) and (6.9) we obtain the value of the current injection network resistance for the optimal third-harmonic current injection as

$$R = \frac{\sqrt{3}}{4\pi} \frac{V_m}{I_{OUT}} . \quad (6.10)$$

Thus, to provide the optimal third-harmonic current injection two constraints should be satisfied: (1) the current injection network phase resonance should be tuned to the triple of the line frequency and (2) the resistance of the current injection network should be as given by (6.10). It should be noted here that the optimal resistance specified by (6.10) is dependent on the load current, thus it should be adjusted according to the load current variations.

Another interesting issue is whether electrolytic capacitors can be applied in the current injection network. Voltage across the capacitors consists of a DC component equal to one half of the output voltage DC component, and an AC component which is dominated by a spectral component at the triple of the line frequency. Neglecting higher order spectral components of the capacitor voltage, which is well justified, the condition that the amplitude of the AC component of the capacitor voltage is lower than the DC component of the capacitor voltage becomes

$$\frac{2}{3\omega_0 C} \frac{3}{4} I_{OUT} < \frac{1}{2} V_{OUT} . \quad (6.11)$$

Substituting (2.11) for the diode bridge output voltage, (6.11) becomes

$$\frac{I_{OUT}}{2\omega_0 C} < \frac{3\sqrt{3}}{2\pi} V_m . \quad (6.12)$$

Using (6.4), (6.5), and (6.10), the condition (6.12) reduces to

$$Q < 4. \quad (6.13)$$

Thus, if the condition of (6.13) is satisfied, electrolytic capacitors can be applied in the current injection network.

To provide the optimal third-harmonic current injection, impedance of the current injection network at the triple of the line frequency should be as specified by (6.8), and at all other frequencies it should be infinitely large. Unfortunately, the circuit of Fig. 6-1 does not have that property. At the triple of the line frequency, the impedance may be tuned to the value of (6.8), but at higher order odd triples of the line frequency the impedance is as specified by (6.7), instead of being infinite.

The next question is to determine the behavior of the current injection network at even triples of the line frequency. At even triples of the line frequency, spectral components of v_A and v_B have the same amplitudes, but the opposite phases,

$$v_{A,2k} = -v_{B,2k}. \quad (6.14)$$

Thus, applying symmetry of the circuit of Fig. 6-1 and the property of v_A and v_B given by (6.14), the current injection network of Fig. 6-1 can be represented by an equivalent circuit shown in Fig. 6-3. Impedance that relates spectral components of the rectifier output terminal voltages to corresponding currents taken from these terminals by the current injection network A, according to the equivalent circuit of Fig. 6-3, is

$$\begin{aligned} Z(j\omega) &= \frac{V_{A,2k}}{I_{IA,2k}} = \frac{V_{B,2k}}{I_{IB,2k}} = 2 \left(aR + j\omega L + \frac{1}{j\omega C} \right) \\ &= 2R \left(a + jQ \left(\frac{\omega}{\omega_R} - \frac{\omega_R}{\omega} \right) \right). \end{aligned} \quad (6.15)$$

At even triples of the line frequency for $\omega = 3(2k)\omega_0$, where the equivalent circuit of Fig. 6-3 is valid, (6.15) reduces to

$$Z(j3(2k)\omega_0) = 2R \left(a + jQ \left(2k - \frac{1}{2k} \right) \right). \quad (6.16)$$

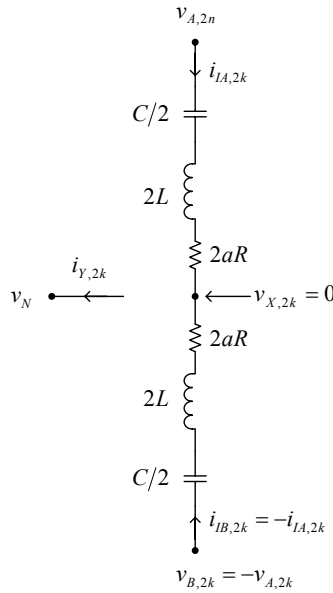


Figure 6-3. Equivalent circuit of current injection network A at even triples of the line frequency.

It should be noted here that due to the symmetry of the current injection network and antisymmetry of $v_{A,2k}$ and $v_{B,2k}$, spectral components at even triples of the line frequency are absent from i_Y ,

$$i_{Y,2k} = 0. \quad (6.17)$$

2. CURRENT INJECTION NETWORK B

The second current injection network to be analyzed in this chapter is proposed in [12], and is referred to as current injection network B. The circuit diagram of the current injection network B is shown in Fig. 6-4, and it consists of two capacitors, one inductor and three resistors. In [12], the resistors were not explicitly included in the circuit diagram of the current injection network. However, without the resistors the phase displacement of the injected current will be either 90° or -90° , and in either of these two cases the current injection cannot improve the input current THD, as shown in Chapter 5. Thus, it seems that parasitic resistance of the reactive elements

was relied on in order to produce the experimental results of [12]. The resistors that are added in the circuit diagram of Fig. 6-4 model losses in the reactive elements of the current injection network, as well as the losses in the current injection device, and some part of the resistance may be externally added by resistors or resistance emulators. The losses of the current injection device are included in the model of the current injection network to make the current injection network solely responsible for the injected current. The current injection network of Fig. 6-4 contains one inductor, in comparison to the current injection network of Fig. 6-1 which contains two.

At odd triples of the line frequency, where spectral components of the output terminal voltages v_A and v_B are the same, as given by (6.2), the equivalent circuit of the current injection network B is the same as for the current injection network A, depicted in Fig. 6-2. Thus, the impedance that relates the output terminal voltages v_A and v_B and the currents that the current injection network takes from the output terminals, i_{IA} and i_{IB} , is the same as for the current injection network A, given by (6.7).

At even triples of the line frequency, the current injection network B is different from the current injection network A. An equivalent circuit that represents the current injection network B at even triples of the line frequency is shown in Fig. 6-5. Again, the injected current i_Y is free of the harmonic components at even triples of the line frequency, the same as in the case of the current injection network A, as given by (6.17). Thus, analyzing the injected current i_Y , the difference between the two current injection networks cannot be observed, provided that parameters L , C , and R are the same for both of circuits. The only difference between the current injection networks is in their behavior for spectral components at even triples of the line frequency, which can be observed in i_{IA} and i_{IB} .

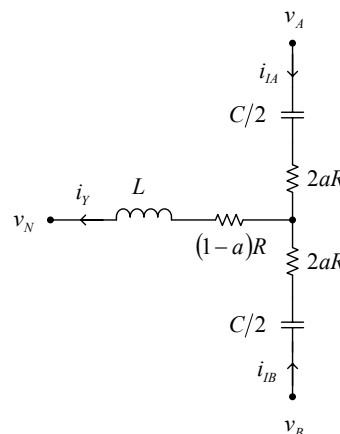


Figure 6-4. Current injection network B. © [1999] IEEE.

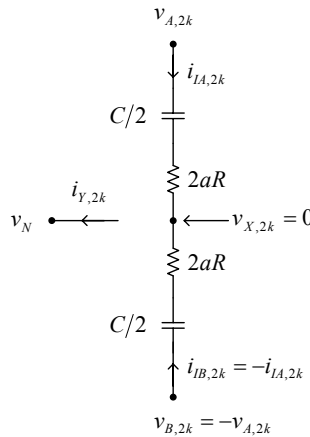


Figure 6-5. Equivalent circuit of current injection network B at even triples of the line frequency.

The impedance relating spectral components of the rectifier output terminal voltages and currents of the current injection network B taken from these terminals, according to the equivalent circuit of Fig. 6-5, is

$$Z(j\omega) = \frac{V_{A,2k}}{I_{IA,2k}} = \frac{V_{B,2k}}{I_{IB,2k}} = 2aR + \frac{2}{j\omega C} = 2R \left(a - jQ \frac{\omega_R}{\omega} \right), \quad (6.18)$$

which for $\omega = 3(2k)\omega_0$, where the equivalent circuit of Fig. 6-5 is valid, reduces to

$$Z(j3(2k)\omega_0) = 2R \left(a - jQ \frac{1}{2k} \right). \quad (6.19)$$

3. VOLT-AMPERE RATING OF AN INDUCTOR CORE

Comparison of the current injection networks A and B indicates so far that behavior of the current injection networks is the same for odd triples of the line frequency, and the most important, at the triple of the line frequency. The behavior is different for even triples of the line frequency, which is a parasitic effect to be analyzed later. On the other hand, the two current

injection networks require different number of inductors—the current injection network A requires two inductors, while the current injection network B requires only one. Voltages and currents across these inductors are different; thus it would be convenient to have a tool to compare the size and cost of these inductors. The inductors for the frequency range to which the current injection networks are exposed are wound applying laminated transformer cores, characterized by the volt-ampere rating. Our task in this section is to relate the core volt-ampere rating to voltages and currents the inductor is exposed to, and to compare the volt-ampere ratings of the inductor cores for the current injection networks A and B.

Assuming that main limiting factors for a transformer core are the maximum flux the core can take without getting saturated and the current handling capability of the core window, the volt-ampere rating is defined as

$$S_T = \frac{\omega_0}{2\sqrt{2}} \Phi_{\max} \sum_{k=1}^{n_w} n_k I_{k RMS}, \quad (6.20)$$

where ω_0 is the rated angular frequency of the core at which the manufacturer provided the volt-ampere data—the same as in (4.3). Since the inductor is assumed to have only one winding, $n_w = 1$, (6.20) reduces to

$$S_L = \frac{\omega_0}{2\sqrt{2}} \Phi_{\max} n I_{L RMS}. \quad (6.21)$$

The flux linkage of the inductor is

$$\lambda = n\Phi = Li, \quad (6.22)$$

and thus

$$n\Phi_{\max} = Li_{L \max}, \quad (6.23)$$

where $i_{L \max}$ is the maximum of the inductor current instantaneous value during the period. Finally, the volt-ampere rating of the inductor core is related to the electrical parameters as

$$S_L = \frac{\omega_0}{2\sqrt{2}} L i_{L \max} I_{L RMS}. \quad (6.24)$$

Now, taking (6.24), let us estimate volt-ampere ratings of the cores required by the inductors of the current injection networks A and B. In the

case of the current injection network A, assuming the optimal third-harmonic current injection and neglecting the influence of the higher order harmonics, we obtain

$$S_{L,A} = \frac{\omega_0}{2\sqrt{2}} 2L \left(\frac{3}{4} I_{OUT} \right) \left(\frac{3}{4\sqrt{2}} I_{OUT} \right), \quad (6.25)$$

which can be simplified to

$$S_{L,A} = \frac{9}{32} \omega_0 L I_{OUT}^2. \quad (6.26)$$

In the special case $Q = 4$, which provides the best filtering of the higher order harmonics and application of electrolytic capacitors, (6.26) reduces to

$$S_{L,A} = \frac{1}{32} V_{OUT} I_{OUT} = \frac{1}{35} P_{IN} = 2.86\% P_{IN}. \quad (6.27)$$

In the case of the current injection network B, for the inductor volt-ampere rating applying (6.24) we obtain

$$S_{L,B} = \frac{\omega_0}{2\sqrt{2}} L \left(\frac{3}{2} I_{OUT} \right) \left(\frac{3}{2\sqrt{2}} I_{OUT} \right), \quad (6.28)$$

which can be simplified to

$$S_{L,B} = \frac{9}{16} \omega_0 L I_{OUT}^2. \quad (6.29)$$

In the special case of $Q = 4$, (6.29) reduces to

$$S_{L,B} = \frac{1}{16} V_{OUT} I_{OUT} = \frac{2}{35} P_{IN} = 5.71\% P_{IN}. \quad (6.30)$$

Comparing (6.26) and (6.29), it can be concluded that for equal electrical performance of the current injection networks at the triple of the line frequency, the volt-ampere rating of the inductor applied in the current injection network B is the double of the volt-ampere rating of each of the inductors applied in the current injection network A. This can be rephrased to the statement that the sum of the volt-ampere ratings of the inductors

applied in the current injection network A is equal to the volt-ampere rating of the current injection network B.

4. COMPARISON OF THE CURRENT INJECTION NETWORKS

According to the analysis performed so far, the current injection networks A and B behave in the same way at odd triples of the line frequency, while their behavior is different at even triples of the line frequency. Analysis of the third-harmonic current injection performed in Chapter 5 ignored the influence of the higher order harmonics of the injected current. In this section, influence of the higher order harmonics is going to be analyzed.

The first of the analyses of the influence of the higher order harmonics is the dependence of the input current THD on the current injection network Q -factor. To determine the input current THD, waveforms of the currents i_{IA} and i_{IB} , that the current injection network takes from the rectifier output terminals, are determined applying

$$i_{IA}(\omega_0 t) = \sum_{n=1}^m \frac{|V_{A,n}|}{|Z(jn\omega_0)|} \cos\left(n\omega_0 t + \arg\left(\frac{V_{A,n}}{Z(jn\omega_0)}\right)\right) \quad (6.31)$$

and

$$i_{IB}(\omega_0 t) = \sum_{n=1}^m \frac{|V_{B,n}|}{|Z(jn\omega_0)|} \cos\left(n\omega_0 t + \arg\left(\frac{V_{B,n}}{Z(jn\omega_0)}\right)\right), \quad (6.32)$$

where $Z(jn\omega_0)$ is defined by (6.7) and (6.16) for the current injection network A, and by (6.7) and (6.19) for the current injection network B. To compute the results presented in this section, for the upper limit of the sums of (6.31) and (6.32) $m=100$ is taken, since harmonic components up to 1.5 kHz are considered relevant. After the waveforms of i_{IA} and i_{IB} are computed, the waveform of the input current i_l is obtained as

$$i_l = d_1(I_{OUT} + i_{IA}) - d_2(I_{OUT} - i_{IB}) - \frac{1}{3}(i_{IA} + i_{IB}), \quad (6.33)$$

where the diode state functions d_1 and d_2 are as defined in Chapter 2. The computation is performed normalizing the voltages by V_m , and the currents by I_{OUT} . After the waveform of i_l is obtained, its THD is computed. The same THD value applies for i_2 and i_3 .

Dependence of the input current THD on the current injection network Q -factor for the current injection network A is depicted in Fig. 6-6 as a parametric family of curves with the resistance distribution a as a parameter. The curves of Fig. 6-6 are presented only for the continuous conduction mode of the rectifier. The curves indicate that with increases of the Q -factor, the input current THD decreases, approaching the limit of 5.12% given by (5.22) asymptotically from above.

The current injection network B has the dependence of the input current THD on the current injection network Q -factor as shown in Fig. 6-7. Comparing the two figures, it can be concluded that the current injection network A provides lower total harmonic distortions of the input currents and a wider range of the continuous conduction mode operation. In both current injection networks, increase of the resistance distribution parameter contributed to the decrease of the input current THD. Thus, to reduce the input current THD it is convenient to locate the added resistors or resistance emulators in “vertical” branches of the current injection networks, i.e., to increase the resistance distribution parameter as much as possible.

Dependence of the input current THD on the current injection network resistance distribution parameter is presented in Fig. 6-8 for current injection network A, and for current injection network B the same dependence is presented in Fig. 6-9. The diagrams are presented as parametric families of curves with the current injection network Q -factor as a parameter. The curves are presented only in the region where the rectifier operates in the continuous conduction mode. Comparing Fig. 6-8 and Fig. 6-9, it can be concluded that current injection network A provided lower values of the input current THD, again. Also, the region where the rectifier operates in the continuous conduction mode is wider in the case of current injection network A than in current injection network B. For example, curves for $Q=0.5$ and $Q=1.0$ are absent from Fig. 6-9, since the rectifier operates in the discontinuous conduction mode in these cases.

To illustrate the influence of the higher order harmonics on operation of the current injection networks, waveforms of i_{IA} , i_{IB} , i_Y , and i_l are presented in Fig. 6-10. Waveforms of the currents in current injection network A are presented in the left column, labeled (a), while the waveforms corresponding to current injection network B are presented in the right column, labeled (b). The diagrams are obtained by simulation, applying (6.31) and (6.32), for $Q=2$ and $a=0.5$. The diagrams of i_{IA} and i_{IB} corresponding to the current injection network A are negligibly polluted by higher order harmonics, in contrast to the waveforms corresponding to the current injection network B that are significantly polluted. However, the waveforms of i_Y are the same for both current injection networks, proving

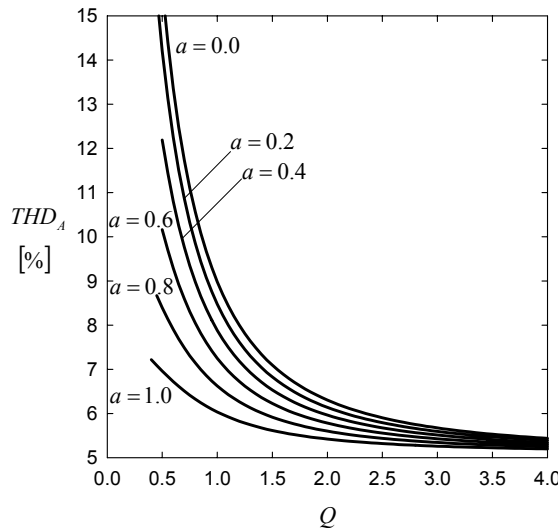


Figure 6-6. Dependence on the input current THD on Q -factor, current injection network A.
© [1999] IEEE.

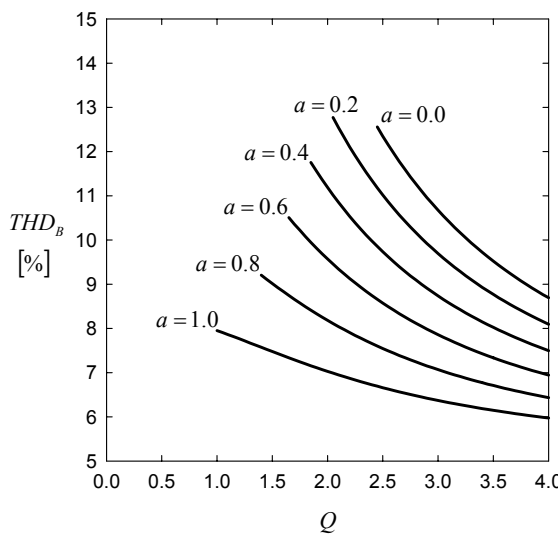


Figure 6-7. Dependence on the input current THD on Q -factor, current injection network B.
© [1999] IEEE.

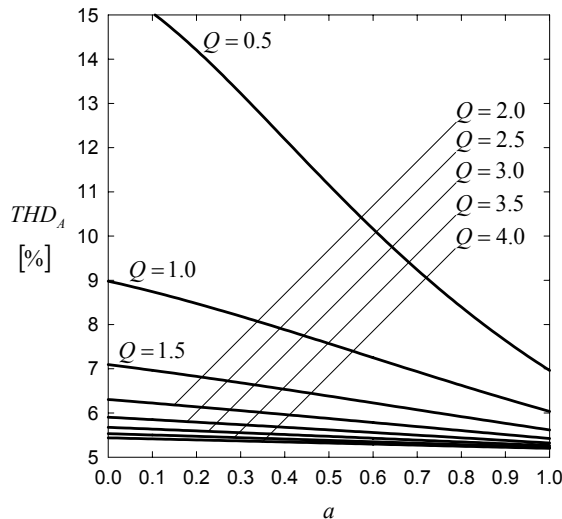


Figure 6-8. Dependence on the input current THD on the resistance distribution parameter, current injection network A. © [1999] IEEE.

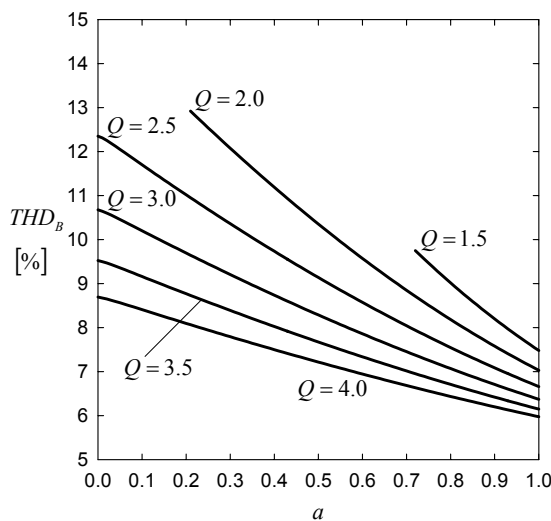


Figure 6-9. Dependence on the input current THD on the resistance distribution parameter, current injection network B. © [1999] IEEE.

that the equivalent circuit of the current injection networks A and B is the same for odd triples of the line frequency. Pollution of i_Y by higher order odd triples of the line frequency is negligible.

Waveforms of the input currents corresponding to the analyzed case are presented in the last row. The total harmonic distortion of the input current for the current injection network A is $THD_A = 5.87\%$, while for the current injection network B the total harmonic distortion is $THD_B = 10.35\%$.

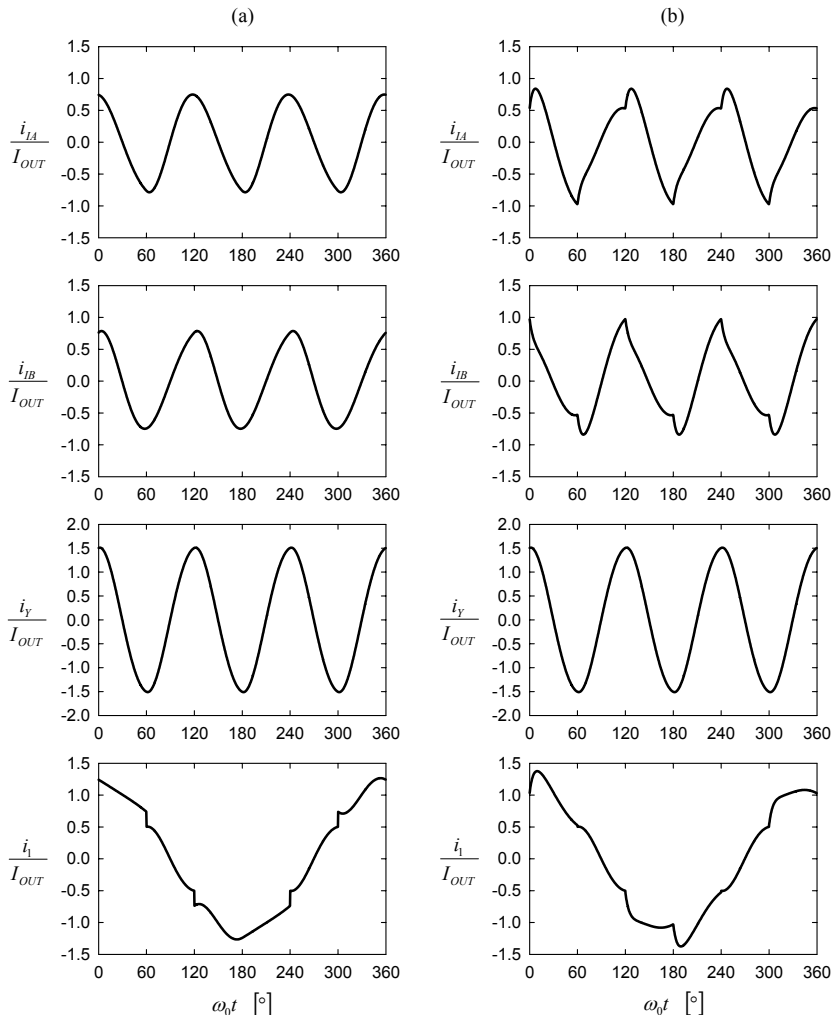


Figure 6-10. Waveforms of the currents for the current injection networks: (a) current injection network A; (b) current injection network B.

According to the analysis presented, current injection network A provides lower total harmonic distortion of the input currents under the constraint that Q -factors and the resistance distribution parameter of the current injection networks are the same. Under these constraints, the current injection networks are built applying the same capacitors and the same resistors or resistance emulators, while the inductors are different. Current injection network B requires one inductor of inductance L , while current injection network A requires two inductors with the inductance $2L$. However, the sum of the volt-ampere ratings of the inductors in current injection network A equals the volt-ampere rating of the inductor in current injection network B. It seems that the only benefit of current injection network B is that it requires only one inductor. This may lead to the conclusion that current injection network A should always be applied. However, there is another current injection network, termed current injection network C, which is the topic of the next section.

5. CURRENT INJECTION NETWORK C

Analysis of current injection networks A and B performed leads to the conclusion that current injection network A provides significantly lower THD values of the rectifier input currents due to the fact that it provides lower content of the harmonics at even triples of the line frequency in i_{IA} and i_{IB} than current injection network B. The harmonics at even triples of the line frequency are blamed for this result, since at odd triples of the line frequency current injection networks A and B behave in the same manner, having the same equivalent circuit, and providing the same current i_Y . The only advantage of current injection network B is that it requires only one inductor, although its volt-ampere rating is the same as the sum of the volt-ampere ratings of the inductors applied in the current injection network A. Thus, it seems reasonable to raise the question: Is there an efficient way to remove harmonic components at even triples of the line frequency from i_{IA} and i_{IB} completely?

Let us consider the current injection network shown in Fig. 6-11, termed current injection network C. Current injection network C is proposed in [30]. In comparison to the current injection network B, depicted in Fig. 6-4, current injection network C applies an extra transformer. The transformer turns ratio is 1:1, and it forces i_{IA} and i_{IB} to be equal,

$$i_{IA} = i_{IB}. \quad (6.34)$$

At odd triples of the line frequency, current injection network C has the same equivalent circuit as current injection networks A and B; thus the same resonant constraint specified by (6.3) and (6.4), and the same value of R specified by (6.10) should be provided in order to obtain the optimal third-harmonic current injection.

At even triples of the line frequency, due to condition (6.34), an equivalent circuit of the current injection network C is the open circuit. In this manner, flow of the harmonics at even triples of the line frequency is completely blocked. Impedance relating spectral components of the rectifier output terminal voltages to corresponding currents taken from these terminals by the current injection network C is at odd triples of the line frequency—the same as for current injection networks A and B,

$$Z(j3(2k-1)\omega_0) = 2R \left(1 + jQ \left(2k-1 - \frac{1}{2k-1} \right) \right), \quad (6.35)$$

while at even triples of the line frequency this impedance is infinitely large,

$$Z(j3(2k)\omega_0) \rightarrow \infty. \quad (6.36)$$

Since the resistance distribution parameter does not appear in (6.35) and (6.36), its value is completely irrelevant for the rectifier operation.

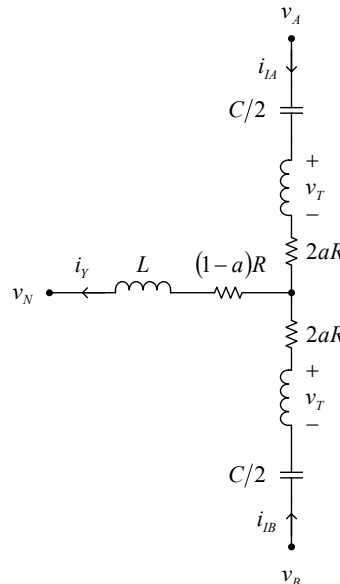


Figure 6-11. Current injection network C.

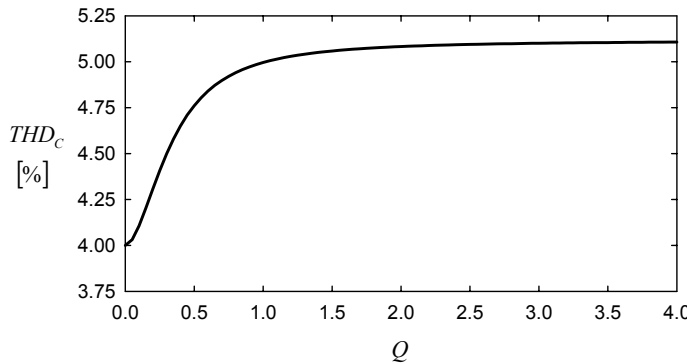


Figure 6-12. Dependence of the input current THD on Q -factor for current injection network C.

Applying the same method as for current injection networks A and B, based on (6.31), (6.32), and (6.33), the dependence of the input current THD on the current injection network Q -factor is obtained, and the resulting curve is presented in Fig. 6-12. The curve does not depend on the resistance distribution parameter, and in contrast to the curves in Figs. 6-6 and 6-7, the THD increases with increases of the current injection network Q -factor, although this increase is not significant. Again, for $Q \rightarrow \infty$ the input current THD asymptotically approaches the limit of (5.22), but from below in this case. Thus, higher order harmonics in the injected currents do not necessarily increase the input current THD and deteriorate the rectifier operation. In contrast, the proper amount of the higher order harmonics can completely remove harmonics from the rectifier input currents, as shown in Chapter 7.

To illustrate the operation of current injection network C, waveforms of its currents are presented in Fig. 6-13 for $Q = 2$, corresponding to the situation in Fig. 6-10 for current injection networks A and B. As can be readily observed, the waveforms of i_{IA} and i_{IB} are free from the harmonic components at even triples of the line frequency, having the same shape as i_Y , since

$$i_{IA} = i_{IB} = \frac{1}{2} i_Y . \quad (6.37)$$

The waveform of the input current is presented in the last diagram of the figure, having the distortion $THD = 5.08\%$. This THD value is the lowest of the THD values for the input current waveforms in Figs. 6.10 and 6.13, obtained for current injection networks A, B, and C for $Q = 2$ and $a = 0.5$.

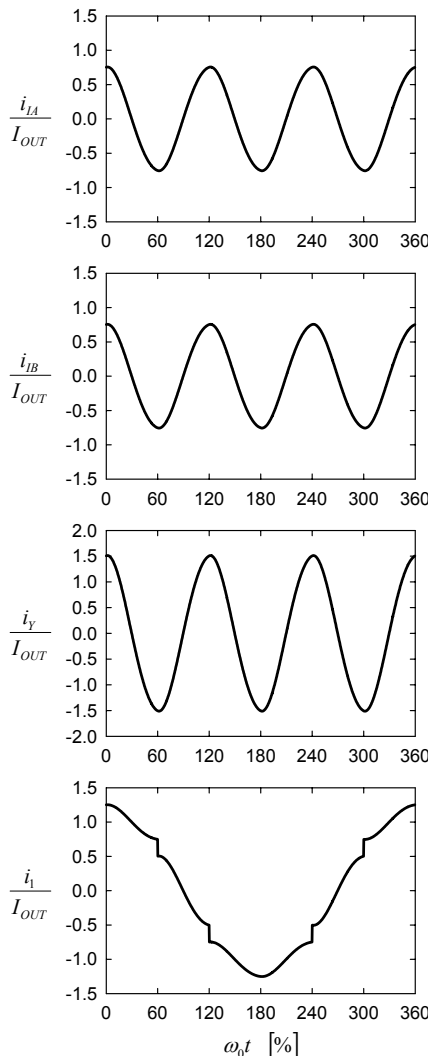


Figure 6-13. Waveforms of the currents for current injection network C.

Thus, since current injection network C provides the lowest THD values of the input currents and requires only one inductor in the current injection network, it can be concluded that it is the best for the design of the rectifiers that apply the third-harmonic current injection.

The volt-ampere rating of the 1:1 transformer in current injection network C is determined by applying (4.3). The waveform of the voltage v_T across one winding of the transformer is one half of the AC component of the

output voltage, and this waveform is shown in the first diagram of Fig. 6-14. The Fourier series expansion of the AC component of the output voltage is given by (2.12), and it contains harmonic components at sixth multiples of the line frequency. Integrating the waveform of the voltage across the transformer windings, the waveform of the flux linkage of the windings is obtained, and this waveform is presented in the second diagram of Fig. 6-14. Dividing the flux linkage by the number of turns n of the winding, the maximum of the core flux is obtained as

$$\Phi_{\max} = \frac{\sqrt{3}}{2\pi} \left(\sqrt{\pi^2 - 9} - 3 \arccos\left(\frac{3}{\pi}\right) \right) \frac{V_m}{n\omega_0}. \quad (6.38)$$

The waveform of the current flowing through the transformer windings is

$$i_T = i_{IA} = i_{IB}, \quad (6.39)$$

and it is shown in the last diagram of Fig. 6-14. The RMS value of this current is

$$I_{T\text{RMS}} = \frac{3}{4\sqrt{2}} I_{OUT} \quad (6.40)$$

in the case of the optimal third-harmonic current injection. Finally, applying (4.3) and normalizing the result to the rectifier input power specified by (5.35), the transformer volt-ampere rating is obtained as

$$S_{T1:1} = \frac{2}{35} \left(\sqrt{\pi^2 - 9} - 3 \arccos\left(\frac{3}{\pi}\right) \right) P_{IN} \approx 0.16\% P_{IN}. \quad (6.41)$$

Thus, the volt-ampere rating of the 1:1 transformer is very low. Applying this transformer, several improvements of current injection network performance are achieved: (a) harmonic components at even triples of the line frequency are completely removed from i_{IA} and i_{IB} ; (b) the resistance distribution parameter has no effect on the rectifier operation; (c) the current injection network requires only one inductor; and (d) the dependence of the input current THD on the current injection network Q -factor is low. According to these advantages obtained at the cost of one 1:1 transformer with a volt-ampere rating of only 0.16% of the input power, current injection network C is the best of the current injection networks for the third-harmonic current injection, and it is used in all of the rectifiers considered in the subsequent text.

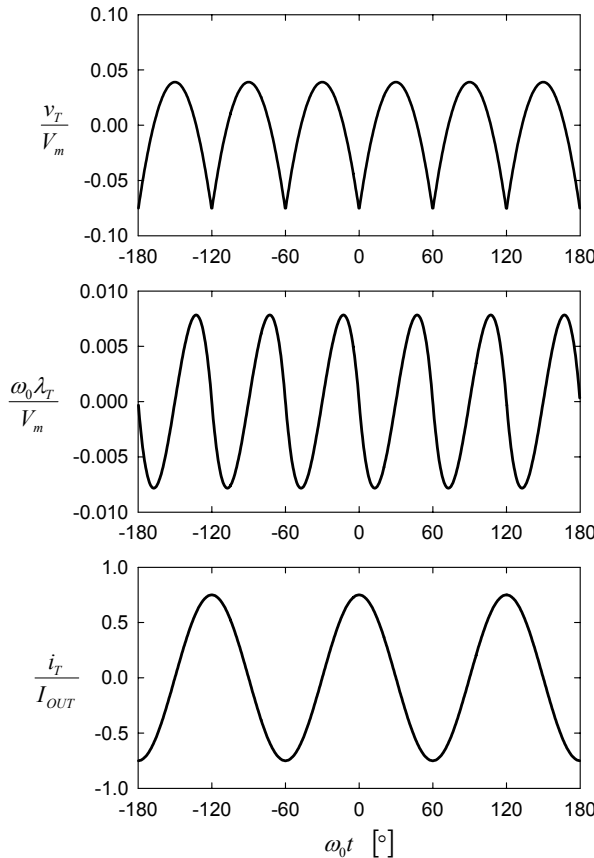


Figure 6-14. Voltage across one winding, flux linkage of the winding, and the current of the winding for the 1:1 transformer of current injection network C.

The volt-ampere rating of the inductor in current injection network C is the same as in the case of current injection network B, specified by (6.29). Transforming the expression (6.29), assuming the optimal third-harmonic current injection provided by the resistance specified by (6.10), and using the definition of the current injection network Q -factor given by (6.5), the inductor volt-ampere rating can be expressed as

$$S_L = \frac{Q}{70} P_{IN}. \quad (6.42)$$

Since THD values of the input currents negligibly depend on the current injection network Q -factor, choice of the Q -factor is dominated by minimization of the rectifier cost.

A special case that deserves to be studied is $Q=0$. In that case, $L=0$ and $C \rightarrow \infty$, which should not be taken literally; if the capacitance of $C/2$ capacitors is large enough to provide negligible ripple of their voltages in comparison to the AC components of the rectifier output terminal voltages v_A and v_B , the capacitors may be considered as infinitely large. In that case,

$$i_Y = \frac{v_{AV}}{R}, \quad (6.43)$$

and the injected current amplitude can be analytically optimized including the higher order harmonics of the injected current into the optimization process. The optimization is performed over parameter

$$\sigma = \frac{V_m}{I_{OUT} R}, \quad (6.44)$$

because the input current THD is dependent only on this parameter since

$$\frac{i_Y}{I_{OUT}} = \sigma \frac{v_{AV}}{V_m}. \quad (6.45)$$

The RMS value of the input currents is obtained as

$$I_{RMS} = \frac{1}{12} \sqrt{96 + \sigma^2 \left(1 - \frac{3\sqrt{3}}{2\pi} \right)}, \quad (6.46)$$

while the RMS value of the fundamental harmonic of the input currents is

$$I_{1RMS} = \frac{48\sqrt{3} + \sigma(2\pi - 3\sqrt{3})}{24\pi\sqrt{2}}. \quad (6.47)$$

The input current THD is obtained applying (2.29), and the result is

$$THD(\sigma) = \frac{\sqrt{(4\pi^2 - 27)\sigma^2 + 96(9 - 2\sqrt{3}\pi)\sigma + 768(\pi^2 - 9)}}{(2\pi - 3\sqrt{3})\sigma + 48\sqrt{3}}. \quad (6.48)$$

From

$$\frac{d(THD(\sigma))}{d\sigma} = 0, \quad (6.49)$$

the minimum of the input current THD is obtained for

$$\sigma = \frac{4\pi}{\sqrt{3}}, \quad (6.50)$$

resulting in a THD value of

$$THD_{min} = THD\left(\frac{4\pi}{\sqrt{3}}\right) = \frac{\sqrt{4\pi^4 - 27\pi^2 + 216\sqrt{3}\pi - 1296}}{2\pi^2 - 3\sqrt{3}\pi + 36} \approx 4.01\%, \quad (6.51)$$

which is in agreement with Fig. 6-12. The input current waveform corresponding to the optimal value of σ is presented in Fig. 6-15.

The resistance of the current injection system that corresponds to the optimal value of σ given by (6.50) is

$$R = \frac{\sqrt{3}}{4\pi} \frac{V_m}{I_{OUT}}, \quad (6.52)$$

which is the same as obtained for the optimal third-harmonic current injection given by (6.10).

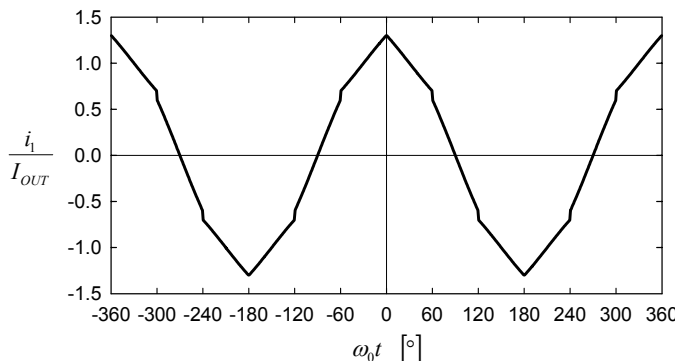


Figure 6-15. Waveform of i_l for $Q = 0$.

In the case $Q=0$, due to the higher order harmonics of the injected current, the power the current injection network takes from the rectifier output is increased in comparison to the optimal third-harmonic current injection, and this power is

$$P_{INJ} = \left(\frac{\pi}{2\sqrt{3}} - \frac{3}{4} \right) V_m I_{OUT}. \quad (6.53)$$

The input power of the rectifier is

$$P_{IN} = P_{OUT} + P_{INJ} = \frac{2\pi^2 - 3\sqrt{3}\pi + 36}{4\sqrt{3}\pi} V_m I_{OUT}, \quad (6.54)$$

and the power the current injection network takes from the rectifier output is, in terms of the input power, expressed as

$$P_{INJ} = \frac{\pi(2\pi - 3\sqrt{3})}{36 + \pi(2\pi - 3\sqrt{3})} P_{IN} \approx 8.66\% P_{IN}. \quad (6.55)$$

Finally, it can be concluded that injection of some amount of higher order harmonics located at odd triples of the line frequency improved the input current THD for somewhat more than 1%, and increased the power the current injection network takes from the rectifier output for negligible amount of 0.09% P_{IN} . The method of injection of the higher order harmonics is analyzed in Chapter 7, and it will be shown that the input current THD can be reduced to zero.

Another issue that will be of interest in Chapters 9 and 11 is the generalized condition that provides that the voltages of the current injection network capacitors do not change polarity during the period. The generalization should be made to cover cases when the amplitude of the injected third-harmonic current is not optimal, while the assumption that the spectral component at the triple of the line frequency dominates currents of the capacitors remains. Let us assume that the injected current is

$$i_Y = I_{Ym} \cos(3\omega_0 t), \quad (6.56)$$

with the amplitude

$$I_{Ym} = kI_{OUT}. \quad (6.57)$$

In that case, conditions (6.12) and (6.13) are generalized to

$$\frac{kI_{OUT}}{3\omega_0 C} \leq \frac{3\sqrt{3}}{2\pi} V_m. \quad (6.58)$$

This condition is normalized and applied in the analysis of suboptimal third-harmonic current injection techniques introduced in Chapters 9 and 11.

Chapter 7

THE OPTIMAL CURRENT INJECTION

The current injection method analyzed so far was based on intentional injection of the third-harmonic current. Other harmonics of the injected currents were side effects, and were not controlled. The first sign that higher order harmonics can improve the input current total harmonic distortion (THD) is the dependence of the input current THD on the current injection network Q -factor for the third-harmonic current injection network C, presented in Fig. 6-12. Decrease of the input current THD at low Q -factor values indicates that higher order harmonic components of the injected current, present for the low Q -factor values, improved the THD. Is it possible to obtain further improvements of the input current THD by injection of an adequate amount of the higher order harmonics? The question is answered in this chapter, with the answer that it is possible to remove harmonics of the input currents completely by proper injection of the higher order harmonics. The line of reasoning that led to the results presented in this chapter can be found in [25], [26], [28], [29], and [35]. The waveforms of the diode bridge load currents that provide purely sinusoidal input currents are also found in [22], [45], [47], and [48].

Let us consider a general form of the current injection based rectifier, shown in Fig. 3-1. Since the rectifier is supplied by a three-wire system, the input currents are subjected to the constraint

$$i_1 + i_2 + i_3 = 0. \quad (7.1)$$

Thus, only two of the input currents are independent; the third one should satisfy (7.1). Let us note that

$$i_X = \frac{1}{3}i_Y = \frac{1}{3}(i_A - i_B), \quad (7.2)$$

thus the input currents are given by

$$i_1 = d_1 i_A - d_2 i_B - \frac{1}{3}(i_A - i_B), \quad (7.3)$$

$$i_2 = d_3 i_A - d_4 i_B - \frac{1}{3} (i_A - i_B), \quad (7.4)$$

and

$$i_3 = d_5 i_A - d_6 i_B - \frac{1}{3} (i_A - i_B), \quad (7.5)$$

where d_1 to d_6 are the diode state functions defined in Chapter 2. Equations (7.3), (7.4), and (7.5) can be presented in a matrix form as

$$\begin{bmatrix} i_1 \\ i_2 \\ i_3 \end{bmatrix} = \begin{bmatrix} d_1 - \frac{1}{3} & -d_2 + \frac{1}{3} \\ d_3 - \frac{1}{3} & -d_4 + \frac{1}{3} \\ d_5 - \frac{1}{3} & -d_6 + \frac{1}{3} \end{bmatrix} \begin{bmatrix} i_A \\ i_B \end{bmatrix}. \quad (7.6)$$

Substituting (7.3), (7.4), and (7.5) in (7.1), we obtain

$$i_1 + i_2 + i_3 = (d_1 + d_3 + d_5 - 1)i_A - (d_2 + d_4 + d_6 - 1)i_B = 0, \quad (7.7)$$

which is always satisfied since

$$d_1 + d_3 + d_5 = 1 \quad (7.8)$$

and

$$d_2 + d_4 + d_6 = 1. \quad (7.9)$$

Since equations (7.6) are linearly dependent, one of them can be omitted from the system in order to compute the diode bridge load currents i_A and i_B as functions of the input currents. Omitting the third equation, i_A and i_B are given by

$$\begin{bmatrix} i_A \\ i_B \end{bmatrix} = \begin{bmatrix} d_1 - \frac{1}{3} & -d_2 + \frac{1}{3} \\ d_3 - \frac{1}{3} & -d_4 + \frac{1}{3} \end{bmatrix}^{-1} \begin{bmatrix} i_1 \\ i_2 \end{bmatrix}. \quad (7.10)$$

It can be proved that the system matrix of (7.10) is invertible for all possible combinations of the diode state functions. Thus, for any waveform of i_1 and i_2 , having $i_3 = -i_1 - i_2$, corresponding waveforms of i_A and i_B can be computed. Additional constraints imposed by the diode bridge are $i_A > 0$ and $i_B > 0$. If these additional constraints are satisfied, the required waveforms of the input currents can be obtained.

Let us assume that the input currents are purely sinusoidal, in phase with corresponding phase voltages,

$$i_1 = I_m \cos(\omega_0 t), \quad (7.11)$$

$$i_2 = I_m \cos\left(\omega_0 t - \frac{2\pi}{3}\right), \quad (7.12)$$

and

$$i_3 = I_m \cos\left(\omega_0 t - \frac{4\pi}{3}\right). \quad (7.13)$$

Substituting (7.11), (7.12), and (7.13) in (7.10), waveforms of the diode bridge load currents that provide undistorted input currents are obtained, and are presented in Fig. 7-1. The waveforms of Fig. 7-1 are periodic with the period equal to one third of the line period. Also, the waveforms are even functions, being symmetric over $\omega_0 t$, i.e.,

$$i_A(\omega_0 t) = i_A(-\omega_0 t) \quad (7.14)$$

and

$$i_B(\omega_0 t) = i_B(-\omega_0 t). \quad (7.15)$$

According to these properties, it is sufficient to define i_A and i_B in the phase angle region $0 < \omega_0 t < 60^\circ$. Expressions for i_A and i_B for $0 < \omega_0 t < 60^\circ$ are obtained from (7.10) as

$$i_A = i_1 - i_2 = I_m \left(\cos(\omega_0 t) - \cos\left(\omega_0 t - \frac{2\pi}{3}\right) \right) \quad (7.16)$$

and

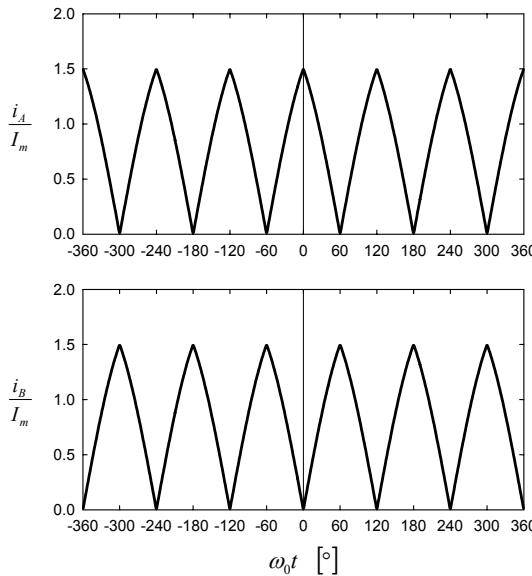


Figure 7-1. Waveforms of i_A and i_B for the ideal current injection.

$$i_B = i_1 + 2i_2 = i_2 - i_3 = I_m \left(\cos\left(\omega_0 t - \frac{2\pi}{3}\right) - \cos\left(\omega_0 t - \frac{4\pi}{3}\right) \right). \quad (7.17)$$

The waveforms of i_A and i_B can be represented by their Fourier series expansions:

$$i_A = \frac{3\sqrt{3}}{\pi} I_m \left(\frac{1}{2} + \sum_{n=1}^{+\infty} \frac{1-2(-1)^n}{9n^2-1} \cos(3n\omega_0 t) \right) \quad (7.18)$$

and

$$i_B = \frac{3\sqrt{3}}{\pi} I_m \left(\frac{1}{2} + \sum_{n=1}^{+\infty} \frac{(-1)^n - 2}{9n^2-1} \cos(3n\omega_0 t) \right). \quad (7.19)$$

The Fourier series expansions of (7.18) and (7.19) contain spectral components at triples of the line frequency, as was expected.

Current i_A that loads the positive output terminal of the diode bridge consists of a DC component equal to the output current, and an AC

component that is taken by the current injection network,

$$i_A = I_{OUT} + i_{IA}. \quad (7.20)$$

According to (7.18), the output current is

$$I_{OUT} = \frac{3\sqrt{3}}{2\pi} I_m, \quad (7.21)$$

while the current taken by the current injection network is given by the Fourier series expansion:

$$i_{IA} = \frac{3\sqrt{3}}{\pi} I_m \sum_{n=1}^{+\infty} \frac{1 - 2(-1)^n}{9n^2 - 1} \cos(3n\omega_0 t). \quad (7.22)$$

The same applies for the other current that loads the diode bridge,

$$i_B = I_{OUT} - i_{IB}, \quad (7.23)$$

and the second current taken by the current injection network is

$$i_{IB} = \frac{3\sqrt{3}}{\pi} I_m \sum_{n=1}^{+\infty} \frac{2 - (-1)^n}{9n^2 - 1} \cos(3n\omega_0 t). \quad (7.24)$$

Waveforms of i_{IA} and i_{IB} accompanied by the injected current $i_Y = i_{IA} + i_{IB}$ are presented in Fig. 7-2.

To analyze the spectra of i_{IA} and i_{IB} further, let us note that a factor of (7.22) equals

$$1 - 2(-1)^n = \begin{cases} 3, & \text{for odd } n \\ -1, & \text{for even } n \end{cases} \quad (7.25)$$

while the corresponding factor of (7.24) is

$$2 - (-1)^n = \begin{cases} 3, & \text{for odd } n \\ 1, & \text{for even } n \end{cases} \quad (7.26)$$

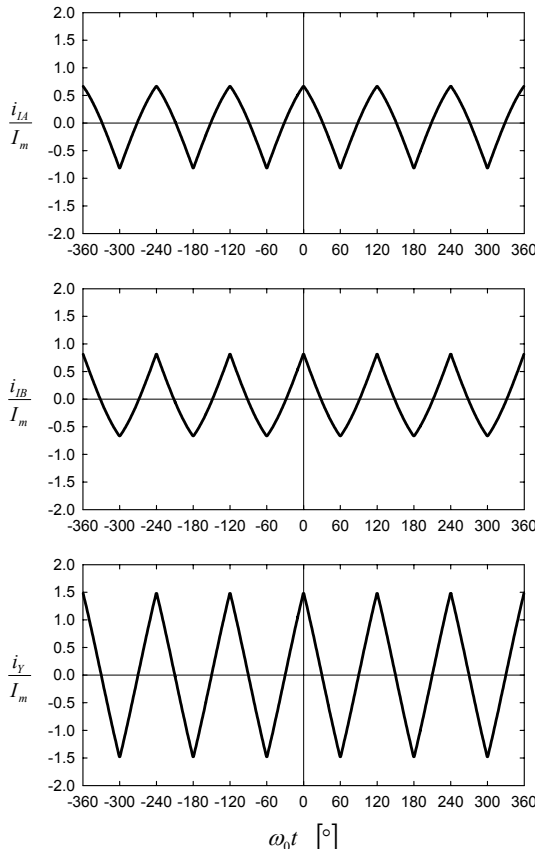


Figure 7-2. Waveforms of i_{IA} , i_{IB} and i_Y for the ideal current injection.

According to (7.25) and (7.26), it can be concluded that the currents from the rectifier output terminals behave in the same manner as the rectifier output terminal voltages, having the same spectral components at odd triples of the line frequency and spectral components with the same amplitudes and opposite phases at even triples of the line frequency. Thus, currents i_{IA} and i_{IB} can be treated as consisting of two components, one containing all spectral components at odd triples of the line frequency, and the other containing all spectral components at even triples of the line frequency. Applying this reasoning, currents of the current injection networks are expressed as

$$i_{IA} = i_{ODD} + i_{EVEN} \quad (7.27)$$

and

$$i_{IB} = i_{ODD} - i_{EVEN}, \quad (7.28)$$

where

$$i_{ODD} = \frac{3\sqrt{3}}{\pi} I_m \sum_{k=1}^{+\infty} \frac{3}{(6k-3)^2 - 1} \cos((6k-3)\omega_0 t) \quad (7.29)$$

and

$$i_{EVEN} = -\frac{3\sqrt{3}}{\pi} I_m \sum_{k=1}^{+\infty} \frac{1}{36k^2 - 1} \cos(6k\omega_0 t). \quad (7.30)$$

Waveforms of i_{ODD} and i_{EVEN} are shown in Fig. 7-3.

Now, let us remember that the spectrum of the average of the output terminal voltages is given by (2.17) as

$$v_{AV} = \frac{3\sqrt{3}}{\pi} V_m \sum_{k=1}^{+\infty} \frac{1}{(6k-3)^2 - 1} \cos((6k-3)\omega_0 t), \quad (7.31)$$

while the spectrum of the output voltage AC component is given by (2.12) as

$$\hat{v}_{OUT} = -\frac{3\sqrt{3}}{\pi} V_m \sum_{k=1}^{+\infty} \frac{2}{36k^2 - 1} \cos(6k\omega_0 t). \quad (7.32)$$

Let us define emulated resistance as the resistance sensed by the supply sources at the rectifier input

$$R_E = \frac{V_m}{I_m}, \quad (7.33)$$

which can be expressed in terms of the rectifier output voltage (2.11) and the output current (7.21) as

$$R_E = \frac{1}{2} \frac{V_{OUT}}{I_{OUT}}. \quad (7.34)$$

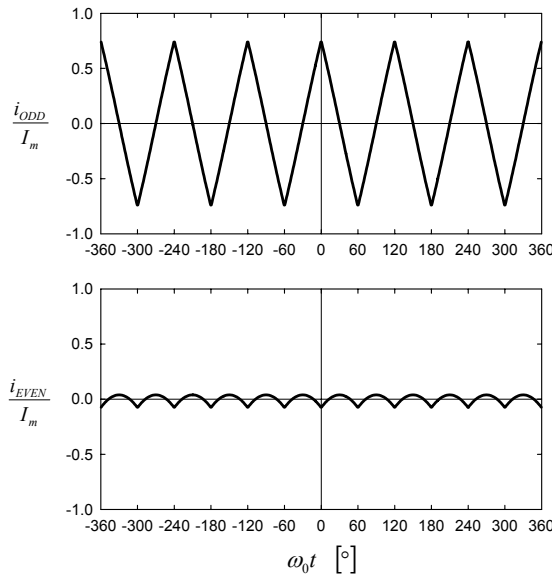


Figure 7-3. Waveforms of i_{ODD} and i_{EVEN} .

Now, from (7.31) and (7.29) we obtain a simple relation:

$$\frac{v_{AV}}{i_{ODD}} = \frac{1}{3} R_E, \quad (7.35)$$

and from (7.32) and (7.30) we obtain

$$\frac{\hat{v}_{OUT}}{i_{EVEN}} = 2R_E. \quad (7.36)$$

The injected current i_Y contains only spectral components at odd triples of the line frequency,

$$i_Y = i_{IA} + i_{IB} = 2i_{ODD} \quad (7.37)$$

resulting in

$$\frac{v_{AV}}{i_Y} = \frac{1}{6} R_E. \quad (7.38)$$

Relations (7.33), (7.36), and (7.38) are used in Chapter 8 in reference to the design of the current injection networks that provide the optimal current injection.

Assuming that power taken by the current injection network is dissipated, the output power of the rectifier is

$$P_{OUT} = V_{OUT} I_{OUT} = \frac{27}{2\pi^2} V_m I_m , \quad (7.39)$$

while the input power is

$$P_{IN} = \frac{3}{2} V_m I_m . \quad (7.40)$$

The difference is taken by the current injection network,

$$P_{INJ} = P_{IN} - P_{OUT} = \left(1 - \left(\frac{3}{\pi}\right)^2\right) P_{IN} = 8.81\% P_{IN} . \quad (7.41)$$

In this case, assuming that the power taken by the current injection network is dissipated, the rectifier efficiency is

$$\eta = \frac{P_{OUT}}{P_{IN}} = \left(\frac{3}{\pi}\right)^2 \approx 91.19\% , \quad (7.42)$$

which is negligibly lower than the efficiency in the case of the optimal third-harmonic current injection given by (5.36). The actual difference between (7.42) and (5.36) is

$$\Delta\eta = \frac{32}{35} - \left(\frac{3}{\pi}\right)^2 = 0.24\% . \quad (7.43)$$

Thus, ideal sinusoidal waveforms of the rectifier input currents can be provided applying current injection, with a negligible decrease in the rectifier efficiency. The problem that remains is a design of adequate current injection networks, which is the topic of the next chapter.

Chapter 8

CURRENT INJECTION NETWORKS FOR THE OPTIMAL CURRENT INJECTION

The optimal current injection analyzed in Chapter 7 offers an attractive opportunity to provide ideally sinusoidal waveforms of the input currents, in phase with corresponding phase voltages. In that case, the three-phase AC power supply observes symmetric and linear resistive load without any distortion of the input currents, with unity power factor. Conditions to provide optimal current injection are derived in Chapter 7, and they are expressed by (7.27), (7.28), (7.35), and (7.36). Since all of these equations are linear and algebraic without any derivatives, it is possible to obtain the current injection network by applying linear resistive circuits if we provide v_{AV} specified by (2.16) and (2.17), and \hat{v}_{OUT} specified by (2.12). In this chapter, the current injection networks that provide the optimal current injection are analyzed. These current injection networks were originally proposed in [26] and [35].

1. BASIC TOPOLOGIES

As shown in Chapter 7, the problem of obtaining a current injection network that provides the optimal current injection reduces to a problem of providing the currents that the current injection network takes from the diode bridge output terminals, specified by

$$i_{IA} = i_{ODD} + i_{EVEN} \quad (8.1)$$

and

$$i_{IB} = i_{ODD} - i_{EVEN}, \quad (8.2)$$

where

$$i_{ODD} = 3 \frac{v_{AV}}{R_E} \quad (8.3)$$

and

$$i_{EVEN} = \frac{\hat{v}_{OUT}}{2R_E} \quad (8.4)$$

The easiest part to obtain is the branch that injects the harmonics at even triples of the line frequency, specified by (8.4). First, we have to obtain \hat{v}_{OUT} , i.e., to remove the DC component of the output voltage. This can be done by applying a capacitor with a capacitance large enough that variations of its voltage can be neglected in comparison to \hat{v}_{OUT} . Second, we have to apply a resistor of resistance equal to $2R_E$ to provide the proper amplitude of the current, according to (8.4). This is achieved via C_{EVEN} and R_{EVEN} in the right-hand branch of the current injection network shown in Fig. 8-1. Since

$$i_{EVEN} = \frac{\hat{v}_{OUT}}{R_{EVEN}}, \quad (8.5)$$

the resistance of R_{EVEN} is

$$R_{EVEN} = 2R_E. \quad (8.6)$$

Calculating the RMS value of the voltage across R_{EVEN} , the power dissipated on this resistor is

$$P_{EVEN} = \frac{2\pi^2 + 3\sqrt{3}\pi - 36}{4\pi^2} P_{IN} = 0.16\% P_{IN}. \quad (8.7)$$

Thus, a very small part of the power taken by the current injection network, given by (7.41), is dissipated on R_{EVEN} .

A somewhat bigger problem is to provide i_{ODD} . In the circuit diagram of Fig. 8-1, capacitors C_{ODD} are applied to remove the DC components of the rectifier output terminal voltages. The capacitance of these capacitors should be large enough to provide small AC components of their voltages in comparison to the AC components of the output terminal voltages. After the DC components of the voltages are removed, a 1:1 transformer can be applied to provide the average of the output terminal voltages, v_{AV} . As discussed in Section 6.5, this transformer completely rejects spectral components at even triples of the line frequency, providing

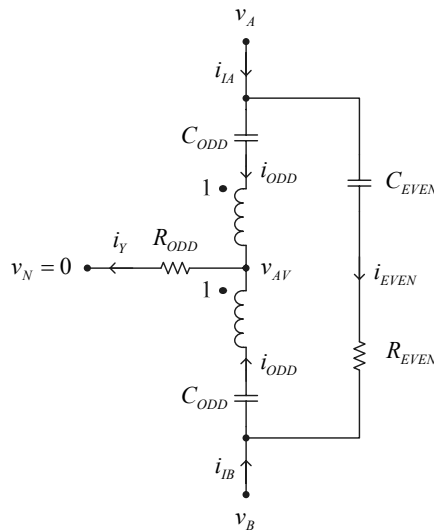


Figure 8-1. Basic current injection network. © [2002] IEEE.

$$i_Y = 2i_{ODD} = \frac{v_{AV}}{R_{ODD}}. \quad (8.8)$$

Thus, to satisfy (8.3), the resistance of R_{ODD} should be

$$R_{ODD} = \frac{1}{6} R_E. \quad (8.9)$$

The power dissipated on R_{ODD} is obtained by computing the RMS value of the voltage v_{AV} across the resistor, and the result is

$$P_{ODD} = \frac{2\pi - 3\sqrt{3}}{4\pi} P_{IN} = 8.65\% P_{IN}. \quad (8.10)$$

The power dissipated on R_{ODD} and on R_{EVEN} add up to the power predicted to be taken by the current injection network

$$P_{INJ} = P_{ODD} + P_{EVEN} = \left(1 - \left(\frac{3}{\pi}\right)^2\right) P_{IN} = 8.81\% P_{IN}. \quad (8.11)$$

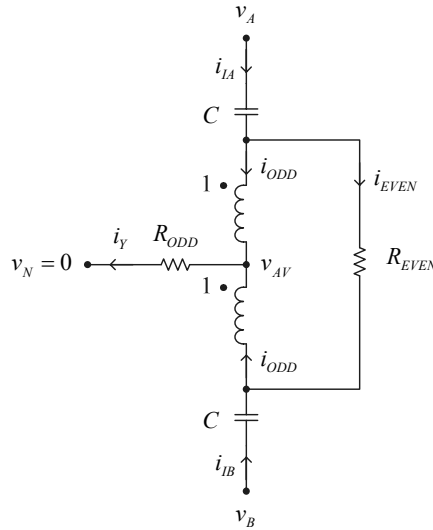


Figure 8-2. Current injection network applying two capacitors. © [2002] IEEE.

The current injection network of Fig. 8-1 can be slightly modified and one capacitor can be omitted, noting that C_{ODD} capacitors are applied to remove the DC component of the output terminal voltages, while the C_{EVEN} capacitor is applied to remove the DC component of the output voltage, being exposed to a voltage equal to double the voltage C_{ODD} capacitors are exposed to, and doing essentially the same job. A modified structure of the current injection network is presented in Fig. 8-2, and assuming low ripple of the capacitor voltages in comparison to the ripple of the output terminal voltages, the voltage across R_{EVEN} is the same as in the current injection network of Fig. 8-1; thus the current is the same: i_{EVEN} . Power dissipations on the resistors are the same as in the current injection network of Fig. 8-1. In all of the subsequent current injection networks, two capacitors are applied to remove the DC components of the output terminal voltages because of the need to construct both the currents i_{ODD} and i_{EVEN} .

2. DERIVED TOPOLOGIES

The current injection network in Fig. 8-2 satisfies all of the requirements imposed on the current injection network to provide the optimal current injection, and requires only two capacitors. Slight modifications of that current injection network are possible, primarily to include some parasitic effects in the current injection network model, and to balance the power dissipated on the current injection network resistors.

The first of the derived topologies is presented in Fig. 8-3. In this current injection network, the resistance distribution is applied in the same manner as in the current injection network for the third-harmonic injection presented in Fig. 6-11, having $0 < a < 1$. In this manner, losses in vertical branches of the current injection network can be included in the calculations, being modeled via $2aR_{ODD}$. The power dissipated on R_{ODD} , given by (8.10), is split on three resistors.

The second of the derived topologies, presented in Fig. 8-4, applies simultaneous injection of harmonics at even and odd triples of the line frequency. Resistors R_2 provide injection of i_{EVEN} ; thus their resistance is

$$R_2 = \frac{1}{2} R_{EVEN} = R_E . \quad (8.12)$$

Besides the injection of i_{EVEN} , a part of i_{ODD} is injected by R_2 . The remaining part of i_{ODD} is injected by applying the 1:1 transformer, and the resistors being fractions of R_1 . To provide the proper amount of harmonics at odd triples of the line frequency, the resistance of R_1 should be

$$R_1 = \frac{1}{4} R_E . \quad (8.13)$$

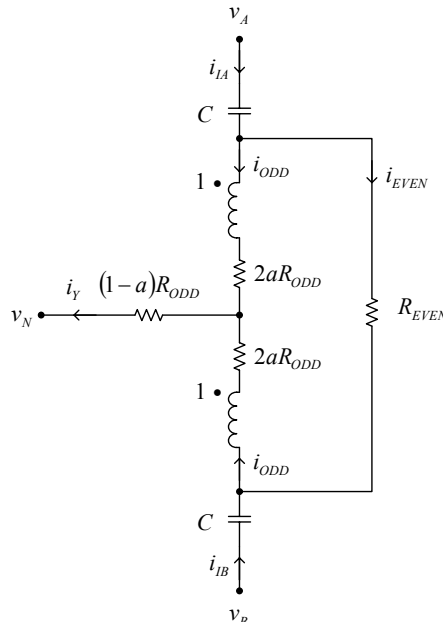


Figure 8-3. Current injection network applying resistance distribution. © [2002] IEEE.

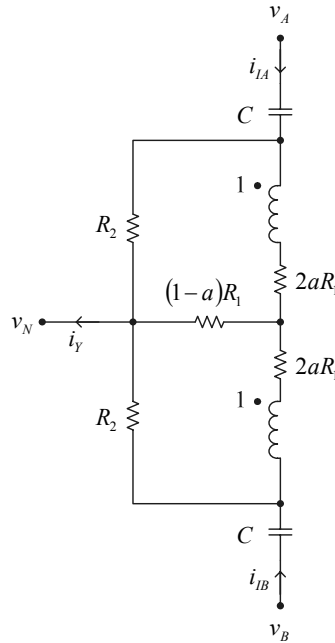


Figure 8-4. Current injection network applying simultaneous injection of odd and even harmonics.

The overall power dissipated on both of the resistors labeled by R_2 is

$$P_2 = \frac{4\pi^2 + 3\sqrt{3}\pi - 54}{6\pi^2} P_{IN} = 3.04\% P_{IN}, \quad (8.14)$$

while the power dissipated on the three resistors being fractions of R_l is

$$P_1 = \frac{2\pi - 3\sqrt{3}}{6\pi} P_{IN} = 5.77\% P_{IN}. \quad (8.15)$$

Again, the power dissipated on the current injection network resistors adds up to the power taken by the current injection network,

$$P_{INJ} = P_1 + P_2 = \left(1 - \left(\frac{3}{\pi}\right)^2\right) P_{IN} = 8.81\% P_{IN}. \quad (8.16)$$

Application of the current injection network in Fig. 8-4 can provide some savings in the 1:1 transformer volt-ampere rating, discussed in Section 8.4.

Applying the described techniques, many more variations of the current injection network in Fig. 8-2 are possible, but besides including losses of the components in the computation, they have limited practical value.

3. CHOICE OF THE CAPACITORS

Another issue of practical interest is the size of the capacitors applied in the current injection network. In the analyses presented so far, the capacitance is considered infinite, i.e., the ripple of the voltage across the capacitors is neglected. For practical application of the optimal current injection, it is important that acceptable values of the capacitance justify the small ripple approximation. To analyze the influence of the capacitors on the input current THD, the same method of equivalent circuits is applied as in Chapter 6 to analyze the dependence of the input current THD on the current injection network Q -factor and the resistance distribution parameter.

Impedance that relates the rectifier output terminal voltages to the currents the current injection network takes from the rectifier output terminals is

$$Z(jn\omega_0 t) = \frac{V_{A,n}}{I_{IA,n}} = \frac{V_{B,n}}{I_{IB,n}} = R_E \begin{cases} \frac{1}{3} + \frac{1}{j\gamma n}, & \text{for odd } n \\ 1 + \frac{1}{j\gamma n}, & \text{for even } n \end{cases} \quad (8.17)$$

where the parameter γ is defined as

$$\gamma = 3\omega_0 R_E C. \quad (8.18)$$

The dependence of the input current THD on the parameter γ is computed by applying the same methods as in Chapter 6, and the result is presented in Fig. 8-5. The solid line in Fig. 8-5 indicates the simulation result, while the dotted line indicates an empirical approximation:

$$THD \approx \frac{40\%}{\gamma}. \quad (8.19)$$

Since the difference between the actual curve and its approximation is negligible in the area of interest, the approximate curve may be used in all of the calculations, and the capacitance of the capacitors is given by

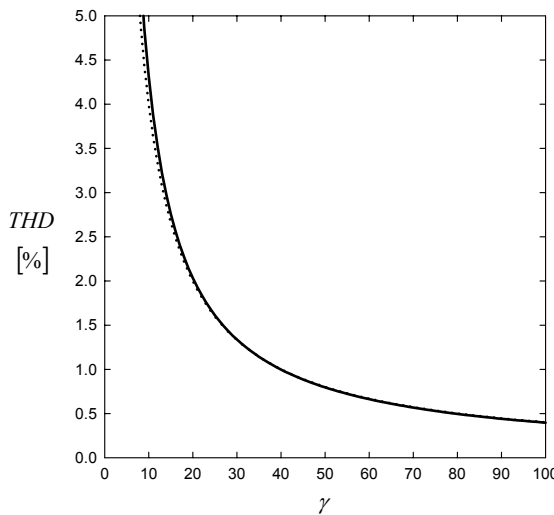


Figure 8-5. Dependence of the input current THD on γ .

$$C = \frac{1}{3\omega_0 R_E} \frac{40\%}{THD}, \quad (8.20)$$

where THD represents the allowed THD of the input current, and R_E represents the emulated resistance at the rectifier input at the considered load current. The capacitance of the capacitors increases with decreases of the emulated resistance under the constraint of fixed THD; thus the capacitance should be computed taking the maximum power of the rectifier as a critical situation.

The voltage across the capacitors is equal to

$$V_C = \frac{3\sqrt{3}}{2\pi} V_m \approx 0.83 V_m \approx 1.17 V_{PRMS}, \quad (8.21)$$

and it can be considered constant since the ripple is neglected. Electrolytic capacitors can be applied since there is no reason to worry about the capacitor voltage polarity caused by the AC component.

4. VOLT-AMPERE RATING OF THE TRANSFORMER

The 1:1 transformer applied in the current injection network for the optimal current injection has a somewhat different volt-ampere rating in comparison to the transformer in the current injection network for the third-harmonic current injection presented in Fig. 6-11, due to the different RMS values of the winding currents. Voltages across the transformer windings are the same as in the third-harmonic current injection case; thus the maximum of the core flux is the same as given by (6.38):

$$\Phi_{\max} = \frac{\sqrt{3}}{2\pi} \left(\sqrt{\pi^2 - 9} - 3 \arccos\left(\frac{3}{\pi}\right) \right) \frac{V_m}{n\omega_0}. \quad (8.22)$$

The RMS values of the winding currents are

$$I_{T\text{RMS}} = \frac{3}{4} I_m \sqrt{2 - \frac{3\sqrt{3}}{\pi}}. \quad (8.23)$$

These values result in the transformer volt-ampere rating, defined by (4.3), equal to

$$S_T = \frac{\omega_0}{2\sqrt{2}} \Phi_{\max} (2nI_{T\text{RMS}}). \quad (8.24)$$

The volt-ampere rating expressed in terms of the rectifier input power is equal to

$$S_T = \frac{1}{4\pi} \sqrt{3 - \frac{9\sqrt{3}}{2\pi}} \left(\sqrt{\pi^2 - 9} - 3 \arccos\left(\frac{3}{\pi}\right) \right) P_{IN} \approx 0.16\% P_{IN}, \quad (8.25)$$

which is very close to the value given by (6.41). Savings in the volt-ampere rating of the 1:1 transformer can be obtained by applying simultaneous injection of harmonics at even and odd triples of the line frequency, applying the current injection network of Fig. 8-4 or its derivatives, since in that way the windings of the transformer will be exposed to the lower currents. However, although a significant percentage of the transformer volt-ampere rating can be saved in this way, the overall savings will not be significant because of the low volt-ampere rating (8.25).

5. VOLT-AMPERE RATING OF THE CURRENT INJECTION DEVICE

In the case of the optimal third-harmonic current injection, the RMS value of the injected current is equal to

$$I_{YRMS3} = \frac{3}{2\sqrt{2}} I_{OUT}. \quad (8.26)$$

On the other hand, in the case of the optimal current injection, the RMS value of the injected current is

$$I_{YRMSI} = \frac{3}{2} I_m \sqrt{2 - \frac{3\sqrt{3}}{\pi}} = I_{OUT} \sqrt{\frac{2\pi^2}{3} - \sqrt{3}\pi}, \quad (8.27)$$

resulting in a slight difference of the volt-ampere ratings of the current injection devices. The ratio of the RMS values of the currents is

$$\frac{I_{YRMSI}}{I_{YRMS3}} = \frac{2}{3} \sqrt{\frac{4\pi^2}{3} - 2\pi\sqrt{3}} \approx 1.00591. \quad (8.28)$$

It is convenient to express volt-ampere ratings of magnetic devices in terms of the rectifier input power, and this practice has been extensively used before. The input power in the case of the optimal third-harmonic current injection is

$$P_{IN3} = \frac{105\sqrt{3}}{32\pi} V_m I_{OUT} = \frac{35}{32} V_{OUT} I_{OUT}, \quad (8.29)$$

while in the case of the optimal current injection it is

$$P_{INI} = \frac{3}{2} V_m I_m = \frac{\pi^2}{9} V_{OUT} I_{OUT}. \quad (8.30)$$

The ratio between the input powers is

$$\frac{P_{IN1}}{P_{IN3}} = \frac{32\pi^2}{315} \approx 1.00262. \quad (8.31)$$

According to the volt-ampere rating definitions given by (4.14) and (4.19), in the case of the ideal current injection, the volt-ampere rating of the current injection device is given by

$$S_{CID1} = S_{CID3} \frac{I_{YRMS1}}{I_{YRMS3}}, \quad (8.32)$$

expressed in terms of the current injection device required by the rectifier that applies the optimal third-harmonic current injection and operates with the same input voltages. In terms of the rectifier input power, the volt-ampere rating is

$$\frac{S_{CID1}}{P_{IN1}} = \frac{S_{CID3}}{P_{IN3}} \frac{I_{YRMS1}}{I_{YRMS3}} \frac{P_{IN3}}{P_{IN1}} = s \frac{S_{CID3}}{P_{IN3}}, \quad (8.33)$$

where s is a scaling factor given by

$$s = \frac{I_{YRMS1}}{I_{YRMS3}} \frac{P_{IN3}}{P_{IN1}} = \frac{105}{16\pi^2} \sqrt{\frac{4\pi^2}{3} - 2\pi\sqrt{3}} \approx 1.00328. \quad (8.34)$$

Thus, the ideal current injection requires an approximately 3.3% higher volt-ampere rating of the current injection device than the third-harmonic current injection, which is a negligible difference. This result applies regardless of the current injection device except in the case of the current injection at the transformer secondary neutral point, which is analyzed separately and in detail in Sections 4.7 and 4.8.

In the case of the current injection device obtained as a zigzag autotransformer described in Section 4.3, which is the most likely to be applied owing to the negligible parasitic inductance of the neutral point and low volt-ampere rating, the volt-ampere rating specified by (4.38) in the case of the ideal current injection becomes

$$S_{CID1} = P_{IN} \sqrt{\frac{1}{3} - \frac{\sqrt{3}}{2\pi}} = 24.01\% P_{IN}. \quad (8.35)$$

6. INFLUENCE OF THE OUTPUT CURRENT RIPPLE

Analytical results presented up to this point neglected the influence of the output current ripple on the input current THD. Here, this influence is studied under the assumption that the load can be represented by a parallel combination of a constant current source and a linear resistor with the conductance G_{OUT} :

$$i_{OUT} = I_{OUT} + G_{OUT}\hat{v}_{OUT}, \quad (8.36)$$

where \hat{v}_{OUT} is the AC component of the output voltage. In practice, all resistive loads that can be encountered in practice can be covered by (8.36), applying linearization. Some characteristic values of G_{OUT} are $G_{OUT} = 1/(2R_E)$ if the load is a linear resistor, and $G_{OUT} = -1/(2R_E)$ if the load is a constant power sink, which is a nonlinear load, thus the conductance is the incremental conductance in the operating point determined by V_{OUT} . In the range $G_{OUT} < 0$, the rectifier operates in the continuous conduction mode, and the input current THD can easily be computed by applying numerical simulation. The result is presented in Fig. 8-6, and indicates that the input current THD is lower than 4% in the entire range of loads, starting from the constant power load and ending at the constant current load. In the case $G_{OUT} > 0$, the rectifier operates in the discontinuous conduction mode, and computation of the input current THD is much more difficult. However, the experimental results indicate that the input current THD is within the range of several percent even in this case. Much more important is the fact that incremental conductance of the load is the parameter that can easily be compensated for. Let us consider the current injection network shown in Fig. 8-2 as the most common one. To provide adequate injection of the harmonics at even triples of the line frequency, a parallel combination of R_{EVEN} and $1/G_{OUT}$ should be equal to $2R_E$,

$$\frac{R_{EVEN}}{1 + G_{OUT}R_{EVEN}} = 2R_E. \quad (8.37)$$

Thus, adjusting R_{EVEN} to the value

$$R_{EVEN} = \frac{2R_E}{1 - 2R_EG_{OUT}}, \quad (8.38)$$

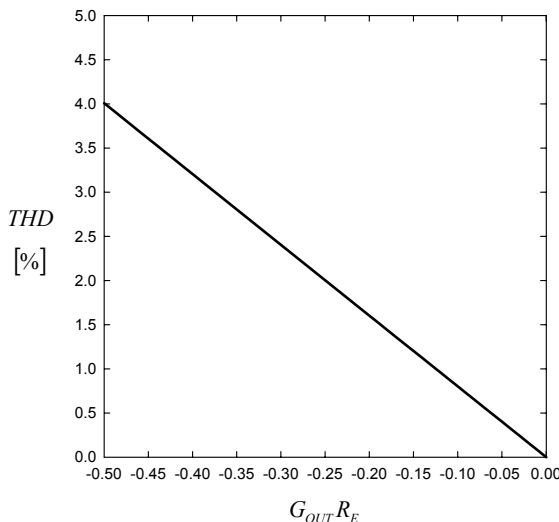


Figure 8-6. Dependence of the input current THD on G_{OUT} .

the optimal current injection can be achieved, and the effects caused by G_{OUT} can be compensated for. With positive value of R_{EVEN} , the entire range of loads starting from constant power load and ending at linear resistor can be covered. Formula (8.38) applies for the current injection networks of Figs. 8.1, 8.2, and 8.3. The technique presented in this section can also be applied to derive proper values for the resistors in the current injection network of Fig. 8-4.

Chapter 9

OPERATION OF THE RECTIFIER IN THE DISCONTINUOUS CONDUCTION MODE

The analysis of the third-harmonic current injection presented so far assumes that in each time point two of the diodes in the three-phase diode bridge conduct—the one connected to the highest of the phase voltages, and the one connected to the lowest of the phase voltages. This operation mode is termed the continuous conduction mode, and it is analyzed in detail in Chapter 2. In the continuous conduction mode, the rectifier circuit can be represented by a periodically switched linear circuit model with the switching controlled by the time variable. This greatly simplifies the analysis and enables extensive application of the Fourier series method, providing closed form solutions in many cases. The most important results of Chapter 2 are spectra of the output terminal voltages and the concept of diode state functions, useful to express the rectifier input currents in terms of the currents that load the rectifier output terminals.

In the case of three-phase diode bridge rectifiers that apply current injection, different operating modes may occur. Let us consider the rectifier

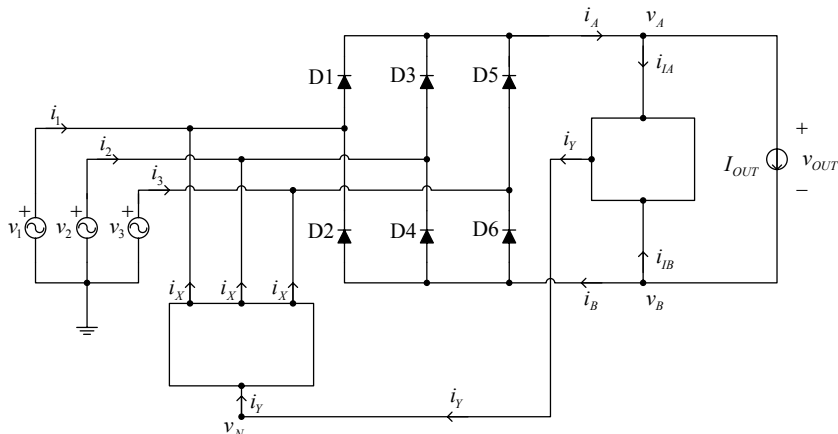


Figure 9-1. The rectifier.

shown in Fig. 9-1. In addition to the three-phase diode bridge, the rectifier in Fig. 9-1 consists of a current injection network and a current injection device. Current injection devices are discussed in detail in Chapter 4. The current injection network C described in Chapter 6 is the type of current injection network that is assumed to be applied. If the current injection is not applied, $i_A = I_{OUT}$ and $i_B = I_{OUT}$, and the rectifier operates in the continuous conduction mode. The current injection network takes currents i_{IA} and i_{IB} from the diode bridge output terminals, causing the waveforms of i_A and i_B to be different than if the current injection is not applied. In the case of the optimal third-harmonic current injection, $i_A > 0$ and $i_B > 0$ during the whole period as depicted in Fig. 5-9, and the rectifier operates in the continuous conduction mode. The amplitude of the injected current is determined by the equivalent resistance of the current injection system in that case, and the optimal value is given by (6.10). Lower values of the equivalent resistance of the current injection system provide a higher amplitude of the injected current. However, this process cannot be extended indefinitely, since the load currents of the three-phase diode bridge have to be positive, $i_A > 0$ and $i_B > 0$. This limits the injected current instantaneous value to the range

$$-2I_{OUT} < i_Y < 2I_{OUT}. \quad (9.1)$$

The boundary between the continuous and the discontinuous conduction mode is reached for

$$R = \frac{3\sqrt{3}}{16\pi} \frac{V_m}{I_{OUT}}, \quad (9.2)$$

and lower values of R result in the discontinuous conduction mode of the rectifier. In the case of the discontinuous conduction mode, there are intervals of time when only one of the diodes in the diode bridge conducts. This results in altered waveforms of v_A and v_B , different than depicted in Fig. 2-3, thus the Fourier series expansions of (2.7) and (2.8) are not applicable. This is the mechanism that limits the amplitude of the injected current.

Now, let us consider an extreme—the case $R = 0$. In that case, the power taken by the current injection network is zero, since the average power on all of the current injection system components is equal to zero. In the case of the continuous conduction mode, improvement of the input current THD is obtained at the expense of the power taken by the current injection network as discussed in Chapter 5, and illustrated in Fig. 5-8. However, experimental experience with the discontinuous conduction mode indicates that improvement in the input current THD can be obtained in this mode with negligible

losses in the current injection network. The amplitude and phase of the injected current are suboptimal in this case, but acceptable. Thus, from the experimental results it became obvious that complete analysis of the rectifier discontinuous conduction mode might be of practical interest. The problem resisted efforts toward a solution for a long time, and the first results were published in 2002, in [6]. Complete analysis of the discontinuous conduction mode is given in [7].

In this chapter, the results of [7] are presented in a somewhat expanded form. The discontinuous conduction mode is analyzed to determine its suitability for practical application. A piecewise linear model of the rectifier is derived first, and normalization of the variables is performed to prepare the model for numerical simulation, as well as to generalize applicability of the results of numerical solution. Four special cases are discussed next, two of them on the boundary with the continuous conduction mode, and the other two on the opposite side with negligible losses in the current injection network. For each of the mode boundaries, the analysis is performed for the case of low and high filtering, where the term “filtering” determines level of reduction of the higher order harmonics of i_y . These four cases are analyzed to determine the possible application area of the discontinuous conduction mode. From the analysis of the rectifier operation in the high filtering case, an approximate method of the rectifier analysis is proposed. The method is based on approximation of the terminal voltage spikes by the δ -function impulses. Results of the rectifier analysis applying numerical methods are presented next, and compared to the approximate method derived previously.

1. THE RECTIFIER MODEL

To start the analysis, let us assume that the rectifier is supplied by an undistorted symmetrical three-phase voltage system

$$v_p = V_m \cos\left(\omega_0 t - (p-1)\frac{2\pi}{3}\right), \quad (9.3)$$

for $p \in \{1, 2, 3\}$, and that the line impedance is low enough to be neglected. The current injection device is characterized by

$$i_X = \frac{1}{3} i_Y \quad (9.4)$$

and

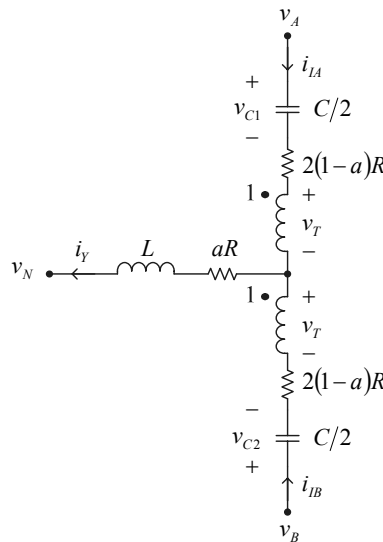


Figure 9-2. The current injection network.

$$v_N = \frac{1}{3}(v_1 + v_2 + v_3) = 0. \quad (9.5)$$

In the analysis that follows, we focus on the current injection network proposed in Section 6.5 and shown in Fig. 9-2. It consists of two capacitors with the capacitance equal to $C/2$, one 1:1 transformer, and an inductor. Losses in the components are modeled by three resistors in Fig. 9-2, and it is assumed that losses in the vertical branches are the same, since the circuit is symmetric. Parameter a is named the resistance distribution parameter and its value is in the range $0 \leq a \leq 1$. Losses in the current injection device are assumed to be modeled by a series resistance, included in aR . Thus, losses of all elements of the current injection system are included in the current injection network model.

To reduce the number of nonlinear elements, the rectifier presented in Fig. 9-1 that applies the current injection network in Fig. 9-2 can be represented by an equivalent circuit presented in Fig. 9-3. In the circuit in Fig. 9-3, the diode bridge is represented by diodes DA and DB to enforce $i_A \geq 0$ and $i_B \geq 0$, respectively. This is crucial to model the rectifier behavior in the discontinuous conduction mode. Operation of D1, D3, and D5 is modeled by the voltage source:

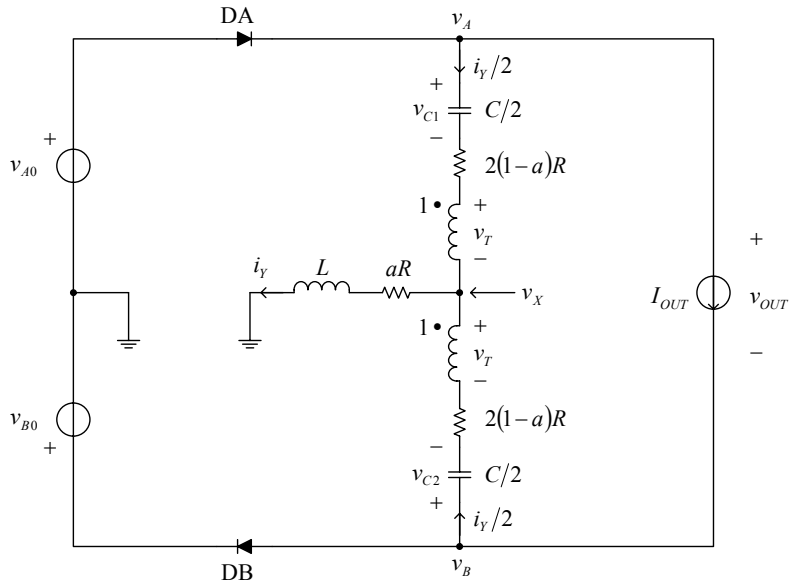


Figure 9-3. Equivalent model of the rectifier.

$$v_{A0} = \max(v_1, v_2, v_3), \quad (9.6)$$

while operation of D2, D4, and D6 is modeled by

$$v_{B0} = \min(v_1, v_2, v_3). \quad (9.7)$$

In this manner, the number of nonlinear elements in the circuit is reduced from six to two, which significantly simplifies the analysis.

To further simplify the analysis of the rectifier, let us note that the transformer forces i_{IA} and i_{IB} are equal:

$$i_{IA} = i_{IB} = \frac{1}{2}i_Y. \quad (9.8)$$

Thus, currents of the capacitors are the same, equal to $i_Y/2$, which results in

$$i_Y = C \frac{dv_{C1}}{dt} = C \frac{dv_{C2}}{dt}. \quad (9.9)$$

This result is applicable regardless of the conduction state of DA and DB.

Let us assume that DA and DB conduct, i.e., $i_A > 0$ and $i_B > 0$. Assuming the diodes are ideal, $v_A = v_{A0}$ and $v_B = v_{B0}$ in this case. Applying Kirchhoff's voltage law, and substituting for some of the element characteristics, in the loop from v_N to v_A we obtain

$$v_A = L \frac{di_Y}{dt} + aRi_Y + v_T + 2(1-a)R \frac{i_Y}{2} + v_{C1}, \quad (9.10)$$

while in the loop from v_N to v_B we obtain

$$v_B = L \frac{di_Y}{dt} + aRi_Y - v_T + 2(1-a)R \frac{i_Y}{2} + v_{C2}. \quad (9.11)$$

Combining the above equations, we obtain an equation in a suitable form for the analysis that follows:

$$\frac{v_A + v_B}{2} = L \frac{di_Y}{dt} + Ri_Y + \frac{v_{C1} + v_{C2}}{2}. \quad (9.12)$$

An average of the voltages across the capacitors will be observed frequently in the equations; thus let us define a special symbol to represent this quantity:

$$v_C = \frac{v_{C1} + v_{C2}}{2}. \quad (9.13)$$

In this manner, (9.12) can be rearranged as

$$L \frac{di_Y}{dt} = -Ri_Y - v_C + \frac{v_{A0} + v_{B0}}{2}, \quad (9.14)$$

taking $v_A = v_{A0}$ and $v_B = v_{B0}$ in this mode, since the diodes conduct. On the other hand, the element characteristics of the capacitors in terms of v_C are expressed as

$$C \frac{dv_C}{dt} = i_Y. \quad (9.15)$$

Equations (9.14) and (9.15) form a system of state equations sufficient to represent the current injection network when DA and DB conduct. Diode DA

conducts for $i_A > 0$, which can be represented in terms of i_Y and I_{OUT} as

$$I_{OUT} + \frac{1}{2}i_Y \geq 0. \quad (9.16)$$

In the same manner, condition $i_B > 0$ can be rephrased as

$$I_{OUT} - \frac{1}{2}i_Y \geq 0. \quad (9.17)$$

If condition (9.16) is violated, diode DA turns off and remains off as long as the condition

$$v_A > v_{A0} \quad (9.18)$$

is satisfied. In that case, the system of differential equations that describes the rectifier survives a dynamic degeneration, since the inductor current is

$$i_Y = -2I_{OUT}, \quad (9.19)$$

while the differential equation that describes the capacitor voltage remains in the same form:

$$C \frac{dv_C}{dt} = -2I_{OUT}. \quad (9.20)$$

To compute the output voltage and to express (9.18) in terms of the state variables, note that node voltage v_X (Fig. 9-3) is given by

$$v_X = L \frac{di_Y}{dt} + aRi_Y = aRi_Y, \quad (9.21)$$

since I_{OUT} is assumed constant. The voltage across the transformer windings can be computed from the loop from v_X to v_B , and since $v_B = v_{B0}$ we obtain

$$v_T = v_X - v_{B0} + v_{C2} + (1-a)Ri_Y. \quad (9.22)$$

The equation for v_A thus takes the form

$$v_A = v_X + v_T + (1-a)Ri_Y + v_{C1}, \quad (9.23)$$

and since $i_Y = -2I_{OUT}$, we finally obtain

$$v_A = -v_{B0} - 4RI_{OUT} + 2v_C. \quad (9.24)$$

On the other hand, when condition (9.17) is violated, DB goes off and remains off while

$$v_B < v_{B0}, \quad (9.25)$$

resulting in the dynamic degeneration of the inductor current

$$i_Y = 2I_{OUT}, \quad (9.26)$$

again. The differential equation over the capacitor voltage takes the form

$$C \frac{dv_C}{dt} = 2I_{OUT}. \quad (9.27)$$

Again, to express (9.25) in terms of the state variables, we determine

$$v_X = aRi_Y, \quad (9.28)$$

$$v_T = v_{A0} - v_{C1} - (1-a)Ri_Y - v_X, \quad (9.29)$$

and since $i_Y = 2I_{OUT}$,

Table 9-1. Piecewise linear model of the rectifier.

State	Equations	Conditions	Transition if the condition is violated
1	$L \frac{di_Y}{dt} = -Ri_Y - v_C + \frac{v_{A0} + v_{B0}}{2}$	$-2I_{OUT} \leq i_Y$	to state 2
	$C \frac{dv_C}{dt} = i_Y$	$i_Y \leq 2I_{OUT}$	
2	$i_Y = -2I_{OUT}$	$v_C > \frac{v_{A0} + v_{B0}}{2} + 2RI_{OUT}$	to state 1
	$C \frac{dv_C}{dt} = -2I_{OUT}$		
3	$i_Y = 2I_{OUT}$	$v_C < \frac{v_{A0} + v_{B0}}{2} - 2RI_{OUT}$	to state 1
	$C \frac{dv_C}{dt} = 2I_{OUT}$		

$$v_B = -v_{A0} + 4RI_{OUT} + 2v_C . \quad (9.30)$$

The results of (9.18) to (9.30) are summarized in Table 9-1, where the state equations are accompanied by the boundary conditions and the transition rules. Two of the modes, mode 2 and mode 3, characterize discontinuous conduction intervals of the rectifier. A direct transition between these two modes is not possible, since the inductor current is continuous in time. From the equations summarized in Table 9-1, we can conclude that the value of the resistance distribution parameter a does not affect the rectifier operation. The model given in Table 9-1 is a piecewise linear model, and it enables simple simulation of the rectifier.

2. NORMALIZATION

Equations summarized in Table 9-1 enable us to analyze any particular rectifier, i.e. to determine waveforms of the voltages and currents for a given set of the rectifier parameters. However, to generalize the results, it is convenient to perform normalization of the rectifier voltages and currents, which reduces the number of variables that affect the rectifier operation.

To normalize the rectifier voltages, the amplitude of the input voltage V_m is chosen and all of the voltages v are substituted by their normalized values m according to

$$m = \frac{v}{V_m} . \quad (9.31)$$

Next, let us define a base resistance for the normalization, and for this quantity a characteristic resistance of the equivalent LC circuit is chosen,

$$R_0 = \sqrt{\frac{L}{C}} . \quad (9.32)$$

Thus, the normalized value of the rectifier parasitic resistance is obtained as

$$\rho = \frac{R}{R_0} . \quad (9.33)$$

As a basis for normalization of currents, V_m/R_0 should be chosen to preserve the form of Ohm's law. Thus, all of the rectifier currents i are represented by their normalized values j according to

$$j = \frac{R_0}{V_m} i . \quad (9.34)$$

Normalization over time is performed representing the time variable by its phase-angle equivalent,

$$\varphi = \omega_0 t , \quad (9.35)$$

where ω_0 is the angular frequency of the input voltage.

The frequency when the equivalent circuit of the current injection network exposes phase resonance is

$$\omega_R = \frac{1}{\sqrt{LC}} . \quad (9.36)$$

Let us define resonance parameter r as

$$r = \frac{\omega_R}{3\omega_0} . \quad (9.37)$$

If the equivalent circuit of the current injection network is in phase resonance with the triple of the line frequency, i.e., the current injection network is tuned to the third harmonic, the value of the resonance parameter is $r=1$; thus parameter r represents a mismatch between the actual resonant and the triple of the line frequency. This parameter, along with R_0 , represents L and C in the set of normalized equations.

Table 9-2. Normalized equations of the rectifier model.

State	Equations	Conditions	Transition if the condition is violated
1	$\frac{dj_Y}{d\varphi} = 3r \left(-\rho j_Y - m_C + \frac{m_{A0} + m_{B0}}{2} \right)$	$-2J_{OUT} \leq j_Y$	to state 2
	$\frac{dm_C}{d\varphi} = 3rj_Y$	$j_Y \leq 2J_{OUT}$	to state 3
2	$j_Y = -2J_{OUT}$	$m_C > \frac{m_{A0} + m_{B0}}{2} + 2\rho J_{OUT}$	to state 1
	$\frac{dm_C}{d\varphi} = -6rJ_{OUT}$		
3	$j_Y = 2J_{OUT}$	$m_C < \frac{m_{A0} + m_{B0}}{2} - 2\rho J_{OUT}$	to state 2
	$\frac{dm_C}{d\varphi} = 6rJ_{OUT}$		

After the normalization, the rectifier piecewise linear model presented in Table 9-1 takes the normalized form presented in Table 9-2.

3. FOUR SPECIAL CASES OF THE DISCONTINUOUS CONDUCTION MODE

To analyze the operation of the rectifier in the discontinuous conduction mode in order to determine the possible application area, four special cases that surround the discontinuous conduction mode region are discussed in this section. One of the boundaries is set by the current injection network parasitic resistance as a parameter, since in the region of interest this value can be in the range starting from zero and ending at the value that causes the rectifier to operate in the continuous conduction mode. The other parameter that affects the rectifier operating mode is characteristic resistance of the series resonant circuit, termed “filtering,” since it is a measure of the content of higher order harmonics in i_Y . The higher the value of R_0 is, the lower the content of the higher order harmonics in i_Y will be. Since R_0 is a parameter essential in normalization of currents, variations of R_0 in the case of a constant output current have the same effect as variations of the normalized output current in the case of constant R_0 . Thus, filtering is also related to the output current, and it is better in the case of higher output current.

3.1 Discontinuous Conduction Mode with Low Filtering and Negligible Losses

The first case to be analyzed corresponds to the current injection network without losses, i.e., $\rho=0$. We assume that the resonance constraint is satisfied with negligible inductance and huge capacitors, resulting in $R_0 \rightarrow 0$. Thus, voltages across the capacitors are constant, and inductance of the inductor is neglected. If this is the case, at any time point only one of the diodes in the bridge conducts, which is an extreme of the discontinuous conduction mode. In the simplified circuit presented in Fig. 9-3, this reduces to the situation that DA conducts if $v_{A0} > -v_{B0}$ and DB conducts if $v_{A0} < -v_{B0}$. Current i_Y takes the value $2I_{OUT}$ when DA conducts, and $-2I_{OUT}$ when DB conducts, and switches between these two values instantaneously. This results in the input current waveform presented in Fig. 9-4, having

$$THD = \frac{1}{3} \sqrt{\pi^2 - 9} \approx 31.08\%. \quad (9.38)$$

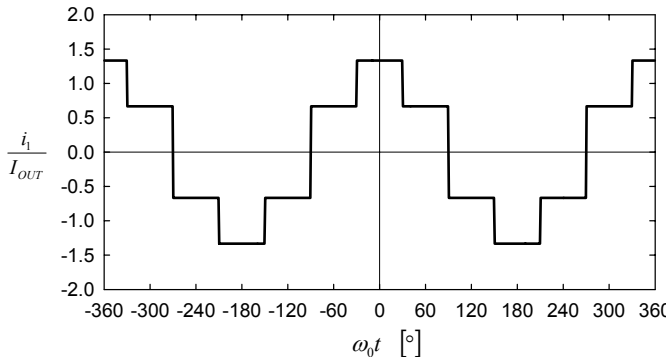


Figure 9-4. Input current of the rectifier for $\rho = 0$ and $R_0 \rightarrow 0$.

In this case, the average of the output voltage is

$$V_{OUT} = \frac{6}{\pi} V_m \approx 1.91 V_m, \quad (9.39)$$

which is greater than the average of the output voltage in the continuous conduction mode. Both of the waveforms of v_A and v_B contain six pulses per period, and do not contain the harmonic components at odd triples of the line frequency. In this manner, the power taken by the current injection network is turned to zero, since it contains only the harmonic components at odd triples of the line frequency. The efficiency that corresponds to this operating mode is $\eta = 100\%$, but the input current THD is the same as when the current injection is not applied, although the waveform of the input current is modified. Thus, this operating mode does not have practical importance, and it is presented here only to illustrate how the modification of the waveforms of v_A and v_B turned the power taken by the current injection network to zero. This mechanism generally occurs in the discontinuous conduction mode.

3.2 Boundary Between the Discontinuous and the Continuous Conduction Mode with Low Filtering

The next case in our study addresses the situation of low filtering and high resistance of the current injection network that causes the rectifier to operate at the boundary between the continuous and the discontinuous conduction mode. This normalized resistance is equal to $\rho = 1/(8J_{OUT})$, and depends on the output current. At the boundary between the modes, the

diodes conduct in the same manner as in the continuous conduction mode; thus the average of the output voltage is

$$V_{OUT} = \frac{3\sqrt{3}}{\pi} V_m \approx 1.65 V_m. \quad (9.40)$$

After the waveform of i_y is determined, the power taken by the current injection network can be computed, and the resulting efficiency of the rectifier is obtained as

$$\eta = \frac{6\sqrt{3}}{3\sqrt{3} + 2\pi} \approx 90.53\%, \quad (9.41)$$

which is slightly lower than in the case of the optimal third harmonic current injection. The corresponding waveform of the input current is presented in Fig. 9-5, and is characterized by

$$THD = \frac{\sqrt{16\pi^2 - 24\sqrt{3}\pi - 27}}{2\pi + 3\sqrt{3}} \approx 4.93\%, \quad (9.42)$$

which is significantly better than (9.38) and slightly better than in the case of the optimal third-harmonic current injection. However, the cost of this reduction of the THD is a significant decrease of efficiency.

From the analysis of the two cases with low filtering, it can be concluded that the input current THD is highly dependent on the current injection network resistance, and that significant improvement in the input current THD can be obtained at the cost of a decrease in efficiency. Unfortunately,

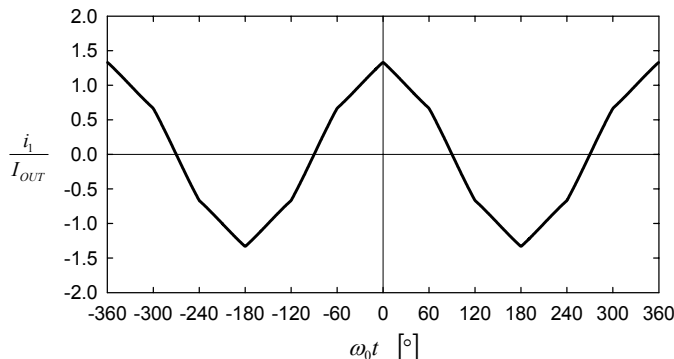


Figure 9-5. Input current of the rectifier for $\rho = 1/(8J_{OUT})$ and $R_0 \rightarrow 0$.

detailed analysis shows that with variations of ρ , the THD of the input current varies from (9.38) to (9.42) in an almost linear fashion, while the efficiency rapidly decreases from 100% to about 90%. Thus to provide an improvement of the input current THD with low filtering, efficiency has to be sacrificed.

3.3 Boundary Between the Discontinuous and the Continuous Conduction Mode with High Filtering

The third case in our study is the boundary between the continuous and the discontinuous conduction mode with high filtering, when i_Y consists only of a component at the triple of the line frequency. In this case, the equivalent resistance of the current injection network is $\rho = (3\sqrt{3})/(16\pi J_{OUT})$. The output voltage is the same as in the case of the continuous conduction mode given by (9.40), and the efficiency is

$$\eta = \frac{8}{9} \approx 88.89\%. \quad (9.43)$$

The waveform of the input current is presented in Fig. 9-6, and it is characterized by

$$THD = \frac{\sqrt{224\pi^2 - 2187}}{27\sqrt{3}} \approx 10.43\%, \quad (9.44)$$

which is about two times higher than in the previous case, with about the same efficiency. Again, this operating mode does not have practical importance since it combines low efficiency that characterizes boundary

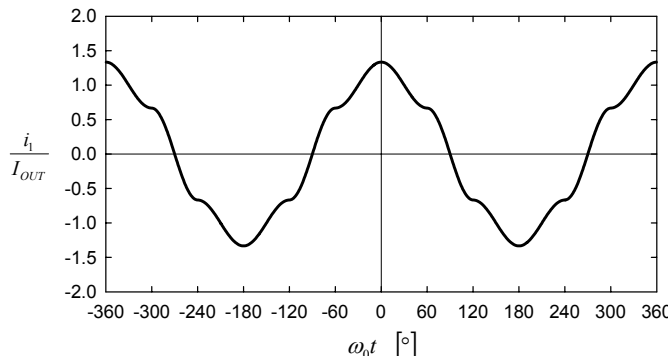


Figure 9-6. Input current of the rectifier for $\rho = (3\sqrt{3})/(16\pi J_{OUT})$ and $R_0 \rightarrow \infty$.

between the modes with the THD value twofold higher than in the low filtering case. However, with high filtering the input current THD slightly depends on losses, as shown next.

3.4 Discontinuous Conduction Mode with High Filtering and Negligible Losses

The last case to be analyzed is characterized by the current injection network with negligible losses, i.e., $\rho = 0$, and the characteristic impedance R_0 of the series resonant circuit large enough to justify ideal filtering approximation, meaning that higher order harmonics of i_y can be neglected. Whenever possible, the results are generalized to the case $\rho \neq 0$. To start the analysis, let us analyze the rectifier waveforms obtained by simulation in the case of a relatively high value of the normalized output current $J_{OUT} = 2$. The waveforms are presented in Fig. 9-7. The first diagram of Fig. 9-7 presents the normalized waveform of i_y , which is almost sinusoidal. This results in the input current waveform presented in the last diagram of Fig. 9-7, similar to the waveform of Fig. 9-6. Actually, in the case $J_{OUT} = 2$, $THD = 11.48\%$ is obtained, which is close to (9.44). Normalized waveforms of v_A and v_B are also presented in Fig. 9-7, and the waveforms are similar to the waveforms in the continuous conduction mode, except for the spikes that exist in the discontinuous intervals. Exact analysis of this operating mode results in bulky equations that cannot be solved in a closed form, requiring application of numerical methods. To avoid these mathematical difficulties, let us approximate waveforms of v_A and v_B as a sum of the corresponding waveform obtained in the continuous conduction mode, i.e., v_{A0} and v_{B0} specified by (9.6) and (9.7), and the spikes observed in the discontinuous conduction intervals approximated by the δ -function impulses,

$$v_A = v_{A0} + V_X \sum_{k=-\infty}^{+\infty} \delta\left(\omega_0 t - \frac{\pi}{3} - k \frac{2\pi}{3}\right) \quad (9.45)$$

and

$$v_B = v_{B0} - V_X \sum_{k=-\infty}^{+\infty} \delta\left(\omega_0 t - k \frac{2\pi}{3}\right), \quad (9.46)$$

where V_X is a constant to be determined. To determine V_X , let us note that the driving voltage of the equivalent series LC circuit is given by

$$\frac{v_A + v_B}{2} = \frac{v_{A0} + v_{B0}}{2} - \frac{V_X}{2} \sum_{k=-\infty}^{+\infty} (-1)^k \delta\left(\omega_0 t - k \frac{\pi}{3}\right). \quad (9.47)$$

The periodic sequence of δ -function impulses can be represented by the Fourier series expansion as

$$\sum_{k=-\infty}^{+\infty} (-1)^k \delta\left(\omega_0 t - k \frac{\pi}{3}\right) = \frac{6}{\pi} \sum_{n=1}^{+\infty} \cos(3(2n-1)\omega_0 t). \quad (9.48)$$

Assuming that i_Y contains only a harmonic component at the triple of the line frequency, the harmonic component of (9.47) at $3\omega_0$ should be large enough to produce amplitude of i_Y equal to $2I_{OUT}$,

$$2RI_{OUT} \cos(3\omega_0 t) = \frac{3\sqrt{3}}{8\pi} V_m \cos(3\omega_0 t) - \frac{3}{\pi} V_X \cos(3\omega_0 t); \quad (9.49)$$

thus V_X is obtained as

$$V_X = \frac{\sqrt{3}}{8} V_m - \frac{2\pi}{3} RI_{OUT}. \quad (9.50)$$

The output voltage waveform is given by

$$v_{OUT} = v_{A0} - v_{B0} + V_X \sum_{k=-\infty}^{+\infty} \delta\left(\omega_0 t - k \frac{\pi}{3}\right), \quad (9.51)$$

and to determine the average value of the output voltage, the average value of the contribution made by the δ -impulses is computed first:

$$\frac{1}{2\pi} \int_{-\pi^+}^{\pi^+} \left(V_X \sum_{k=-\infty}^{+\infty} \delta\left(\omega_0 t - k \frac{\pi}{3}\right) \right) d(\omega_0 t) = \frac{3}{\pi} V_X = \frac{3\sqrt{3}}{8\pi} V_m - 2RI_{OUT}, \quad (9.52)$$

which for $R = 0$ results in the output voltage average

$$V_{OUT} = \frac{27\sqrt{3}}{8\pi} V_m \approx 1.86 V_m, \quad (9.53)$$

while the normalized output voltage in the general case of high filtering and the discontinuous conduction mode is

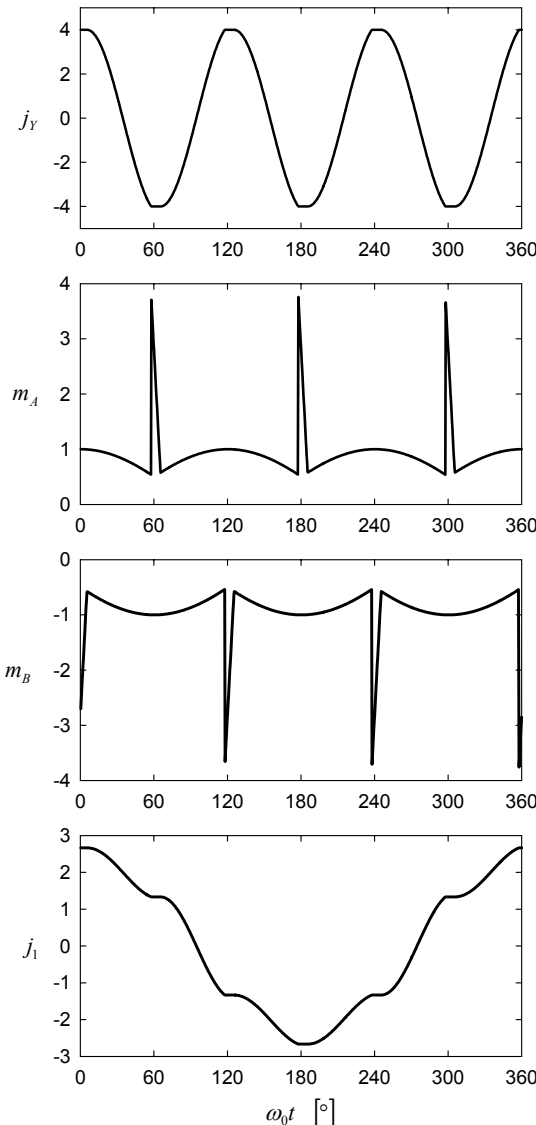


Figure 9-7. The rectifier waveforms for $\rho = 0$ and $J_{OUT} = 2$.

$$M_{OUT} = \frac{27\sqrt{3}}{8\pi} - 2\rho J_{OUT}. \quad (9.54)$$

In the case $R=0$, the input current THD is close to (9.44), i.e., $THD \approx 10.43\%$, while the efficiency is $\eta=100\%$. In this manner, reduction

of the input current THD is combined by high efficiency, and this is provided by a simple circuit—which was our goal.

Since the desired operating mode is found, stress on the components within the current injection network should be discussed. In the high filtering case, regardless of the current injection network resistance, the normalized current of the inductor reaches its maximum of $j_{Y\max} = 2J_{OUT}$, and the maximum of the AC component of the capacitor voltage is $m_{C\max} \approx 2J_{OUT}$. Another quantity of interest is the maximum instantaneous value of the output voltage, although the importance of this parameter is reduced if an inductive filter is applied at the output. Assuming that the discontinuous conduction intervals are short, the output voltage spikes are adequately represented by triangular waveforms, and equating the area of the triangle with V_X , the maximum of the output voltage is obtained as

$$M_{OUT\max} = \frac{3}{2} + \sqrt{3\sqrt{3} J_{OUT} - 16\pi\rho J_{OUT}^2}. \quad (9.55)$$

In the case of the high filtering, the injected current is close to sinusoidal, and under this assumption the efficiency is

$$\eta = 1 - \frac{16\pi}{27\sqrt{3}} \rho J_{OUT}. \quad (9.56)$$

3.5 Summary of the Special Cases

The results of the analysis of the four special cases are summarized in Table 9-3. The cases are chosen to correspond to the corners of the discontinuous conduction mode area in the plane determined by R_0 , which characterizes the filtering, and ρ , which characterizes the losses. Analyzing the low filtering cases, when $R_0 \rightarrow 0$, it is shown that a wide range of THD values can be obtained, but the reduction of the THD is at the cost of a reduction of efficiency. Analyzing the dependence of the THD on the efficiency in the low filtering case, it can be concluded that this case is not

Table 9-3. Summary of the special cases.

Case	R_0	ρ	η (%)	THD (%)	M_{OUT}
1	$\rightarrow 0$	0	100	31.08	1.91
2	$\rightarrow 0$	$\rho = 1/(8J_{OUT})$	90.53	4.93	1.65
3	$\rightarrow \infty$	$\rho = (3\sqrt{3})/(16\pi J_{OUT})$	88.89	10.43	1.65
4	$\rightarrow \infty$	0	100	10.43	1.86

attractive for practical application since the continuous conduction mode provides about the same THD with somewhat better efficiency. On the other hand, the discontinuous conduction mode in the high filtering case is characterized by an almost constant THD value of 10.43%, regardless of the efficiency. In cases with low losses, an increase of the output voltage in the discontinuous conduction mode is observed, and the increase is within 16% of the average output voltage in the continuous conduction mode. Thus, in applications where a THD value of about 10% is acceptable, the rectifier analyzed in this chapter might be a suitable choice. In the analysis of the discontinuous conduction mode with low losses and high filtering, a method to analyze the rectifier is proposed. The method is based on an approximation of the voltage spikes in the output terminal voltages during the discontinuous conduction intervals by the δ -function impulses, and applying the harmonic balance technique to determine the amplitude of these impulses. Application of this technique enables us to circumvent transcendental equations in the rectifier analysis, and it provided closed form approximate expressions for the output voltage, the maximum of the output voltage, and the efficiency.

4. EFFECTS OF VARIATIONS IN J_{OUT} , ρ , AND R

From the analysis performed so far, it is concluded that the rectifier operation parameters such as THD, efficiency, average of the output voltage, and the maximum of the output voltage depend on the normalized output current and the normalized value of the current injection network equivalent resistance. Four special cases were analyzed in the previous section, and in the analysis of the high filtering case with low losses an approximate analysis method was introduced, which resulted in expressions for the THD (9.44), the average of the output voltage (9.54), and the maximum of the output voltage (9.55). From the application point of view, it would be interesting to see how the listed parameters depend on the normalized output current and the normalized resistance of the current injection network in the case the approximations are not applied. The results presented in this section are obtained by numerical integration of the rectifier model given in Table 9-2. The range for the normalized output current is limited to $0 < J_{OUT} < 0.4$, which guarantees unipolar voltages across the current injection network capacitors, and thus enables application of electrolytic capacitors. The curves are computed taking the normalized resistance of the current injection network as a parameter, and for five values of the parameter: $\rho_1 = 0$, $\rho_2 = 0.1$, $\rho_3 = 0.2$, $\rho_4 = 0.3$, and $\rho_5 = 0.4$. The curves obtained are presented in Figs. 9-8 to 9-11, labeled from 1 to 5, corresponding to the list of values of ρ .

In Fig. 9-8, the dependence of the input current THD on the normalized output current is presented. All of the curves start from the THD value specified by (9.38), which corresponds to the low filtering case and low losses. Curves 1 to 3 converge to the THD value specified by (9.44), corresponding to the discontinuous conduction mode at high filtering. In curves 4 and 5, transition of the rectifier to the continuous conduction mode can be observed at the points where the curves expose discontinuous derivative and rapid decrease of the THD. Curve 5 captures the absolute minimum of the THD of 5.125%, which is predicted for the optimal third-harmonic current injection in the continuous conduction mode. All of the diagrams illustrate that increase of the output current in the discontinuous conduction mode causes a decrease of the input current THD, converging to the value of 10.43%. An increase of the current injection network resistance results in a slight decrease of the THD.

Dependence of the efficiency on J_{OUT} is shown in Fig. 9-9. In the discontinuous conduction mode, all of the curves are monotonically decreasing in an almost linear fashion, being in close correspondence with the analytical prediction of the approximate formula (9.56). In curves 4 and 5, a transition to the continuous conduction mode can be observed.

Dependence of the maximum instantaneous value of the output voltage on J_{OUT} is shown in Fig. 9-10. The curves in the discontinuous conduction mode are in close correspondence to the analytical prediction (9.55), with slightly higher difference for the curve labeled 1. The maximum of the

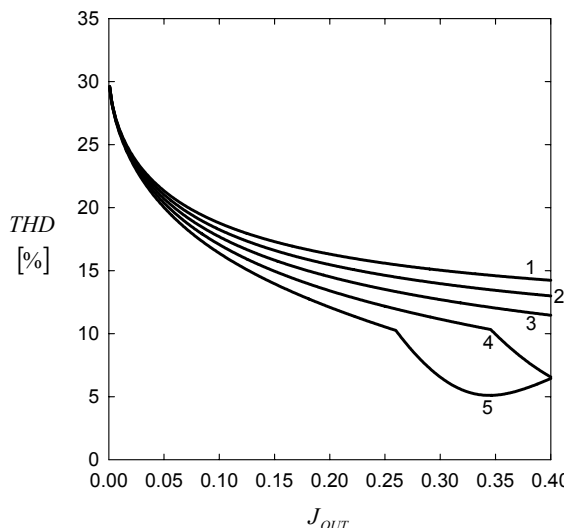


Figure 9-8. Dependence of the THD on J_{OUT} .

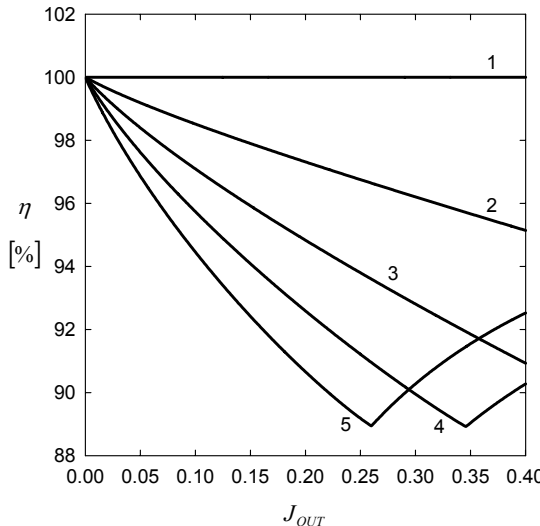


Figure 9-9. Dependence of the efficiency on J_{OUT} .

output voltage is highly dependent on losses in the current injection network, and this quantity might be used for precise indirect measurement of the losses. Curves labeled 4 and 5 captured transition to the continuous conduction mode in which the maximum of the output voltage is not dependent on J_{OUT} .

Dependence of the average of the output voltage on J_{OUT} is shown in Fig. 9-11. All of the curves start from the value specified by (9.39), corresponding to the low filtering and low losses. This value is 15.47% higher than the output voltage in the continuous conduction mode. The output voltage decreases with an increase of the output current, the decrease being faster for the higher values of ρ . Again, curves 4 and 5 capture the transition to the continuous conduction mode.

Another important issue for the rectifier design is dependence of the rectifier operation on the resonance parameter r , defined by (9.37). Ideally, the resonance parameter is $r=1$, but due to the component tolerances and temperature variations, the value of r varies within a certain range. Variation of r is a hard problem for the analytical approach, and thus the numerical approach is applied. The dependence of the input current THD on r is presented in Fig. 9-12 for $\rho=0$, and for five distinct values of J_{OUT} , $J_{OUT1}=0.1$, $J_{OUT2}=0.2$, $J_{OUT3}=0.3$, $J_{OUT4}=0.4$, and $J_{OUT5}=0.5$. The curves in Fig. 9-12 are labeled from 1 to 5, according to the given list of values for J_{OUT} . The curves expose two different regions, one with high THD values in the range from 30% to 35%, and the region with low THD

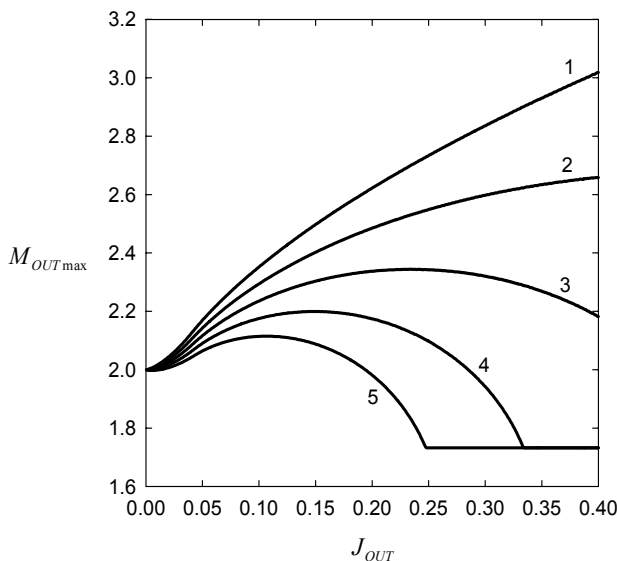


Figure 9-10. Dependence of $M_{OUT,\max}$ on J_{OUT} .

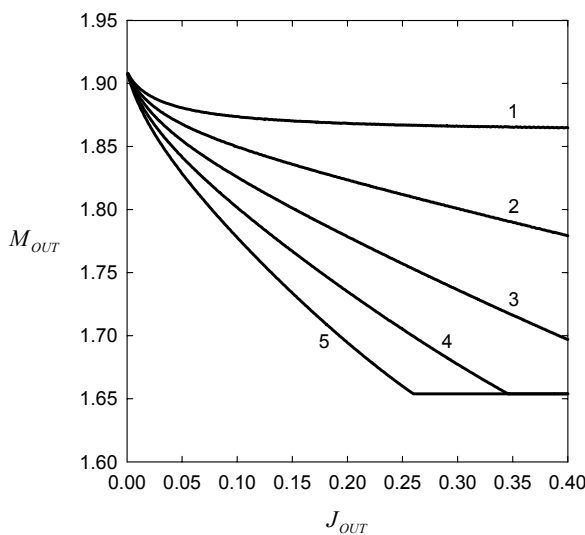


Figure 9-11. Dependence of M_{OUT} on J_{OUT} .

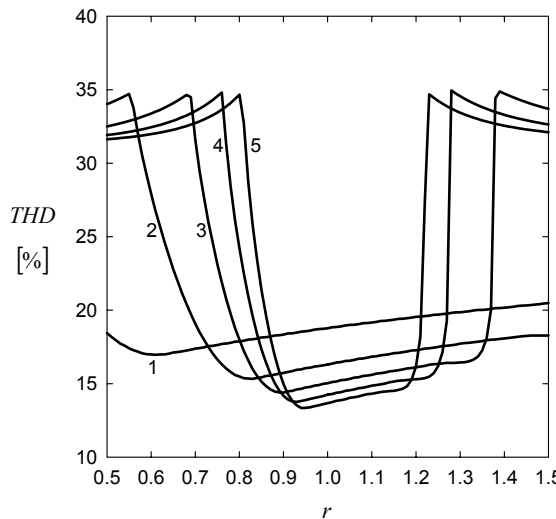


Figure 9-12. Dependence of the THD on the resonance parameter.

values around $r = 1$. The high THD values correspond to the continuous conduction mode of the rectifier, caused by the high mismatch of the resonant frequency. Transition between the regions is rapid, and it should be noted that the transitions are not symmetrical with respect to $r = 1$. The region of low THD values is wider for the lower values of J_{OUT} . If we take $J_{OUT} = 0.4$ as a reasonable upper limit for the output current, the allowable range for r is $0.85 < r < 1.25$ to remain in the low THD region. According to this conclusion, tolerances for the current injection network inductor and the capacitors should be chosen.

The simulation results presented in Fig. 9-12 indicate that there is a region over r in which the input current THD values are acceptable. The region almost coincides with the region over r in which the rectifier operates in the discontinuous conduction mode. This region can be analytically obtained by analyzing the rectifier in the continuous conduction mode and searching the values of r when the amplitude of the injected current becomes equal to $2I_{OUT}$, which corresponds to the transition to the discontinuous conduction mode. The two values that limit the region are obtained as a solution of a second-order algebraic equation as

$$\sqrt{1+x^2} - x < r < \sqrt{1+x^2} + x , \quad (9.57)$$

where

$$x = \frac{1}{2} \sqrt{\left(\frac{3\sqrt{3}}{16\pi} \frac{1}{J_{OUT}} \right)^2 - \rho^2}. \quad (9.58)$$

The derivation is almost straightforward. The region in r defined by (9.57) and (9.58) exactly defines the range where the rectifier operates in the discontinuous conduction mode, and approximately the range of low THD values of the input currents.

Chapter 10

RECOVERY OF THE CURRENT INJECTION NETWORK POWER APPLYING A CURRENT-LOADED RESISTANCE EMULATOR

Analysis of the third-harmonic current injection method presented so far indicates that the method can significantly improve total harmonic distortion (THD) of the input currents of three-phase diode bridge rectifiers. In Chapter 5, optimization of the injected current amplitude and phase is performed, and it is shown that for the minimum of the input current THD the injected current i_y supplied to the current injection device should be in phase with the spectral component of the diode bridge output terminal voltages at the triple of the line frequency, with the amplitude equal to $3/2$ of the output current. This requires a power to be taken by the current injection network from the diode bridge output terminals in order to provide the optimal third-harmonic current injection. This power is shown in Chapter 5 to be equal to 8.57% of the rectifier input power. In the current injection networks analyzed in Chapter 6, this power is dissipated on the current injection network resistors. The approach to dissipate the power taken by the current injection network is inconvenient for two reasons: first, the power dissipated on the resistors reduces the rectifier efficiency, imposing the theoretical limit for the efficiency of 91.43% in the case of the optimal third-harmonic current injection; and second, the equivalent resistance of the current injection network, specified by (6.10) in the case of the optimal third-harmonic current injection, is dependent on the rectifier output current, being

$$R = \frac{\sqrt{3}}{4\pi} \frac{V_m}{I_{OUT}}. \quad (10.1)$$

Thus, adjustment of the current injection network resistance to the load current variations is required. As suggested in [35] and [36], this can be achieved by applying a switching resistance emulator, being essentially a single-phase high power factor rectifier. Since the scope of this book is oriented to the converters that do not apply high-frequency switching, this

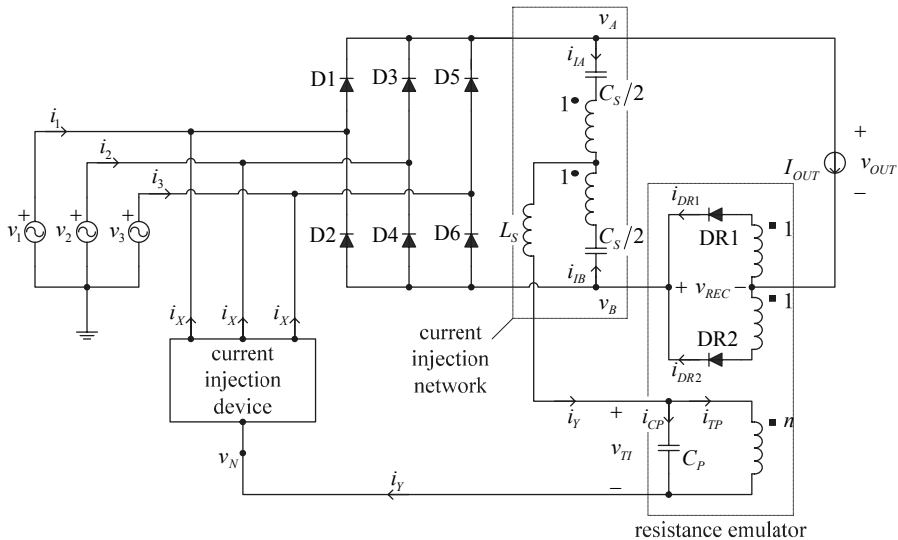


Figure 10-1. The third-harmonic current injection rectifier applying a current-loaded resistance emulator.

solution is not discussed here, although it is efficient and not difficult to achieve. In this chapter, another approach is applied that completely avoids high-frequency switching. The equivalent resistance of the current injection network specified by (10.1) is the focus of this chapter, with an aim of its lossless emulation and automatic adjustment to the load current variations.

The structure of the rectifier analyzed is presented in Fig. 10-1. The rectifier consists of a three-phase diode bridge accompanied by a current injection device, a current injection network, and a resistance emulator. The current injection device is applied to divide the current supplied from the current injection network into three equal parts, and to inject them back to the supply lines. Any of the current injection devices discussed in Chapter 4 will suffice. For the current injection network C introduced in Section 6.5 is applied, since its performance is superior when compared to the other current injection networks. The new part of the system is the resistance emulator, the unit identified in Fig. 10-1. The resistance emulator consists of two diodes, one transformer with the turns ratio $n:1:1$, and one capacitor, C_p . The purpose of the resistance emulator is to adjust the amplitude of the injected current according to the load current, and to restore the power taken by the current injection network at the rectifier output. In this manner, automatic regulation of the injected current amplitude is achieved, and the rectifier efficiency is improved as well.

The inspiration for the design of the resistance emulator is found in [14], where a circuit similar to the one presented in Fig. 10-1 is applied in a current injection based multipulse rectifier. First thoughts about simple resistance emulation circuits indicated that the power taken by the current injection network should be restored at the rectifier output, not the input, since the voltages and currents there are DC, thus simpler circuitry would be required. Second, information about the rectifier output current is required to provide the optimal resistance in the current injection network, specified by (10.1). These two facts, when put together, lead to the conclusion that the output of the resistance emulator should be connected in series with the load, taking the information about the load current and restoring the power taken by the current injection network at the same time. In this arrangement, the power taken by the current injection network is restored by an increase of the output voltage. The importance of [14] is the fact that it indicated a right way to apply a transformer and two diodes to link the rectifier output and the third-harmonic injection system. The remaining parts of the current injection network and the resistance emulator are added to smoothen the waveforms in order to provide the third-harmonic current injection. This provides better THD values of the input currents than the multipulse rectifier of [14], which provides a staircase approximation of a sine wave for the input currents.

In the analysis of the resistance emulator, the sinusoidal approximation techniques described in [8] (pages 709 to 713) will be extensively applied. The resistance emulator that is the focus of this chapter was originally proposed in references [32] and [34].

1. THE CURRENT-LOADED RESISTANCE EMULATOR

Let us assume that the rectifier shown in Fig. 10-1 is supplied by a three-phase voltage system:

$$v_p = V_m \cos\left(\omega_0 t - (p-1)\frac{2\pi}{3}\right), \quad (10.2)$$

for $p \in \{1, 2, 3\}$. Assuming the continuous conduction mode of the three-phase diode bridge, the rectifier output terminal voltages are given by their Fourier series expansions:

$$v_A = \frac{3\sqrt{3}}{\pi} V_m \left(\frac{1}{2} + \sum_{n=1}^{+\infty} \frac{(-1)^{n+1}}{9n^2 - 1} \cos(3n\omega_0 t) \right) \quad (10.3)$$

and

$$v_B = \frac{3\sqrt{3}}{\pi} V_m \left(-\frac{1}{2} + \sum_{n=1}^{+\infty} \frac{1}{9n^2 - 1} \cos(3n\omega_0 t) \right), \quad (10.4)$$

as derived in Chapter 2. The voltage between the two output terminals of the diode bridge is

$$v_{AB} = \frac{3\sqrt{3}}{\pi} V_m \left(1 - \sum_{k=1}^{+\infty} \frac{2}{36k^2 - 1} \cos(6k\omega_0 t) \right). \quad (10.5)$$

This voltage is named the diode bridge output voltage, and it is no longer the rectifier output voltage since the rectifier output voltage is increased for the voltage at the resistance emulator output. The DC component of the diode bridge output voltage is

$$V_{AB} = \frac{3\sqrt{3}}{\pi} V_m, \quad (10.6)$$

and the power at the diode bridge output is

$$P_{AB} = \frac{3\sqrt{3}}{\pi} V_m I_{OUT}. \quad (10.7)$$

In the case of the optimal third-harmonic current injection, the currents that the current injection network takes from the rectifier output terminals are

$$i_{IA} = i_{IB} = \frac{3}{4} I_{OUT} \cos(3\omega_0 t), \quad (10.8)$$

resulting in the current supplied to the current injection device

$$i_Y = \frac{3}{2} I_{OUT} \cos(3\omega_0 t). \quad (10.9)$$

Since $v_N = 0$, the power taken by the current injection network cannot be restored through the current injection device, thus the power taken by the current injection network, equal to

$$P_{INJ} = \frac{9\sqrt{3}}{32\pi} V_m I_{OUT} = \frac{3}{32} P_{AB}, \quad (10.10)$$

has to be either dissipated or restored at the rectifier output in some way.

The rectifier input power is

$$P_{IN} = P_{AB} + P_{INJ} = \frac{105\sqrt{3}}{32\pi} V_m I_{OUT} = \frac{35}{32} P_{AB}. \quad (10.11)$$

For the analyses that follow, the Fourier series expansion of the average of the output terminal voltages is needed:

$$v_{AV} = \frac{v_A + v_B}{2} = \frac{3\sqrt{3}}{\pi} V_m \sum_{k=1}^{+\infty} \frac{1}{(6k-3)^2 - 1} \cos((6k-3)\omega_0 t). \quad (10.12)$$

Now, let us apply the method of equivalent circuits used to analyze current injection networks in Chapter 6. For the harmonic components at odd triples of the line frequency, the current injection network C of Section 6.5 reduces to a series resonant circuit consisting of C_s and L_s , as shown in Fig. 10-2. The transformer applied in the resistance emulator, with the turns ratio $n:1:1$, is assumed to have perfect coupling and a magnetizing inductance L_p . The magnetizing inductance is assumed to be placed at the primary winding of the transformer model, which is the winding with n turns. Thus, the transformer could be represented by an inductor with the inductance L_p , connected in parallel to a primary of an ideal transformer with the turns ratio $(1:1:n)$. The magnetizing inductance of the transformer plays an important role in providing the current injection, and it is fine-tuned by an air gap placed in the transformer core. After the transformer is modeled, the resistance emulator is in the equivalent circuit of Fig. 10-2 represented by the capacitor C_p , the magnetizing inductance of the resistance emulator transformer, L_p , and the current source i_{TI} that represents the primary current of the ideal transformer part of the resistance emulator transformer. The current i_{TI} is the input current of a full-wave single-phase rectifier consisting of the ideal transformer and the diodes DR1 and DR2. This rectifier is loaded by constant current I_{OUT} , and its input current is

$$i_{TI} = \frac{1}{n} I_{OUT} \operatorname{sgn}(v_{TI}). \quad (10.13)$$

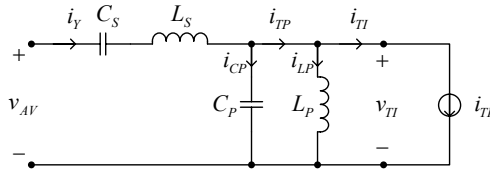


Figure 10-2. Equivalent circuit of the current injection network for odd triples of the line frequency. © [2000] IEEE.

At even triples of the line frequency, the current injection network is represented by an open circuit, due to the 1:1 transformer. Thus, flow of the currents at even triples of the line frequency in the current injection system is blocked.

Now, let us assume that resonance of the series resonant circuit consisting of C_S and L_S is tuned to the triple of the line frequency, as well as the resonance of the parallel resonant circuit consisting of C_P and L_P ,

$$\omega_R = 3\omega_0 = \frac{1}{\sqrt{L_S C_S}} = \frac{1}{\sqrt{L_P C_P}}. \quad (10.14)$$

In that case, at the triple of the line frequency the series resonant circuit is represented by a short circuit, while the parallel resonant circuit is represented by an open circuit. This results in an equivalent circuit of the current injection network for the triple of the line frequency presented in Fig. 10-3.

According to the equivalent circuit of Fig. 10-3, at the triple of the line frequency $v_{AV} = v_{Tl}$, thus corresponding to the Fourier series expansion of v_{AV} given by (10.12), the waveform of the ideal transformer primary current neglects the higher order harmonics of v_{Tl} obtained as

$$i_{Tl} = \frac{1}{n} I_{OUT} \operatorname{sgn}(\cos(3\omega_0 t)), \quad (10.15)$$

and its Fourier series expansion is

$$i_{Tl} = \frac{4}{\pi} \frac{I_{OUT}}{n} \sum_{k=1}^{+\infty} \frac{(-1)^{k+1}}{2k-1} \cos((2k-1)\omega_0 t). \quad (10.16)$$

The fundamental harmonic of i_{Tl} should be equal to the amplitude of the injected current i_Y , I_{Ym} ,

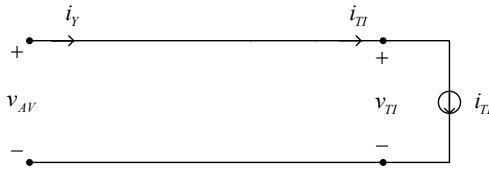


Figure 10-3. Equivalent circuit of the current injection network at the triple of the line frequency. © [2000] IEEE.

$$\frac{4}{\pi} \frac{I_{OUT}}{n} = I_{Ym} = \frac{3}{2} I_{OUT}. \quad (10.17)$$

To satisfy (10.17), turns ratio of the resistance emulator transformer should be

$$n = \frac{8}{3\pi}. \quad (10.18)$$

In this manner, the amplitude of the injected current is automatically adjusted to the load current.

At higher order odd triples of the line frequency, the series resonant circuit of Fig. 10-2 can be approximated by an open circuit. On the other hand, the parallel resonant circuit can be approximated by a short circuit. This results in the equivalent circuit of the current injection network for higher order odd triples of the line frequency shown in Fig. 10-4. The equivalent circuit of Fig. 10-4 is an approximation, since the behavior of the resonant circuits is idealized. On the other hand, the equivalent circuit for the triple of the line frequency, presented in Fig. 10-3, is exact.

According to the equivalent circuits of Figs. 10-3 and 10-4, the only spectral component of the voltage at the resistance emulator rectifier input is at the triple of the line frequency, being equal to the corresponding spectral component of v_{AV} ,

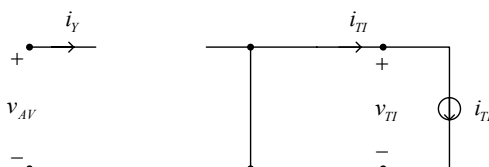


Figure 10-4. Idealized equivalent circuit of the current injection network for the higher order odd triples of the line frequency. © [2000] IEEE.

$$v_{AV,1} = \frac{3\sqrt{3}}{8\pi} V_m \cos(3\omega_0 t). \quad (10.19)$$

Since

$$v_{REC} = \frac{1}{n} |v_{TI}|, \quad (10.20)$$

the voltage at the resistance emulator output is

$$v_{REC} = \frac{9\sqrt{3}}{64} V_m |\cos(3\omega_0 t)| = \frac{9\sqrt{3}}{32\pi} V_m \left(1 - 2 \sum_{k=1}^{+\infty} \frac{(-1)^k}{4k^2 - 1} \cos(6k\omega_0 t) \right). \quad (10.21)$$

Finally, the rectifier output voltage is given as a sum of the diode bridge output voltage and the resistance emulator output voltage

$$\begin{aligned} v_{OUT} &= v_{AB} + v_{REC} \\ &= \frac{3\sqrt{3}}{\pi} V_m \left(\frac{35}{32} - \sum_{k=1}^{+\infty} \left(\frac{2}{36k^2 - 1} + \frac{3}{16} \frac{(-1)^k}{4k^2 - 1} \right) \cos(6k\omega_0 t) \right). \end{aligned} \quad (10.22)$$

The DC component of the rectifier output voltage is

$$V_{OUT} = \frac{35}{32} \frac{3\sqrt{3}}{\pi} V_m, \quad (10.23)$$

which for the DC component of the resistance emulator output voltage is

$$V_{REC} = \frac{9\sqrt{3}}{32\pi} V_m, \quad (10.24)$$

increased in comparison to the rectifier output voltage if the resistance emulator is not applied. In this manner, by the increase of the rectifier output voltage, the power taken by the current injection network is restored at the rectifier output. This results in the output power

$$P_{OUT} = \frac{105\sqrt{3}}{32\pi} V_m I_{OUT} = \frac{35}{32} P_{AB} = P_{IN}. \quad (10.25)$$

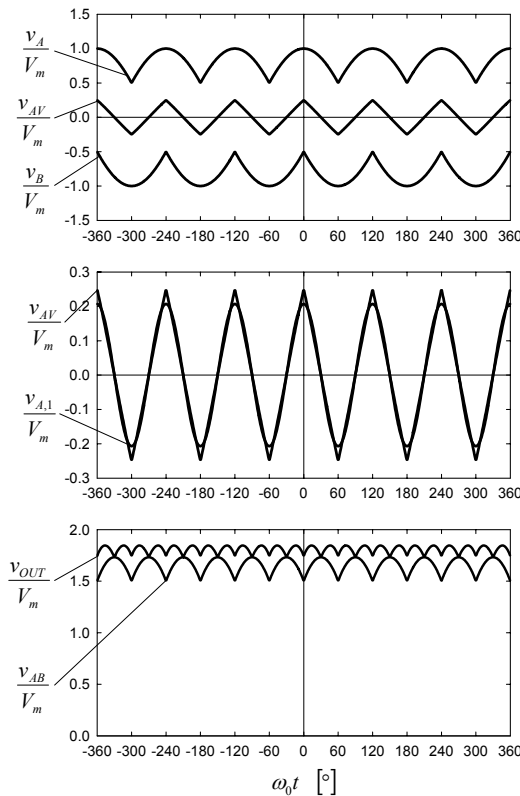


Figure 10-5. Waveforms of v_A , v_B , v_{AV} , $v_{AV,1}$, v_{AB} , and v_{OUT} .

Waveforms for some of the rectifier voltages are presented in Fig. 10-5. In the first diagram, waveforms of the diode bridge output terminal voltages are presented, as well as their average, $v_{AV} = (v_A + v_B)/2$. The voltage v_{AV} is effectively applied at the input of the equivalent circuit presented in Fig. 10-2, and its magnified waveform is presented in the second diagram of Fig. 10-5, accompanied with the waveform of its fundamental harmonic. From the diagram, it can be concluded that the waveform of v_{AV} consists primarily of the fundamental harmonic, with a small amount of pollution by higher order harmonics. Finally, the waveforms of the diode bridge output voltage and the rectifier output voltage are presented in the last diagram. It can be observed that the waveform of the output voltage has a higher DC component, corresponding to the recovery of the power taken by the current injection network. It can also be observed that the spectral component at the sixth multiple of the line frequency, being the fundamental harmonic of v_{AB} , is almost eliminated from the output voltage. However, as can be seen from

(10.22), this harmonic component is not completely eliminated from the output voltage, but it is significantly reduced, having the amplitude of only $0.54\% V_m$. Overall ripple of the output voltage is reduced, which is a side effect of resistance emulation.

Waveforms of some currents in the current injection network are presented in Fig. 10-6. In the first diagram, the injected current i_y and the current of an ideal transformer part of the resistance emulator transformer model, i_{Tl} , are presented. The waveforms have the same fundamental harmonic, while current i_{Tl} is polluted by higher order harmonics. The difference between the two currents, $i_y - i_{Tl}$, is the current that flows through the parallel resonant circuit that consists of C_P and L_P . The diagrams of Fig. 10-6 apply for idealized resonant circuits of the current injection network, corresponding to ideal filtering of the higher order harmonics. Thus, i_y is free from the higher order harmonics, since the higher order harmonics of v_{AV} are filtered by the series resonant circuit, while the higher order harmonics of i_{Tl} are closed through the parallel resonant circuit.

2. CHOICE OF COMPONENTS

In the analysis of the resistance emulator, the behavior of the resonant circuits is idealized, assuming ideal selectivity. However, there are some limitations for the choice of the components, which are discussed in this section.

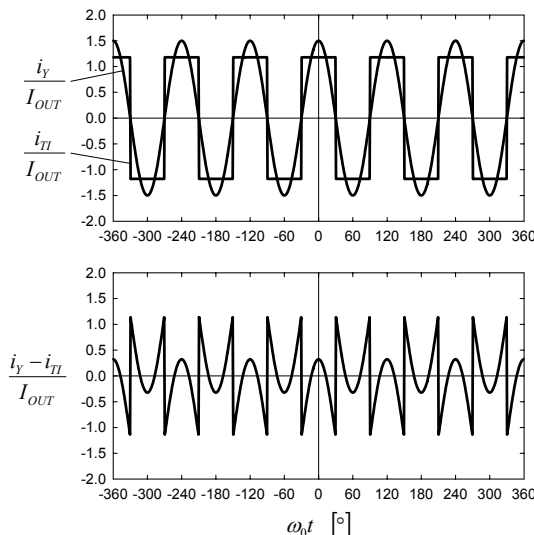


Figure 10-6. Waveforms of the rectifier currents.

First, let us assume that the rectifier is supplied by a symmetrical undistorted three-phase voltage system with the amplitude of phase voltages equal to V_m . The maximum of the rectifier output current is assumed to be $I_{OUT\max}$. To normalize the rectifier voltages and currents, let us define a normalizing resistance R_X as

$$R_X = \frac{V_m}{I_{OUT\max}}. \quad (10.26)$$

The first part of the current injection system is the current injection network that consists of two $C_S/2$ capacitors, inductor L_S , and the transformer with the turns ratio 1:1. In the equivalent circuit of Fig. 10-2, the current injection network reduces to a series resonant circuit consisting of L_S and C_S . The choice of these two values is subjected to the resonance constraint (10.14); thus only one of these two values can be chosen independently. To reject harmonic components of the injected current, the impedance of the series resonant circuit should be large, and the idealized representation of the series resonant circuit in the equivalent circuit of Fig. 10-4 is an open circuit. To provide high impedance above the resonant frequency, inductance of the series resonant circuit should be large, since it dominates the impedance above the resonant frequency. However, the inductance cannot be increased unlimitedly, since high inductance values result in a high volt-ampere rating of the inductor core and high voltage stress on the resonant circuit elements. If application of electrolytic capacitors for $C_S/2$ is required, the voltage across these capacitors should not change polarity during the whole period. In that case, the DC component of the capacitor voltage, equal to one half of the diode bridge output voltage DC component,

$$V_{CSDC} = \frac{3\sqrt{3}}{2\pi} V_m, \quad (10.27)$$

should be lower than the amplitude of the AC component of the capacitor voltage,

$$V_{CSACm} = \frac{I_{OUT\max}}{2\omega_0 C_S}. \quad (10.28)$$

This results in a minimum value for the capacitance C_S of

$$C_s = \frac{\pi}{3\sqrt{3}} \frac{1}{\omega_0 R_X}. \quad (10.29)$$

The corresponding value of the inductance L_s is obtained from the resonance constraint (10.14):

$$L_s = \frac{1}{\pi\sqrt{3}} \frac{R_X}{\omega_0}, \quad (10.30)$$

and this is the maximum value that allows application of electrolytic capacitors. The volt-ampere rating of the core for such an inductor is

$$S_L = \frac{2}{35} P_{OUT} \approx 5.71\% P_{OUT}. \quad (10.31)$$

Lower values for the inductance accompanied by higher capacitance values are valid choices, but leakage of the higher order harmonics of v_{AV} would be higher.

The current injection network transformer, with the turns ratio 1:1 discussed in Section 6.5, and its volt-ampere rating is derived there as

$$S_{T1:1} = \frac{2}{35} \left(\sqrt{\pi^2 - 9} - 3 \arccos \frac{3}{\pi} \right) P_{OUT} = 0.16\% P_{OUT}. \quad (10.32)$$

The elements of the parallel resonant circuit, C_p and L_p , are parts of the resistance emulator. The purpose of the parallel resonant circuit is to block the current spectral component at the triple of the line frequency, forcing it to flow through the ideal transformer primary, and to short-circuit the higher order harmonic components of the ideal transformer primary current. To achieve the first of these two goals, it is sufficient to satisfy the resonance constraint (10.14). The second constraint cannot be fully satisfied, and to reduce the impedance of the parallel resonant circuit above the line frequency, the capacitance C_p should be as large as possible. On the other hand, voltage across the parallel resonant circuit primarily consists of the fundamental component of v_{AV} , and huge C_p values would result in a huge amplitude of the parallel resonant circuit ringing current. This would increase the volt-ampere rating of the components, as well as the losses. On the other hand, there is a lower limit for the amplitude of the ringing current, imposed by a requirement that switching in the resistance emulator rectifier should provide i_{TT} waveform as depicted in Fig. 10-6. This requirement

imposes the condition that the amplitude of the ringing current is greater than the amplitude of the ideal transformer primary current,

$$\frac{1}{3\omega_0 L_P} \frac{3\sqrt{3}}{8\pi} V_m > \frac{1}{n} I_{OUT\max}. \quad (10.33)$$

If this requirement is not fulfilled, the resistance emulator rectifier will operate in the discontinuous conduction mode, characterized by time intervals when both of the diodes conduct. This situation is the same as in the discontinuous conduction mode of the parallel resonant converter, described in [8] (pages 749 to 751). Thus, for the elements of the parallel resonant converter, values that provide the minimum of the ringing current for which the discontinuous conduction mode is avoided are chosen. The value for L_P is obtained from (10.33),

$$L_P = \frac{1}{\pi^2 \sqrt{3}} \frac{R_X}{\omega_0}, \quad (10.34)$$

and the corresponding value of C_P that meets the resonance constraint (10.14) is

$$C_P = \frac{\pi^2}{3\sqrt{3}} \frac{1}{\omega_0 R_X}. \quad (10.35)$$

Lower values of L_P , and corresponding higher values of C_P that meet the resonance constraint, are valid choices for the elements of the parallel resonant circuit that would result in higher ringing currents, higher volt-ampere ratings of the components, and better filtering.

Waveforms of the resistance emulator transformer currents in the case of the parallel resonant circuit elements specified by (10.35) are presented in Fig. 10-7. All of the diagrams are presented using the same scale for current axes to illustrate the high amplitude of the transformer primary current, $i_{TP} = i_{LP} + i_{TI}$, caused by the ringing current of the parallel resonant circuit inductance, which is obtained as a magnetizing inductance of the transformer. These waveforms are essential in computation of the resistance emulator transformer volt-ampere rating. Having the waveforms of the transformer currents as presented in Fig. 10-7, and since the voltage across the transformer primary is given by (10.19), being the fundamental harmonic of v_{AV} , the transformer volt-ampere rating is obtained as

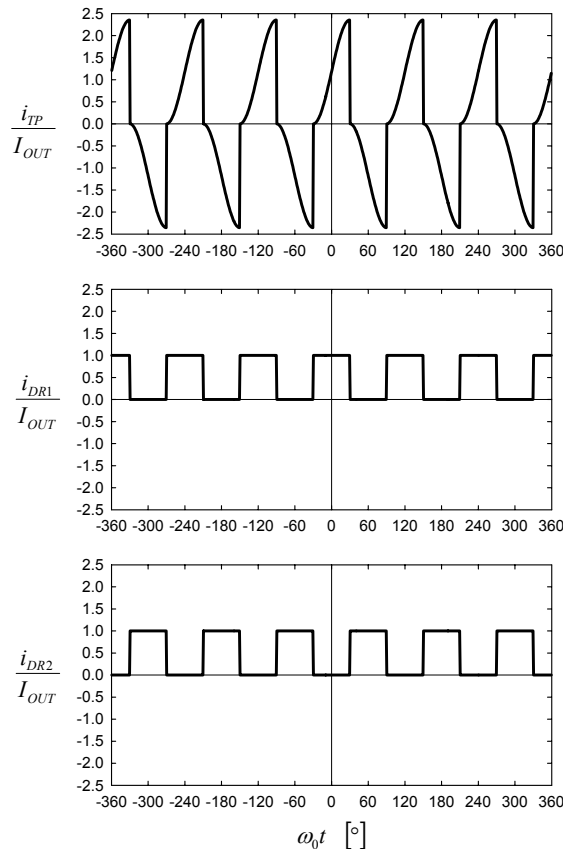


Figure 10-7. Waveforms of the transformer currents.

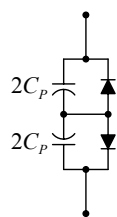


Figure 10-8. Obtaining C_P by applying electrolytic capacitors.

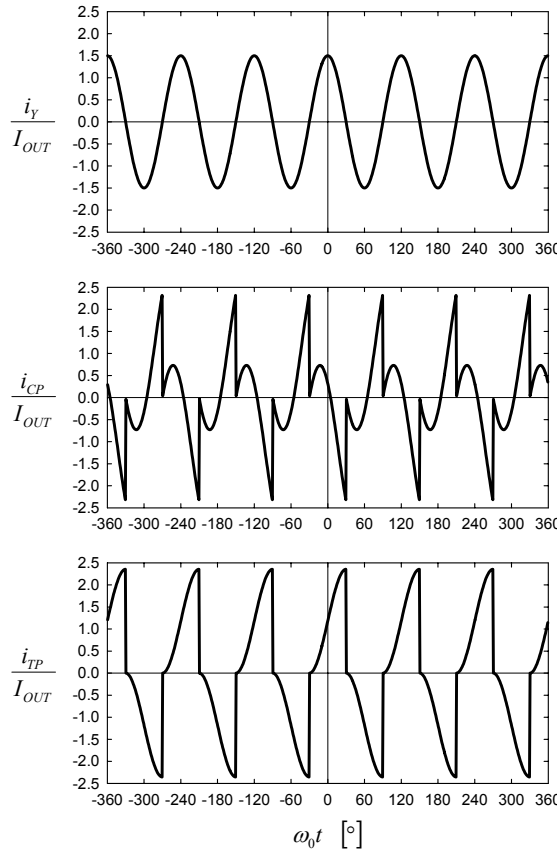


Figure 10-9. Waveforms of the currents at the resistance emulator AC side.

$$S_{TRE} = \frac{\pi}{140} \left(1 + \frac{\sqrt{3}}{2} \right) P_{OUT} \approx 4.19\% P_{OUT}. \quad (10.36)$$

This value is slightly different from the value given in [34] by equation (47) of the reference. The value of [34] is obtained by erroneous computation of the transformer secondary RMS values, thus (10.36) is a correction of that value.

The voltage across the parallel resonant circuit capacitor is specified by (10.19), consisting only of the AC component. Thus, direct application of electrolytic capacitors is not possible. However, an arrangement of two electrolytic capacitors and two diodes shown in Fig. 10-8 is applied in all

of the experimental setups. The electrolytic capacitors required have a capacitance equal to twice the C_P , and their maximum voltage is equal to twice the voltage across C_P . The diodes in the arrangement conduct a negligible average current in the steady state, only to compensate the leakage of the capacitors. However, during the transients the currents through the diodes may have significant instantaneous values. The transient process corresponds to DC biasing of the capacitors, and it is determined both by the C_P value and the remaining part of the circuit.

Waveforms of the currents at the resistance emulator AC side are presented in Fig. 10-9. The first diagram presents the resistance emulator input current, i_Y , which splits up to a component i_{CP} that flows to the resistance emulator capacitor, C_P , and the component i_{TP} which flows through the resistance emulator transformer primary. The waveform of i_{CP} is presented in the second diagram of Fig. 10-9. The waveform touches zero at the switching instants when diodes change state. This corresponds to the boundary between the discontinuous and the continuous conduction modes of the resistance emulator rectifier, which is the situation chosen to compute the values of L_P and C_P . Lower values of C_P and corresponding higher values of L_P would provide the rectifier operation deeper in the continuous conduction mode, and thus some margin in the instantaneous value of i_{CP} at the switching instants.

3. INFLUENCE OF THE HIGHER ORDER HARMONICS

The analysis of the resistance emulator circuit presented so far is based on idealized equivalent circuits shown in Figs. 10-3 and 10-4. Exact analysis of the rectifier presents mathematical difficulties of solving the fourth-order nonlinear circuit. Fortunately, the problem can be significantly simplified if a reasonable assumption of the three-phase diode bridge continuous conduction mode is accepted. In that case, voltages of the diode bridge output terminals are given by (10.3) and (10.4), and the diode bridge operation is represented by these two voltages. In this manner, six nonlinear elements, the diodes that form the three-phase diode bridge, are removed from the circuit analysis, and the only remaining nonlinear elements are two diodes of the resistance emulator rectifier. In this section, effects caused by previously neglected harmonics of the injected current i_Y are studied via numerical simulation of a normalized state-space model of the current injection system. The state-space model is derived, normalized, and the simulation results are presented.

First, let us simplify the current injection network in the part that consists of the $C_S/2$ capacitors and 1:1 transformer. This part of the current injection network has been previously simplified by applying the analysis in the frequency domain, resulting in the equivalent circuits for odd and even triples of the line frequency introduced in Chapter 6. Here, the problem is approached in time domain, to prepare the model for the time domain simulation.

Let us consider a part of the current injection network applied in the rectifier of Fig. 10-1, presented in Fig. 10-10. The part of the circuit consists of the $C_S/2$ capacitors and 1:1 transformer. The transformer forces currents of the capacitors to be the same, equal to one half of the injected current,

$$i_{IA} = i_{IB} = \frac{1}{2} i_Y . \quad (10.37)$$

The voltage v_X at the output of the considered part of the current injection network starts from v_A , given by

$$v_X = v_A - v_{C1} - v_T , \quad (10.38)$$

while starting from v_B we obtain

$$v_X = v_B - v_{C2} + v_T . \quad (10.39)$$

Adding (10.38) and (10.39), the voltage v_T across the transformer windings is eliminated,

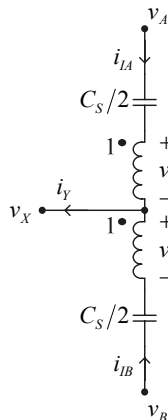


Figure 10-10. A part of the current injection network.

$$2v_X = v_A + v_B - v_{C1} - v_{C2}, \quad (10.40)$$

and the voltage at the output of the considered part of the current injection network is obtained as

$$v_X = v_{AV} - \frac{1}{2}(v_{C1} + v_{C2}), \quad (10.41)$$

where v_{AV} is defined by (10.12). Differentiating and rearranging (10.41), we obtain

$$\frac{1}{2}\left(\frac{dv_{C1}}{dt} + \frac{dv_{C2}}{dt}\right) = \frac{d}{dt}(v_{AV} - v_X). \quad (10.42)$$

Applying element characteristics of the $C_S/2$ capacitors,

$$\frac{C_S}{2} \frac{dv_{C1}}{dt} = \frac{C_S}{2} \frac{dv_{C2}}{dt} = \frac{i_Y}{2}, \quad (10.43)$$

we obtain

$$\frac{dv_{C1}}{dt} + \frac{dv_{C2}}{dt} = 2 \frac{i_Y}{C_S}. \quad (10.44)$$

After (10.44) is substituted in (10.42), the final relation between v_{AV} , v_X , and i_Y is obtained as

$$i_Y = C_S \frac{d}{dt}(v_{AV} - v_X). \quad (10.45)$$

Equation (10.45) applies regardless of the way the waveforms of v_A and v_B are obtained, and regardless of the conduction mode of the diode bridge. An equivalent circuit that corresponds to (10.45) and replaces the part of the current injection network of Fig. 10-10 is shown in Fig. 10-11. This equivalent circuit is used in all of the subsequent analyses.

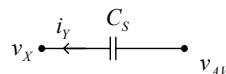


Figure 10-11. Equivalent representation of a part of the current injection network.

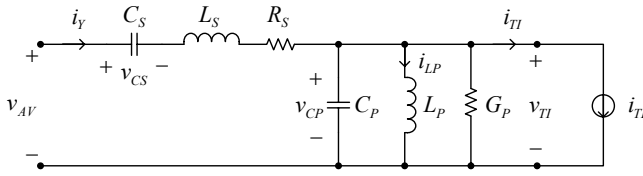


Figure 10-12. Generalized equivalent representation of the current injection system AC side in the continuous conduction intervals.

Applying the equivalent circuit of Fig. 10-11, and somewhat generalizing the representation of the current injection network and the resistance emulator circuit, a model of the current injection system is obtained as shown in Fig. 10-12. The generalization is done in the sense that parasitic resistance of the current injection network and the current injection device is modeled by R_S , and leakage of the parallel resonant circuit at the resonant frequency is modeled by G_P . The input current of the ideal transformer part of the resistance emulator transformer model is in the continuous conduction intervals, for $v_{CP} \neq 0$, represented by a nonlinear voltage controlled current source i_{Tl} . Since $v_{Tl} = v_{CP}$, and since v_{CP} is going to be a state variable of the state-space model for the circuit of Fig. 10-12, it is convenient to express the current i_{Tl} as

$$i_{Tl} = \frac{1}{n} I_{OUT} \operatorname{sgn}(v_{CP}). \quad (10.46)$$

To simplify the analysis, in [34] for the control voltage of the current source specified by (10.46), voltage v_{AV} is applied instead of v_{CP} . This is an approximation that significantly simplifies the analysis, since it reduces the nonlinear circuit to a periodically switched linear circuit. However, the approximation is not well justified, since the results obtained simulating the accurate model are significantly different from the results of the analysis of the approximate periodically switched linear circuit, as shown here.

The state-space model of the circuit of Fig. 10-12 is given by a set of four differential equations:

$$\frac{d}{dt} \begin{bmatrix} i_Y \\ v_{CS} \\ i_{LP} \\ v_{CP} \end{bmatrix} = \begin{bmatrix} -\frac{R_S}{L_S} & -\frac{1}{L_S} & 0 & -\frac{1}{L_S} \\ \frac{1}{C_S} & 0 & 0 & 0 \\ 0 & 0 & 0 & \frac{1}{L_P} \\ \frac{1}{C_P} & 0 & -\frac{1}{C_P} & -\frac{G_P}{C_P} \end{bmatrix} \begin{bmatrix} i_Y \\ v_{CS} \\ i_{LP} \\ v_{CP} \end{bmatrix} + \begin{bmatrix} \frac{v_{AV}}{L_S} \\ 0 \\ 0 \\ -\frac{1}{nC_P} I_{OUT} \operatorname{sgn}(v_{CP}) \end{bmatrix}. \quad (10.47)$$

The model of (10.47) applies for continuous conduction intervals, where only one of the diodes DR1 and DR2 of the resistance emulator rectifier is conducting. In this case, $v_{CP} \neq 0$. However, if the amplitude of the ringing current in the parallel resonant circuit is not large enough, the discontinuous conduction intervals occur. In the discontinuous conduction intervals both of the diodes DR1 and DR2 conduct, and the ideal transformer primary is represented by a short circuit, as shown in Fig. 10-13. The circuit survives a dynamic degeneration, and v_{CP} is not a state variable during the discontinuous intervals, since $v_{CP} = 0$. This results in the current of C_P equal to zero, as well as the current of G_P . The current of the parallel resonant circuit inductor, i_{LP} , remains constant during the discontinuous conduction interval. The state-space model of the circuit of Fig. 10-13 is given by

$$\frac{d}{dt} \begin{bmatrix} i_Y \\ v_{CS} \\ i_{LP} \end{bmatrix} = \begin{bmatrix} -\frac{R_S}{L_S} & -\frac{1}{L_S} & 0 \\ \frac{1}{C_S} & 0 & 0 \\ 0 & 0 & 0 \end{bmatrix} \begin{bmatrix} i_Y \\ v_{CS} \\ i_{LP} \end{bmatrix} + \begin{bmatrix} \frac{v_{AV}}{L_S} \\ 0 \\ 0 \end{bmatrix}, \quad (10.48)$$

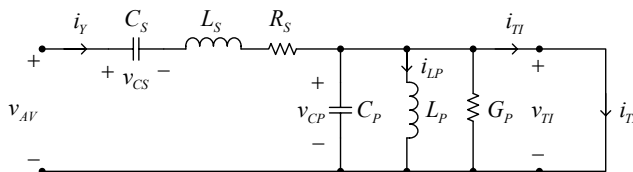


Figure 10-13. Generalized equivalent representation of the current injection system AC side in the discontinuous conduction interval.

and the system is of the third order, owing to the dynamic degeneration. In comparison to the state-space model of (10.47), the last equation, i.e., the equation over v_{CP} , is omitted, and in the remaining equations $v_{CP} = 0$ is substituted. In numerical simulation, the system (10.48) is going to be treated as a second-order system, since i_{LP} remains constant during the discontinuous conduction interval, and there is no need for numerical integration over this variable. The state-space model of (10.48) applies for

$$-\frac{1}{n}I_{OUT} < i_{TI} \quad (10.49)$$

and

$$i_{TI} < \frac{1}{n}I_{OUT}, \quad (10.50)$$

where

$$i_{TI} = i_Y - i_{LP} \quad (10.51)$$

due to the dynamic degeneration. When i_{TI} violates (10.49), the current injection system switches to the state that corresponds to negative v_{CP} . On the other hand, if (10.50) is violated, the current injection system switches to the state that corresponds to positive v_{CP} . In cases when occurrence of the discontinuous conduction intervals are not expected, equations for the discontinuous conduction mode can be omitted from the simulation program. However, all of the results presented here are obtained using a simulation program that had the discontinuous conduction mode programmed.

The derived model of the current injection system is nonlinear, and cannot be solved in a closed form. However, the model can be solved applying numerical methods if the rectifier parameters are known. To generalize the simulation results, normalization of the variables should be performed.

Let us define a characteristic resistance of the series resonant circuit of Fig. 10-12 as

$$R_{0S} = \sqrt{\frac{L_S}{C_S}}. \quad (10.52)$$

Resonant frequency of the series resonant circuit is given by

$$\omega_{RS} = \frac{1}{\sqrt{L_S C_S}}, \quad (10.53)$$

and the assumption that the resonant frequency is exactly tuned to the triple of the line frequency (10.14) no longer applies. In terms of the characteristic resistance and the resonant frequency, inductance of the series resonant circuit is expressed as

$$L_S = \frac{R_{0S}}{\omega_{RS}}, \quad (10.54)$$

while the capacitance is given by

$$C_S = \frac{1}{R_{0S} \omega_{RS}}. \quad (10.55)$$

Next, let us define the *Q*-factor of the series resonant circuit as

$$Q_S = \frac{1}{R_S} \sqrt{\frac{L_S}{C_S}}. \quad (10.56)$$

In a similar manner, parameters of the parallel resonant circuit are defined, and the characteristic resistance of the parallel resonant circuit is

$$R_{0P} = \sqrt{\frac{L_P}{C_P}}, \quad (10.57)$$

and the resonant frequency is

$$\omega_{RP} = \frac{1}{\sqrt{L_P C_P}}. \quad (10.58)$$

Inductance of the parallel resonant circuit is in terms of the characteristic resistance and the resonant frequency given by

$$L_P = \frac{R_{0P}}{\omega_{RP}}, \quad (10.59)$$

and the capacitance is

$$C_P = \frac{1}{R_{0P}\omega_{RP}}. \quad (10.60)$$

For the parallel resonant circuit, the *Q*-factor is defined as

$$Q_P = \frac{1}{G_P} \sqrt{\frac{C_P}{L_P}}, \quad (10.61)$$

which is different than in the case of the series resonant converter.

Let us start with normalization of variables by normalization of the time variable, which is replaced by a phase-angle defined as

$$\varphi = \omega_0 t. \quad (10.62)$$

Voltages are normalized by the amplitude of the phase voltage,

$$m = \frac{v}{V_m}, \quad (10.63)$$

and the currents are normalized by the output current of the rectifier,

$$j = \frac{i}{I_{OUT}}. \quad (10.64)$$

Let us define a resonant parameter of the series resonant circuit as

$$r_S = \frac{\omega_{RS}}{3\omega_0}, \quad (10.65)$$

and a resonance parameter of the parallel resonant circuit as

$$r_P = \frac{\omega_{RP}}{3\omega_0}. \quad (10.66)$$

The resonance parameters are ideally equal to one, and if the resonance constraints are not met, the resonant parameters represent mismatch of the resonant circuit resonant frequency and the triple of the line frequency.

Next, let us define the load level parameter α as

$$\alpha = \frac{I_{OUT}}{I_{OUT\max}}. \quad (10.67)$$

The definition of the load level parameter is necessary to relate the natural normalizing resistance to R_X defined by (10.26),

$$R_0 = \frac{V_m}{I_{OUT}} = \frac{R_X}{\alpha}. \quad (10.68)$$

After the normalization of the variables, the state-space model (10.47) becomes

$$\frac{d}{d\varphi} \begin{bmatrix} j_Y \\ m_{CS} \\ j_{LP} \\ m_{CP} \end{bmatrix} = \begin{bmatrix} -\frac{3r_S}{Q_S} & -\frac{3r_S}{\alpha\rho_S} & 0 & -\frac{3r_S}{\alpha\rho_S} \\ 3r_S\alpha\rho_S & 0 & 0 & 0 \\ 0 & 0 & 0 & \frac{3r_P}{\alpha\rho_P} \\ 3r_P\alpha\rho_P & 0 & -3r_P\alpha\rho_P & -\frac{3r_P}{Q_P} \end{bmatrix} \begin{bmatrix} j_Y \\ m_{CS} \\ j_{LP} \\ m_{CP} \end{bmatrix} + \begin{bmatrix} \frac{3r_S}{\alpha\rho_S}m_{AV} \\ 0 \\ 0 \\ -3r_P\alpha\rho_P \frac{\text{sgn}(m_{CP})}{n} \end{bmatrix}, \quad (10.69)$$

where

$$\rho_S = \frac{R_{0S}}{R_X} \quad (10.70)$$

and

$$\rho_P = \frac{R_{0P}}{R_X}. \quad (10.71)$$

In the same manner, the state-space model of (10.48) can be normalized.

Since the continuous conduction mode of the three-phase diode bridge is assumed, and the diode bridge is analyzed as a periodically switched linear circuit, the input current at the first phase of the rectifier is obtained as

$$\frac{i_1}{I_{OUT}} = j_1 = d_1 \left(1 + \frac{1}{2} j_Y \right) - d_2 \left(1 - \frac{1}{2} j_Y \right) - \frac{1}{3} j_Y, \quad (10.72)$$

after the normalized waveform j_Y of the injected current is obtained by numerical simulation of (10.65). The diode state functions d_1 and d_2 are defined in Chapter 2. Waveforms of the remaining two rectifier phases have the same shape, but displaced for $2\pi/3$ and $4\pi/3$. After the input current waveform is obtained, total harmonic distortion, power factor, displacement power factor, and all other parameters can be computed.

The most important analysis of the influence of the higher order harmonics is dependence of the input current THD on the load level parameter, defined by (10.63). At first, let us assume that the resonance constraints (10.14) are satisfied. This results in

$$\omega_{RS} = \omega_{RP} = 3\omega_0, \quad (10.73)$$

and corresponding values of the resonance parameters are

$$r_S = r_P = 1. \quad (10.74)$$

If the current injection system parameters have the values derived in Section 10.2,

$$\rho_S = \frac{\sqrt{3}}{\pi} \quad (10.75)$$

and

$$\rho_P = \frac{\sqrt{3}}{\pi^2}. \quad (10.76)$$

Since $R_S = 0$ and $G_P = 0$ in the analyzed case, $Q_S \rightarrow \infty$ and $Q_P \rightarrow \infty$, and the system (10.69) reduces to

$$\frac{d}{d\varphi} \begin{bmatrix} j_Y \\ m_{CS} \\ j_{LP} \\ m_{CP} \end{bmatrix} = \begin{bmatrix} 0 & -\frac{\pi\sqrt{3}}{\alpha} & 0 & -\frac{\pi\sqrt{3}}{\alpha} \\ \frac{3\sqrt{3}}{\pi}\alpha & 0 & 0 & 0 \\ 0 & 0 & 0 & \frac{\pi^2\sqrt{3}}{\alpha} \\ \frac{3\sqrt{3}}{\pi^2}\alpha & 0 & -\frac{3\sqrt{3}}{\pi^2}\alpha & 0 \end{bmatrix} \begin{bmatrix} j_Y \\ m_{CS} \\ j_{LP} \\ m_{CP} \end{bmatrix} + \begin{bmatrix} \frac{\pi\sqrt{3}}{\alpha}m_{AV} \\ 0 \\ 0 \\ -\frac{9\sqrt{3}}{8\pi}\alpha \operatorname{sgn}(m_{CP}) \end{bmatrix}. \quad (10.77)$$

The system (10.77), followed by the accompanying model for the discontinuous conduction intervals, is solved by applying numerical methods for a set of values for the load level parameter α , and corresponding input current waveforms are computed applying (10.72). The resulting dependence of the input current THD on the load level parameter is represented in Fig. 10-14 by the solid line. The dotted line presents the result obtained in the case the states of the diodes in the resistance emulator rectifier are controlled by v_{AV} , which is an approximation introduced in [34]. The result presented by the dotted line is obtained by applying numerical simulation of the state-space model, and the result is the same as the result obtained in [34] by applying Fourier series method for the corresponding periodically switched linear circuit. Comparing the results presented in Fig. 10-14 to those in Fig. 10 of [34], it can be concluded that the approximation of [34] is not well justified, and that simulation of the nonlinear circuit has to be performed in order to provide accurate results.

The simulation results presented in Fig. 10-14 are of low practical importance. As shown in [34], experiments provide quite different dependence of the input current THD on the load level parameter α . The reason for this is leakage of the parallel resonant circuit at the triple of the line frequency, which is the most pronounced parasitic effect. The simulation method presented here can easily capture the leakage, since G_P is included in the current injection system model.

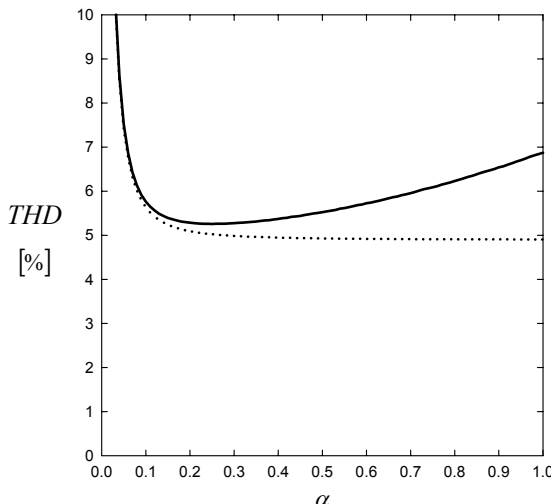


Figure 10-14. Dependence of the input current THD on α .

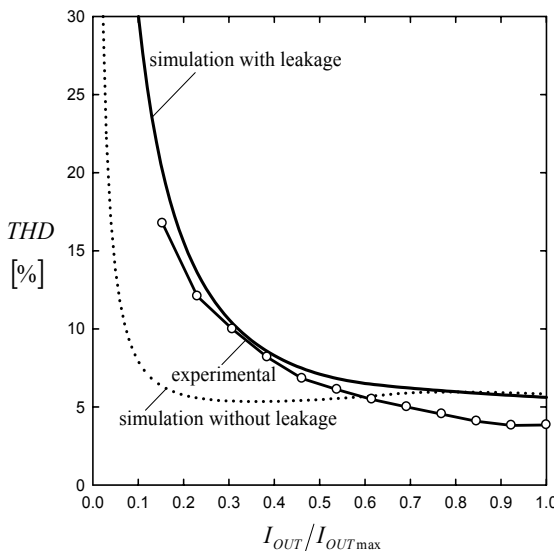


Figure 10-15. Dependence of the input current THD on α with the leakage of the parallel resonant circuit taken into account.

The simulation results in the case the leakage is taken into account are presented in Fig. 10-15 in the case of the experimental rectifier presented in [34]. The simulation results differ slightly from the results of [34], but capture the behavior of the experimental curve. The dotted curve in Fig. 10-15 presents the dependence of the input current THD for the considered rectifier in the case the leakage is neglected. This curve significantly differs from the experimental curve and the curve obtained by simulation with the leakage taken into account. From experimental results and Fig. 10-15, it can be concluded that the leakage of the parallel resonant circuit at the triple of the line frequency significantly affects the input current THD, and should be taken into account when the analyses are performed.

Chapter 11

RECOVERY OF THE CURRENT INJECTION NETWORK POWER APPLYING A VOLTAGE-LOADED RESISTANCE EMULATOR

In Chapter 10, a current-loaded passive resistance emulator is proposed. This type of resistance emulator does not require high-frequency switching, and it restores the power taken by the current injection network at the rectifier output by increasing the output voltage DC component. In addition, the output voltage ripple is reduced. The main advantage of the current-loaded resistance emulator is automatic adjustment to the load current variations. Although the concept works well with ideal resonant circuits, the selectivity of the resonant circuits that can be afforded in practice somewhat degrades the results. Finally, the main disadvantage of the current-loaded resistance emulator is the application of two resonant circuits, requiring two resonant constraints to be satisfied. To avoid one of the resonant circuits, application of a voltage-loaded resistance emulator is proposed in this chapter. In comparison to the current-loaded resistance emulator, one of the resonant circuits is going to be omitted, and straightforward adjustment to the load current variations will be lost. However, due to the low sensitivity of the input current total harmonic distortion (THD) on suboptimal operation of the rectifier, acceptable THD values of the input currents are obtained within a wide range of the load current variations.

The rectifier discussed in this chapter is presented in Fig. 11-1, and it consists of a three-phase diode bridge and a current injection system. The current injection system consists of three blocks: a current injection device, a current injection network, and a voltage-loaded resistance emulator. For the current injection device, any of the devices described in Chapter 4 will suffice. Current injection network C, analyzed in Section 6.5, is applied since its performance is superior in comparison to the other third-harmonic current injection networks. A new part of the rectifier is the voltage-loaded resistance emulator, which consists of a transformer with the turns ratio $1:n$, and a single-phase diode bridge consisting of diodes DR1 to DR4.

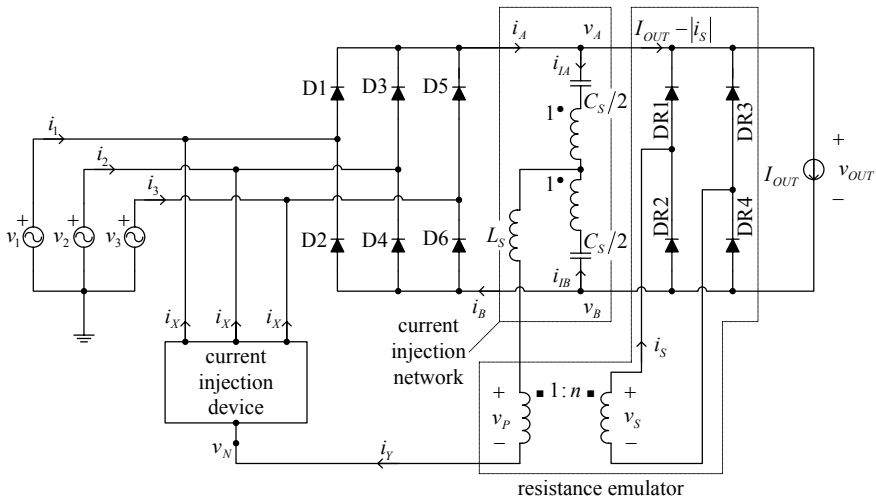


Figure 11-1. The third-harmonic current injection rectifier applying a voltage-loaded resistance emulator. © [2005] IEEE.

The resistance emulator is connected in parallel to the load; thus the voltage at the resistance emulator output is the same as the rectifier output voltage. In contrast to the resistance emulator described in Chapter 10, the voltage-loaded resistance emulator recovers the power taken by the current injection network, increasing the output current instead of increasing the output voltage. Actually, the resistance emulator output current reduces the current the load takes from the three-phase diode bridge. The transformer of the resistance emulator is assumed to be modeled by an ideal transformer with a huge magnetizing inductance. Thus, fine-tuning of the magnetizing inductance, required for the current-loaded resistance emulator transformer, is not needed. Choice of the elements of the current injection network is subject to the same constraints as discussed in Section 6.5.

It might be interesting to note here that the original ideas about the voltage-loaded resistance emulator included an additional filter at the resistance emulator output, consisting of an inductor and a capacitor, intended to remove the ripple of the resistance emulator output current. During the experimental work, one fortunate mistake left the filter out of the circuit, which was noticed while an amazing fact—that unexpectedly good results were obtained—was investigated. After the fact that the resistance emulator output current ripple improves the input current THD was discovered, instead of an incorrectly expected degradation, everything else was simple, including the mathematical model, optimization, simulation, etc. It seems that sometimes it might be a good practice to make a mistake during experimental work.

Let us assume that the rectifier is supplied by an undistorted symmetrical three-phase voltage system:

$$v_p = V_m \cos\left(\omega_0 t - (p-1)\frac{2\pi}{3}\right), \quad (11.1)$$

where $p \in \{1, 2, 3\}$. In that case, assuming $i_A > 0$ and $i_B > 0$, the diode states are determined by the diode state functions introduced in Chapter 2. The input current of the first phase is given by

$$i_1 = d_1 i_A - d_2 i_B - i_X, \quad (11.2)$$

while the currents at the remaining two phases have the same waveforms, but delayed for $2\pi/3$ and $4\pi/3$ in phase. Current i_A that loads the positive output terminal of the three-phase diode bridge is

$$i_A = I_{OUT} - |i_S| + \frac{1}{2}i_Y, \quad (11.3)$$

while the current that loads the negative output terminal of the three-phase diode bridge is

$$i_B = I_{OUT} - |i_S| - \frac{1}{2}i_Y. \quad (11.4)$$

The current injection device splits the injected current i_Y into three equal parts,

$$i_X = \frac{1}{3}i_Y. \quad (11.5)$$

The resistance emulator transformer secondary current is

$$i_S = \frac{1}{n}i_Y. \quad (11.6)$$

Substituting equations (11.3) to (11.6) in (11.2), the input current is obtained as

$$i_1 = d_1 \left(I_{OUT} - \frac{1}{n} |i_Y| + \frac{1}{2} i_Y \right) - d_2 \left(I_{OUT} - \frac{1}{n} |i_Y| - \frac{1}{2} i_Y \right) - \frac{1}{3} i_Y. \quad (11.7)$$

Up to this point, the rectifier analysis was exact; only element characteristics and Kirchhoff's current law were applied. At this point, let us make an approximation, assuming that the injected current consists only of a spectral component at the triple of the line frequency,

$$i_Y = kI_{OUT} \cos(3\omega_0 t), \quad (11.8)$$

where k is the normalized amplitude of the injected current. The injected current is assumed to be in phase with the fundamental harmonic of the three-phase diode bridge output terminal voltages, corresponding to the optimization results of Chapter 5. Under the assumption of (11.8), the waveform of the input current becomes

$$\begin{aligned} \frac{i_1}{I_{OUT}} &= j_1 = d_1 \left(1 - \frac{k}{n} |\cos(3\omega_0 t)| + \frac{k}{2} \cos(3\omega_0 t) \right) \\ &\quad - d_2 \left(1 - \frac{k}{n} |\cos(3\omega_0 t)| - \frac{k}{2} \cos(3\omega_0 t) \right) - \frac{k}{3} \cos(3\omega_0 t). \end{aligned} \quad (11.9)$$

An expanded representation of the waveform specified by (11.9) is given in Table 11-1, in a form convenient to compute the input current characterization parameters.

After the waveform of the input current is obtained in a convenient form, the input current parameters are computed. The RMS value of the input current fundamental harmonic is obtained as

$$I_{1RMS} = \frac{\sqrt{6}(k(n-10)+16n)}{16\pi n} I_{OUT}, \quad (11.10)$$

while the RMS value of the input current waveform is

$$I_{RMS} = \frac{\sqrt{\pi k^2(n^2+12)-96kn+24\pi n^2}}{6\sqrt{\pi}n} I_{OUT}. \quad (11.11)$$

Total harmonic distortion of the input current is computed by applying

Table 11-1. Analytical description of the input current waveform.

Interval	d_1	d_2	$\text{sgn}(i_Y)$	i_1/I_{OUT}
$0 < \omega_0 t < 30^\circ$	1	0	+1	$1 + k \left(\frac{1}{6} - \frac{1}{n} \right) \cos(3\omega_0 t)$
$30^\circ < \omega_0 t < 60^\circ$	1	0	-1	$1 + k \left(\frac{1}{6} + \frac{1}{n} \right) \cos(3\omega_0 t)$
$60^\circ < \omega_0 t < 90^\circ$	0	0	-1	$-\frac{k}{3} \cos(3\omega_0 t)$
$90^\circ < \omega_0 t < 120^\circ$	0	0	+1	$-\frac{k}{3} \cos(3\omega_0 t)$
$120^\circ < \omega_0 t < 150^\circ$	0	1	+1	$-1 + k \left(\frac{1}{6} + \frac{1}{n} \right) \cos(3\omega_0 t)$
$150^\circ < \omega_0 t < 180^\circ$	0	1	-1	$-1 + k \left(\frac{1}{6} - \frac{1}{n} \right) \cos(3\omega_0 t)$
$180^\circ < \omega_0 t < 210^\circ$	0	1	-1	$-1 + k \left(\frac{1}{6} - \frac{1}{n} \right) \cos(3\omega_0 t)$
$210^\circ < \omega_0 t < 240^\circ$	0	1	+1	$-1 + k \left(\frac{1}{6} + \frac{1}{n} \right) \cos(3\omega_0 t)$
$240^\circ < \omega_0 t < 270^\circ$	0	0	+1	$-\frac{k}{3} \cos(3\omega_0 t)$
$270^\circ < \omega_0 t < 300^\circ$	0	0	-1	$-\frac{k}{3} \cos(3\omega_0 t)$
$300^\circ < \omega_0 t < 330^\circ$	1	0	-1	$1 + k \left(\frac{1}{6} + \frac{1}{n} \right) \cos(3\omega_0 t)$
$330^\circ < \omega_0 t < 360^\circ$	1	0	+1	$1 + k \left(\frac{1}{6} - \frac{1}{n} \right) \cos(3\omega_0 t)$

$$THD(k, n) = \frac{\sqrt{I_{RMS}^2 - I_{1RMS}^2}}{I_{1RMS}}, \quad (11.12)$$

and a bulky expression

$$THD(k, n) = \frac{\sqrt{3} \sqrt{k^2 (h^2 (32\pi^2 - 27) + 540n + 12(32\pi^2 - 225) - 96kn(9n + 2(16\pi - 45))) + 768h^2 (\pi^2 - 9)}}{9(k(n-10) + 16n)} \quad (11.13)$$

is obtained as a result. At this point, the input current THD is obtained as a function of the transformer turns ratio n and the injected current normalized amplitude k , regardless of the way the injected current is provided and its

amplitude controlled. The injected current amplitude may be limited by the rectifier transition to the discontinuous conduction mode, and by the current injection network parasitic resistance. Both of these cases are analyzed in subsequent sections.

1. ANALYSIS OF THE RECTIFIER IN THE CONTINUOUS CONDUCTION MODE

The rectifier in Fig. 11-1 contains two diode bridges: the main three-phase diode bridge, D1 to D6, and the resistance emulator diode bridge, DR1 to DR4. When addressing the conduction modes, the focus is on the main three-phase rectifier bridge, and the continuous conduction mode of the resistance emulator diode bridge is assumed, unless otherwise explicitly stated. In the continuous conduction mode, in each time point two of the diodes in the three-phase diode bridge conduct—one connected by its anode to the highest of the phase voltages, and the other connected by its cathode to the lowest of the phase voltages. This results in

$$v_A = \max(v_1, v_2, v_3) \quad (11.14)$$

and

$$v_B = \min(v_1, v_2, v_3). \quad (11.15)$$

To provide the continuous conduction mode, it is necessary to have $i_A > 0$ and $i_B > 0$ in each time point during the period.

Now, let us assume that the injected current i_Y is

$$i_Y = kI_{OUT} \cos(3\omega_0 t). \quad (11.16)$$

This assumption implies continuous conduction mode of the resistance emulator diode bridge. In that case, voltage v_P at the input of the resistance emulator is

$$v_P = \frac{1}{n} v_{OUT} \operatorname{sgn}(i_Y). \quad (11.17)$$

Waveforms of the currents and the voltages at the input and the output of the resistance emulator are shown in Fig. 11-2. The waveform of the resistance emulator input voltage, v_P , contains spectral components at odd triples of

the line frequency, and its Fourier series expansion is

$$v_p = \frac{6\sqrt{3}}{\pi} \frac{V_m}{n} \sum_{k=0}^{+\infty} \frac{6(-1)^{k+1}(2k-1)-1}{9(2k-1)^2-1} \cos(3(2k-1)\omega_0 t). \quad (11.18)$$

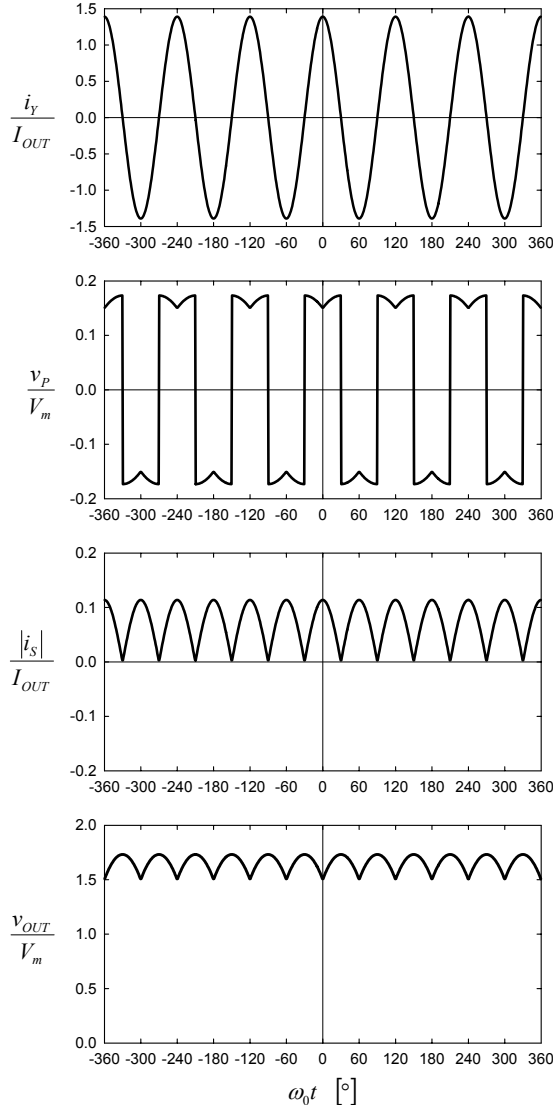


Figure 11-2. Currents and voltages at the resistance emulator input and the output.

To apply the method of equivalent circuits introduced in Chapter 6, it is convenient to represent the Fourier series expansion as a sum of particular harmonic components,

$$v_{P,2k-1} = \frac{6\sqrt{3}}{\pi} \frac{V_m}{n} \frac{6(-1)^{k+1}(2k-1)-1}{9(2k-1)^2 - 1} \cos(3(2k-1)\omega_0 t). \quad (11.19)$$

The amplitude of the fundamental harmonic of v_P is

$$V_{P,1} = \frac{15\sqrt{3}}{4\pi} \frac{V_m}{n}. \quad (11.20)$$

After the waveforms of the current injection network system are determined, it can be represented by an equivalent circuit shown in Fig. 11-3 that applies for odd triples of the line frequency. Losses in the current injection network, the resistance emulator, and the current injection device are represented by a resistor with the resistance R in the equivalent circuit of Fig. 11-3. At even triples of the line frequency, the current injection system can be represented by an open circuit.

Analyzing the equivalent circuit of Fig. 11-3 at the triple of the line frequency, the injected current i_Y is related to the voltages applied over the current injection network,

$$v_{A,1} = R i_Y + v_{P,1}. \quad (11.21)$$

Substituting expressions for the fundamental harmonics, (11.21) is reduced to an equation over amplitudes of the fundamental harmonics,

$$\frac{3\sqrt{3}}{8\pi} V_m = R k I_{OUT} + \frac{15\sqrt{3}}{4\pi} \frac{V_m}{n}, \quad (11.22)$$

which can be rearranged to

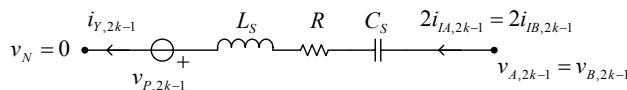


Figure 11-3. Equivalent circuit of the current injection system for odd triples of the line frequency.

$$kI_{OUT} = \frac{3\sqrt{3}}{8\pi} \left(1 - \frac{10}{n}\right) \frac{V_m}{R}. \quad (11.23)$$

Thus, amplitude of the injected current is primarily determined by the parasitic resistance of the current injection system. In the special case that $R = 0$, from (11.22) the turns ratio of the resistance emulator transformer is obtained as

$$n = 10. \quad (11.24)$$

This value of the transformer turns ratio, for $R = 0$, leaves the injected current amplitude undetermined. Lower values of the turns ratio, $n < 10$, cause the resistance emulator diode bridge to operate in the discontinuous conduction mode, resulting in high values of the input current THD. Situation $n > 10$ causes the main three-phase diode bridge to operate in the discontinuous conduction mode.

In the case $n = 10$, (11.13) reduces to a function of one variable, $THD(k, 10)$, where the optimal amplitude of the injected current is determined from

$$\frac{d THD(k, 10)}{d k} = 0, \quad (11.25)$$

and the minimum of the THD is achieved for

$$k = \frac{30}{7\pi} \approx 1.36. \quad (11.26)$$

The optimal amplitude of the injected current is lower than if the resistance emulation is not applied, where the optimum is reached for $k = 1.5$, as shown in Chapter 5. The minimal value of the THD is

$$THD = \frac{1}{3} \sqrt{\pi^2 - \frac{69}{7}} \approx 3.72\%, \quad (11.27)$$

which is lower than if the resistance emulation is not applied, when the minimum of the THD is 5.12%. These differences are caused by the output current of the resistance emulator, $|i_S|$, presented in the third diagram of Fig. 11-2. This current contains significant harmonics at even triples of the line frequency, and alters the current that loads the three-phase diode bridge.

The waveform of the current that loads the main diode bridge, $I_{OUT} - |i_S|$, is presented in the first diagram of Fig. 11-4 for $n=10$. The harmonics of the diode bridge load current reduce the input current THD in the same manner as the input current THD is reduced to zero by adequate injection of the higher order harmonics described in Chapter 8. The waveform of the load current of the positive output terminal of the diode bridge, i_A , is shown in the second diagram of Fig 11-4, proving that the diode bridge operates in the continuous conduction mode, since $i_A > 0$ during the whole period. The waveform of i_B has the same shape, but it is displaced in phase for 60° in comparison to i_A , i.e., for one half of its period. The corresponding waveform of the input current of the rectifier first phase is presented in the last diagram of Fig. 11-4.

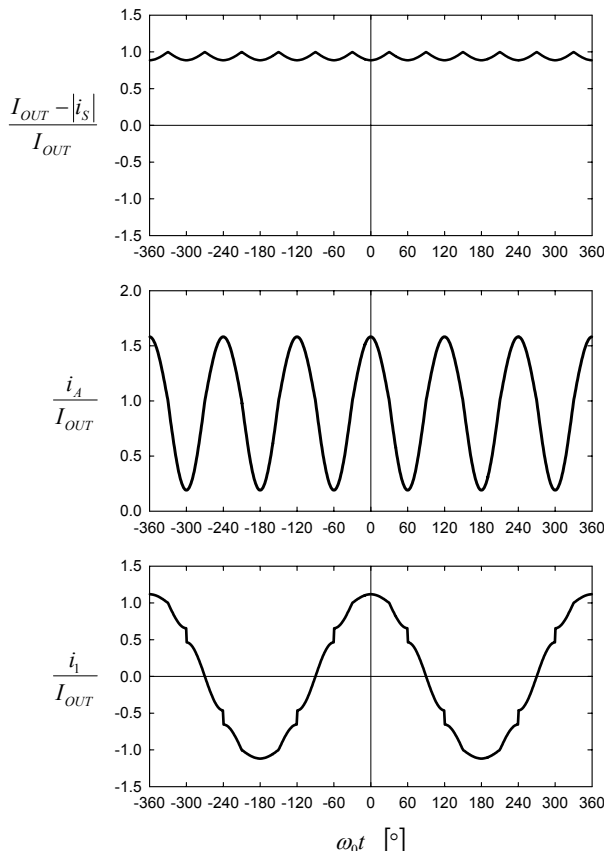


Figure 11-4. Waveforms of the rectifier currents for $n=10$ and $k=1.36$.

Dependence of the input current THD on the transformer turns ratio n and the normalized amplitude of the injected current k is a smooth function of these two variables. For a fixed value of n , the function reaches the minimum for

$$\frac{\partial \text{THD}(k, n)}{\partial k} = 0. \quad (11.28)$$

This results in the optimal value of k for specified n , given by

$$k_{opt}(n) = \frac{3n(\pi n - 2(5\pi - 16))}{2(\pi n^2 + 3n + 6(2\pi - 5))}. \quad (11.29)$$

Substituting (11.29) in (11.13), the input current THD becomes a function of only one variable, the transformer turns ratio, $\text{THD}(k_{opt}(n), n)$, and the minimum is reached for

$$\frac{d \text{THD}(k_{opt}(n), n)}{d n} = 0, \quad (11.30)$$

corresponding to the global minimum of the THD. Applying a symbolic computation program to handle bulky equations, optimal values of k and n , when the input current THD reaches a global minimum, are obtained as

$$k_{OPT} = \frac{3(\pi^2 - 8)}{\pi(2\pi - 5)} \approx 1.39 \quad (11.31)$$

and

$$n_{OPT} = \frac{6(\pi^2 - 8)}{\pi(16 - 5\pi)} \approx 12.23. \quad (11.32)$$

The optimal values for k and n provide the minimal THD of

$$\begin{aligned} \text{THD}_{MIN} &= \text{THD}(k_{OPT}, n_{OPT}) \\ &= \frac{1}{3} \sqrt{\frac{8\pi^4 - 199\pi^2 + 360\pi + 54}{15\pi^2 - 40\pi - 6}} \approx 3.64\%. \end{aligned} \quad (11.33)$$

This value is somewhat lower than the minimal value obtained for $n = 10$,

but the difference is so small that it can be neglected in practice. Another conclusion that can be drawn is that the input current THD is weakly sensitive on the choice of the transformer turns ratio, since similar THD values are obtained for $n = 10$ and $n = 12.23$.

The current injection system equivalent resistance is obtained from (11.22) as

$$R = \frac{3\sqrt{3}}{8\pi} \left(1 - \frac{10}{n}\right) \frac{V_m}{kI_{OUT}}, \quad (11.34)$$

and for the optimal values of k and n given by (11.31) and (11.32), the corresponding value of the current injection system equivalent resistance is

$$R_{OPT} = \frac{\sqrt{3}(2\pi - 5)(7\pi^2 - 20\pi - 6)}{6(\pi^2 - 8)^2} \frac{V_m}{I_{OUT}} \approx 2.71\% \frac{V_m}{I_{OUT}}. \quad (11.35)$$

In terms of the rectifier output voltage, the resistance value corresponding to k_{OPT} and n_{OPT} is

$$R_{OPT} = \frac{\pi(2\pi - 5)(7\pi^2 - 20\pi - 6)}{18(\pi^2 - 8)^2} \frac{V_{OUT}}{I_{OUT}} \approx 1.64\% \frac{V_{OUT}}{I_{OUT}}. \quad (11.36)$$

The power dissipated on the equivalent resistance of the current injection system in this case equals

$$P_R = \frac{7\pi^2 - 20\pi - 6}{4\pi(2\pi - 5)} P_{OUT} \approx 1.58\% P_{OUT}, \quad (11.37)$$

which is significantly lower than 9.38% in the case of the optimal third-harmonic current injection without the resistance emulator. Thus, application of the resistance emulator reduced the power dissipated by the current injection system, improved the input current THD, and reduced the optimal amplitude of the injected current, reducing the current stress on applied components.

In practice, the rectifier design cannot afford to choose the optimal value for the current injection system equivalent resistance R . Instead, the value of R is given by the choice of components, primarily the components of the current injection network discussed in Section 6.5, and the current injection device discussed in Chapter 4. Thus, the turns ratio of the resistance emulator transformer has to be adjusted to the given value of R to provide the optimal

performance in that case. Assuming that the normalized amplitude of the injected current has the optimal value specified by (11.29), and since the resistance of the current injection system is related to other parameters by (11.34), eliminating k from these equations a relation between the transformer turns ratio, the equivalent resistance, the output current, and the input voltage amplitude is obtained as

$$\frac{RI_{OUT}}{V_m} = \frac{\sqrt{3}}{4\pi} \frac{n-10}{n^2} \frac{\pi n^2 + 3n + 6(2\pi - 5)}{\pi n - 2(5\pi - 16)}. \quad (11.38)$$

The optimal value of the transformer turns ratio, n_{opt} , that provides the optimal amplitude of the injected current for given values of R , I_{OUT} , and V_m is obtained from (11.38). The closed form expression for n_{opt} is too bulky to be applicable; thus a diagram that relates n_{opt} to RI_{OUT}/V_m is presented in Fig. 11-5. Hence the rectifier design should start from the current injection network and the current injection device, and after their parameters are determined, the resistance emulator transformer turns ratio should be determined to minimize the input current THD at the desired operating point.

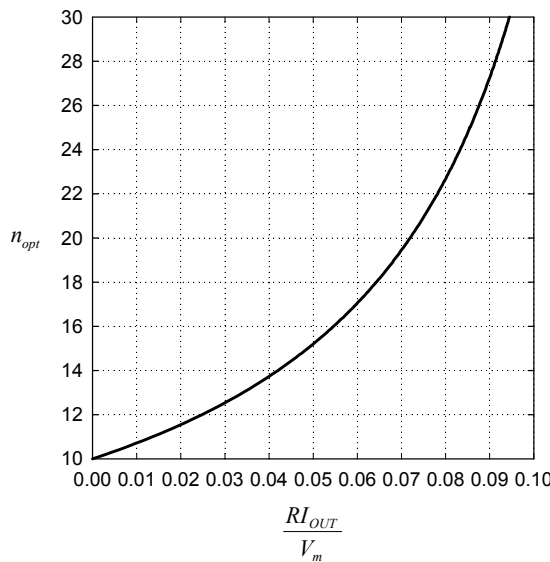


Figure 11-5. Dependence of the resistance emulator transformer optimal turns ratio on RI_{OUT}/V_m .

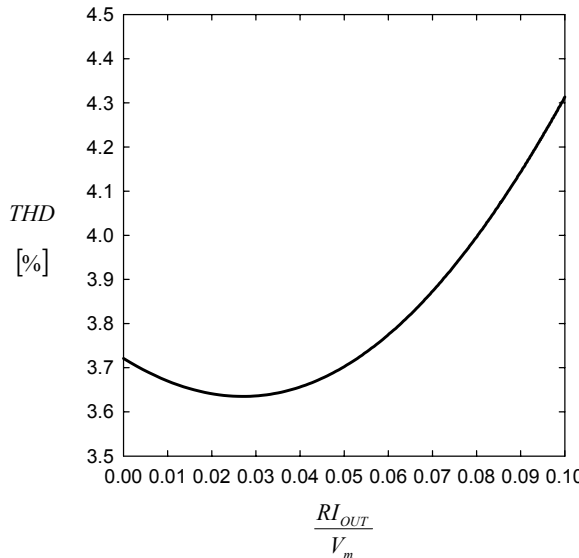


Figure 11-6. Dependence of the input current THD on RI_{OUT}/V_m .

Dependence of the input current THD on RI_{OUT}/V_m is presented in Fig. 11-6. The curve is obtained from (11.13), substituting the value of n obtained from (11.38) and the value of k obtained from (11.29), $k_{opt}(n)$. The diagram illustrates that the minimal value of the input current THD is dependent on RI_{OUT}/V_m , but this dependence is small enough not to be relevant in practice. Thus, the most important issue for proper design of the resistance emulator is the choice of the transformer turns ratio, the value of which should provide the optimal amplitude of the injected current.

Obviously, it would be very hard to design the rectifier to operate with the optimal amplitude of the injected current specified by (11.31) and the optimal turns ratio of the transformer given by (11.32). Even if achievable, the optimum would apply to only one operating point of the rectifier. A somewhat easier task is to design the rectifier to provide minimal THD for the specified RI_{OUT}/V_m , but this constrained optimum applies for only one value of the output current. Thus, of essential importance for applicability of the rectifier discussed in this chapter is sensitivity of the input current THD on the two parameters that affect it, the normalized injected current amplitude k and the transformer turns ratio n , since the most likely situation is that the rectifier operates in a suboptimal mode.

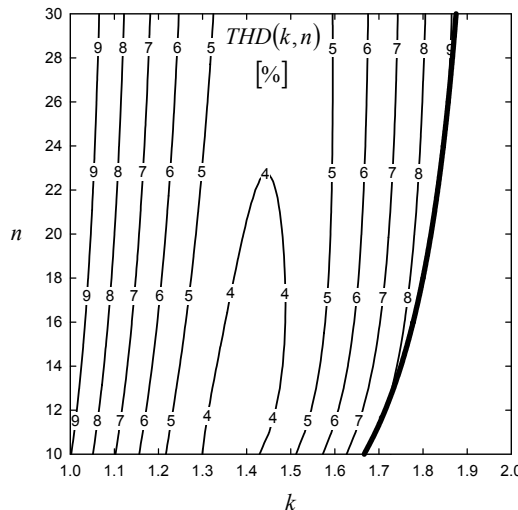


Figure 11-7. Dependence of the input current THD on k and n .

Dependence of the input current THD on k and n is presented in a contour plot shown in Fig. 11-7 in the range where both rectifier bridges operate in the continuous conduction mode. The area in the (k, n) diagram on the right-hand side of the thick line corresponds to the discontinuous conduction mode, which is discussed in the next section. The contour plot shows wide regions where the input current THD is lower than 4%, and lower than 5%. These values are considered acceptable in almost all of the situations. An important conclusion from the contour plot is that the input current THD is more sensitive on the injected current normalized amplitude than on the resistance emulator turns ratio. Thus, the turns ratio should be carefully adjusted to provide near optimal normalized amplitude of the injected current, around 1.4, for a wide range of the rectifier output current.

2. ANALYSIS OF THE RECTIFIER IN THE DISCONTINUOUS CONDUCTION MODE

Results presented in the previous section apply for the continuous conduction mode of both diode bridges in the rectifier shown in Fig. 11-1. If the equivalent resistance of the current injection system is low, the three-phase diode bridge operates in the discontinuous conduction mode, which limits the amplitude of the injected current. The boundary between the continuous and the discontinuous conduction mode is determined by the

three-phase diode bridge load current that touches zero at one point during the period. A critical point is the minimum of i_A that occurs at the phase angle of 60° , according to the second diagram of Fig. 11-4. At the boundary between the modes, i_A touches zero at 60° , and according to (11.3), (11.6), and (11.8) we obtain

$$\begin{aligned} i_A(60^\circ) &= I_{OUT} \left(1 - \left| \frac{k}{n} \cos 180^\circ \right| + \frac{k}{2} \cos 180^\circ \right) \\ &= I_{OUT} \left(1 - k \frac{n+2}{2n} \right) = 0. \end{aligned} \quad (11.39)$$

This results in a relation between the normalized amplitude of the injected current and the transformer turns ratio in the discontinuous conduction mode:

$$k = \frac{2n}{n+2}. \quad (11.40)$$

When $n \rightarrow \infty$, the normalized amplitude of the injected current $k \rightarrow 2$, corresponding to the discontinuous conduction mode of the rectifier without the resistance emulator.

From (11.40), the upper boundary of the continuous conduction mode is

$$k < \frac{2n}{n+2} \quad (11.41)$$

which can be expressed in terms of the output current as

$$I_{OUT} > \frac{3\sqrt{3}}{16\pi} \frac{V_m}{R} \frac{n^2 - 8n - 20}{n^2}. \quad (11.42)$$

Thus, the discontinuous conduction mode of the three-phase diode bridge occurs for the output current values lower than specified by (11.42), which is likely to occur at the rectifier light loads. On the other hand, the normalized value of the injected current amplitude in the continuous conduction mode from (11.22) is given by

$$k = \frac{3\sqrt{3}}{8\pi} \left(1 - \frac{10}{n} \right) \frac{V_m}{RI_{OUT}}. \quad (11.43)$$

For

$$n > 10, \quad (11.44)$$

the injected current amplitude computed from (11.43) is positive and the rectifier operates in the continuous conduction mode. However, for lower values of the turns ratio, the injected current amplitude does not become negative, but the resistance emulator diode bridge switches to the discontinuous conduction mode instead. This mode of operation is characterized by time intervals when all of the diodes in the resistance emulator diode bridge do not conduct, resulting in the injected current instantaneous value equal to zero during these intervals. The transformer turns ratio $n = 10$ may be considered as a lower boundary for the continuous conduction operation mode of the rectifier. However, this boundary is not that precise as the upper boundary, since at low amplitudes of the injected current the higher order harmonics dominate the injected current waveform. The value $n = 10$ is used as a lower continuous conduction mode boundary in the contour plot of Fig. 11-7.

In the analysis of the discontinuous conduction mode that follows, the “high filtering” approximation introduced in Chapter 9 is used. According to the approximation, the injected current i_Y contains only a spectral component at the triple of the line frequency, with the normalized amplitude given by (11.40). In that case, the input current THD is determined by (11.13) substituting (11.40) for k ,

$$THD_{DCM}(n) = THD\left(\frac{2n}{n+2}, n\right). \quad (11.45)$$

Thus, the input current THD is a function of only one variable, the transformer turns ratio. The input current THD reaches the minimum for

$$\frac{d}{dn}(THD_{DCM}(n)) = 0, \quad (11.46)$$

resulting in

$$n_{DCM\ OPT} = 6 \frac{7\pi - 20}{36 - 11\pi} \approx 8.28, \quad (11.47)$$

and corresponding to the THD value of

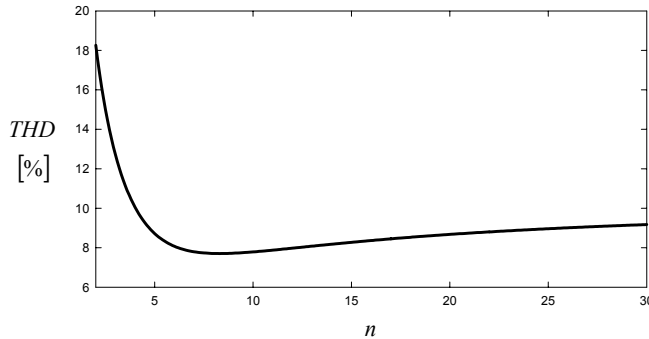


Figure 11-8. Dependence of the THD on n in the discontinuous conduction mode.

$$THD_{DCM}(n_{DCM\ OPT}) = \frac{\sqrt{936\pi^4 - 3424\pi^3 - 16377\pi^2 + 89640\pi - 104976}}{9(13\pi - 36)} \approx 7.71\%. \quad (11.48)$$

The optimization result is obtained assuming the sinusoidal waveform of i_Y given by (11.8). However, the optimized transformer turns ratio of (11.47) corresponds to the discontinuous conduction mode of the resistance emulator diode bridge, where i_Y is equal to zero during intervals of time; thus the sinusoidal waveform of (11.8) is not a valid approximation. The lowest value of n where assumed waveform of i_Y applies is $n = 10$, providing a somewhat higher THD value of

$$THD_{DCM}(10) = \frac{1}{9} \sqrt{\frac{61\pi^2 - 36\pi - 486}{6}} \approx 7.79\%. \quad (11.49)$$

Increasing the transformer turns ratio, the input current THD approaches the value computed in Chapter 9 for the discontinuous conduction mode without the resistance emulator,

$$\lim_{n \rightarrow \infty}(THD_{DCM}(n)) = \frac{1}{27} \sqrt{\frac{224\pi^2 - 2187}{3}} \approx 10.43\%. \quad (11.50)$$

In Fig. 11-8, the dependence of the input current THD on the transformer turns ratio in the discontinuous conduction mode is presented. The diagram is valid for $n > 10$, where both of the diode bridges operate in the continuous conduction mode. It is important to observe that in the region of interest, for

$n > 10$, the input current THD weakly depends on the transformer turns ratio, varying from 7.79% to 10.43%. Thus, application of the resistance emulator reduces the input current THD in the discontinuous conduction mode. It is important to underline here that according to the high filtering approximation introduced in Chapter 9, once the discontinuous conduction mode is reached, the input current THD remains the same as it was at the boundary of the discontinuous mode. The validity of this approximation is studied by applying simulation methods as described in subsequent sections.

Waveforms of the rectifier currents in the discontinuous conduction mode for $n = 10$ are presented in Fig. 11-9. In the first diagram, the normalized value of i_A is presented, showing that the waveform touches zero once per its period. The current that loads the diode bridge is presented in the second diagram, showing the ripple caused by the resistance emulator. This ripple, along with the reduced amplitude of the injected current, results in the input current THD value lower than in the case the resistance emulator is not applied. The last diagram presents the input current waveform with $THD = 7.79\%$.

In the discontinuous conduction mode, during the discontinuous intervals voltage spikes at the three-phase diode bridge output terminals occur, as shown in Chapter 9. These voltage spikes play an essential role in control of the injected current amplitude, since they affect the harmonic balance of the equivalent circuit of Fig. 11-3 at the triple of the line frequency. In this manner, the amplitude of the voltage that drives the fundamental harmonic of i_Y is reduced to the level required to provide the amplitude determined by (11.40). Applying the same technique introduced in [7], described in detail in Chapter 9, in the discontinuous conduction mode voltage at the rectifier positive output terminal can be approximated by

$$v_A = \max(v_1, v_2, v_3) + V_X \sum_{l=-\infty}^{+\infty} \delta\left(\omega_0 t - l \frac{2\pi}{3}\right), \quad (11.51)$$

while the voltage at the rectifier negative output terminal is

$$v_B = \min(v_1, v_2, v_3) - V_X \sum_{l=-\infty}^{+\infty} \delta\left(\omega_0 t - l \frac{2\pi}{3}\right), \quad (11.52)$$

where $\delta(\varphi)$ is the Dirac impulse δ -function. The average of the two voltages that effectively drives the current injection system is given by

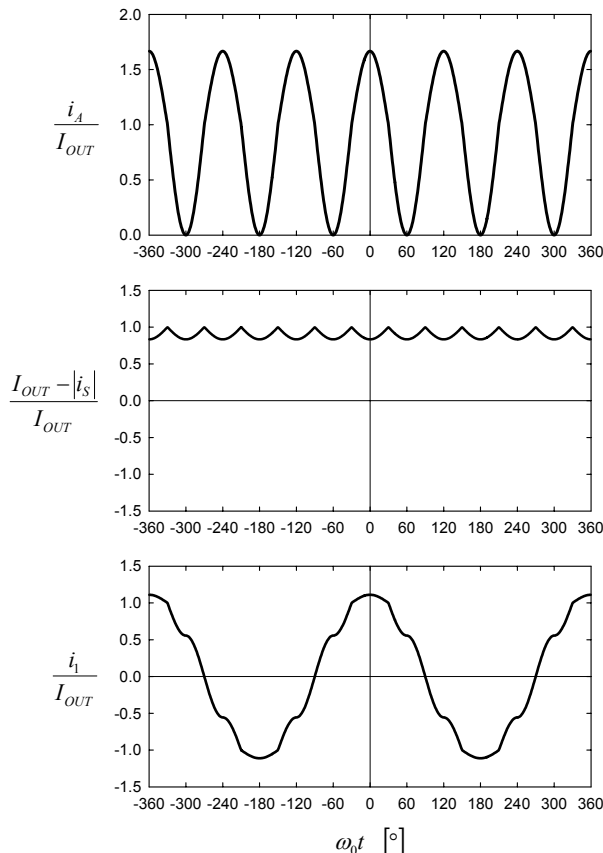


Figure 11-9. Waveforms of the rectifier currents in the discontinuous conduction mode for $n = 10$.

$$\frac{v_A + v_B}{2} = v_{AV} - \frac{V_X}{2} \sum_{l=-\infty}^{+\infty} (-1)^l \delta\left(\omega_0 t - l \frac{\pi}{3}\right). \quad (11.53)$$

On the other hand, the modified output voltage affects the resistance emulator input voltage, which can be approximated by

$$v_p = \frac{v_A - v_B}{n} \operatorname{sgn}(i_Y) = \frac{\max(v_1, v_2, v_3) - \min(v_1, v_2, v_3)}{n} \operatorname{sgn}(i_Y) + \frac{V_X}{n} \sum_{l=-\infty}^{+\infty} (-1)^l \delta\left(\omega_0 t - l \frac{\pi}{3}\right). \quad (11.54)$$

The sequence of δ -impulses that appears in (11.53) and (11.54) can be expanded in the Fourier series as

$$\sum_{l=-\infty}^{+\infty} (-1)^l \delta\left(\omega_0 t - l \frac{\pi}{3}\right) = \frac{6}{\pi} \sum_{m=1}^{+\infty} \cos(3(2m-1)\omega_0 t). \quad (11.55)$$

The amplitude of the impulses is determined by balancing the harmonics of the equivalent circuit of Fig. 11-3 at the triple of the line frequency, and

$$V_X(n) = \frac{\pi}{3} \frac{n}{n+2} \left(\frac{3\sqrt{3}}{8\pi} \left(1 - \frac{10}{n} \right) V_m - \frac{2n}{n+2} RI_{OUT} \right) \quad (11.56)$$

is obtained. In the case $n \rightarrow \infty$, the result approaches the result for the discontinuous conduction mode without the resistance emulation,

$$\lim_{n \rightarrow \infty} (V_X(n)) = \frac{\sqrt{3}}{8} V_m - \frac{2\pi}{3} RI_{OUT}. \quad (11.57)$$

After the amplitude of the δ -impulses is determined, the methods of Chapter 9 could be directly applied to determine the average of the output voltage in the discontinuous conduction mode and the maximum of the output voltage instantaneous value. Since bulky expressions are obtained, they are not presented here.

Substituting parameter values of actual rectifiers in (11.56), it can be concluded that the resistance emulation significantly reduces the amplitude of the voltage spikes, reducing the maximum instantaneous value of the output voltage and the increase of the output voltage DC component in the discontinuous conduction mode.

3. CHOICE OF COMPONENTS

Two parts of the current injection system applied in the rectifier of Fig. 11-1 have already been discussed: the current injection device and the

current injection network. Application of the voltage-loaded resistance emulator did not affect operating conditions of the current injection device; thus the results of Chapter 4 are directly applicable. The same applies for the choice of components in the current injection network; the results of Section 6.5 are directly applicable regardless of the way the resistance in the current injection network is obtained—applying a resistor or a resistance emulator. Thus, elements of the resistance emulator, the transformer and the diodes, remain to be discussed.

Choice of the transformer turns ratio has been discussed previously, and its value is determined by the requirement to provide minimal total harmonic distortions of the input currents. The volt-ampere rating of the device is computed using (4.3), and according to the transformer primary voltage given by (11.17), and shown in the second diagram of Fig. 11-2, Φ_{\max} is computed. Root-mean-square (RMS) values of the transformer currents are obtained assuming the injected current waveform specified by (11.8). Finally, the volt-ampere rating of the transformer is obtained as

$$S_{Tl:n} = \frac{\sqrt{3}}{4} \frac{k}{n} V_m I_{OUT}, \quad (11.58)$$

and it is dependent on actual values of k and n . In the optimized situation for the rectifier without losses in the current injection system, when $k = 30/(7\pi)$ and $n = 10$, the volt-ampere rating is

$$S_{Tl:n} = \frac{1}{28} V_{OUT} I_{OUT} \approx 3.57\% P_{OUT}. \quad (11.59)$$

The diode bridge of the resistance emulator is connected in parallel to the three-phase diode bridge; thus the diodes have the same maximum of the reverse voltage, equal to the maximum of the line-to-line voltages, $\sqrt{3}V_m$. However, current stress on the diodes in the resistance emulator bridge is significantly lower than in the main diode bridge, since the average current in the diodes of the resistance emulator diode bridge is

$$I_{DR} = \frac{k}{\pi} I_{OUT}. \quad (11.60)$$

In the optimized case of the current injection system without losses, for $k = 30/(7\pi)$ and $n = 10$,

$$I_{DR} = \frac{30}{7\pi^2} I_{OUT} \approx 4.34\% I_{OUT}. \quad (11.61)$$

Application of the resistance emulator also affected average currents of the diodes in the three-phase diode bridge, somewhat reducing the average current of the diodes. The average currents of the diodes are

$$I_D = \frac{1}{3} \left(1 - \frac{2}{\pi} \frac{k}{n} \right) I_{OUT}, \quad (11.62)$$

which for $k = 30/(7\pi)$ and $n = 10$ reduces to

$$I_D = \frac{1}{3} \left(1 - \frac{6}{7\pi^2} \right) I_{OUT} = 30.44\% I_{OUT}. \quad (11.63)$$

4. NORMALIZED STATE-SPACE MODEL OF THE RECTIFIER

The analysis of the rectifier presented so far is based on approximations. In the continuous conduction mode, a sinusoidal waveform of the injected current is assumed, and its harmonics are neglected. In the discontinuous conduction mode, besides neglecting the higher order harmonics of the injected current, voltage spikes at the rectifier output terminals are approximated by δ -function impulses. In the continuous conduction mode, when the rectifier can be analyzed as a periodically switched linear circuit, a Fourier series technique introduced in [24] and [27], used in the analysis in Chapter 6, could be applied. However, since the rectifier may operate in two distinct discontinuous conduction modes as well as in the continuous conduction mode, a numerical simulation technique applied on a normalized state-space model is chosen as a better method. The normalized state-space model, similar to the one derived for the analysis of the discontinuous conduction mode in Chapter 9, applies for all of the rectifier operating modes. The derivation of such model is presented in this section.

To simplify derivation of the normalized state-space model, the rectifier in Fig. 11-1 is represented by an equivalent circuit shown in Fig. 11-10. Voltages and currents of all reactive elements of the circuit of Fig. 11-10 are

the same as in the rectifier in Fig. 11-1, and the modifications are made in order to reduce the number of nonlinear elements.

Operation of the three-phase diode bridge of Fig. 11-1 is represented by voltage sources:

$$v_{A0} = \max(v_1, v_2, v_3) \quad (11.64)$$

and

$$v_{B0} = \min(v_1, v_2, v_3), \quad (11.65)$$

accompanied by diodes DA and DB. The diodes play an essential role in modeling of the three-phase diode bridge discontinuous conduction mode. Let us define auxiliary voltage waveforms as

$$v_{AB0} = v_{A0} - v_{B0} \quad (11.66)$$

and

$$v_{AV} = \frac{1}{2}(v_{A0} + v_{B0}). \quad (11.67)$$

After the steady-state solution of the circuit in Fig. 11-10 is obtained, the input current waveform is computed by applying

$$i_l = d_1 \left(I_{OUT} + \frac{1}{2} i_Y \right) - d_2 \left(I_{OUT} - \frac{1}{2} i_Y \right) - \frac{1}{3} i_Y. \quad (11.68)$$

For the diode state functions, waveforms shown in Chapter 2 may be applied, although they are not valid in the discontinuous conduction mode. This simplification is possible because simulation of the circuit in Fig. 11-10 provides currents of the diodes DA and DB equal to zero in the time intervals of discontinuous conduction, i.e., $i_A = 0$ or $i_B = 0$. Thus, it is irrelevant whether the diode bridge output terminal current equal to zero is added to the input current waveform or not.

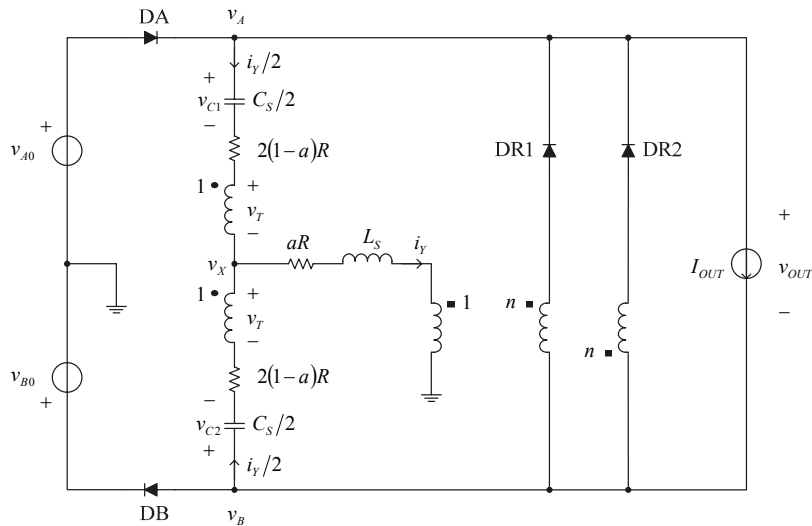


Figure 11-10. An equivalent circuit of the rectifier.

Table 11-2. States of the equivalent circuit.

State	DA	DB	DR1	DR2
1	1	1	1	0
2	1	1	0	1
3	1	1	0	0
4	0	1	0	1
5	1	0	1	0

The circuit in Fig. 11-10 consists of four nonlinear elements, the diodes, each of them having two states that can be represented by an equivalent linear circuit. A network state is defined by states of its nonlinear elements. In each of the network states, the circuit in Fig. 11-10 may be represented by a linear equivalent circuit. Assuming the diode states are mutually independent, an overall number of $2^4 = 16$ network states may occur. However, the states of the diodes are mutually dependent, which significantly reduces the number of possible states. To reduce the number of states, let us assume that $I_{OUT} > 0$, $n > 0$, and the input voltages given by (11.1). Under these assumptions, DR1 and DR2 cannot conduct simultaneously, which eliminates four of the network states, leaving 12 possibilities. Both diodes DA and DB cannot be simultaneously reverse biased, which eliminates another three

combinations, leaving nine possibilities. If DA is on and DB is off, the diode DR1 has to conduct, which eliminates another two combinations, leaving seven possibilities. In the same manner, when DB is on and DA is off, DR2 has to conduct, which eliminates another two combinations, leaving the final number of five possible network states. The possible network states are summarized in Table 11-2, each combination of the diode states defining one state of the circuit of Fig. 11-10. The notation in Table 11-2 is such that DA = 1 means that DA is on, while DA = 0 means that DA is off. The same notation applies for the other diodes.

In the analysis that follows, the diodes are assumed as ideal, meaning that a diode is represented by a short circuit while conducting, and as an open circuit while reverse biased. Since all of the nonlinear elements of the circuit in Fig. 11-10 are diodes, the circuit can be represented by an equivalent linear circuit in each of its states, for which a state-space model of an equivalent linear circuit is presented, accompanied by the boundary conditions that limit the area where the model applies. The boundary conditions are followed by state transition rules that define the next state the circuit moves to, after the boundary condition is violated.

The circuit in Fig. 11-10 is the third-order system; thus it is characterized by a state-space model with three state variables: v_{C1} , v_{C2} , and i_Y . However, since the capacitors are assumed to have the same capacitance, equal to $C_S/2$, and share the same current, $i_Y/2$, one of the system poles is at the origin, resulting in the capacitor voltages with the same AC component and different DC components. This fact can be utilized and the system of the state equations can be reduced in order by one, taking the average value of the capacitor voltages

$$v_C = \frac{v_{C1} + v_{C2}}{2} \quad (11.69)$$

as a state variable. In simulation of the circuit in Fig. 11-10, the waveform of interest is the waveform of i_Y , utilized to compute the input current according to (11.68), while waveforms of v_{C1} and v_{C2} are not of particular interest although they can be computed indirectly. Thus, taking v_C as a state variable is a particularly useful technique.

4.1 State 1

The first state is defined by DA = 1, DB = 1, DR1 = 1, and DR2 = 0 (see Table 11-2). A system of state-space equations of the equivalent linear circuit corresponding to this state is

$$\frac{d}{dt} \begin{bmatrix} i_Y \\ v_C \end{bmatrix} = \begin{bmatrix} -\frac{R}{L_S} & -\frac{1}{L_S} \\ \frac{1}{C_S} & 0 \end{bmatrix} \begin{bmatrix} i_Y \\ v_C \end{bmatrix} + \begin{bmatrix} \frac{1}{L_S} \left(v_{AV} - \frac{v_{AB0}}{n} \right) \\ 0 \end{bmatrix}. \quad (11.70)$$

The first of the boundary conditions originates from DR1, which becomes reverse biased when the injected current becomes negative. Thus, the boundary condition is

$$i_Y > 0. \quad (11.71)$$

If this boundary condition is violated, two transitions may occur. The first possibility is transition to state 3, which occurs if

$$v_C < v_{AV} + \frac{v_{AB0}}{n} \quad (11.72)$$

at the state transition time instant. In the case

$$v_C > v_{AV} + \frac{v_{AB0}}{n}, \quad (11.73)$$

the circuit switches to state 2.

The second boundary condition originates from diode DB, which might become reverse biased if i_Y becomes too large. The boundary condition is

$$i_Y < \frac{2n}{n+2} I_{OUT} \quad (11.74)$$

and if it is violated the circuit switches to state 5.

Since the injected current i_Y , being the current of an inductor, is continuous in time, the circuit cannot change its state from 1 to 4 directly.

4.2 State 2

The second state is defined by $DA = 1$, $DB = 1$, $DR1 = 0$, and $DR2 = 1$ (see Table 11-2). A system of state-space equations of the equivalent linear circuit corresponding to this state is

$$\frac{d}{dt} \begin{bmatrix} i_Y \\ v_C \end{bmatrix} = \begin{bmatrix} -\frac{R}{L_S} & -\frac{1}{L_S} \\ \frac{1}{C_S} & 0 \end{bmatrix} \begin{bmatrix} i_Y \\ v_C \end{bmatrix} + \begin{bmatrix} \frac{1}{L_S} \left(v_{AV} + \frac{v_{AB0}}{n} \right) \\ 0 \end{bmatrix}. \quad (11.75)$$

The first of the boundary conditions originates from DR2, which becomes reverse biased when the injected current becomes positive. Thus, the boundary condition is

$$i_Y < 0. \quad (11.76)$$

If this boundary condition is violated, two transitions may occur. The first possibility is transition to state 3, which occurs if

$$v_C > v_{AV} - \frac{v_{AB0}}{n} \quad (11.77)$$

at the state transition time instant. In the case

$$v_C < v_{AV} - \frac{v_{AB0}}{n}, \quad (11.78)$$

the circuit switches to state 1.

The second boundary condition originates from diode DA, which might become reverse biased if the absolute value of i_Y becomes too large. The boundary condition is

$$i_Y > -\frac{2n}{n+2} I_{OUT} \quad (11.79)$$

and if it is violated the circuit switches to state 4.

Since the injected current i_Y is continuous in time, the circuit cannot change its state from 2 to 5 directly.

4.3 State 3

The third state is defined by DA=1, DB=1, DR1=0, and DR2=0 (see Table 11-2). This state corresponds to the discontinuous conduction interval of the resistance emulator diode bridge. In this state, a dynamic degeneration of the inductor current occurs, and the system of differential

equations is reduced in order by one. The dynamically degenerated inductor current is

$$i_Y = 0, \quad (11.80)$$

and the remaining differential equation of the capacitor voltage is

$$\frac{dv_C}{dt} = 0. \quad (11.81)$$

This means that in state 3 the inductor current, i.e., the injected current, is equal to zero, while the capacitor voltage AC component remains the same as it was at the time instant the circuit entered state 3.

Since the injected current is continuous in time, being an inductor current, the boundary conditions for state 3 allow transitions only to states 1 and 2. The first boundary condition is caused by DR1,

$$v_C > v_{AV} - \frac{v_{AB0}}{n}, \quad (11.82)$$

and if it is violated the network state makes a transition to 1.

The second boundary condition is caused by DR2, the state 3 is valid for

$$v_C < v_{AV} + \frac{v_{AB0}}{n}, \quad (11.83)$$

and if the condition is violated the network switches to state 2.

Boundary conditions (11.82) and (11.83) may be used to derive another interesting property of the rectifier of Fig. 11-1. In the case the diodes in the resistance emulator diode bridge are reverse biased during the whole period, the injected current $i_Y = 0$, and $v_C = 0$. The converter is in state 3, and it will never exit this state if the value of the transformer turns ratio n is such that conditions (11.82) and (11.83) are satisfied during the whole period. This situation is termed “completely discontinuous conduction mode of the diode bridge rectifier,” and it occurs for

$$n < 6. \quad (11.84)$$

Thus, values of the turns ratio $n < 6$ should not be considered in the analysis since there is no current injection in that case.

4.4 State 4

The fourth state is defined by DA = 0, DB = 1, DR1 = 0, and DR2 = 1 (see Table 11-2). This state corresponds to the discontinuous conduction interval of the main three-phase diode bridge. A dynamic degeneration of the inductor current occurs again, and the system of differential equations is reduced in order by one. The dynamically degenerated inductor current is

$$i_Y = -\frac{2n}{n+2} I_{OUT}. \quad (11.85)$$

The remaining equation, over the capacitor voltage AC component, is given by

$$C_s \frac{dv_C}{dt} = -\frac{2n}{n+2} I_{OUT}, \quad (11.86)$$

and it causes the capacitor voltage to change linearly. Since the inductor current is continuous in time, transition from this state to states 1, 3, and 5 is not possible, and the only transition that is possible is to state 2, when diode DA starts to conduct. The boundary condition to remain in state 4 is

$$v_C > v_{AV} + \frac{v_{AB0}}{n} + \frac{2n}{n+2} RI_{OUT}, \quad (11.87)$$

and in the case of violation, the network switches to state 2.

During state 4, the voltage of the positive output terminal of the diode bridge is

$$v_A = \frac{2n}{n+2} (v_C + Ri_Y) - \frac{n-2}{n+2} v_{B0}, \quad (11.88)$$

while the voltage of the negative output terminal is $v_B = v_{B0}$.

4.5 State 5

The fifth state is defined by DA = 1, DB = 0, DR1 = 1, and DR2 = 0 (see Table 11-2). This state corresponds to the discontinuous conduction interval of the main three-phase diode bridge, again. In this state, a dynamic degeneration of the inductor current occurs, and the system of differential

equations is reduced in order by one. The dynamically degenerated inductor current is

$$i_Y = \frac{2n}{n+2} I_{OUT}. \quad (11.89)$$

The remaining equation, over the capacitor voltage AC component, is given by

$$C_S \frac{dv_C}{dt} = \frac{2n}{n+2} I_{OUT}, \quad (11.90)$$

and it causes the capacitor voltage to change linearly. Since the inductor current is continuous in time, transition from this state to states 2, 3, and 4 is not possible, and the only transition that is possible is to state 1, when diode DB starts to conduct. The boundary condition to remain in state 5 is

$$v_C < v_{AV} - \frac{v_{AB0}}{n} - \frac{2n}{n+2} RI_{OUT}, \quad (11.91)$$

and in the case of violation, the network switches to state 1.

During state 5, voltage of the negative output terminal of the diode bridge is

$$v_B = \frac{2n}{n+2} (v_C + R i_Y) - \frac{n-2}{n+2} v_{A0}, \quad (11.92)$$

while the voltage of the positive output terminal is $v_A = v_{A0}$.

4.6 Normalization of the Variables

The equations derived so far in this section allow direct numerical simulation of the rectifier. However, the results obtained in this manner lack generality, since they apply only to a particular rectifier. Thus, to increase generality of the results, normalization of variables is applied. The normalization is done in the same manner as in the analysis of the discontinuous conduction mode presented in Chapter 9.

To normalize the voltages, for the normalization the amplitude of the phase voltage is used as a base voltage. Thus, all of the voltages v are represented by their normalized equivalents m according to

$$m = \frac{V}{V_m} . \quad (11.93)$$

As a base resistance for normalization, the characteristic resistance of the resonant circuit applied in the current injection network is used,

$$R_0 = \sqrt{\frac{L_S}{C_S}} . \quad (11.94)$$

Thus, normalized resistance of the current injection system is

$$\rho = \frac{R}{R_0} . \quad (11.95)$$

To preserve the form of Ohm's law, V_m/R_0 is used as a base current to normalize currents

$$j = \frac{R_0}{V_m} i . \quad (11.96)$$

In normalized equations, the time variable is replaced by the phase angle

$$\varphi = \omega_0 t . \quad (11.97)$$

The resonant frequency of the series resonant circuit applied in the current injection network is

$$\omega_R = \frac{1}{\sqrt{L_S C_S}} . \quad (11.98)$$

To simplify the notation further, a resonance parameter is defined as

$$r = \frac{\omega_R}{3\omega_0} , \quad (11.99)$$

and its value is $r=1$ in the case the resonance of the series resonant circuit of the current injection network is tuned exactly to the triple of the line frequency.

Applying the introduced normalization, capacitance C_S is expressed as

$$C_S = \frac{1}{3r\omega_0 R_0}, \quad (11.100)$$

while the inductance L_S is

$$L_S = \frac{R_0}{3r\omega_0}. \quad (11.101)$$

Resistance of the current injection system is expressed as

$$R = \rho R_0, \quad (11.102)$$

while time derivatives are

$$\frac{d}{dt} = \omega_0 \frac{d}{d\varphi}. \quad (11.103)$$

Finally, the obtained normalized state-space model of the rectifier is presented in Table 11-3, prepared for numerical simulation. To integrate the equations, the trapezoidal integration method is applied. Direct numerical integration of the equations until the steady state is reached is a time-consuming process. To accelerate the convergence to the steady state, an extrapolation algorithm of [51] is applied. The extrapolation algorithm turned out to be an essential element in providing practical applicability of the simulation method.

Assuming that waveforms of m_{AV} and m_{AB0} , related to the input voltages, are known and fixed, the simulation result is uniquely determined by four parameters: J_{OUT} , ρ , r , and n . Various simulation analyses in the space determined by these four degrees of freedom can be made, some of which are presented next.

5. SIMULATION RESULTS

The state-space model derived in Section 11.4 is suitable for a numerical simulation program. Four parameters of the normalized state-space model affect the simulation result: the transformer turns ratio, n , the normalized

Table 11-3. States of the equivalent circuit.

State	Equations	Boundary conditions
1	$\frac{d}{d\varphi} \begin{bmatrix} j_Y \\ m_C \end{bmatrix} = \begin{bmatrix} -3r\rho & -3r \\ 3r & 0 \end{bmatrix} \begin{bmatrix} j_Y \\ m_C \end{bmatrix} + \begin{bmatrix} 3r \left(m_{AV} - \frac{m_{AB0}}{n} \right) \\ 0 \end{bmatrix}$	$j_Y > 0$ $j_Y < \frac{2n}{n+2} J_{OUT}$
2	$\frac{d}{d\varphi} \begin{bmatrix} j_Y \\ m_C \end{bmatrix} = \begin{bmatrix} -3r\rho & -3r \\ 3r & 0 \end{bmatrix} \begin{bmatrix} j_Y \\ m_C \end{bmatrix} + \begin{bmatrix} 3r \left(m_{AV} + \frac{m_{AB0}}{n} \right) \\ 0 \end{bmatrix}$	$j_Y < 0$ $j_Y > -\frac{2n}{n+2} J_{OUT}$
3	$j_Y = 0$ $\frac{dm_C}{d\varphi} = 0$	$m_C > m_{AV} - \frac{m_{AB0}}{n}$ $m_C < m_{AV} + \frac{m_{AB0}}{n}$
4	$j_Y = -\frac{2n}{n+2} J_{OUT}$ $\frac{dm_C}{d\varphi} = -3r \frac{2n}{n+2} J_{OUT}$	$m_C > m_{AV} + \frac{m_{AB0}}{n} + \frac{2n}{n+2} \rho J_{OUT}$
5	$j_Y = \frac{2n}{n+2} J_{OUT}$ $\frac{dm_C}{d\varphi} = 3r \frac{2n}{n+2} J_{OUT}$	$m_C < m_{AV} - \frac{m_{AB0}}{n} - \frac{2n}{n+2} \rho J_{OUT}$

output current, J_{OUT} ; the resonance parameter, r ; and the normalized resistance of the current injection system, ρ . Several analyses in the space determined by these four variables are presented here.

The first of the analyses is the dependence of the input current THD on the transformer turns ratio. For the analysis, the normalized output current is chosen to be $J_{OUT} = 0.4$, which is the value close to the upper limit of the output current that guarantees unipolar voltage across the current injection network capacitors, regardless of the rectifier operating mode (continuous or discontinuous) and the transformer turns ratio. The resonance parameter is assumed to be $r=1$. The analysis is performed for five values of the normalized resistance: $\rho_1 = 0$, $\rho_2 = 0.05$, $\rho_3 = 0.10$, $\rho_4 = 0.15$, $\rho_5 = 0.20$, and the result is presented as a parametric family of curves in Fig. 11-11.

Curve 1 corresponds to $\rho_1 = 0$, where losses in the current injection system are neglected. In that case, the analytically obtained optimal value for the transformer turns ratio is $n = 10$, (11.24). For lower values of n , the THD value is high, in the range from 31.08%, corresponding to the situation $n < 6$ when the injected current is equal to zero during the whole period, to about 25%.

These high values correspond to the discontinuous conduction mode of the resistance emulator diode bridge, and this operating mode should be avoided in practice. Values of the turns ratio $n > 10$ correspond to the discontinuous conduction mode of the three-phase diode bridge, which in contrast to the discontinuous conduction mode of the resistance emulator diode bridge provided good values for the input current THD. The case of the optimal amplitude of the injected current for $n = 10$ cannot be captured by simulation, since in that case the injected current amplitude is not firmly defined by the circuit parameters, being highly sensitive to numerical error. The same situation would occur in practice.

The second curve corresponds to $\rho_2 = 0.05$. This relatively low value for normalized resistance of the current injection system is sufficient to illustrate all of the relevant features: the discontinuous conduction mode of the resistance emulator diode bridge, the continuous conduction mode, and the discontinuous conduction mode of the three-phase diode bridge. The discontinuous conduction mode of the resistance emulator diode bridge is characterized by high values of the input current THD, and this mode cannot be utilized in practice. In the continuous conduction mode, the minimum of the THD occurs, in this case for $n \approx 11.7$, which according to (11.38) provides the minimum of the THD for $\rho = 0.05418$. The boundary between the resistance emulator bridge discontinuous conduction mode and the continuous conduction mode is not clearly observable. On the other hand, the discontinuous derivative of curve 2 in Fig. 11-11 clearly indicates the boundary between the continuous conduction mode and the discontinuous conduction mode of the three-phase diode bridge. In the discontinuous conduction mode of the three-phase diode bridge, the input current THD depends weakly on n . It can be concluded that the range for n suitable for practical application corresponds to the narrow interval of the rectifier continuous conduction mode around the point where the minimum of the THD is reached, and the wider interval of the three-phase diode bridge discontinuous conduction mode.

Curves in Fig. 11-11 corresponding to the higher values of the current injection system normalized resistance show the same features as curve 2, but with lower sensitivity on variations of the turns ratio. A conclusion that can be drawn from the simulation results in Fig. 11-11 is that the transformer turns ratio should be chosen to enable operation of the rectifier in the discontinuous conduction mode of the three-phase rectifier bridge and in the continuous conduction mode in the narrow area around the minimum of the THD, for the whole range of expected values for the output current. The discontinuous conduction mode of the resistance emulator diode bridge should be avoided.

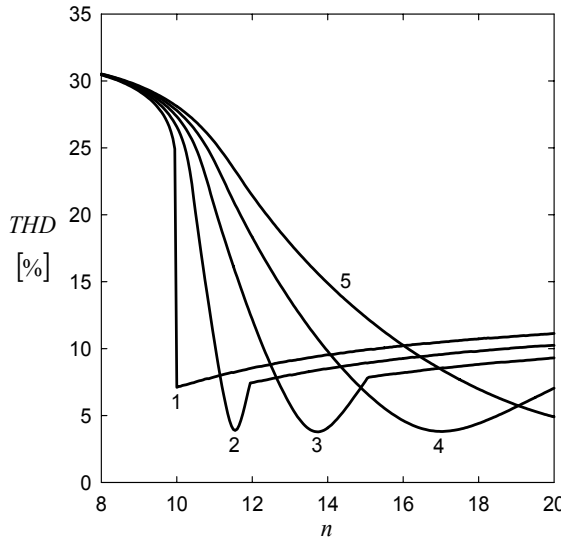


Figure 11-11. Dependence of the input current THD on the transformer turns ratio: $\rho_1 = 0$, $\rho_2 = 0.05$, $\rho_3 = 0.10$, $\rho_4 = 0.15$, $\rho_5 = 0.20$; $r = 1$, $J_{OUT} = 0.4$.

The second of the analyses shows the dependence of the input current THD on J_{OUT} for the same set of values for ρ as in the first simulation analysis: $\rho_1 = 0$, $\rho_2 = 0.05$, $\rho_3 = 0.10$, $\rho_4 = 0.15$, $\rho_5 = 0.20$. In the analysis, it is assumed that the resonance of the current injection network is tuned to the triple of the line frequency, i.e., $r = 1$. The purpose of this analysis is to verify an empirical algorithm for the choice of the resistance emulator turns ratio, given by

$$n = \frac{10}{1 - 2.5\rho}. \quad (11.104)$$

The range of the normalized output current $0 < J_{OUT} < 0.4$ was considered, since in that range voltages of the current injection capacitors do not change polarity during the period, and application of electrolytic capacitors is allowed.

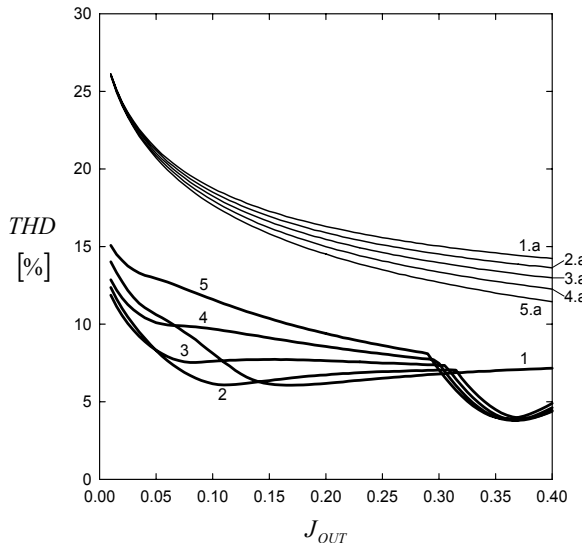


Figure 11-12. Dependence of the input current THD on J_{OUT} : $\rho_1 = 0$, $\rho_2 = 0.05$, $\rho_3 = 0.10$, $\rho_4 = 0.15$, $\rho_5 = 0.20$; $r = 1$, $n = 10/(1 - 2.5\rho)$. Thin lines: $n \rightarrow \infty$.

The simulation results are presented in Fig. 11-12. Thick lines in Fig. 11-12 present the results for the circuit that applies the resistance emulator with the transformer turns ratio chosen according to (11.104), while the thin lines, labeled 1a to 5a, correspond to the situation when the resistance emulator is not applied, i.e., $n \rightarrow \infty$. Comparison of the two sets of curves clearly indicates the advantages of application of the resistance emulator. Dependence of the input current THD on the output current is good, although there is no mechanism to adjust to the load current automatically, as in the case of the rectifier proposed in Chapter 10. Transition of the rectifier from the three-phase diode bridge discontinuous conduction mode to the continuous conduction mode can be observed in curves 2 to 5 by the derivative discontinuity.

Conclusions that can be drawn from the presented simulation results are that the empirical algorithm of (11.104) for choosing the resistance emulator transformer turns ratio provides good results, and that application of the resistance emulator significantly improves the input current THD in comparison to the corresponding rectifier without the resistance emulator.

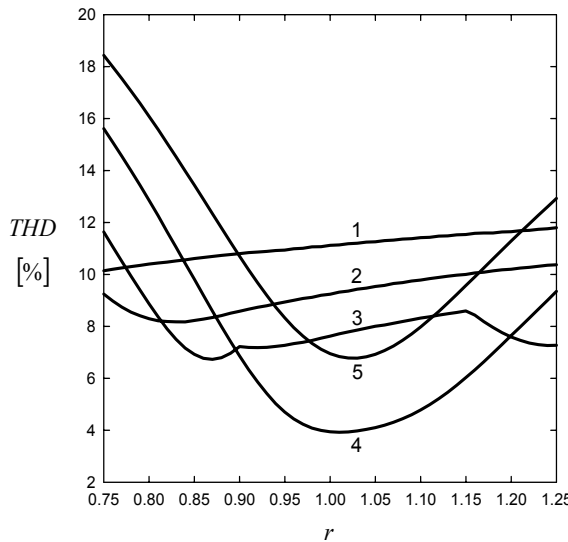


Figure 11-13. Dependence of the input current THD on the resonance parameter for $J_{OUT1} = 0.05$, $J_{OUT2} = 0.10$, $J_{OUT3} = 0.15$, $J_{OUT4} = 0.20$, $J_{OUT5} = 0.25$; $n = 19$, $\rho = 0.34$.

The last of the simulation analyses presented in this section illustrates dependence of the input current THD on the resonance parameter for a set of values of J_{OUT} taken as a parameter: $J_{OUT1} = 0.05$, $J_{OUT2} = 0.10$, $J_{OUT3} = 0.15$, $J_{OUT4} = 0.20$, and $J_{OUT5} = 0.25$. The results are presented in Fig. 11-13, and they are obtained for $\rho = 0.34$ and $n = 19$, which corresponds to the experimental rectifier that is discussed in the next section. Curves 1, 2, and 3 in Fig. 11-13 correspond to the discontinuous conduction mode of the three-phase diode bridge of the rectifier. These curves are characterized by weak sensitivity of the input current THD on the resonance parameter, the sensitivity being weaker the deeper the rectifier in the discontinuous conduction mode is. Curves 4 and 5 correspond to the continuous conduction mode, where the input current THD is sensitive to the resonance parameter. Thus, for the rectifiers intended to operate in the continuous conduction mode, fine-tuning of the resonance in the current injection network might be needed.

6. EXPERIMENTAL RESULTS

To verify feasibility of the proposed rectifier experimentally and to analyze effects caused by parasitic effects that are not modeled, an

experimental rectifier is built. The rectifier operates with the input voltage amplitude of $V_m = 140$ V and the output current up to $I_{OUT\max} = 10$ A. This results in the rectifier output power somewhat above 2 kW. Parameters of the current injection network are $L_s = 4.3$ mH and $C_s/2 = 140 \mu\text{F}$. The turns ratio of the resistance emulator transformer is $n = 19$. Parasitic resistance of the current injection system is measured as $R = 1.34 \Omega$, and the biggest part of this resistance is located in the current injection device. Applied components result in normalized parameters $r = 0.97$ and $\rho = 0.34$. The base current for the normalization is $V_m/R_0 = 35.7$ A.

In Fig. 11-14, dependence of the input current THD on the output current is presented. The curve with filled symbols, labeled 1, corresponds to the rectifier that applies the resistance emulator, while the curve with hollow symbols, labeled 2, is obtained on the rectifier with the resistance emulator excluded from the circuit. Advantages of the rectifier that applies the resistance emulator can be readily observed. Curves 1a and 2a are obtained by numerical simulation, and correspond to curves 1 and 2. A discrepancy between the simulation and the experimental results in curves 1 and 1a can be observed at light loads, where ripple of the output current affects the rectifier operation. Besides this, the rectifier operation is slightly affected by the output resistance of the transformer applied to supply the experimental rectifier, equal to 0.5Ω . Owing to this resistance, the amplitude of the phase voltages varies with the load current variations, which is not included in the derived models. On the other hand, in curves 2 and 2a a discrepancy can be observed at high output currents, which is caused by saturation effects in the core of L_s . This effect is pronounced in the rectifier without the resistance emulator, since the inductor current amplitude is higher in that case.

Dependence of the output voltage on the output current is presented in Fig. 11-15. Curve 1 applies for the rectifier with the resistance emulator, while curve 2 applies for the rectifier without the resistance emulator. It can be concluded that application of the resistance emulator significantly reduced dependence of the output voltage on the output current. In contrast to the analytical predictions, the output voltage is dependent on the output current even in the continuous conduction mode of the rectifier, owing to the output resistance of the supply sources.

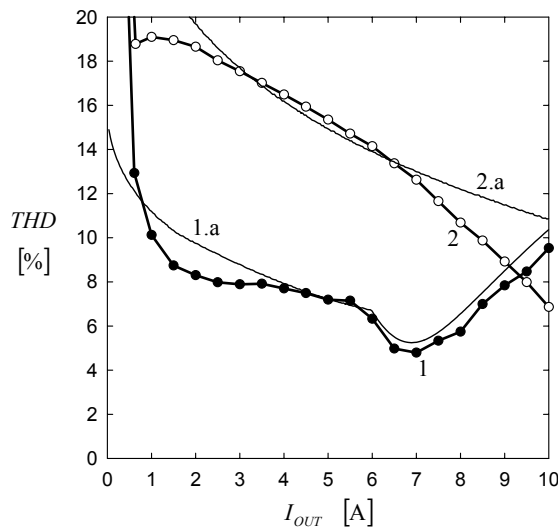


Figure 11-14. Dependence of the input current THD on I_{OUT} .

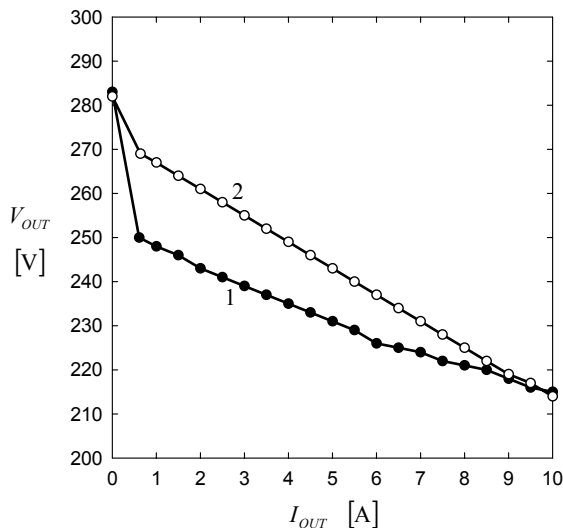


Figure 11-15. Dependence of V_{OUT} on I_{OUT} .

Chapter 12

CURRENT INJECTION APPLYING A SWITCHING CURRENT INJECTION DEVICE

The discussion of current injection principles presented in Chapter 3 indicated that the main reason for degradation of the input current total harmonic distortion (THD) in three-phase diode bridge rectifiers are the gaps in the input currents that occur during the intervals the corresponding input voltage is neither minimal nor maximal among the three of the supply voltages. To remedy these gaps, the current injection method is proposed. The current injection methods analyzed so far apply magnetic current injection devices that simultaneously inject currents in all three of the rectifier phases. Magnetic current injection devices are robust, but bulky and expensive. The exception is the case when a transformer should be applied at the rectifier input, and the current injection can be achieved at the same time as the voltage level adjustment, by the same transformer, without any increase of the transformer volt-ampere rating. Another drawback of magnetic current injection devices is the fact that they inject current in all three of the supply phases simultaneously, although only one of the phases needs the injected current. The question addressed in this chapter is another type of current injection device based on controlled semiconductor switches. The basic idea behind the concept is that the current should be injected in only one of the phases, the one with a voltage that is neither minimal nor maximal at the considered time point. In this manner, the injected current is directed only to the phase that needs the injected current. The topological inspiration for this type of current injection device is found in the rectifiers proposed in [48] and [49]. However, instead of the high-frequency switching applied in [48] and [49], here the switches are operated at low frequency, equal to the double of the line frequency, and the rectifier operates in a completely different manner than the rectifiers proposed in [48] and [49]. The concept was originally proposed in [32] and [37].

The rectifier that applies the switching current injection device is presented in Fig. 12-1. It consists of a three-phase diode bridge, a current injection network, and a switching current injection device. Let us assume that the rectifier shown in Fig. 12-1 is supplied by an undistorted symmetrical three-phase voltage set specified by

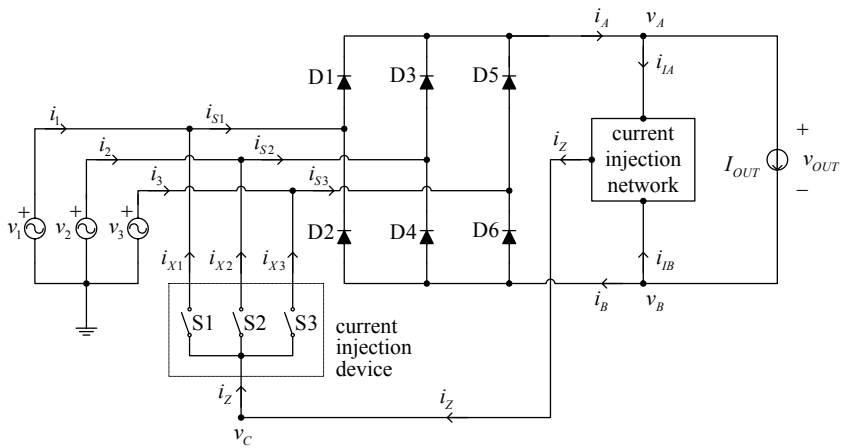


Figure 12-1. Current injection based rectifier that applies the switching current injection device. © [2002] IEEE.

$$v_p = V_m \cos\left(\omega_0 t - (p-1)\frac{2\pi}{3}\right), \quad (12.1)$$

for $p \in \{1, 2, 3\}$. These supply voltages and the diode bridge that operates in the continuous conduction mode result in the voltages of the rectifier output terminals as derived in Chapter 2, given by

$$v_A = \max(v_1, v_2, v_3) = \frac{3\sqrt{3}}{\pi} V_m \left(\frac{1}{2} + \sum_{n=1}^{+\infty} \frac{(-1)^{n+1}}{9n^2 - 1} \cos(3n\omega_0 t) \right) \quad (12.2)$$

and

$$v_B = \min(v_1, v_2, v_3) = \frac{3\sqrt{3}}{\pi} V_m \left(-\frac{1}{2} + \sum_{n=1}^{+\infty} \frac{1}{9n^2 - 1} \cos(3n\omega_0 t) \right). \quad (12.3)$$

As discussed in Chapter 2, voltages v_A and v_B contain the same spectral components at odd triples of the line frequency, while the spectral components at even triples of the line frequency have the same amplitudes, but the opposite phases. Thus it is convenient to express voltages v_A and v_B as sums of two components, one of these components containing harmonic components at odd triples of the line frequency, defined as

$$v_{ODD} = \frac{3\sqrt{3}}{\pi} V_m \sum_{k=1}^{+\infty} \frac{1}{9(2k-1)^2 - 1} \cos(3(2k-1)\omega_0 t), \quad (12.4)$$

and the other one containing spectral components at even triples of the line frequency,

$$v_{EVEN} = -\frac{3\sqrt{3}}{\pi} V_m \sum_{k=1}^{+\infty} \frac{1}{36k^2 - 1} \cos(6k\omega_0 t). \quad (12.5)$$

The DC component of the diode bridge output voltage is

$$V_{OUT} = \frac{3\sqrt{3}}{\pi} V_m. \quad (12.6)$$

Applying (12.4), (12.5), and (12.6), the output terminal voltages are expressed as

$$v_A = \frac{1}{2} V_{OUT} + v_{ODD} + v_{EVEN} \quad (12.7)$$

and

$$v_B = -\frac{1}{2} V_{OUT} + v_{ODD} - v_{EVEN}. \quad (12.8)$$

Waveforms of v_A and v_B are presented in the first two diagrams of Fig. 12-2.

Switches in the current injection device are operated such that at each time point one of the switches is turned on, while the remaining two are off. The switch that is turned on is connected to the phase with a voltage that is neither minimal nor maximal at the considered time point. Since $v_1 + v_2 + v_3 = 0$, and thus $v_A + v_B + v_C = 0$, the voltage at the current injection device common point is

$$v_C = -v_A - v_B = -2v_{ODD}. \quad (12.9)$$

The waveform of v_C is presented in the third diagram of Fig. 12-2. This voltage makes the difference in comparison to the current injection based rectifiers that apply magnetic current injection devices, where the

corresponding voltage is $v_N = 0$. This fact is one of the reasons for writing this chapter, since the current injection methods and the current injection networks have to be adjusted to the modified voltages across the current injection network.

The voltages across the current injection network are

$$v_{AC} = \frac{1}{2}V_{OUT} + 3v_{ODD} + v_{EVEN} \quad (12.10)$$

and

$$v_{BC} = -\frac{1}{2}V_{OUT} + 3v_{ODD} - v_{EVEN}. \quad (12.11)$$

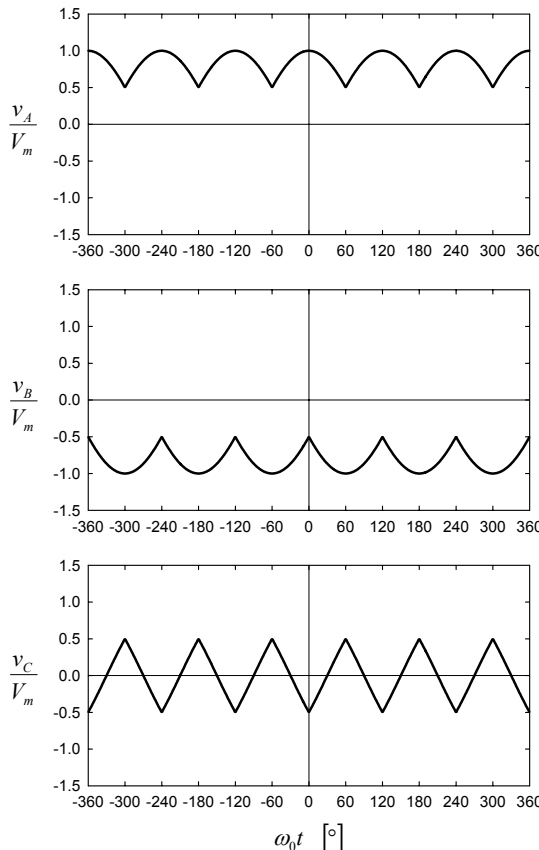


Figure 12-2. Waveforms of the voltages at the current injection network terminals.

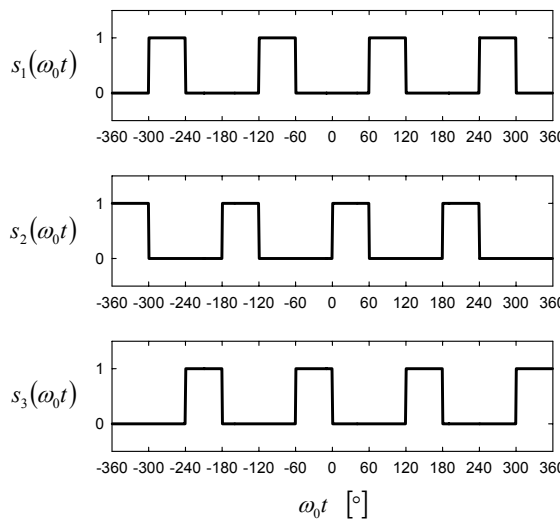


Figure 12-3. States of the switches in the current injection device.

According to the method of equivalent circuits introduced in Chapter 6, the voltage effectively applied to the equivalent circuit for odd triples of the line frequency is

$$\frac{1}{2}(v_{AC} + v_{BC}) = 3v_{ODD}, \quad (12.12)$$

which is three times higher than in the case of the rectifiers that apply magnetic current injection devices.

Another voltage of interest is the average of the output terminal voltages, effectively applied across the equivalent circuit for odd triples of the line frequency in the case a magnetic current injection device is applied. In terms of v_{ODD} this voltage is

$$v_{AV} = \frac{1}{2}(v_A + v_B) = \frac{1}{2}(v_{AN} + v_{BN}) = v_{ODD}, \quad (12.13)$$

and it is three times lower than the voltage specified by (12.12).

The current injection device in the rectifier of Fig. 12-1 consists of three switches operated such that the switch connected to the phase with a voltage that is neither minimal nor maximal at the considered time point is turned on. States of the switches are presented in the diagrams in Fig. 12-3. According to Fig. 12-3, it can be concluded that the switches are switched at the

frequency equal to the double of the line frequency. The current supplied to the current injection device in the case of the switching current injection device is denoted by i_Z , in contrast to the cases when magnetic current injection devices have been applied, where the corresponding current is denoted by i_Y .

1. THE THIRD-HARMONIC CURRENT INJECTION APPLYING A SWITCHING CURRENT INJECTION DEVICE

In the analysis of the rectifier that applies a switching current injection device, operation of the switches in the current injection device and the resulting voltages across the current injection network have been discussed so far. At this point, injected currents are introduced into the analysis, and the first to be analyzed is the third-harmonic current injection. Let us consider the rectifier input current at the first phase, i_1 . Currents of the remaining two phases have the same form, but they are delayed in phase for $2\pi/3$ and $4\pi/3$ in comparison to i_1 . In the analysis that follows, it is assumed that the injected current i_Z contains only a spectral component at the triple of the line frequency, the same as assumed for the injected current i_Y in Chapter 5. Depending on the states of the diodes D1 and D2 in the diode bridge, according to the diode state functions defined in Chapter 2, the input current can be represented by three analytical expressions, presented in Table 12-1. In contrast to the rectifiers that apply magnetic current injection devices (CID), in the case of the switching current injection device the injected current is directed only to the phase that needs the injected current to patch the gap caused by the reverse biased diodes in the diode bridge connected to that phase in the considered time interval.

According to the equations presented in Table 12-1, the input current of the rectifier that applies the switching current injection device has the same waveform as the input current of the rectifier that applies magnetic current injection device in the case

Table 12-1. Expressions for the input current.

d_1	d_2	i_1 , magnetic CID	i_1 , switching CID
1	0	$I_{OUT} + \frac{1}{6}i_Y$	$I_{OUT} + \frac{1}{2}i_Z$
0	1	$-I_{OUT} + \frac{1}{6}i_Y$	$-I_{OUT} + \frac{1}{2}i_Z$
0	0	$-\frac{1}{3}i_Y$	$-i_Z$

$$i_Z = \frac{1}{3} i_Y . \quad (12.14)$$

Thus, all of the optimization results of Chapter 5 are directly applicable, and for

$$i_Z = \frac{1}{2} I_{OUT} \cos(3\omega_0 t) \quad (12.15)$$

the minimum of the input current THD equal to

$$THD_{min} = \sqrt{\frac{32\pi^2}{315}} - 1 \approx 5.12\% \quad (12.16)$$

is reached.

In Fig. 12-4, waveforms of i_A , i_B and i_Z are presented for the optimal third-harmonic current injection. In comparison to the waveforms of the same currents in the case a magnetic current injection device is applied (presented in Fig. 5-9 in Chapter 5), reduced AC components of i_A and i_B can be readily observed. This is caused by a reduced amplitude of the injected current i_Z in comparison to i_Y . Currents in the current injection network if the switching current injection device is applied are three times lower than if a magnetic current injection device is applied, since the current is injected only into one phase, instead of three.

Waveforms of the input currents in the diode bridge, i_{S1} , i_{S2} , i_{S3} , are presented in Fig. 12-5. In comparison to the waveforms of Fig. 2-6, obtained for the diode bridge rectifier without current injection and presented in Chapter 2, the waveforms are shaped in the area when the diodes conduct, but the gaps in the waveforms are present during the time intervals when the corresponding phase voltage is neither minimal nor maximal. These gaps are patched by the injected currents, presented in Fig. 12-6. The waveforms presented in Fig. 12-6 illustrate how the output current of the current injection network, i_Z , is directed to the phase that needs injected current by the switching current injection device, according to the states of the switches in Fig. 12-3.

The final result of the current injection are the waveforms of the input currents shown in Fig. 12-7. The waveforms are the same as in the case of the optimal third-harmonic current injection with a magnetic current injection device, shown in Fig. 5-10 of Chapter 5, having the same THD value given by (12.16).

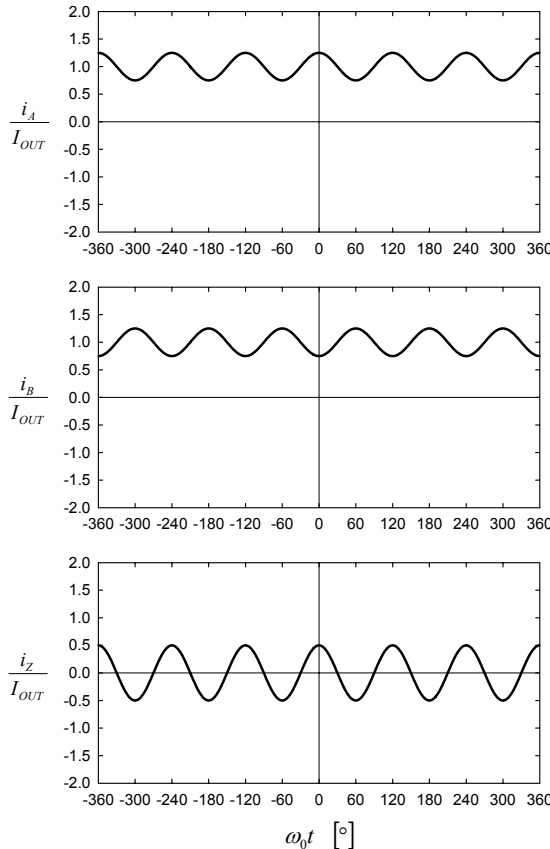


Figure 12-4. Waveforms of i_A , i_B , and i_Z in the case of the optimal third-harmonic current injection.

Another issue of interest is the power taken by the current injection network in the case the switching current injection device is applied. Since the currents of the current injection device are assumed to contain only one harmonic component located at the triple of the line frequency, the power taken by the current injection device is affected only by the spectral component of the voltages across the current injection network located at the triple of the line frequency. The harmonic component of the voltages across the current injection network at the triple of the line frequency is

$$v_{AC,3} = v_{BC,3} = \frac{9\sqrt{3}}{8\pi} V_m \cos(3\omega_0 t). \quad (12.17)$$

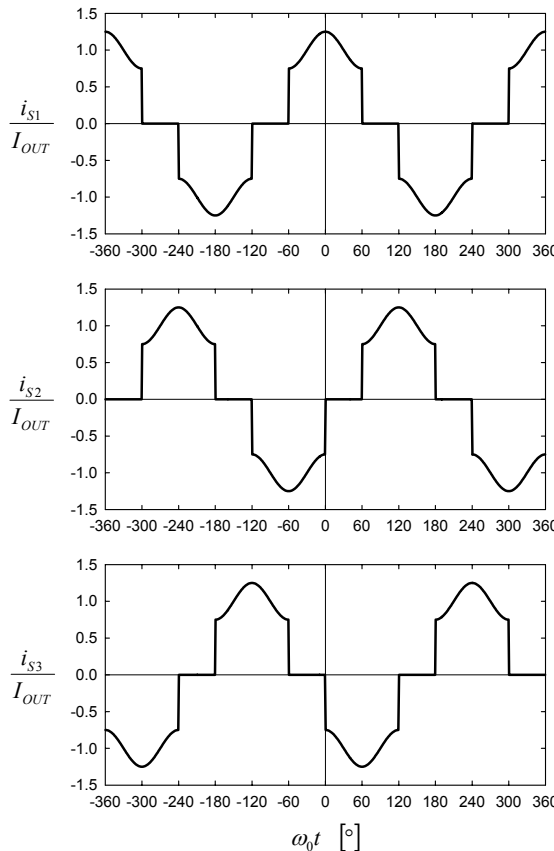


Figure 12-5. Waveforms of the diode bridge input currents, i_{S1} , i_{S2} , and i_{S3} .

These voltages with the injected current i_Z specified by (12.15) result in the power taken by the current injection network equal to

$$P_{INJ} = \frac{9\sqrt{3}}{32\pi} V_m I_{OUT} = \frac{3}{32} P_{OUT} = \frac{3}{35} P_{IN} \approx 8.57\% P_{IN}, \quad (12.18)$$

which is the same as specified by (5.35) in the case of the optimal third-harmonic current injection and a magnetic current injection device. In the case the power taken by the current injection network is dissipated within the network, the corresponding efficiency of the rectifier is

$$\eta = \frac{32}{35} P_{IN} \approx 91.43\%. \quad (12.19)$$

These results are the same as obtained in Chapter 5, since if the switching current injection device is applied the third-harmonic voltages across the current injection networks are three times higher, while the currents are three times lower.

To conclude the analysis of the optimal third-harmonic current injection applying the switching current injection device, it can be stated that the same results are obtained as in the case a magnetic current injection device is applied, presented in Chapter 5. The differences are that the results are obtained with three times lower currents and three times higher voltages of the current injection network at the triple of the line frequency. These differences require somewhat different parameters of the current injection network and cause a completely different behavior of the rectifier in the discontinuous conduction mode.

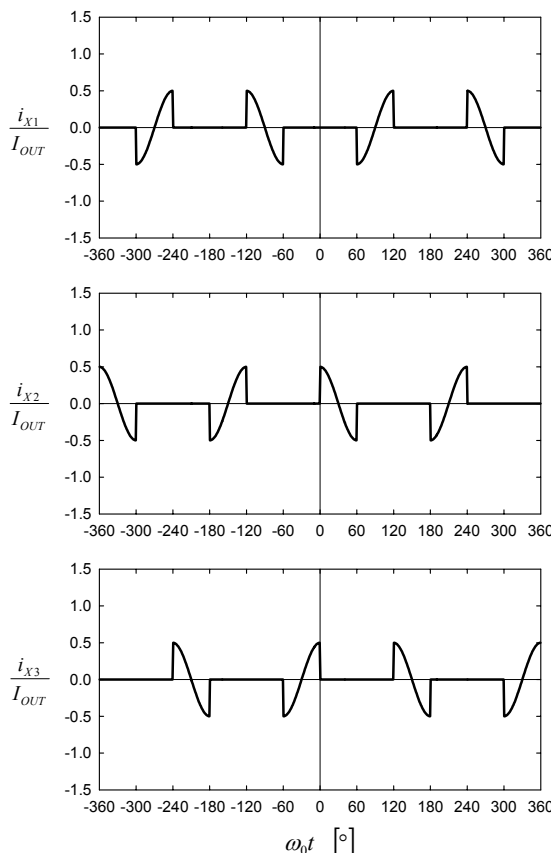


Figure 12-6. Waveforms of the injected currents i_{X1} , i_{X2} , and i_{X3} .

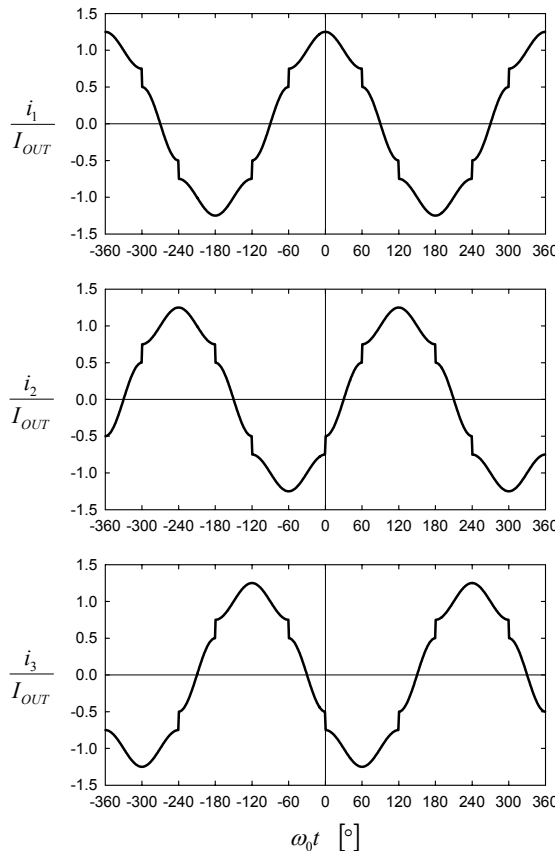


Figure 12-7. Waveforms of the input currents i_1 , i_2 , and i_3 .

2. DISCONTINUOUS CONDUCTION MODE IN THE RECTIFIERS THAT APPLY A SWITCHING CURRENT INJECTION DEVICE

The discontinuous conduction mode of the current injection based rectifiers that apply magnetic current injection devices is discussed in Chapter 9, where it is shown that acceptable THD values of the input currents and high efficiency can be obtained with simple rectifier structures that apply suboptimal current injection in the discontinuous conduction mode. The continuous conduction mode is characterized by the diode bridge

output terminal currents $i_A > 0$ and $i_B > 0$ during the whole period. If these currents reach zero in some points during the period, the discontinuous conduction mode occurs. In this section, the discontinuous conduction mode is analyzed for the rectifiers that apply the switching current injection device.

Let us assume that the injected current i_Z is free from higher order harmonics and contains only a harmonic component at the triple of the line frequency,

$$i_Z = I_{Zm} \cos(3\omega_0 t). \quad (12.20)$$

Since the load current at the positive output terminal of the diode bridge is

$$i_A = I_{OUT} + \frac{1}{2}i_Z, \quad (12.21)$$

the discontinuous conduction mode of the diode bridge occurs when the injected current amplitude is equal to

$$I_{Zm} = 2I_{OUT}. \quad (12.22)$$

The same conclusion can be drawn if the load current at the negative output terminal of the diode bridge i_B is analyzed.

If the injected current is specified by (12.20), with the amplitude of (12.22) that corresponds to the discontinuous conduction mode, the THD of the input current is

$$THD = \frac{\sqrt{160\pi^2 - 1089}}{33} \approx 67.09\%. \quad (12.23)$$

According to the results of Chapter 9, even in the case the high filtering assumption of (12.20) is not exactly satisfied, the input current THD will be around the value given by (12.23). Thus, an important conclusion can be made: the discontinuous conduction mode in the rectifiers that apply switching current injection device is not of practical interest.

3. CURRENT INJECTION NETWORKS FOR THE THIRD-HARMONIC CURRENT INJECTION APPLYING A SWITCHING CURRENT INJECTION DEVICE

To provide the injected current i_Z , a current injection network is needed. Since current injection network C is shown in Chapter 6 to provide the best performance, this current injection network is applied here for the third-harmonic current injection. The current injection network is shown in Fig. 12-8, and it consists of two capacitors, one inductor, one transformer with the turns ratio 1:1, and a resistor or a resistance emulator applied to control the amplitude of the injected current. The inductor and the capacitors form a series resonant circuit in the equivalent circuit of the current injection network for odd triples of the line frequency, introduced in Chapter 6, and the resonant frequency is

$$\omega_R = \frac{1}{\sqrt{LC}} . \quad (12.24)$$

The current injection network has to satisfy the resonance constraint

$$\omega_R = 3\omega_0 . \quad (12.25)$$

If (12.25) is satisfied, and the resonance of the current injection network is tuned to the triple of the line frequency, the amplitude of the injected current is controlled by R , and the value that provides the optimal amplitude specified by (12.15) is

$$R = \frac{9\sqrt{3}}{4\pi} \frac{V_m}{I_{OUT}} . \quad (12.26)$$

This value is nine times higher than the value of (6.10) for the current injection networks designed for application with magnetic current injection devices, since in this case the current injection network is exposed to three times higher voltages and conducts three times lower currents than in the case of a magnetic current injection device.

Let us define the current injection network Q -factor as

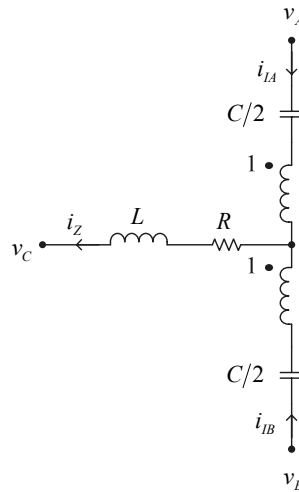


Figure 12-8. Current injection network for the third-harmonic current injection.

$$Q = \frac{1}{R} \sqrt{\frac{L}{C}}, \quad (12.27)$$

in the same manner as in Chapter 6. To provide single polarity of the voltages across the current injection network capacitors, the amplitude of the AC component of the capacitor voltages has to be lower than the DC component, which reduces to a condition

$$\frac{2}{3\omega_0 C} \frac{1}{4} I_{OUT} < \frac{1}{2} V_{OUT}. \quad (12.28)$$

In terms of the current injection network *Q*-factor, the condition for single polarity of the voltage across the current injection network capacitors is expressed as

$$Q < \frac{4}{3}. \quad (12.29)$$

If (12.29) is satisfied, electrolytic capacitors can be applied in construction of the current injection network.

Dependence of the input current THD on the current injection network *Q*-factor can be computed applying the method of equivalent circuits,

introduced in Chapter 6. In comparison to current injection network C described in Section 6.5, the differences are in three times higher voltages at odd triples of the line frequency the current injection network is exposed to, and the nine times higher equivalent resistance of the current injection system, specified by (12.26). The simulation result is presented in Fig. 12-9, and it indicates that the choice of the current injection network Q -factor negligibly affects the input current THD. Thus, the choice of the Q -factor should be dominated by economical arguments, rather than technical.

Another issue of interest are the volt-ampere ratings of magnetic components applied in the current injection network. Voltages across the transformer are the same as in the case of current injection network C discussed in Section 6.5, while the currents are three times lower. This results in the volt-ampere rating of the transformer equal to

$$S_{THI} = \frac{2}{105} \left(\sqrt{\pi^2 - 9} - 3 \arccos\left(\frac{3}{\pi}\right) \right) P_{IN} \approx 0.054\% P_{IN}. \quad (12.30)$$

Again, the volt-ampere rating of the transformer is very low, even three times lower than in the case of the current injection device designed for application with magnetic current injection devices.

The volt-ampere rating of the core for the current injection network inductor is obtained assuming that the current through the device is purely sinusoidal, and the obtained result is

$$S_L = \frac{Q}{70} P_{IN}, \quad (12.31)$$

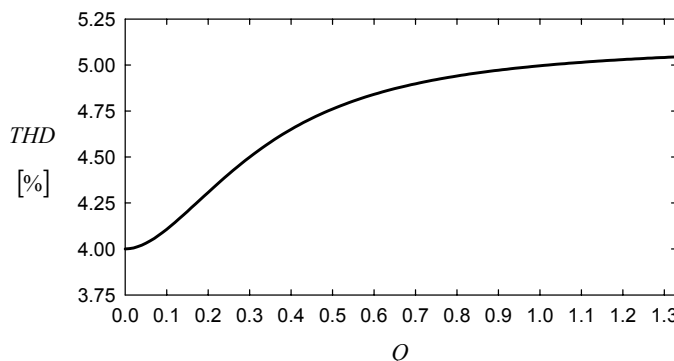


Figure 12-9. Dependence of the input current THD on the current injection network Q -factor.

the same as given by (6.42) for the current injection network C. The result is expected, since the inductance is increased three times, while the RMS value of the current going through the inductor and the maximum of the inductor current are reduced three times. According to (6.24), these values result in a three times lower value for the inductor core volt-ampere rating. To avoid misunderstanding, let us underline here that the range for Q in (12.31) is reduced three times according to (12.29).

To conclude, it can be stated that current injection network C described in Section 6.5 should be adjusted to be applied with the switching current injection device. The equivalent resistance of the current injection system should be increased nine times; the capacitors and the inductor should be chosen to satisfy $Q < 4/3$, which allows three times higher maximal value of the inductance and three times lower minimal value of the capacitance of the current injection network capacitors. Volt-ampere ratings of the magnetic components in the current injection network are reduced three times in comparison to the situation when a magnetic current injection device is applied.

4. RECOVERY OF THE CURRENT INJECTION NETWORK POWER BY THE CURRENT-LOADED RESISTANCE EMULATOR

The power taken by the current injection network should be either dissipated or restored at the rectifier output by applying resistance emulation techniques. Since the high-frequency switching resistance emulation is not within the scope of this book, only passive resistance emulation techniques are analyzed here. Two methods of this kind are presented in this book, the first in Chapter 10, and the other in Chapter 11. Application of the current-loaded resistance emulator is discussed in this section, since the voltage-loaded resistance emulator relies on the discontinuous conduction mode of the three-phase diode bridge, which is not applicable in the case of the switching current injection device. The rectifier that applies the switching current injection device is presented in Fig. 12-10. The rectifier is different than the rectifier presented in Fig. 10-1 only in the current injection device part, since the rectifier presented in Fig. 12-10 applies the switching current injection device. As discussed in previous sections of this chapter, this results in different voltages across the current injection network, as well as different currents in the current injection network. To adjust to these changes, some of the rectifier parameters have to be modified. Application of the current-loaded resistance emulator in the rectifier that applies switching current injection device was originally proposed in [35].

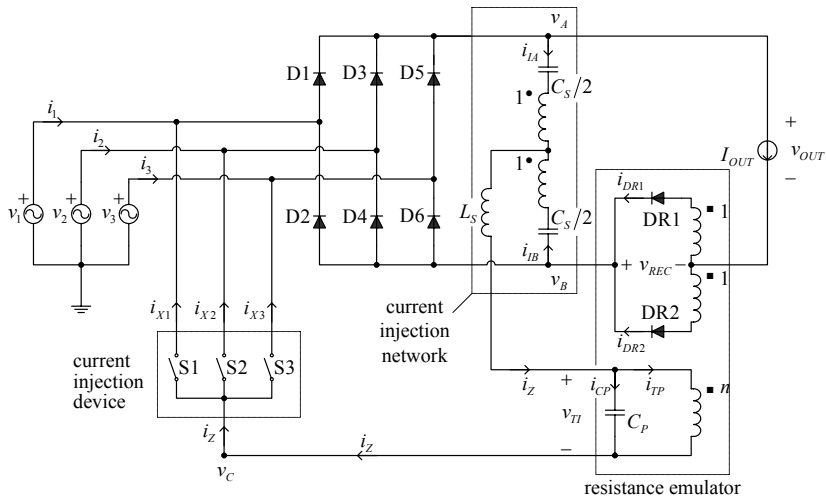


Figure 12-10. The third-harmonic current injection rectifier applying a current-loaded resistance emulator and a switching current injection device.

To provide an adequate amplitude of the injected current which is three times lower than if a magnetic current injection device is applied, the 1:1: n transformer turns ratio has to be modified to be

$$n = \frac{8}{\pi}. \quad (12.32)$$

Elements of the current injection network should satisfy the resonance constraint of (12.25) and the constraint that the voltages across the current injection network capacitors do not change polarity during the period. Applying the same methods as in Chapter 10, this results in

$$L_s = \frac{\sqrt{3}}{\pi} \frac{R_X}{\omega_0} \quad (12.33)$$

and

$$C_s = \frac{\pi}{9\sqrt{3}} \frac{1}{\omega_0 R_X}, \quad (12.34)$$

where

$$R_X = \frac{V_m}{I_{OUT \max}}. \quad (12.35)$$

In comparison to the rectifier proposed in Chapter 10, the inductance is increased three times, while the capacitance is reduced three times.

Elements of the parallel resonant circuit, capacitor C_P and the magnetizing inductance of the $1:1:n$ transformer L_P observed at the winding with n turns, should satisfy the resonance constraint for the triple of the line frequency, and the ringing current of the parallel resonant circuit should be large enough to avoid discontinuous conduction operation of the resistance emulator rectifier. The values of these parameters that satisfy both of the conditions are

$$L_P = \frac{3\sqrt{3}}{\pi^2} \frac{R_X}{\omega_0} \quad (12.36)$$

and

$$C_P = \frac{\pi^2}{27\sqrt{3}} \frac{1}{\omega_0 R_X}. \quad (12.37)$$

In comparison to the rectifier proposed in Chapter 10, the inductance is increased nine times, while the capacitance is reduced nine times.

In the case the parameters of the rectifier are chosen according to (12.32), (12.33), (12.34), (12.36), and (12.37), the volt-ampere rating of the $1:1:n$ transformer is the same as in the case of the rectifier that applies a magnetic current injection device, and it is

$$S_{TRE} = \frac{\pi}{140} \left(1 + \frac{\sqrt{3}}{2}\right) P_{OUT} \approx 4.19\% P_{OUT}. \quad (12.38)$$

Volt-ampere ratings of the $1:1$ transformer and the current injection network inductor are given by (12.30) and (12.31), where (12.31) for the values specified by (12.33) and (12.34) reduces to

$$S_L = \frac{2}{105} P_{IN} \approx 1.90\% P_{IN}, \quad (12.39)$$

which is three times lower than in the case of the rectifier proposed in Chapter 10.

Before the rectifier of the type analyzed in this section is built, the parameters of the current injection network should be carefully selected and optimized applying the simulation method described in Section 10.3.

5. OPTIMAL CURRENT INJECTION APPLYING SWITCHING CURRENT INJECTION DEVICE

In the case of optimal current injection, the rectifier input currents are purely sinusoidal and in phase with corresponding phase voltages, given by

$$i_p = \frac{v_p}{R_E} \quad (12.40)$$

for $p \in \{1, 2, 3\}$. If the switching current injection device is applied, each of the phase currents is equal either to i_A , $-i_B$, or $-i_Z$. Thus, these currents should be proportional to the voltages of the nodes they are taken from. Since i_A is the load current of the diode bridge positive output terminal, in the case of the optimal current injection its waveform should be

$$i_A = \frac{v_A}{R_E} = \frac{1}{R_E} \left(\frac{1}{2} V_{OUT} + v_{ODD} + v_{EVEN} \right). \quad (12.41)$$

On the other hand, current i_B is the load current of the negative output terminal of the diode bridge, and taking the direction of i_B into account its waveform in the case of the optimal current injection is

$$i_B = -\frac{v_B}{R_E} = \frac{1}{R_E} \left(\frac{1}{2} V_{OUT} - v_{ODD} + v_{EVEN} \right). \quad (12.42)$$

The remaining phase, the voltage of which is neither minimal nor maximal in the considered time point, is connected to the output terminal of the current injection network by the switching current injection device. Taking the direction of i_Z into account, its waveform is given by

$$i_Z = -\frac{v_C}{R_E} = \frac{2}{R_E} v_{ODD}. \quad (12.43)$$

The waveforms of i_A , i_B , and i_Z that provide purely sinusoidal input currents are shown in Fig. 12-11. The waveforms are slightly different than

the waveforms presented in Fig. 12-4 for the case of the optimal third-harmonic current injection, and the difference is caused by the higher order harmonics of the current injection network currents.

Now, let us define waveforms for two auxiliary currents,

$$i_{ODD} = \frac{v_{ODD}}{R_E} \quad (12.44)$$

and

$$i_{EVEN} = \frac{v_{EVEN}}{R_E} . \quad (12.45)$$

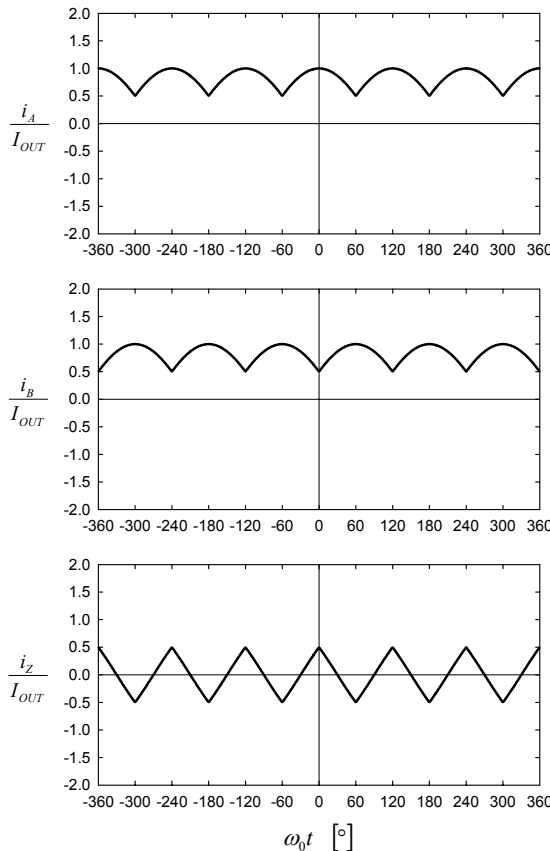


Figure 12-11. Waveforms of i_A , i_B , and i_Z that provide ideal sinusoidal waveforms of the input currents, in phase with corresponding phase voltages.

Since the DC components of v_{ODD} and v_{EVEN} are equal to zero according to (12.4) and (12.5), the DC components of i_{ODD} and i_{EVEN} are also equal to zero. Thus, the DC components of i_A and i_B are equal to the output current,

$$I_{OUT} = \frac{1}{2} \frac{V_{OUT}}{R_E} = \frac{3\sqrt{3}}{2\pi} \frac{V_m}{R_E}. \quad (12.46)$$

The AC components of i_A and i_B are taken by the current injection network, and according to the circuit diagram of Fig. 12-1 these currents are

$$i_{IA} = i_A - I_{OUT} = i_{ODD} + i_{EVEN} \quad (12.47)$$

and

$$i_{IB} = I_{OUT} - i_B = i_{ODD} - i_{EVEN}. \quad (12.48)$$

After i_{IA} and i_{IB} are determined, the injected current in the case of the optimal current injection is obtained as

$$i_Z = i_{IA} + i_{IB} = 2i_{ODD}. \quad (12.49)$$

Thus, the injected current contains only harmonic components at odd triples of the line frequency, the same as in the case of the optimal current injection in the case a magnetic current injection device is applied.

Waveforms of the diode bridge input currents i_{S1} , i_{S2} , and i_{S3} are presented in Fig. 12-12. This figure corresponds to Fig. 12-5 for the optimal third-harmonic current injection. Again, gaps in the diode bridge input currents can be observed during the intervals the phase voltage is neither minimal nor maximal among the phase voltages. These gaps are going to be patched by the injected current. During the time intervals the currents are not equal to zero, segments of sinusoidal input currents can be observed.

To patch the gaps in the currents of Fig. 12-12, the injected currents i_{X1} , i_{X2} , and i_{X3} are utilized. These currents are obtained by directing the injected current i_Z to the phase that needs the injected current to patch the gap. The waveforms of i_{X1} , i_{X2} , and i_{X3} in the case of the optimal current injection are shown in Fig. 12-13. The currents flow during the same intervals of time as the currents of Fig. 12-6, but the waveforms are different owing to the higher order harmonics in the injected current i_Z .

From the waveforms of i_{Sp} and i_{Xp} for $p \in \{1, 2, 3\}$, the input currents i_1 , i_2 , and i_3 can be obtained taking

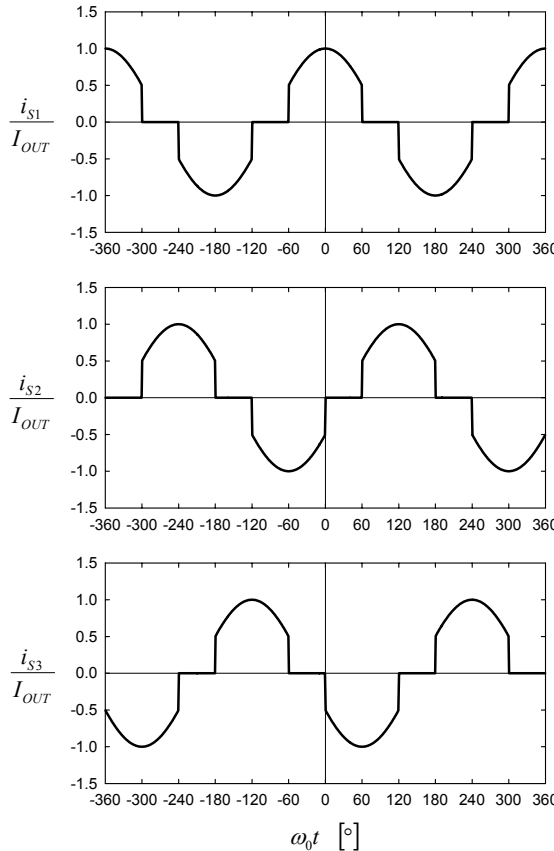


Figure 12-12. Waveforms of the diode bridge input currents, i_{S1} , i_{S2} , and i_{S3} .

$$i_p = i_{Sp} - i_{Xp}. \quad (12.50)$$

The waveforms of Figs. 12-12 and 12-13 indicate that the input current waveforms are purely sinusoidal.

The power taken by the current injection network in the case of the optimal current injection can be computed from the waveforms of the voltages and currents of the current injection network, and the result is

$$P_{INJ} = \frac{3}{2} \frac{\pi^2 - 9}{\pi^2} \frac{V_m^2}{R_E} \approx 8.81\% P_{IN}, \quad (12.51)$$

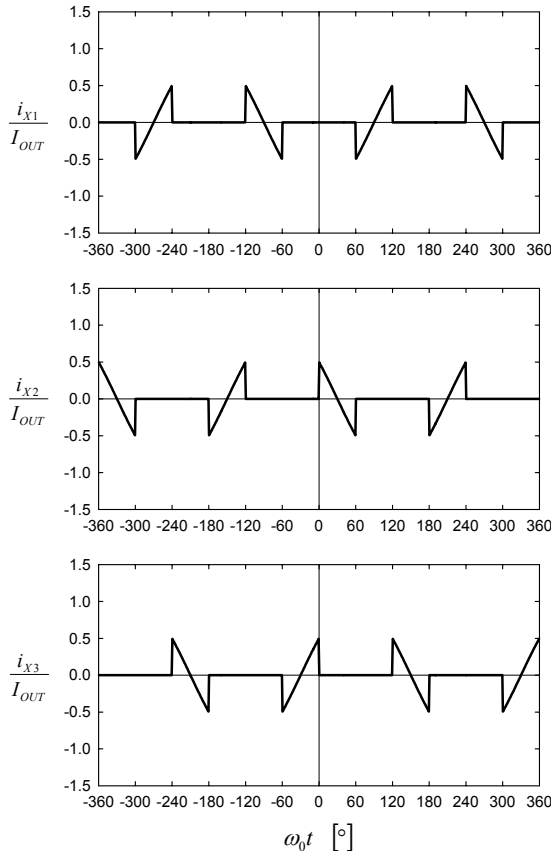


Figure 12-13. Waveforms of the injected currents i_{X1} , i_{X2} , and i_{X3} .

which is the same as in the case of the optimal current injection with a magnetic current injection device. If the power taken by the current injection network is dissipated, the rectifier efficiency is

$$\eta = \frac{9}{\pi^2} \approx 91.19\% P_{IN}. \quad (12.52)$$

Again, the same result is obtained as in Chapter 7 for the rectifiers that apply magnetic current injection devices.

6. CURRENT INJECTION NETWORKS FOR THE OPTIMAL CURRENT INJECTION APPLYING A SWITCHING CURRENT INJECTION DEVICE

The purpose of the current injection network for the optimal current injection is to provide the injected currents i_{IA} , i_{IB} , and i_Z specified by (12.47), (12.48), and (12.49) applying voltages v_A , v_B , and v_C present at the current injection network terminals. In the design of the current injection networks, the same methods are applied as in Chapter 8; thus some of the steps are omitted.

The first current injection network for the optimal current injection is presented in Fig. 12-14, and it consists of two capacitors and three resistors. The capacitors are applied to remove the DC components of the output terminal voltages. The injected currents are given by

$$i_A = i_{R \text{ ODD } A} + i_{R \text{ EVEN}} \quad (12.53)$$

and

$$i_B = i_{R \text{ ODD } B} - i_{R \text{ EVEN}}. \quad (12.54)$$

The currents of R_{ODD} resistors are

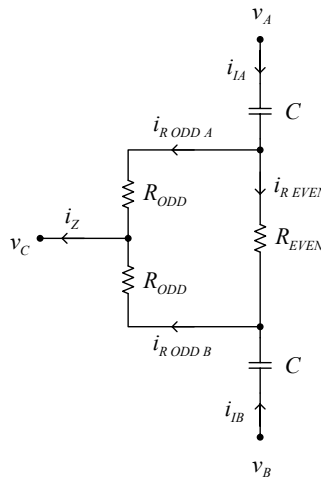


Figure 12-14. The first current injection network for the optimal current injection.
© [2002] IEEE.

$$i_{R\text{ODD}\text{A}} = \frac{3v_{ODD} + v_{EVEN}}{R_{ODD}} \quad (12.55)$$

and

$$i_{R\text{ODD}\text{B}} = \frac{3v_{ODD} - v_{EVEN}}{R_{ODD}}, \quad (12.56)$$

which gives the injected current

$$i_Z = i_{R\text{ODD}\text{A}} + i_{R\text{ODD}\text{B}} = \frac{6v_{ODD}}{R_{ODD}}. \quad (12.57)$$

Equating (12.57) and (12.43), the value of R_{ODD} is obtained as

$$R_{ODD} = 3R_E. \quad (12.58)$$

Applying this value of R_{ODD} , the currents of R_{ODD} resistors are

$$i_{R\text{ODD}\text{A}} = i_{ODD} + \frac{1}{3}i_{EVEN} \quad (12.59)$$

and

$$i_{R\text{ODD}\text{B}} = i_{ODD} - \frac{1}{3}i_{EVEN}. \quad (12.60)$$

The remaining part of $2/3 i_{EVEN}$ in i_{IA} and i_{IB} is added applying R_{EVEN} , whose current is

$$i_{R\text{EVEN}} = \frac{2v_{EVEN}}{R_{EVEN}} = \frac{2}{3}i_{EVEN} = \frac{2}{3} \frac{v_{EVEN}}{R_E}. \quad (12.61)$$

From (12.61) the resistance of R_{EVEN} is obtained as

$$R_{EVEN} = 3R_E. \quad (12.62)$$

Computing RMS values of the voltages across the current injection network resistors, the power dissipated on each of the resistors can be computed. The

power dissipated on each of the R_{ODD} resistors is obtained as

$$P_{R_{ODD}} = \frac{4\pi^2 - 3\sqrt{3}\pi - 18}{12\pi^2} P_{IN} \approx 4.35\% P_{IN}, \quad (12.63)$$

while the power dissipated on R_{EVEN} is

$$P_{R_{EVEN}} = \frac{2\pi^2 + 3\sqrt{3}\pi - 36}{6\pi^2} P_{IN} \approx 0.11\% P_{IN}. \quad (12.64)$$

The sum of the powers dissipated on the resistors is equal to the power taken by the current injection network given by (12.51).

As in the case of the magnetic current injection devices, the solution for the current injection network is not unique. The second current injection network proposed here is presented in Fig. 12-15, and it consists of two capacitors, one 1:1 transformer, and two resistors. The current injection network is topologically the same as the current injection network shown in Fig. 8-2, but the parameters of the network are different. Application of two resistors instead of three might be interesting if the switching resistance emulation is applied, since the number of resistance emulators is reduced. In the current injection network of Fig. 12-15, for the injection of harmonics at odd triples of the line frequency R_1 is solely responsible, and for the injection of harmonics at even triples of the line frequency R_2 is solely responsible.

The resistance of R_1 that provides optimal injection of the harmonics at odd triples of the line frequency is

$$R_1 = \frac{3v_{ODD}}{2i_{ODD}} = \frac{3}{2} R_E, \quad (12.65)$$

while the resistance of R_2 is

$$R_2 = \frac{2v_{EVEN}}{i_{EVEN}} = 2R_E. \quad (12.66)$$

The power dissipated on R_1 is

$$P_{R1} = \left(\frac{1}{2} - \frac{3\sqrt{3}}{4\pi} \right) P_{IN} \approx 8.65\% P_{IN}, \quad (12.67)$$

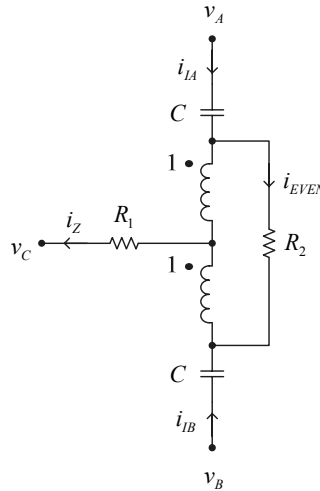


Figure 12-15. The second current injection network for the optimal current injection.
© [2002] IEEE.

while the power dissipated on R_2 is

$$P_{R2} = \frac{2\pi^2 + 3\sqrt{3}\pi - 36}{4\pi^2} P_{IN} \approx 0.16\% P_{IN}. \quad (12.68)$$

The powers dissipated on the resistors add up to the power taken by the current injection network given by (12.51).

The volt-ampere rating of the transformer in the current injection network shown in Fig. 12-15 is

$$S_T = \frac{1}{4\pi} \sqrt{\frac{1}{3} - \frac{\sqrt{3}}{2\pi}} \left(\sqrt{\pi^2 - 9} - 3 \arccos\left(\frac{3}{\pi}\right) \right) P_{IN} \approx 0.054\% P_{IN}, \quad (12.69)$$

which is three times lower than if a magnetic current injection device is applied, when the volt-ampere rating is given by (8.25). The result is expected since the voltages across the transformer windings are the same, while the currents are three times lower in the case the switching current injection device is applied.

In the analyses previously presented in this section, it has been assumed that the capacitance of the current injection network capacitors is infinite, and that the ripple of their voltages can be neglected. Degradation of the input current THD caused by finite capacitance of the capacitors can be studied applying the method introduced in Section 8.3. The input current THD is computed as a function of parameter γ defined as

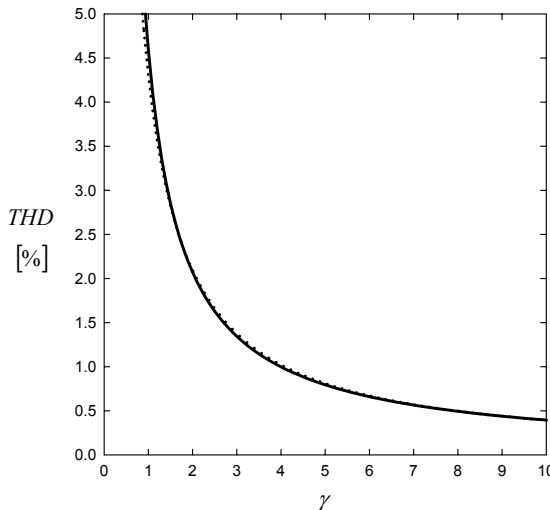


Figure 12-16. Dependence of the input current THD on γ .

$$\gamma = 3\omega_0 CR_E, \quad (12.70)$$

and the resulting curve is shown by the solid line in Fig. 12-16. From the diagram of Fig. 12-16, it can be concluded that the input current THD falls rapidly with γ until the THD values of about 1% are reached, and after that the input current THD slowly decays with γ . The solid line in Fig. 12-16 is accompanied by the dotted line computed from

$$THD \approx \frac{4.31\%}{\gamma^{1.04}}, \quad (12.71)$$

which is obtained fitting the curve obtained by numerical simulation. In practice, the value of C should be chosen to provide $\gamma > 4$ at the maximum of the rectifier power, i.e. the minimum of the emulated resistance at the rectifier input.

The analytical results presented so far are derived under the assumption that the output current is free from ripple, containing only the DC component. However, the effects the output current ripple causes in the input current THD deserve to be studied. The first of the analyses of this kind assumes that the ripple is caused by finite incremental conductance of the load. In this case, the load can be represented by a parallel combination of a constant current source and the incremental conductance G_{OUT} in the vicinity of the operating point,

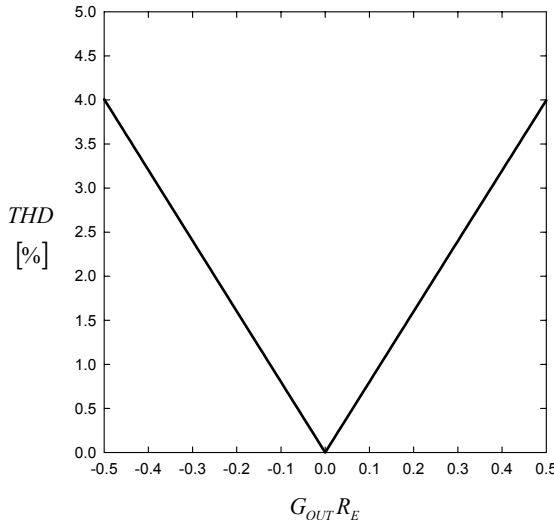


Figure 12-17. Dependence of the input current THD on γ . © [2002] IEEE.

$$i_{OUT} = I_{OUT} + G_{OUT} \hat{v}_{OUT}, \quad (12.72)$$

where \hat{v}_{OUT} is the AC component of the output voltage. The input current THD is obtained by numerical simulation in this case, and the resulting diagram is presented in Fig. 12-17. The range for normalized incremental resistance of the load is chosen such that the minimum of $G_{OUT} = -1/(2R_E)$ corresponds to the constant power load, while the maximum of $G_{OUT} = 1/(2R_E)$ corresponds to the linear resistor as the load. Thus, this range covers all loads that might be encountered in practice. According to the diagram of Fig. 12-17, the input current THD almost linearly depends on $|G_{OUT}|$, and an empirical formula that gives the input current THD as a function of incremental conductance of the load is

$$THD \approx 8|G_{OUT} R_E|. \quad (12.73)$$

It is worth mentioning that effects caused by the output current ripple in this case can be compensated for adjusting the resistor R_{EVEN} in the current injection network of Fig. 12-14 or R_2 in the current injection network of Fig. 12-15 such that the parallel combination of R_{EVEN} and $1/G_{OUT}$ or R_2 and $1/G_{OUT}$ is made equal to $2R_E$. The current injection network shown in Fig. 12-15 allows more freedom in compensation of the load incremental conductance, and the whole range of the incremental conductance variations $-1/(2R_E) < G_{OUT} < 1/(2R_E)$ can be ideally compensated for adjusting R_2 .

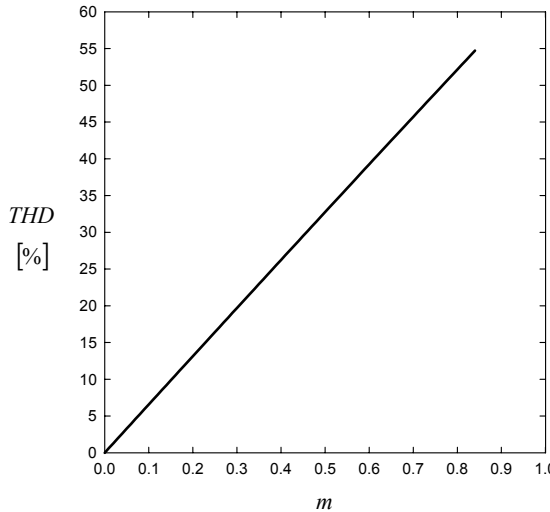


Figure 12-18. Dependence of the input current THD on m .

If the load is connected to the rectifier by an inductive filter, the load current takes the form

$$i_{OUT} = I_{OUT}(1 - m \sin(6\omega_0 t)), \quad (12.74)$$

where m is the normalized amplitude of the output current ripple. Again, the input current THD is obtained applying numerical simulation, and the resulting diagram is presented in Fig. 12-18. The dependence is almost linear, and an empirical relation between the normalized amplitude of the input current THD and the normalized amplitude of the output current ripple is

$$THD \approx 65\% m. \quad (12.75)$$

This result is different than the result presented in [37].

The current injection network resistors should depend on the resistance emulated at the rectifier input. On the other hand, the emulated resistance is dependent on the output power, i.e., on the output current. To provide the optimal current injection, resistors in the current injection network should be adjusted to the load current. If expected variations of the load current are small, fixed resistors may be used in the current injection network. Variations of the output current cause degradation of the input current THD in this case, and such a degradation is analyzed now. Let us assume that there is a rated output current that corresponds to the resistance R_E emulated at each phase of the rectifier input. Next, let us assume that the output current is

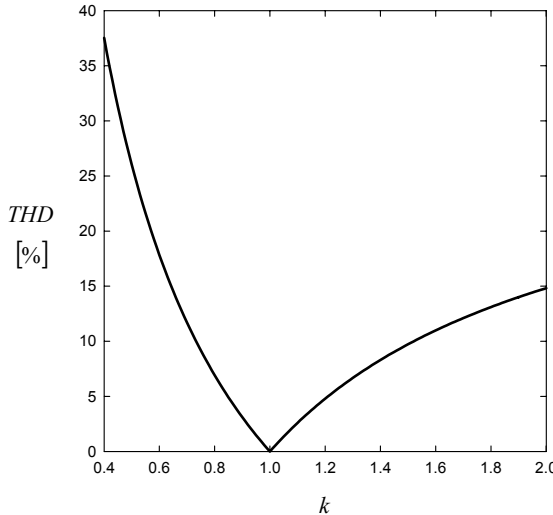


Figure 12-19. Dependence of the input current THD on the output current.

$$I_{OUT} = k \frac{1}{2} \frac{V_{OUT}}{R_E} = k \frac{3\sqrt{3}}{2\pi} \frac{V_m}{R_E}, \quad (12.76)$$

where $k=1$ corresponds to the rated value of the output current. Dependence of the input current THD on k is computed applying numerical simulation, and the result is presented in Fig. 12-19. For output current values lower than the rated value, the input current THD grows relatively fast, being higher than 5% at the output current equal to 80% of the rated value. The increase of the input current THD is significantly lower for the output current values above the rated value, and the curve asymptotically reaches the value of 31.08% as $k \rightarrow \infty$, that corresponds to the rectifier without the current injection system.

7. DESIGNING THE SWITCHING CURRENT INJECTION DEVICE

The current injection method achieved using a switching current injection device offers some advantages in comparison to the case a magnetic current injection device is applied. Currents of the current injection network are three times lower, as well as the volt-ampere ratings of the magnetic components applied in the current injection network. This reduces losses

in the current injection system and improves efficiency. However, the switching current injection device is not that easy to design as a magnetic current injection device, and its robustness is lower. The design of the switching current injection device is not a closed topic yet, and the opinion of the author is that some research in that area still needs to be done.

According to Figs. 12-6 and 12-13, the switches in the current injection device have to be bidirectional, i.e., they have to conduct current in both directions. To generate experimental results presented in [32] and [37], realization of a bidirectional switch shown in Fig. 12-20 is applied. This realization consists of a diode bridge and one controlled switch, being a MOSFET in this case. The realization is not considered the best, since the realizations that apply two controlled switches can be controlled with higher precision, but it is simple. The controlled switch should be precisely controlled to avoid interphase short circuits caused by two switches that are turned on, and to avoid the situation when all of the switches are turned off and the injected current does not have a path to close, which is especially important in the case of the current injection networks for the third-harmonic current injection that apply series inductor. Techniques developed for control of the switches in matrix converters may be utilized in the design of the switching current injection network.

To control the switches in the current injection device, let us define three logic functions, A , B , and C , according to the specification given in Table 12-2. The logic functions contain information about mutual relations of the phase voltages, and they are used to determine the voltage that is neither minimal nor maximal at the considered time point. States of the switches in the current injection device, shown in Fig. 12-3, are generated applying the logic signals A , B , and C according to

$$s_1 = \overline{A} \overline{B} \overline{C} + \overline{A} \overline{B} C, \quad (12.77)$$

$$s_2 = A \overline{B} \overline{C} + \overline{A} \overline{B} C, \quad (12.78)$$

and

$$s_3 = A \overline{B} \overline{C} + \overline{A} BC. \quad (12.79)$$

A circuit that generates control signals for the switches applying three comparators, one 8-bit decoder/demultiplexer, and three NAND gates, is shown in Fig. 12-21. The comparators provide information about mutual relations of the phase voltages, and their output signals are further processed

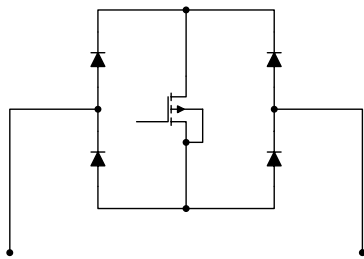


Figure 12-20. Construction of a bidirectional switch. © [2002] IEEE.

Table 12-2. Definition of logic functions A, B, and C.

Function	0	1
A	$v_1 < v_2$	$v_1 > v_2$
B	$v_2 < v_3$	$v_2 > v_3$
C	$v_3 < v_1$	$v_3 > v_1$

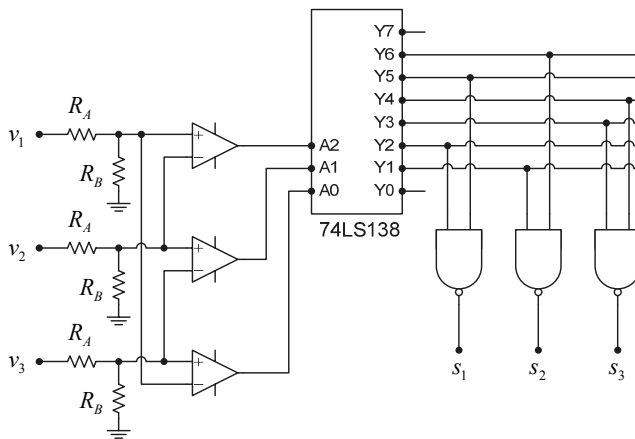


Figure 12-21. The circuit applied to generate control signals for the switches. © [2002] IEEE.

by the digital part of the circuit of Fig. 12-21 that consists of one 74LS138 decoder/demultiplexer and three NAND gates of a 74LS00 chip. The circuit is simple and precise enough to generate control signals for the switches in the current injection device of the rectifier built to generate the experimental results. During the experiments, the experience with such design of the current injection device is that interphase short circuits appeared, resulting in spikes in the input currents. Fortunately, due to the line to line voltages that

are close to zero at the commutation instants, these current spikes were low. However, the opinion of the author is that robustness and performance of the circuit may be improved by applying the techniques developed for matrix converters. The drawback of the bidirectional switches developed for matrix converters is that they require two controlled switches with a relatively complex control strategy.

Chapter 13

RECTIFIERS THAT APPLY A SQUARE-WAVE CURRENT INJECTION

Current injection based rectifiers analyzed so far apply either sinusoidal current injection, analyzed in Chapter 5, or the optimal current injection, analyzed in Chapter 7. Sinusoidal current injection in its various implementations provided total harmonic distortion (THD) values of the input currents of about 5%. The optimal current injection provides purely sinusoidal input currents, in phase with corresponding phase voltages. These two approaches require different current injection networks. If losses in the current injection network of about 9% of the input power can be tolerated, resulting in the rectifier efficiency of about 90%, the current injection networks are almost equally simple. However, in a more realistic case that these losses cannot be tolerated, simple passive resistance emulators can be applied in the case of the sinusoidal current injection, while the optimal current injection would require switching resistance emulators. Thus, implementation of the sinusoidal current injection, either applying current-loaded resistance emulator discussed in Chapter 10, or applying voltage-loaded resistance emulator discussed in Chapter 11, is more likely in the high power area.

Besides the sinusoidal and the optimal current injection, there is another class of current injection based rectifiers, characterized by square-wave current injection, or rectangular current injection, as classified in [23]. This type of current injection was inspired by difficulties in obtaining the injected current with sinusoidal waveform in the early days of current injection, and resulted in the rectifiers proposed in [3], [4], and [5]. A modern rectifier of this kind presented in [14] is of particular interest, and is analyzed in detail in this chapter. The rectifiers that apply square-wave current injection are characterized by somewhat higher THD of the input currents (around 15%), but their current injection networks are extremely simple—they do not require any resonance constraints to be satisfied, neither do they require switching converters to shape the injected current. The only components required in square-wave current injection rectifiers are diodes, transformers, and capacitors. Thus, the application area of these simple and robust rectifiers is in the high power area, where they compete with classical

12-pulse rectifiers, having the same THD values of the input currents but different constructions.

In this chapter, two rectifiers that apply square-wave current injection are analyzed. In both rectifiers, a limiting case of the current injection network discussed in Section 6.5 is applied. The limiting case refers to the situation in which the inductor of the current injection network is omitted, and the capacitance of the capacitors is considered to be infinitely large. In practice, this reduces to the requirement that AC components of the capacitor voltages are small enough in comparison to the output voltage ripple that they do not affect the rectifier operation. This results in acceptable values for the capacitance of the capacitors, and makes this kind of rectifier interesting for practical application. To provide current injection, both of the rectifiers require current injection device or a transformer with wye-connected secondary. Choice of the current injection device type is limited to the devices with small inductance of the neutral point, since the injected currents are not continuous in time.

Besides the current injection network and the current injection device or a transformer, the rectifiers to be analyzed in this chapter apply resistance emulators. The first of the rectifiers, proposed in [14], applies a current-loaded resistance emulator, while the second of the rectifiers applies a voltage-loaded resistance emulator. Thus, the rectifiers proposed in this chapter may be considered as special cases of the rectifiers proposed in Chapter 10 and Chapter 11, in the case that the inductor of the current injection network is omitted, avoiding the resonance constraint and imposing the constraint that the capacitor voltage ripple should be small. These two rectifiers may even be applied as retrofit upgrades of existing 6-pulse rectifiers.

To introduce notation used throughout this chapter, some waveforms are defined here. Both rectifiers to be analyzed in this chapter are assumed to be supplied by a balanced undistorted three-phase voltage system

$$v_p(\omega_0 t) = V_m \cos\left(\omega_0 t - (p-1)\frac{2\pi}{3}\right), \quad (13.1)$$

where $p \in \{1, 2, 3\}$. In the case the three-phase diode bridge supplied by the voltage system of (13.1) operates in the continuous conduction mode, the voltage of the positive output terminal is given by

$$v_{A0}(\omega_0 t) = \max(v_1(\omega_0 t), v_2(\omega_0 t), v_3(\omega_0 t)), \quad (13.2)$$

while the voltage of the negative output terminal of the diode bridge is

$$v_{B0}(\omega_0 t) = \min(v_1(\omega_0 t), v_2(\omega_0 t), v_3(\omega_0 t)). \quad (13.3)$$

The output voltage of the diode bridge in the continuous conduction mode is

$$v_{AB0}(\omega_0 t) = v_{A0}(\omega_0 t) - v_{B0}(\omega_0 t). \quad (13.4)$$

Another quantity that needs to be defined here is the average of the output terminal voltages in the continuous conduction mode, present at the center tap of the current injection network transformer in that mode. This voltage is

$$v_{AV0}(\omega_0 t) = \frac{v_{A0}(\omega_0 t) + v_{B0}(\omega_0 t)}{2}. \quad (13.5)$$

Waveforms and spectra of the waveforms specified by (13.2) to (13.5) are given in Chapter 2.

1. **SQUARE-WAVE CURRENT INJECTION RECTIFIER THAT APPLIES A CURRENT-LOADED RESISTANCE EMULATOR**

The first rectifier to be analyzed in this chapter is presented in Fig. 13-1. It is proposed in [14], and consists of a three-phase diode bridge, a current injection device, a current injection network, and a current-loaded resistance emulator. The current injection device should have a small inductance of the neutral point, since the current to be injected has discontinuities in its waveform. The current injection network consists of two capacitors and a transformer with the turns ratio 1:1. Capacitance of the capacitors should be large enough to provide a small ripple of the capacitor voltages in comparison to the output voltage ripple. The resistance emulator consists of a transformer with the turns ratio $n:1:1$ and two diodes, DR1 and DR2. Output of the resistance emulator is connected in series with the load, which is assumed to have constant current, free from ripple.

To reduce the number of nonlinear elements, the technique proposed in Chapter 9 is applied, and the equivalent circuit is presented in Fig. 13-2. In the circuit of Fig. 13-2, operation of the three-phase diode bridge of Fig. 13-1 is represented by voltage sources v_{A0} and v_{B0} , accompanied by diodes DA and DB to model the diode bridge discontinuous conduction mode. Resistor R models losses in the current injection system, consisting of the current injection network, resistance emulator, and the current injection device.

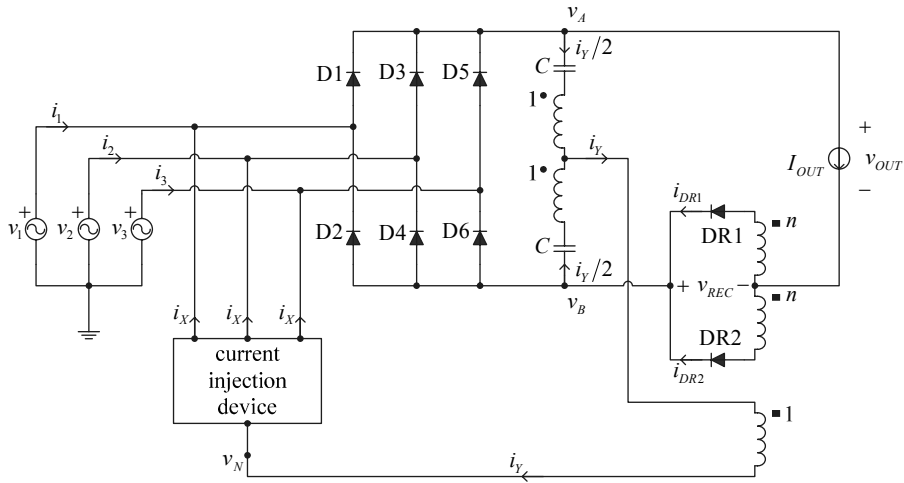


Figure 13-1. Square-wave current injection rectifier with current-loaded resistance emulator.

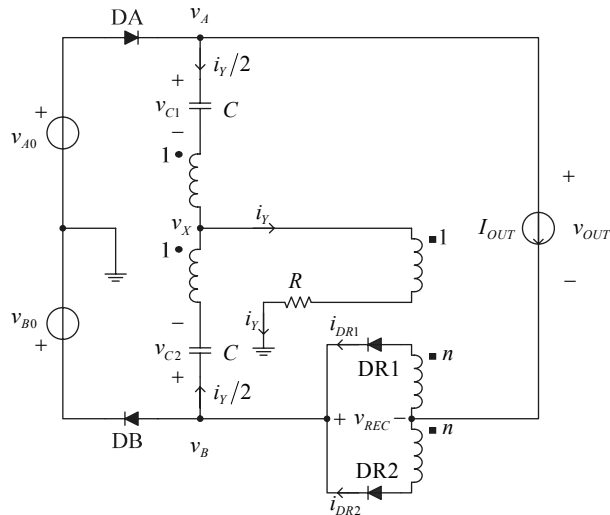


Figure 13-2. Equivalent circuit of the rectifier with current-loaded resistance emulator.

1.1 Analysis of the Rectifier Operation Neglecting Losses

Assuming negligible losses in the current injection system, states of the resistance emulator diodes DR1 and DR2 are determined solely by the

polarity of the voltage at the center tap of the 1:1 transformer. In this case, only one of the diodes DR1 or DR2 conducts in each point in time, resulting in the injected current

$$i_Y = nI_{OUT} \operatorname{sgn}(v_X). \quad (13.6)$$

In the case

$$0 < n < 2, \quad (13.7)$$

the range of the injected current instantaneous values is limited to

$$-2I_{OUT} < i_Y < 2I_{OUT}, \quad (13.8)$$

resulting in the continuous conduction mode of the diode bridge. In that case, diodes DA and DB are constantly conducting; thus

$$v_X = v_{AV0}. \quad (13.9)$$

Knowing the voltage that controls the resistance emulator diodes, specified by (13.5), the waveform of the injected current is obtained applying (13.6), and is depicted in the second diagram of Fig. 13-3. After the injected current is determined, the input currents are determined by applying

$$i_p = \left(I_{OUT} + \frac{i_Y}{2} \right) d_{2p-1} - \left(I_{OUT} - \frac{i_Y}{2} \right) d_{2p} - \frac{i_Y}{3}, \quad (13.10)$$

for $p \in \{1, 2, 3\}$, where the diode state functions d_{2p-1} and d_{2p} are defined in Chapter 2. The resulting waveform of the first phase current is presented in the first diagram of Fig. 13-3.

To analyze dependence of the input current THD on n , the RMS value of the input current is determined as

$$\frac{I_{RMS}(n)}{I_{OUT}} = \frac{1}{3} \sqrt{\frac{n^2}{2} + 6}, \quad (13.11)$$

while the RMS value of the input current fundamental harmonic is

$$\frac{I_{1RMS}(n)}{I_{OUT}} = \frac{2\sqrt{3} + (2 - \sqrt{3})n}{\pi\sqrt{2}}. \quad (13.12)$$

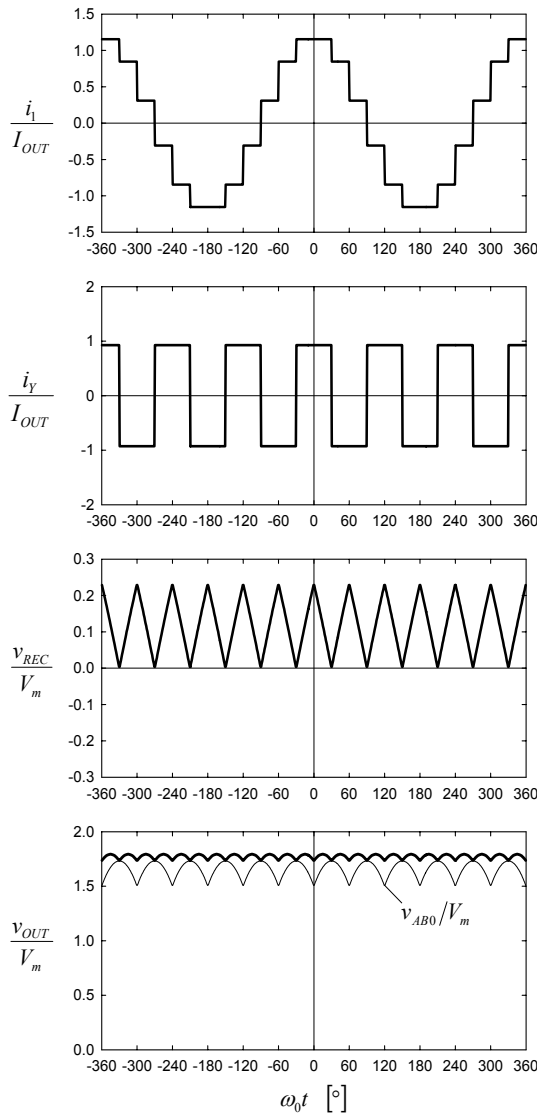


Figure 13-3. Waveforms of i_l , i_Y , v_{REC} , and v_{OUT} .

The input current THD is defined as

$$THD(n) = \sqrt{\frac{I_{RMS}^2(n) - I_{1RMS}^2(n)}{I_{1RMS}^2(n)}} = \sqrt{\frac{I_{RMS}^2(n)}{I_{1RMS}^2(n)} - 1}, \quad (13.13)$$

and its minimum is found from

$$\frac{d \text{THD}(n)}{dn} = 0. \quad (13.14)$$

Performing the calculation, for $R = 0$ the optimal value of the resistance emulator transformer turns ratio is obtained as

$$n_{OPT} = 4\sqrt{3} - 6 \approx 0.9282, \quad (13.15)$$

which coincides with the numerical value given in [14]. Waveforms of the rectifier voltages and currents presented in Fig. 13-3 are obtained for $R = 0$ and $n = n_{OPT}$.

For the optimal value of n , the THD value of the input currents is

$$\text{THD}_{\min} = \text{THD}(n_{OPT}) = \frac{\sqrt{(2 + \sqrt{3})\pi^2 - 36}}{6} \approx 15.22\%, \quad (13.16)$$

which is somewhat higher than for the sinusoidal and for the optimal current injection. However, the current injection network is not required to satisfy resonance constraint in this case, and the current injection network inductor is omitted.

The waveform of the output voltage of the current-loaded resistance emulator is determined by

$$v_{REC} = n_{OPT} |v_{AV0}|, \quad (13.17)$$

and is presented in the third diagram of Fig. 13-3. The waveform of v_{REC} can be represented by its Fourier series expansion as

$$v_{REC} = \frac{6\sqrt{3}}{\pi} V_m \left(\frac{7 - 4\sqrt{3}}{2} + \sum_{k=1}^{+\infty} \frac{(-1)^k (2\sqrt{3} - 4) + 2\sqrt{3} - 3}{36k^2 - 1} \cos(6k\omega_0 t) \right). \quad (13.18)$$

The output voltage of the rectifier is given by

$$v_{OUT} = v_{AB0} + v_{REC}, \quad (13.19)$$

and its waveform is presented in the fourth diagram of Fig. 13-3, accompanied by the waveform of the three-phase diode bridge output

voltage, plotted with the thin line. The DC component of the output voltage is

$$V_{OUT} = \frac{24\sqrt{3} - 36}{\pi} V_m \approx 1.77 V_m. \quad (13.20)$$

In (13.19), substituting v_{AB0} expressed by its Fourier series expansion given by (2.10), and substituting v_{REC} by its Fourier series expansion given by (13.18), Fourier series expansion of the rectifier output voltage is obtained as

$$v_{OUT} = V_m \frac{24\sqrt{3} - 36}{\pi} \left(1 - 2 \sum_{k=1}^{+\infty} \frac{1}{144k^2 - 1} \cos(12k\omega_0 t) \right). \quad (13.21)$$

From (13.21) it can be concluded that the output voltage contains harmonic components only at multiples of the twelfth multiple of the line frequency, which is the situation observed in multipulse rectifiers. The same conclusion can be made, although with less rigor, observing the waveforms presented in the fourth diagram of Fig. 13-3. Since the output voltage of the three-phase diode bridge is plotted with the thin line in the same diagram, it can be easily compared to the output voltage waveform, and it can be observed that application of the resistance emulator increased the DC component of the output voltage, reduced the output voltage ripple, and doubled the frequency of the output voltage ripple fundamental harmonic.

The output power of the rectifier is determined as a product of the output current and the DC component of the output voltage as

$$P_{OUT} = \frac{12(2\sqrt{3} - 3)}{\pi} V_m I_{OUT}. \quad (13.22)$$

The power taken by the current injection network is obtained as

$$P_{INJ} = \frac{3(7\sqrt{3} - 12)}{\pi} V_m I_{OUT}, \quad (13.23)$$

and the same power is restored at the rectifier output by the resistance emulator. Thus, the power processed by the resistance emulator normalized to the rectifier input power is

$$\frac{P_{INJ}}{P_{IN}} = \frac{2 - \sqrt{3}}{4} \approx 6.70\%, \quad (13.24)$$

which is less than in the cases of sinusoidal and optimal current injection.

The RMS value of the injected current for $n = n_{OPT}$ is

$$I_{YRMS} = n_{OPT} I_{OUT} = (4\sqrt{3} - 6) I_{OUT} \approx 0.93 I_{OUT}. \quad (13.25)$$

This value is used to compute the volt-ampere rating of the transformer applied in the current injection network, with the turns ratio 1:1, and the result is

$$S_{T1:1} = \frac{\sqrt{6}}{48} \left(\sqrt{\pi^2 - 9} - 3 \arccos\left(\frac{3}{\pi}\right) \right) P_{OUT} \approx 0.145\% P_{OUT}, \quad (13.26)$$

which is smaller than in the case of the sinusoidal current injection, where the corresponding volt-ampere rating is given by (6.41), and in the case of the optimal current injection, where the corresponding volt-ampere rating is given by (8.25).

The volt-ampere rating of the resistance emulator transformer is computed as

$$S_{Tn:n:1} = \frac{(2 - \sqrt{3})(1 + \sqrt{2})\pi}{48\sqrt{2}} P_{OUT} \approx 2.99\% P_{OUT}, \quad (13.27)$$

which is lower than the volt-ampere rating given by (10.36) for the resistance emulator transformer applied to provide a sinusoidal current injection with current-loaded resistance emulator.

Modified waveform of the injected current in a square-wave current injection rectifier also affects the volt-ampere rating of the current injection device. For the square-wave current injection it is required that the parasitic inductance of the current injection device neutral point is low, thus the device realized as a zigzag autotransformer is a suitable choice. In this case, the volt-ampere rating of the device is

$$S_{CID} = (2\sqrt{2} - \sqrt{6}) V_m I_{OUT} = \frac{\pi}{6\sqrt{6}} P_{OUT} \approx 21.38\% P_{OUT}. \quad (13.28)$$

The volt-ampere rating of the wye-wye transformer applied to provide the current injection would be

$$S_{YY} = \frac{3}{\sqrt{2}} \left(1 - \frac{1}{\sqrt{3}} + \frac{1}{3} \sqrt{33 - 18\sqrt{3}} \right) V_m I_{OUT}, \quad (13.29)$$

and normalized to the rectifier output power this volt-ampere rating becomes

$$S_{YY} = \frac{\pi\sqrt{2}}{24} \left(1 + \sqrt{3} + \sqrt{5 + 2\sqrt{3}} \right) P_{OUT} \approx 104.43\% P_{OUT}. \quad (13.30)$$

The wye-wye transformer is not a likely choice for application in rectifiers that apply square-wave current injection due to the high parasitic inductance of the neutral point. The delta-wye connected transformer is a better choice, and its volt-ampere rating would be

$$S_{DY} = \sqrt{66 - 36\sqrt{3}} V_m I_{OUT} = \frac{\pi}{12} \sqrt{10 + 4\sqrt{3}} P_{OUT} \approx 107.71\% P_{OUT}. \quad (13.31)$$

Thus, the delta-wye transformer could adjust the rectifier output voltage and provide the current injection with negligible inductance of the neutral point on expense of negligible increase in the volt-ampere rating.

1.2 Analysis of the Rectifier Taking Losses into Account

Another issue of interest is influence of losses in the current injection system on the rectifier operation. The losses in the current injection system are represented by resistor R in the equivalent circuit of Fig. 13-2. The resistance could be distributed in the current injection network branches in the same manner as analyzed in Chapter 11, but the resistance distribution would not cause any effect on the rectifier operation, again. Thus, it would be assumed that the resistance is located in the branch where i_Y flows.

The presence of the resistance R introduces the third state of the resistance emulator in the analysis. In that state, both diodes DR1 and DR2 conduct and voltages across the windings of the resistance emulator transformer are equal to zero. The injected current is determined by

$$i_Y = \frac{v_{AV0}}{R}, \quad (13.32)$$

and the currents of the diodes in the resistance emulator are given by

$$i_{DR1} = \frac{1}{2} \left(I_{OUT} + \frac{v_{AV0}}{nR} \right) \quad (13.33)$$

and

$$i_{DR2} = \frac{1}{2} \left(I_{OUT} - \frac{v_{AV0}}{nR} \right). \quad (13.34)$$

The rectifier remains in this state as long as these currents are positive. Thus, the injected current is determined by

$$i_Y = \begin{cases} nI_{OUT}, & \text{for } v_{AV0} > nRI_{OUT} \\ \frac{v_{AV0}}{R}, & \text{for } |v_{AV0}| < nRI_{OUT} \\ -nI_{OUT}, & \text{for } v_{AV0} < -nRI_{OUT} \end{cases}. \quad (13.35)$$

After the injected current is computed, the input currents are readily determined applying (13.10). Depending on the states of the diodes in the resistance emulator, the output voltage of the rectifier is given by

$$v_{OUT} = \begin{cases} v_{A0} - v_{B0} + nv_{AV0} - n^2 RI_{OUT}, & \text{for } v_{AV0} > nRI_{OUT} \\ v_{A0} - v_{B0}, & \text{for } |v_{AV0}| < nRI_{OUT} \\ v_{A0} - v_{B0} - nv_{AV0} - n^2 RI_{OUT}, & \text{for } v_{AV0} < -nRI_{OUT} \end{cases}. \quad (13.36)$$

Thus, losses in the current injection system also affect the output voltage.

Time intervals during the line period when both of the diodes in the resistance emulator conduct increase with increases of R . Since

$$\max(v_{AV0}) = \frac{1}{4}V_m, \quad (13.37)$$

as shown in Chapter 2, for the current injection system resistance

$$R > \frac{V_m}{4nI_{OUT}} \quad (13.38)$$

the diodes in the resistance emulator are constantly turned on. In this case, voltages across the resistance emulator transformer windings are equal to zero during the whole period, and the resistance emulator does not process any power.

To analyze the influence of the current injection system resistance on the rectifier parameters, it is convenient to define the normalized value of the current injection system resistance as

$$\rho = \frac{RI_{OUT}}{V_m}. \quad (13.39)$$

Introducing this normalization, parameters that characterize the rectifier behavior become dependent solely on ρ . For example, dependence of the minimal value of the input current THD that can be achieved on ρ is depicted in Fig. 13-4. Figure 13-4 is obtained by applying (13.35) to compute i_Y . For each value of ρ , the optimal value of the resistance emulator transformer turns ratio that minimizes the input current THD, $n_{opt}(\rho)$, is determined numerically, and the minimum of the THD that can be achieved in this manner is presented in Fig. 13-4. The optimal values of the transformer turns ratio are given in Fig. 13-5. It can be observed that increases in the current injection system parasitic resistance contribute to the reduction of the THD. The optimal value of the resistance emulator transformer turns ratio is sensitive on the current injection system resistance, and this parameter should be taken into account when designing the transformer. Increased parasitic resistance of the current injection system results in reduced power processed by the resistance emulator. Thus, the volt-ampere rating of the resistance emulator is also reduced.

The power lost on the current injection system resistance reduces the rectifier efficiency. If $n = n_{opt}(\rho)$, the dependence of the rectifier efficiency on ρ is depicted in Fig. 13-6. To analyze tradeoff between the input current THD and the rectifier efficiency, Figs. 13-4 and 13-6 are combined to plot THD as a function of efficiency, which is presented in Fig. 13-7. In Fig. 13-7, it can be observed that the input current THD depends on the rectifier efficiency in almost linear fashion. However, it should be noted that each of the points of the diagram of Fig. 13-7 corresponds to a specific value of ρ , which is defined by (13.39), and depends on the output current. On the other hand, the results obtained for the rectifier without losses apply for the whole range of the output current since the THD of the input currents is independent on the output current in this case.

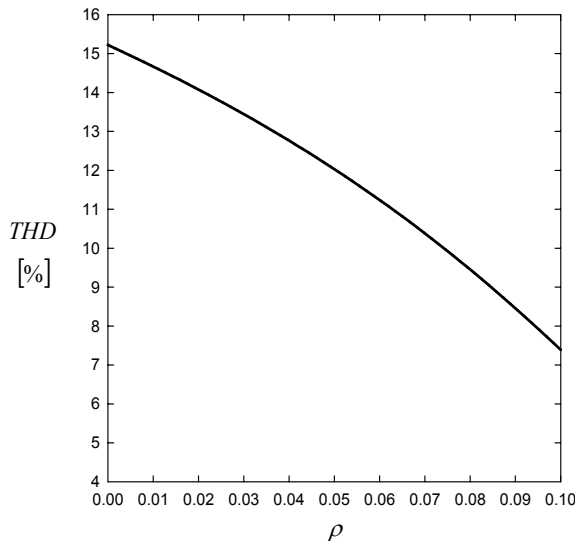


Figure 13-4. Dependence of the input current THD on ρ .

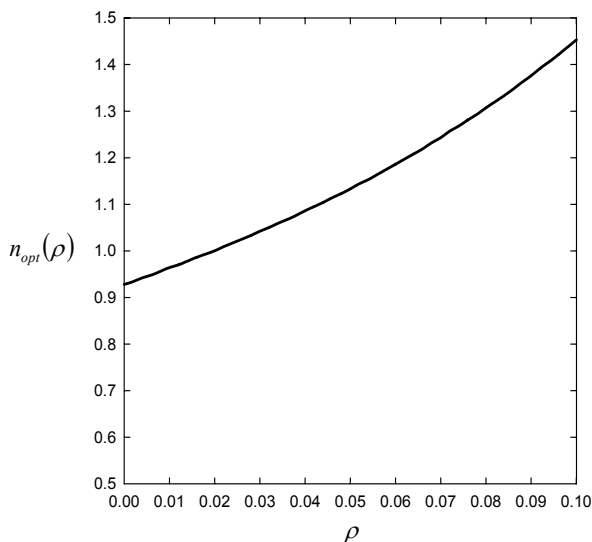


Figure 13-5. Dependence of n_{opt} on ρ .

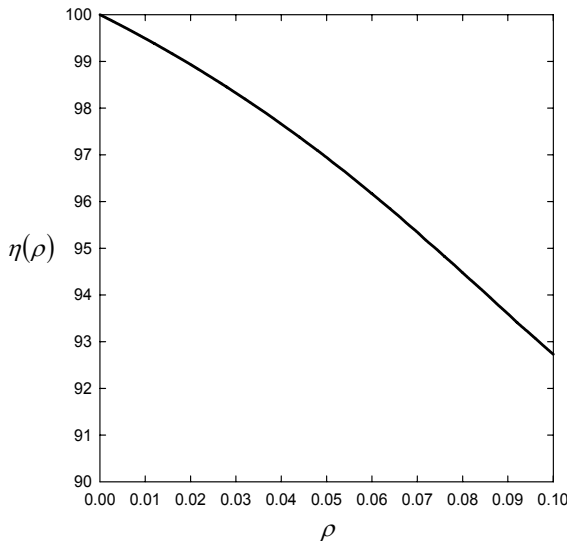


Figure 13-6. Dependence of the rectifier efficiency on ρ .

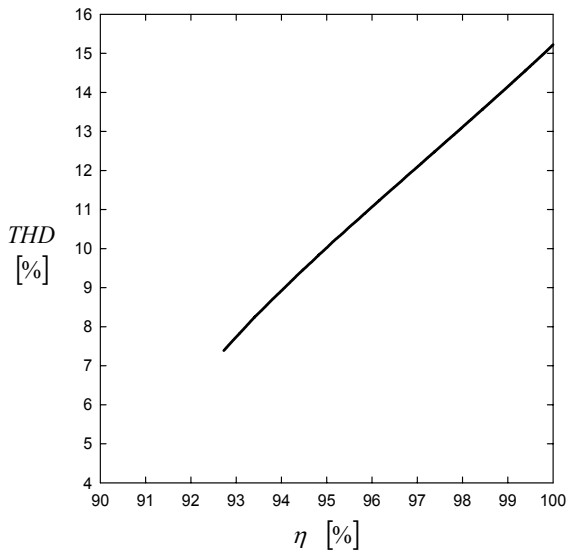


Figure 13-7. Dependence of the input current THD on η .

2. **SQUARE-WAVE CURRENT INJECTION RECTIFIER THAT APPLIES VOLTAGE-LOADED RESISTANCE EMULATOR**

The second circuit topology to be analyzed in this chapter is presented in Fig. 13-8, and it applies voltage-loaded resistance emulator. The circuit is a special case of the circuit analyzed in Chapter 11, obtained omitting the current injection network inductor and increasing the capacitance of the capacitors. Like in the previous rectifier, there are no resonance constraints to be satisfied—the only requirement is that the capacitance of the capacitors is large enough to provide negligible ripple of their voltages in comparison to the output voltage ripple. The rectifier of Fig. 13-8 consists of a three-phase diode bridge, a current injection network, a current injection device, and a voltage-loaded resistance emulator. The current injection network consists of the capacitors and the 1:1 transformer, while the resistance emulator is consisted of the diodes DR1 to DR4 and the 1: n transformer. The current injection device should have low inductance of the neutral point, since the injected current i_y is going to have discontinuities. Thus, constructions with zigzag autotransformer, with two single-phase transformers, and with the delta-wye connected transformer are preferred choices.

To simplify the circuit analysis, the rectifier of Fig. 13-8 is represented by the equivalent circuit in Fig. 13-9. In the equivalent circuit of Fig. 13-9, the three-phase diode bridge is represented by voltage sources v_{A0} and v_{B0} , accompanied by diodes DA and DB to model the three-phase diode bridge discontinuous conduction mode. The transformer and the diodes of the resistance emulator are replaced by their equivalents in the circuit of Fig. 13-9 such that the transformer operation is modeled by a transformer with two secondary windings to reduce the number of diodes. The equivalent circuit of Fig. 13-9 will have the same output voltage and the injected current as the original circuit, but the number of nonlinear elements is reduced from 10 to 4, i.e. the number of possible combinations of nonlinear element states is reduced from 1024 to 16. Resistor R in the circuit of Fig. 13-9 models losses in the current injection system.

2.1 **Analysis of the Rectifier Operation Neglecting Losses**

The analysis presented in this subsection is performed neglecting losses in the current injection system, i.e., assuming $R = 0$. In the case

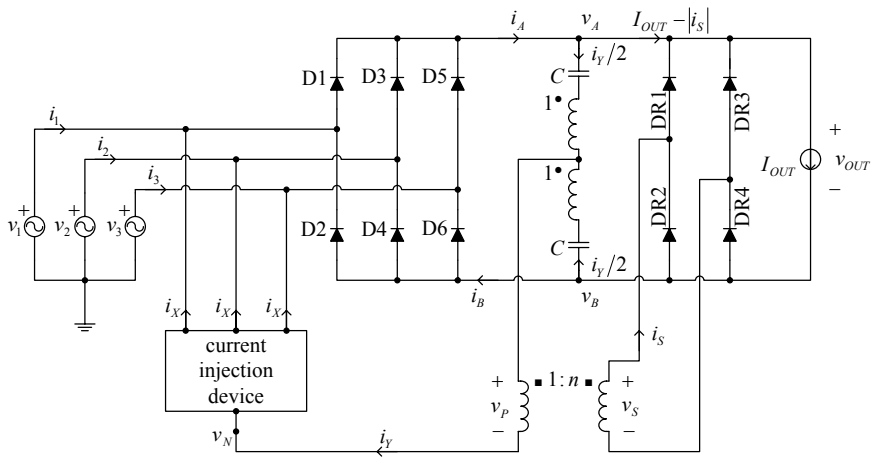


Figure 13-8. Square-wave current injection rectifier with voltage-loaded resistance emulator.

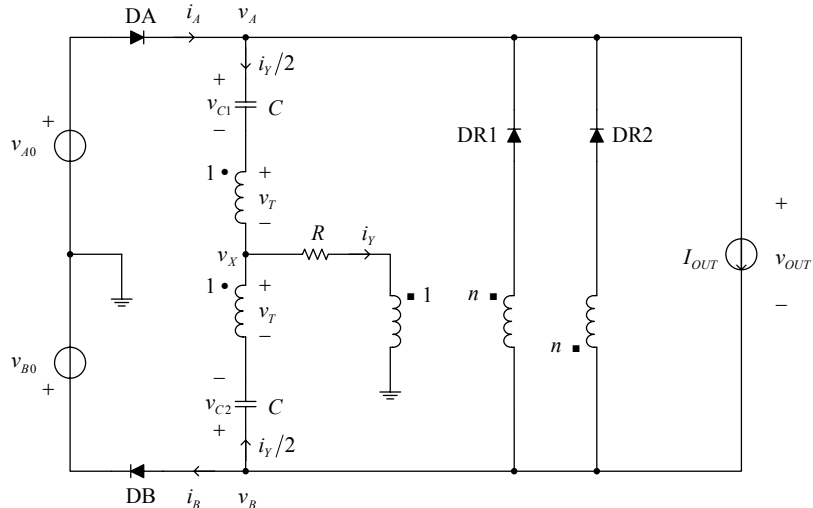


Figure 13-9. Equivalent circuit of the rectifier with current-loaded resistance emulator.

$$-v_{AB0} < nv_{AV0} < v_{AB0}, \quad (13.40)$$

both diodes DR1 and DR2 are reverse biased; thus

$$i_Y = 0. \quad (13.41)$$

In this state, both diodes DA and DB have to conduct, since

$$i_A = I_{OUT} \quad (13.42)$$

and

$$i_B = I_{OUT}. \quad (13.43)$$

The output voltage corresponds to the three-phase diode bridge continuous conduction mode,

$$v_{OUT} = v_{A0} - v_{B0}, \quad (13.44)$$

and the voltage at the primary of the resistance emulator transformer is

$$v_X = v_{AV0}. \quad (13.45)$$

To simplify determination of the phase angle intervals in which the rectifier is in this state, in Fig. 13-10 waveforms of nv_{AV0} , v_{AB0} , and $-v_{AB0}$ are plotted in the same diagram. The diagram is obtained assuming $n=10$, which is close to the optimal value of n , which is going to be determined. Since the maximum of v_{AV0} is $V_m/4$, for

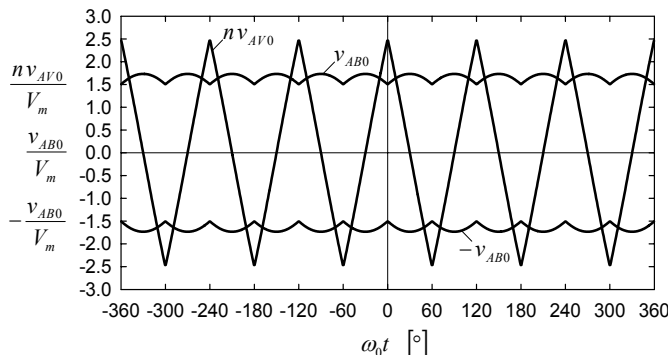


Figure 13-10. Waveforms of nv_{AV0} , v_{AB0} , and $-v_{AB0}$ for $n=10$.

$$n < 6 \quad (13.46)$$

the rectifier is in the described state during the whole period, the injected current is equal to zero, and the rectifier behaves as a common three-phase diode bridge rectifier without the current injection system. Thus, only values $n > 6$ are of interest.

In the remaining part of this subsection, the described state of nonlinear elements in which DA and DB are conducting, while DR1 and DR2 are reverse biased, is referred to as state 1.

If

$$nv_{AV0} > v_{AB0}, \quad (13.47)$$

diode DR1 conducts. This causes the injected current to be positive, $i_Y > 0$; thus DA is going to conduct, resulting in $v_A = v_{A0}$. As a consequence, this would cause DB to be reverse biased, resulting in $i_B = 0$. Thus, according to Kirchhoff's current law for the node with the voltage v_B , i.e., the negative output terminal of the three-phase diode bridge, the injected current is computed as

$$i_Y = \frac{2n}{n+2} I_{OUT} \quad (13.48)$$

in this case. The current that loads positive terminal of the three-phase diode bridge is

$$i_A = I_{OUT} + \frac{i_Y}{2} - \frac{i_Y}{n} = \frac{2n}{n+2} I_{OUT}. \quad (13.49)$$

Assuming

$$v_{C2} = -v_{C1}, \quad (13.50)$$

which is justified by the circuit symmetry and the fact that the capacitor voltages are assumed to be free from ripple, the voltage at the negative output terminal of the diode bridge is obtained as

$$v_B = -\frac{n-2}{n+2} v_{A0}. \quad (13.51)$$

The rectifier remains in this state as long as

$$v_B < v_{B0} , \quad (13.52)$$

and substituting (13.51) this condition is transformed to

$$-\frac{n-2}{n+2}v_{A0} < v_{B0} , \quad (13.53)$$

which is only a different form of (13.47). In this state,

$$v_{OUT} = v_{A0} - v_B = \frac{2n}{n+2}v_{A0} \quad (13.54)$$

and

$$v_X = \frac{v_{OUT}}{n} . \quad (13.55)$$

In the case the boundary condition for this state (expressed by (13.47) or (13.53)) is violated, the rectifier switches to the previously described state 1.

The state of the circuit of Fig. 13-9 in which DA and DR1 conduct, while DB and DR2 are reverse biased, would be referred to as state 2.

If

$$nv_{AV0} < -v_{AB0} , \quad (13.56)$$

diode DR2 conducts. This causes i_Y to be negative, $i_Y < 0$, thus DB is going to conduct, resulting in $v_B = v_{B0}$. This, in turn, causes DA to be reverse biased, resulting in $i_A = 0$. Applying Kirchhoff's current law on the positive output terminal of the diode bridge, i.e., the node with the voltage v_A , the injected current is obtained as

$$i_Y = -\frac{2n}{n-2}I_{OUT} . \quad (13.57)$$

Thus, the current that loads the negative output terminal of the three-phase diode bridge is

$$i_B = \frac{2n}{n-2}I_{OUT} . \quad (13.58)$$

Under the same assumption about the capacitor voltages as in the previous state, the voltage of the positive terminal of the three-phase diode bridge is obtained as

$$v_A = -\frac{n-2}{n+2} v_{B0}. \quad (13.59)$$

The rectifier remains in this state as long as $v_A > v_{A0}$, and substituting (13.59) this becomes

$$-\frac{n-2}{n+2} v_{B0} > v_{A0}, \quad (13.60)$$

which is equivalent to (13.56). In this state,

$$v_{OUT} = v_A - v_{B0} = -\frac{2n}{n+2} v_{B0} \quad (13.61)$$

and

$$v_X = -\frac{v_{OUT}}{n}. \quad (13.62)$$

If the boundary condition for this state (expressed by (13.56) or (13.60)) is violated, the rectifier switches to the previously described state 1.

The state of the circuit of Fig. 13-9 in which DB and DR2 conduct, while DA and DR1 are reverse biased, would be referred to as state 3.

States of the diodes and the boundary conditions are summarized for all three states in Table 13-1. The state of the circuit is determined by mutual relation of nv_{AV0} and v_{AB0} . If a boundary condition for state 1 is violated, the circuit can switch to state 2 or to state 3, depending on the boundary condition violated. However, from states 2 and 3 the circuit can switch only to state 1, and direct transition between states 2 and 3 is not possible. In Table 13-2, expressions for i_Y , v_A , v_B , and v_{OUT} are summarized for all three network states. These equations form the rectifier model, which consists only of algebraic equations, since all differential equations are avoided assuming that voltages of the capacitors are constant in time without any ripple, and neglecting magnetizing currents of the transformers.

After the circuit in Fig. 13-9 is analyzed, waveforms of i_Y , v_A , v_B , and v_{OUT} are determined. Waveforms of the input currents are determined from the circuit of Fig. 13-8 as

Table 13-1. States of the rectifier and boundary conditions.

State	DA	DB	DR1	DR2	Condition 1	Condition 2
1	1	1	0	0	$-v_{AB0} < nv_{AV0}$	$nv_{AV0} < v_{AB0}$
2	1	0	1	0	$v_{AB0} < nv_{AV0}$	
3	0	1	0	1	$nv_{AV0} < -v_{AB0}$	

Table 13-2. Expressions for i_Y , v_A , v_B , and v_{OUT} .

State	i_Y	v_A	v_B	v_{OUT}
1	0	v_{A0}	v_{B0}	v_{AB0}
2	$\frac{2n}{n+2} I_{OUT}$	v_{A0}	$-\frac{n-2}{n+2} v_{A0}$	$\frac{2n}{n+2} v_{A0}$
3	$-\frac{2n}{n+2} I_{OUT}$	$-\frac{n-2}{n+2} v_{B0}$	v_{B0}	$-\frac{2n}{n+2} v_{B0}$

$$i_p = i_A d_{2p-1} - i_B d_{2p} - \frac{1}{3} i_Y \quad (13.63)$$

for $p \in \{1, 2, 3\}$, where the diode state functions d_{2p-1} and d_{2p} are defined in Chapter 2. Typical waveforms of i_l and i_Y are presented in the first two diagrams of Fig. 13-11. The absolute value of the resistance emulator transformer secondary current, $|i_S|$, which is the output current of the resistance emulator, is presented in the third diagram of Fig. 13-11. By this current, the power taken by the current injection network is restored at the rectifier output applying resistance emulator. The last diagram of Fig. 13-11 presents the output voltage, accompanied by the waveform of v_{AB0} plotted with a thin line.

To express the waveforms of the input currents in analytic form, phase angles when the circuit of Fig. 13-9 changes its state are of particular interest. These phase angles are determined by intersections of the waveforms presented in Fig. 13-10. Let us determine the phase angle when the first intersection of v_{AB0} and v_{AV0} for $\omega_0 t > 0$ occurs. Since the values of interest for the resistance emulator transformer turns ratio are located in $6 < n < \infty$, the phase angle to be determined is located in

$$0 < \varphi < \frac{\pi}{6}, \quad (13.64)$$

and φ is formally defined by

$$v_{AV0}(\varphi) = \frac{1}{n} v_{AB0}(\varphi). \quad (13.65)$$

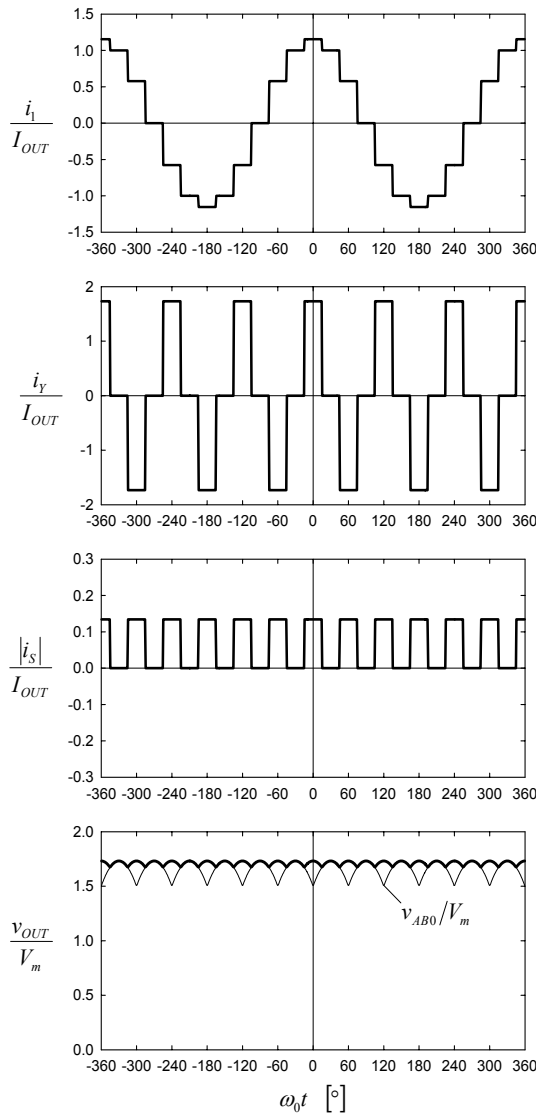


Figure 13-11. Waveforms of i_l , i_Y , v_{REC} , and v_{OUT} .

Substituting expressions for v_{AV0} and v_{AB0} in (13.65), it is transformed to

$$\frac{1}{2} \left(\cos(\varphi) + \cos\left(\varphi - \frac{4\pi}{3}\right) \right) = \frac{1}{n} \left(\cos(\varphi) - \cos\left(\varphi - \frac{4\pi}{3}\right) \right). \quad (13.66)$$

This equation relates phase angle φ to the resistance emulator transformer turns ratio n as

$$n = 2\sqrt{3} \frac{\sqrt{3} + \tan \varphi}{1 - \sqrt{3} \tan \varphi} \quad (13.67)$$

or

$$\tan \varphi = \frac{1}{\sqrt{3}} \frac{n-6}{n+2}. \quad (13.68)$$

Applying symmetries in Fig. 13-10, all phase angles where the state changes occur could be expressed as functions of φ , thus the waveform of the injected current i_Y during the phase interval $0 < \omega_0 t < \pi/2$ is expressed as

$$i_Y(\omega_0 t) = \begin{cases} \frac{2n}{n+2} I_{OUT}, & \text{for } 0 < \omega_0 t < \varphi \\ 0, & \text{for } \varphi < \omega_0 t < \frac{\pi}{3} - \varphi \\ -\frac{2n}{n+2} I_{OUT}, & \text{for } \frac{\pi}{3} - \varphi < \omega_0 t < \frac{\pi}{3} + \varphi \\ 0, & \text{for } \frac{\pi}{3} + \varphi < \omega_0 t < \frac{\pi}{2}. \end{cases} \quad (13.69)$$

This results in the waveform of the input current of the first phase given on the phase interval $0 < \omega_0 t < \pi/2$ by

$$i_I(\omega_0 t) = \begin{cases} \frac{4n}{3(n+2)} I_{OUT}, & \text{for } 0 < \omega_0 t < \varphi \\ I_{OUT}, & \text{for } \varphi < \omega_0 t < \frac{\pi}{3} - \varphi \\ \frac{2n}{3(n+2)} I_{OUT}, & \text{for } \frac{\pi}{3} - \varphi < \omega_0 t < \frac{\pi}{3} + \varphi \\ 0, & \text{for } \frac{\pi}{3} + \varphi < \omega_0 t < \frac{\pi}{2}, \end{cases} \quad (13.70)$$

which is computed according to (13.63). The phase interval $0 < \omega_0 t < \pi/2$ is chosen because it is sufficient to determine the input current THD applying symmetry properties of the waveform. Analyzing the waveform of the input current of the first phase specified by (13.70), its RMS value is obtained as

$$I_{RMS} = I_{OUT} \sqrt{\frac{2}{3} + \frac{4}{3} \frac{n^2 - 12n - 12}{(n+2)^2} \frac{\varphi}{\pi}}, \quad (13.71)$$

while the RMS value of its fundamental harmonic is

$$I_{1RMS} = I_{OUT} \frac{\sqrt{2}}{\pi} \left(\sqrt{3} \cos \varphi + \frac{n-6}{n+2} \sin \varphi \right). \quad (13.72)$$

Applying (13.68), the sine and cosine of φ in (13.72) are expressed in terms of n as

$$\cos \varphi = \frac{\sqrt{3}}{2} \frac{n+2}{\sqrt{n^2 + 12}} \quad (13.73)$$

and

$$\sin \varphi = \frac{n-6}{2\sqrt{n^2 + 12}}. \quad (13.74)$$

Substituting (13.73) and (13.74) in (13.72), the RMS value of the input current fundamental harmonic is obtained as a function of n as

$$I_{1RMS} = I_{OUT} \frac{2\sqrt{2}}{\pi} \frac{\sqrt{n^2 + 12}}{n+2}. \quad (13.75)$$

The THD of the input current is defined by

$$THD = \frac{\sqrt{I_{RMS}^2 - I_{1RMS}^2}}{I_{1RMS}} = \sqrt{\frac{I_{RMS}^2}{I_{1RMS}^2} - 1}, \quad (13.76)$$

and the goal is to determine the transformer turns ratio that minimizes the THD. Since the expressions for I_{RMS} and I_{1RMS} are bulky, applying the fact that the square root is a monotonous function, it is sufficient to minimize

$$f(n) = \frac{I_{RMS}^2}{I_{1RMS}^2}. \quad (13.77)$$

The minimum is reached for

$$\frac{d f(n)}{dn} = 0, \quad (13.78)$$

which results in

$$\arctan \frac{n-6}{\sqrt{3}(n+2)} = \frac{(\pi - \sqrt{3})n^2 + 4(3\sqrt{3} - \pi)n + 12(\sqrt{3} - \pi)}{6(n+6)(n-2)}. \quad (13.79)$$

The equation of (13.79) has a closed-form solution

$$n_{OPT} = 6 + 4\sqrt{3} \approx 12.93, \quad (13.80)$$

which is the optimal value of the resistance emulator transformer turns ratio that minimizes the input current THD. Waveforms of the diagrams presented in Fig. 13-11 are obtained for $n = n_{OPT}$. In this case, the phase angle that determines the state transition instants is

$$\varphi_{OPT} = \frac{\pi}{12}, \quad (13.81)$$

while the input current RMS value is

$$I_{RMS} = \frac{\sqrt{6}}{\pi} I_{OUT}, \quad (13.82)$$

and its fundamental harmonic is

$$I_{1RMS} = \frac{6 - 2\sqrt{3}}{\pi} I_{OUT}. \quad (13.83)$$

The value of the input current THD that corresponds to $n = n_{OPT}$ is

$$THD_{min} = THD(n_{OPT}) = \frac{\sqrt{(2 + \sqrt{3})\pi^2 - 36}}{6} \approx 15.22\%, \quad (13.84)$$

which is the same distortion as given by (13.16) for the rectifier that applies current-loaded resistance emulator. It should be noted that the input current waveforms presented in the first diagrams of Figs. 13-3 and 13-11 are

different, but they have the same THD. Detailed analysis of the waveforms shows that they have the same normalized amplitude spectra, while their phase spectra are different. This results in the same THD values that are determined solely by the amplitude spectra, and different waveforms that are affected both by the amplitude and the phase spectra. The THD value of (13.84) is the same as achieved by classic twelve-pulse rectifiers.

The waveform of the rectifier output voltage is presented in the fourth diagram of Fig. 13-11, accompanied by the waveform of the v_{AB0} . Fourier series expansion of the output voltage waveform is given by

$$v_{OUT} = V_m \frac{9\sqrt{2} - 3\sqrt{6}}{\pi} \left(1 - 2 \sum_{k=1}^{+\infty} \frac{(-1)^k}{144k^2 - 1} \cos(12k\omega_0 t) \right), \quad (13.85)$$

and its DC component is

$$V_{OUT} = \frac{9\sqrt{2} - 3\sqrt{6}}{\pi} V_m \approx 1.71 V_m. \quad (13.86)$$

The DC component of the output voltage is somewhat lower than the output voltage of the rectifier that applies current-loaded resistance emulator, given by (13.20). This is expected, given the waveforms of the output voltages presented in Figs. 13-3 and 13-11.

The rectifier output power is obtained as a product of the output voltage DC component and the output current,

$$P_{OUT} = \frac{9\sqrt{2} - 3\sqrt{6}}{\pi} V_m I_{OUT}. \quad (13.87)$$

The power taken by the current injection network from the three-phase diode bridge output terminals is

$$P_{INJ} = \frac{2 - \sqrt{3}}{4} P_{OUT} \approx 6.70\% P_{OUT}, \quad (13.88)$$

which is the same as in the case the current-loaded resistance emulator is applied. Again, the result is lower than in cases of the sinusoidal and the optimal current injection.

If $n = n_{OPT}$, the RMS value of the injected current is obtained as

$$I_{Y\text{ RMS}} = I_{OUT} \sqrt{\frac{3}{2}} \approx 1.22 I_{OUT}, \quad (13.89)$$

applying (13.69), and this value is used to compute the volt-ampere ratings of the magnetic components.

Analyzing the waveform of the voltage across the windings of the current injection network transformer, i.e., the transformer with the turns ratio 1:1, and applying (13.89) to compute the RMS value of the currents of the windings, its volt-ampere rating is obtained as

$$\begin{aligned} S_{T\text{ 1:1}} &= \left(\frac{\sqrt{3}}{8} \arcsin \frac{3\sqrt{2}(\sqrt{3}-1)}{\pi} + \frac{3+\sqrt{3}}{48\sqrt{2}} \sqrt{\pi^2 + 36\sqrt{3} - 72} - \frac{2\pi\sqrt{3}}{32} \right) P_{OUT} \\ &\approx 0.025\% P_{OUT}. \end{aligned} \quad (13.90)$$

This is significantly lower than in all of the rectifiers previously analyzed. This result is caused by the significantly reduced value of the flux linkage of the transformer windings, since the voltage applied across the windings is periodic with one twelfth of the line period in comparison to one sixth of the line period in previously analyzed rectifiers, as well as the voltage amplitude being reduced. However, overall savings are not significant since the transformer already had a small volt-ampere rating.

The volt-ampere rating of the resistance emulator transformer is computed as

$$S_{T\text{ 1:n}} = \frac{\pi\sqrt{2}}{48} (1 + \sqrt{3} - \sqrt{6}) P_{OUT} \approx 2.62\% P_{OUT}, \quad (13.91)$$

which is slightly lower than in the case of the current-loaded resistance emulator.

Like in the case of the rectifier that applies current-loaded resistance emulator, due to the discontinuities in the waveform of the injected current, a current injection device with low inductance of the neutral point is required. In the case the current injection device is realized as a zigzag auto-transformer, its volt-ampere rating is

$$S_{CID} = \frac{1}{2} V_m I_{OUT} = \frac{\pi}{18\sqrt{2} - 6\sqrt{6}} P_{OUT} \approx 29.20\% P_{OUT}, \quad (13.92)$$

which is higher than in the case the current-loaded resistance emulator is applied, due to the increased RMS value of the injected current. In the case the wye-wye transformer is applied at the rectifier input, its volt-ampere rating would be

$$S_{YY} = \frac{\sqrt{3}(2+\sqrt{5})}{4} V_m I_{OUT} = \frac{\pi\sqrt{3}(2+\sqrt{5})}{36\sqrt{2}-12\sqrt{6}} P_{OUT} \approx 107.12\% P_{OUT}, \quad (13.93)$$

again slightly higher than in the case of the rectifier that applies current-loaded resistance emulator. Finally, in the case the delta-wye transformer is applied, its volt-ampere would be

$$S_{DY} = \frac{\sqrt{15}}{2} V_m I_{OUT} = \frac{\pi\sqrt{15}}{18\sqrt{2}-6\sqrt{6}} P_{OUT} \approx 113.09\% P_{OUT}. \quad (13.94)$$

Application of the delta-wye transformer is a better choice than the wye-wye transformer because it provides negligible inductance of the secondary neutral point, as well as negligible stray flux.

2.2 Analysis of the Rectifier Taking Losses into Account

To analyze the effects caused by the losses in the current injection system, the equivalent circuit of Fig. 13-9 will be analyzed. The goal of that analysis will be to determine the waveforms of i_Y , v_A , and v_B . Currents that load the three-phase diode bridge output terminals, i_A and i_B , are regardless of the network state determined by

$$i_A = I_{OUT} + \frac{i_Y}{2} - \frac{|i_Y|}{n} \quad (13.95)$$

and

$$i_B = I_{OUT} - \frac{i_Y}{2} - \frac{|i_Y|}{n}, \quad (13.96)$$

which is obtained analyzing the circuit of Fig. 13-8. After these waveforms are determined, waveforms of the input currents are obtained applying

$$i_p = i_A d_{2p-1} - i_B d_{2p} - \frac{1}{3} i_Y, \quad (13.97)$$

for $p \in \{1, 2, 3\}$, where the diode state functions d_{2p-1} and d_{2p} are defined in Chapter 2.

Regardless of the network state, assumption $v_{C1} = -v_{C2}$ yields

$$v_A - v_X = v_X - v_B, \quad (13.98)$$

thus voltage v_X is obtained as

$$v_X = \frac{v_A + v_B}{2}. \quad (13.99)$$

Also, the rectifier output voltage is regardless of the network state defined by

$$v_{OUT} = v_A - v_B. \quad (13.100)$$

Thus, by (13.95) to (13.99) all relevant rectifier waveforms are related to i_Y , v_A , and v_B , and these waveforms are going to be determined analyzing the circuit of Fig. 13-9.

Since one of the conclusions of the analysis of the rectifier without losses is that states of the rectifier nonlinear elements are determined comparing nv_{AV0} to $\pm v_{AB0}$, the analysis of the rectifier with losses will be started assuming the same control variables. For

$$-v_{AB0} < nv_{AV0} < v_{AB0} \quad (13.101)$$

the three-phase diode bridge is in the continuous conduction mode, and diodes DR1 and DR2 do not conduct. This state is equivalent to state 1 of the rectifier without losses, and it is characterized by the same equations. This is caused by $i_Y = 0$, thus there is no voltage drop on R , and its existence cannot be observed. This state is defined as state 1 in Table 13-3, and conditions that bound this state are summarized there. Equations that define i_Y , v_A , and v_B are summarized in Table 13-4.

In the case the second of the conditions for state 1 is violated, i.e.,

$$nv_{AV0} > v_{AB0}, \quad (13.102)$$

diode DR1 starts to conduct. However, in contrast to the case the rectifier had no losses, this does not cause immediate turn-off of diode DB. Thus, there is a state where DA, DB, and DR1 are conducting simultaneously. This state will be referred to as state 2, and in this state $v_X = v_{AV0}$, according to (13.99), since $v_A = v_{A0}$ and $v_B = v_{B0}$. Thus, the injected current is

$$i_Y = \frac{1}{R} \left(v_{AV0} - \frac{v_{AB0}}{n} \right). \quad (13.103)$$

The rectifier remains in this state as long as $i_B > 0$, and this condition can be rephrased to

$$v_{AV0} < \frac{v_{AB0}}{n} + \frac{2n}{n+2} RI_{OUT}, \quad (13.104)$$

applying (13.96) and (13.103). Equations that define this state are summarized in Tables 13-3 and 13-4.

In the case the boundary condition of (13.104) is violated, DB turns off, and the rectifier switches to state 4. This state is the equivalent of state 2 of the rectifier without losses. In this state

$$i_Y = \frac{2n}{n+2} I_{OUT}, \quad (13.105)$$

which is obtained in the same manner as for the rectifier without losses, applying Kirchhoff's current law. Voltage v_X in this state is determined by

$$v_X = \frac{v_{OUT}}{n} + \frac{2n}{n+2} RI_{OUT}, \quad (13.106)$$

resulting in

$$v_B = -\frac{n-2}{n+2} v_{A0} + \left(\frac{2n}{n+2} \right)^2 RI_{OUT}, \quad (13.107)$$

since $v_A = v_{A0}$ because DA is conducting. The rectifier remains in this state as long as $v_B < v_{B0}$, which can be rephrased to

$$\frac{v_{AB0}}{n} + \frac{2n}{n+2} RI_{OUT} < v_{AV0}. \quad (13.108)$$

Again, the equations that describe this state are summarized in Tables 13-3 and 13-4.

State 3 is characterized by conducting of DA, DB, and DR2, and it is symmetric to state 2. These two states are new, and they are initiated by the nonzero value for R . In this state, the injected current is given by

Table 13-3. States of the rectifier and boundary conditions.

State	DA	DB	DR1	DR2	Condition 1	Condition 2
1	1	1	0	0	$-\frac{v_{AB0}}{n} < v_{AV0}$	$v_{AV0} < \frac{v_{AB0}}{n}$
2	1	1	1	0	$\frac{v_{AB0}}{n} < v_{AV0}$	$v_{AV0} < \frac{v_{AB0}}{n} + \frac{2n}{n+2} RI_{OUT}$
3	1	1	0	1	$v_{AV0} < -\frac{v_{AB0}}{n}$	$-\frac{v_{AB0}}{n} - \frac{2n}{n+2} RI_{OUT} < v_{AV0}$
4	1	0	1	0	$\frac{v_{AB0}}{n} + \frac{2n}{n+2} RI_{OUT} < v_{AV0}$	
5	0	1	0	1	$v_{AV0} < -\frac{v_{AB0}}{n} - \frac{2n}{n+2} RI_{OUT}$	

Table 13-4. Expressions for i_Y , v_A , and v_B .

State	i_Y	v_A	v_B
1	0	v_{A0}	v_{B0}
2	$\frac{1}{R} \left(v_{AV0} - \frac{v_{AB0}}{n} \right)$	v_{A0}	v_{B0}
3	$\frac{1}{R} \left(v_{AV0} + \frac{v_{AB0}}{n} \right)$	v_{A0}	v_{B0}
4	$\frac{2n}{n+2} I_{OUT}$	v_{A0}	$-\frac{n-2}{n+2} v_{A0} + \left(\frac{2n}{n+2} \right)^2 RI_{OUT}$
5	$-\frac{2n}{n+2} I_{OUT}$	$-\frac{n-2}{n+2} v_{B0} - \left(\frac{2n}{n+2} \right)^2 RI_{OUT}$	v_{B0}

$$i_Y = \frac{1}{R} \left(v_{AV0} + \frac{v_{AB0}}{n} \right), \quad (13.109)$$

while $v_A = v_{A0}$ and $v_B = v_{B0}$, since DA and DB are conducting. The rectifier remains in this state as long as $i_A > 0$, and this condition could be rephrased to

$$-\frac{v_{AB0}}{n} - \frac{2n}{n+2} RI_{OUT} < v_{AV0}, \quad (13.110)$$

applying (13.95) and (13.109). The equations for this state are given in Tables 13-3 and 13-4.

Finally, the rectifier switches to state 5 if the condition of (13.110) is violated, since diode DA turns off then. This state corresponds to state 3 of the rectifier without losses, and it is symmetric to state 4 of the rectifier with

losses. In this state, the injected current is computed by applying Kirchhoff's current law, in the same manner as for state 4, and is given by

$$i_Y = -\frac{2n}{n+2} I_{OUT}. \quad (13.111)$$

This results in

$$v_X = -\frac{v_{OUT}}{n} - \frac{2n}{n+2} RI_{OUT}. \quad (13.112)$$

Since $v_B = v_{B0}$, the voltage of the three-phase diode bridge positive output terminal is

$$v_A = -\frac{n-2}{n+2} v_{B0} - \left(\frac{2n}{n+2} \right)^2 RI_{OUT}. \quad (13.113)$$

The rectifier remains in this state as long as $v_A > v_{A0}$, which is rephrased to

$$v_{AV0} < -\frac{v_{AB0}}{n} - \frac{2n}{n+2} RI_{OUT}, \quad (13.114)$$

applying (13.113). Again, the equations that describe this state are summarized in Tables 13-3 and 13-4.

Equations summarized in Tables 13-3 and 13-4, accompanied by the equations (13.95)-(13.97), (13.99), and (13.100), constitute the model of the rectifier with losses. Like in the case of the rectifier without losses, the rectifier state is determined by comparing the value of v_{AV0} to time dependent thresholds, and all of the rectifier waveforms are computed algebraically, without solving any differential equations. Thus, it is not difficult to compute the rectifier waveforms numerically and to perform necessary optimizations.

Like in the case of the rectifier that applies current-loaded resistance emulator, optimization of the transformer turns ratio is performed to minimize the input current THD in the presence of losses. To apply numerical methods, normalization is performed and all of the rectifier parameters are shown to be dependent only on normalized parasitic resistance of the current injection system, defined as

$$\rho = \frac{RI_{OUT}}{V_m}. \quad (13.115)$$

Applying a brute force numerical method, the optimization is performed and in Fig. 13-12, dependence of the minimal value of the input current THD on ρ is presented. The values of THD plotted in Fig. 13-12 correspond to the optimal values of the resistance emulator transformer turns ratio, $n_{opt}(\rho)$, plotted in Fig. 13-13. From Figs. 13-12 and 13-13 it can be concluded that the parasitic resistance of the current injection system contributes to reduction of the input current THD, and that it significantly affects the optimal value of the resistance emulator transformer turns ratio. Besides these effects, the parasitic resistance reduces the power processed by the resistance emulator, and thus affects the volt-ampere rating of the resistance emulator transformer.

Losses in the current injection system affect the rectifier efficiency. For $n = n_{opt}(\rho)$, the rectifier efficiency is plotted as a function of ρ in Fig. 13-14. As expected, the efficiency is reduced by increases of ρ .

To analyze the tradeoff between the input current THD and the rectifier efficiency, Figs. 13-12 and 13-14 are combined in Fig. 13-15, providing the input current THD plotted as a function of the rectifier efficiency. Figure 13-15 is similar to Fig. 13-7 that applies for the rectifier with current-loaded resistance emulator, but the rectifier that applies a voltage-loaded resistance emulator provided lower values of the input current THD with the same efficiency.

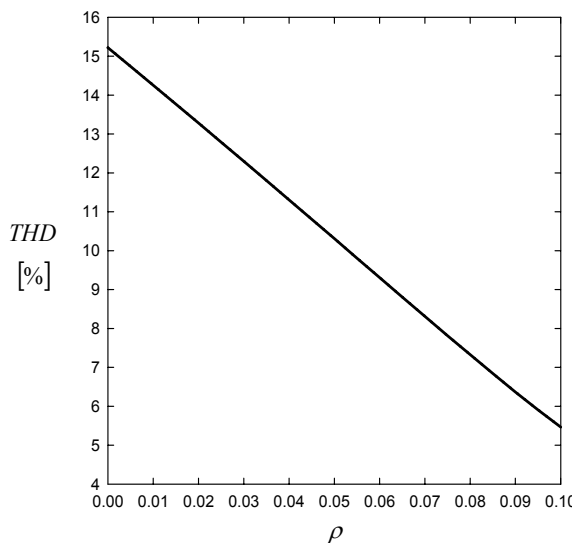


Figure 13-12. Dependence of the input current THD on ρ .

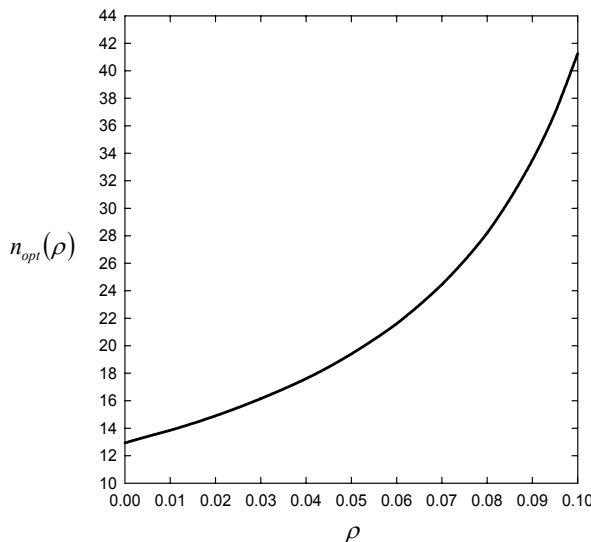


Figure 13-13. Dependence of n_{opt} on ρ .

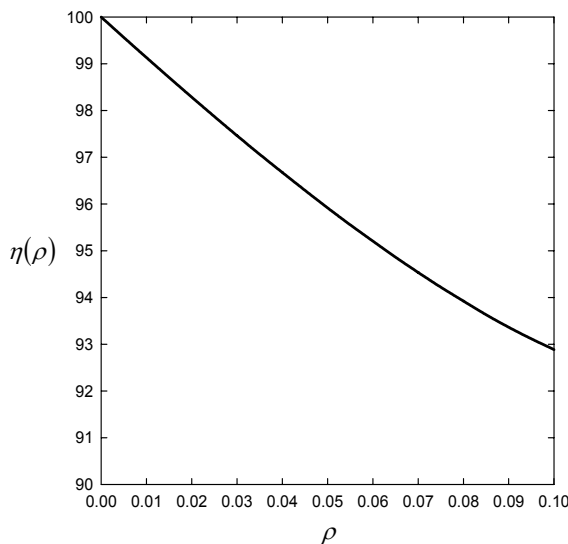


Figure 13-14. Dependence of the rectifier efficiency on ρ .

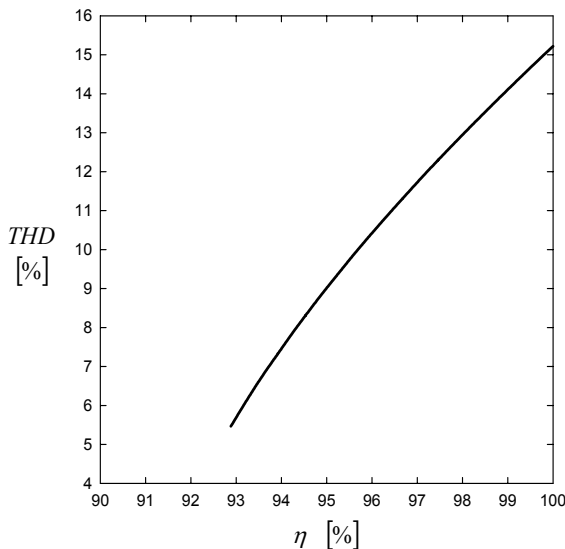


Figure 13-15. Dependence of the input current THD on η .

Chapter 14

CONCLUSIONS

In this book, three-phase rectifiers that provide low harmonic distortions of the input currents applying current injection principle are analyzed. Three types of current injection are analyzed and compared: the third-harmonic sinusoidal current injection, the optimal current injection, and the square-wave current injection. The book focuses on the rectifiers that do not apply high-frequency switching. Instead, the rectifiers that provide current injection applying passive elements are analyzed. Results provided in references [7], [10], [11], and [24]–[40] related to the defined scope of the book are systematized and presented, as well as some new results that have not been published previously.

Chapter 2 presents basic results regarding three-phase diode bridge rectifiers. These results include spectra of the output terminal voltages, spectrum of the output voltage, and definitions of the diode state functions, which are the basic tools for the analyses that follow. Waveforms of the input currents are presented, and their total harmonic distortion (THD) values are computed. Notches in the rectifier input voltages caused by discontinuities in the input currents and parasitic inductances of the supply lines are illustrated for experimental results.

Current injection principles are presented in Chapter 3, where a current injection system consisting of a current injection network and a current injection device is introduced. Basic ideas behind the method are discussed. It is shown that the injected currents should contain spectral components at triples of the line frequency only, in order to provide the same waveforms of the input currents at all three of the phases, with the same amplitude spectra, but mutually shifted in phase for one third of the line period. A common misunderstanding that the third-harmonic current injection is a sort of compensation for the third-harmonic component in the input currents is clarified. It is clearly stated that spectral components at triples of the line frequency did not exist in the input currents before the current injection was applied, nor do they exist after the current injection is applied, since the system considered is a balanced three-wire system. The path where the harmonic currents at odd triples of the line frequency flow is shown, as well as how they affect the input current waveforms.

In Chapter 4, magnetic current injection devices are analyzed in detail, which provides information not available in the references. Volt-ampere rating of a magnetic device is defined, extending the volt-ampere concept of [9]. This quantity is used as a measure to compare various constructions of the current injection devices. Various current injection devices are presented, and their performance compared. According to the results in Chapter 4, it can be concluded that in most applications it would be best to apply a current injection device based on a zigzag autotransformer. In Section 4.6, a novel magnetic device that integrates the current injection device and the inductor of the current injection network is proposed. This result has not been previously published. Application of a three-phase wye-wye connected transformer to adjust the voltage level and to provide current injection, as it is utilized in [13] and [15], is discussed next. Issues regarding the volt-ampere rating are clarified, and it is shown that the transformer can provide the current injection with negligible increase of the volt-ampere rating. Application of a delta-wye connected transformer in the same purpose is discussed in Section 4.8. This transformer arrangement provides a voltage level adjustment, current injection, and negligible inductance of the neutral point, with a minor increase in the device volt-ampere rating.

The third-harmonic current injection is discussed in Chapter 5. Theoretical study of the third-harmonic current injection, in which the amplitude and the phase of the injected current are optimized in order to minimize the input current THD, is presented. It is shown that the input current THD can be improved only at the cost of the power taken by the current injection network. Improvement of the input current THD is related to the power taken by the current injection network, and it is shown that in the case of the optimal third-harmonic current injection the input current THD equals 5.12%, while the power taken by the current injection network equals 8.57% of the input power.

Constructions of the current injection networks are discussed in Chapter 6, where the current injection networks proposed in [12] and [13] are compared. It is shown that these current injection networks behave in the same way at odd triples of the line frequency, while their different overall behavior is caused by their different behavior at even triples of the line frequency. After the harmonics at even triples of the line frequency are identified as the reason that the current injection network proposed in [13] provides lower THD values than the current injection network proposed in [12], a novel current injection network is proposed. The novel current injection network, originally proposed in [30], is analyzed in detail, and it is shown that it provides the lowest THD values of the input currents, with low dependence on the current injection network Q -factor. The case when the current injection network Q -factor approaches zero is separately analyzed,

showing that the lowest input current THD is obtained here. The last of the current injection networks analyzed in Chapter 6 is utilized in all of subsequently analyzed rectifiers that apply the third-harmonic current injection.

The optimal current injection, the topic of Chapter 7, provides ideal sinusoidal waveforms of the input currents, and it relies on injection of the currents containing spectral components at triples of the line frequency, i.e., the injected current is enriched by higher order harmonics. Basic principles of the optimal current injection are presented in Chapter 7. Waveforms of the diode bridge load currents that provide the optimal current injection are derived, as well as the requirements imposed to the current injection network in order to provide the optimal current injection.

In Chapter 8, current injection networks that provide the optimal current injection are presented. This chapter presents systematized and expanded results of [26] and [35]. Several current injection networks are analyzed, all of them being built applying capacitors, resistors or resistance emulators, and transformers, without any need for inductors. The influence of finite capacitance of the capacitors on the input current THD is analyzed, as well as the influence of the output current ripple.

Chapter 9 is somewhat specific, and it presents the analysis of the discontinuous conduction mode in three-phase diode bridge rectifiers. The problem is mathematically complex, and requires application of numerical methods to be solved. A piecewise linear state-space model of the rectifier is developed, normalization of variables is applied to generalize the results, and special mathematical techniques proposed in [51] are applied to solve the problem numerically. It is shown that the rectifier discontinuous conduction mode might be of practical interest, since it provides acceptable values of the input current THD and high efficiency applying simple and robust circuitry. Dependence of the input current THD, the rectifier efficiency, and the output voltage on various of the rectifier parameters is analyzed.

Application of a current-loaded resistance emulator to recover the power taken by the current injection network is the topic of Chapter 10. The current-loaded passive resistance emulator is described, and it is shown that it provides automatic adjustment of the injected current amplitude to the load current. Choice of the rectifier parameters is discussed. A novel simulation method to analyze dependence of the input current THD on the load current, caused by the higher order harmonics of the injected current, is presented in Section 10.3. This method has not been presented before.

Chapter 11 presents a completely new rectifier that applies voltage-loaded resistance emulator. This rectifier is presented in this book for the first time. The rectifier is simple, requires only one resonant circuit, and a small number of other components that are exposed to relatively low voltage

and current stress. Operation of the rectifier is analyzed in the continuous and the discontinuous conduction modes, and optimization of the rectifier parameters to minimize the input current THD is performed in both of the operating modes. Although adjustment of the injected current amplitude to the load current is not as straightforward as it is in the rectifier presented in Chapter 10, even better results are experimentally obtained.

The switching current injection device is analyzed in Chapter 12. The concepts developed for the rectifiers that apply magnetic current injection devices are adjusted to the switching current injection device. It is shown that application of the switching current injection device provides an attractive opportunity to obtain the same results as obtained applying magnetic current injection devices, but with three times lower amplitude of the injected current and three times lower volt-ampere ratings of the magnetic devices applied in the current injection network. Design of the current injection networks intended for application with the switching current injection device is discussed; one current injection network for the third-harmonic current injection, and two current injection networks for the optimal current injection are proposed. Dependence of the input current THD on various parasitic effects is analyzed. It is shown that operation of the rectifier that applies switching current injection device in the discontinuous conduction mode results in unacceptably high values of the input current THD. This restricted application of the resistance emulators to the current-loaded resistance emulator.

The rectifiers that apply square-wave current injection are analyzed in Chapter 13. In the first part of Chapter 13, the rectifier proposed in [14] is subjected to detailed analysis. It is shown that this rectifier can be treated as a special case of the rectifier analyzed in Chapter 10, which applies the third-harmonic current injection and current-loaded passive resistance emulator. Thus, it was natural to analyze the same special case in the rectifier proposed in Chapter 11, which applies a voltage-loaded resistance emulator. This is the second rectifier analyzed in Chapter 13, and it has not been published before. The rectifier provides the same THD of the input currents as the rectifier proposed in [14], with some differences in regard to realization and sensitivity to losses in the current injection system.

REFERENCES

1. A. Ametani, "Generalised Method of Harmonic Reduction in A.C.-D.C. Convertors by Harmonic Current Injection," *IEE Proceedings*, vol. 1991, no. 7, pp. 857–864, July 1972.
2. A. Ametani, "Harmonic Reduction in Thyristor Converters by Harmonic Current Injection," *IEEE Transactions on Power Apparatus and Systems*, vol. Pas-95, no. 2, pp. 441–449, March/April 1976.
3. J. Arillaga, A. P. B. Joosten, and J. F. Baird, "Increasing the Pulse Number of AC-DC Convertors by Current Rejection Techniques," *IEEE Transactions on Power Apparatus and Systems*, vol. PAS-102, no. 8, pp. 2649–2655, August 1983.
4. J. F. Baird, and J. Arillaga, "Harmonic Reduction in D.C.-Ripple Rejection," *IEE Proceedings, Part C*, vol. 127, no. 5, pp. 294–303, September 1980.
5. B. M. Bird, J. F. Marsh, and P. R. McLellan, "Harmonic Reduction in Multiplex Convertors by Triple-Frequency Current Injection," *IEE Proceedings*, vol. 116, no. 10, pp. 1730–1734, October 1969.
6. Predrag Božović, and Predrag Pejović, "Three-Phase High Power Factor Rectifier Based on the Third Harmonic Current Injection in Discontinuous Conduction Mode," *PCIM Europe 2002, Power Electronics*, Nuremberg, pp. 501–506, May 2002.
7. Predrag Božović, and Predrag Pejović, "Current Injection Based Low Harmonic Three-Phase Diode Bridge Rectifier Operating in Discontinuous Conduction Mode," *IEE Proceedings-Electric Power Applications*, vol. 152, no. 2, pp. 199–208, April 2005.
8. Robert W. Erickson, and Dragan Maksimović, *Fundamentals of Power Electronics*, Second Edition, Kluwer Academic Publishers, 1999.
9. William M. Flanagan, *Handbook of Transformer Design & Applications*, Second Edition, McGraw-Hill, 1993.
10. Žarko Janda, and Predrag Pejović, "A Novel Low-Harmonic Three-Phase Diode Rectifier Type Utility Interface Applying Passive Resistance Emulation," *Power Electronics and Motion Control*, PEMC'98, Prague, pp. 7.24–7.29, September 1998.
11. Žarko Janda, and Predrag Pejović, "A High Power Factor Three Phase Rectifier Based on Adaptive Current Injection Applying Buck Converter," *Power Electronics and Motion Control*, PEMC'00, Košice, pp. 3.140–3.144, September 2000.
12. Sikyung Kim, Prasad N. Enjeti, Paul Packebush, and Ira J. Pitel, "A New Approach to Improve Power Factor and Reduce Harmonics in a Three-Phase Diode Rectifier Type Utility Interface," *IEEE Transactions on Industry Applications*, vol. 30, no. 6, pp. 1557–1564, November/December 1994.
13. William B. Lawrence, and Wladyslaw Mielczarski, "Harmonic Current Reduction in a Three-Phase Diode Bridge Rectifier," *IEEE Transactions on Industrial Electronics*, vol. 39, no. 6, pp. 571–576, December 1992.
14. Shigeo Masukawa, and Shoji Iida, "An Improved Three-Phase Diode Rectifier for Reducing AC Line Current Harmonics," *7th European Conference on Power Electronics and Applications*, EPE'97, Trondheim, Norway, pp. 4.227–4.232, September 1997.

15. Wladyslaw Mielczarski, William B. Lawrence, Rafal Nowacki, and Donald Grahame Holmes, "Harmonic Current Reduction in Three-Phase Bridge-Rectifier Circuits Using Controlled Current Injection," *IEEE Transactions on Industrial Electronics*, vol. 44, no. 5, pp. 604–611, October 1997.
16. Ned Mohan, Mukul Rastogi, and Rajendra Naik, "Analysis of a New Power Electronics Interface with Approximately Sinusoidal 3-Phase Utility Currents and a Regulated DC Output," *IEEE Transactions on Power Delivery*, vol. 8, no. 2, pp. 540–546, April 1993.
17. Ned Mohan, Tore M. Undeland, and William P. Robbins, *Power Electronics: Converters, Applications, and Design*, John Wiley & Sons, 2003.
18. Rajendra Naik, Mukul Rastogi, and Ned Mohan, "Third-Harmonic Modulated Power Electronics Interface with 3-Phase Utility to Provide a Regulated DC Output and to Minimize Line-Current Harmonics," *Industry Applications Society Annual Meeting*, pp. 689–694, 1992.
19. Rajendra Naik, Mukul Rastogi, Ned Mohan, Robert Nilssen, and Chris P. Henze, "A Magnetic Device for Current Injection in a Three-Phase, Sinusoidal-Current Utility Interface," *Industry Applications Society Annual Meeting*, pp. 926–930, 1993.
20. Rajendra Naik, Mukul Rastogi, and Ned Mohan, "Third-Harmonic Modulated Power Electronics Interface with Three-Phase Utility to Provide a Regulated DC Output and to Minimize Line-Current Harmonics," *IEEE Transactions on Industry Applications*, vol. 31, no. 3, pp. 598–601, May/June 1995.
21. Rajendra Naik, Ned Mohan, Mark Rogers, and Alec Bulawka, "A Novel Grid Interface, Optimized for Utility-Scale Applications of Photovoltaic, Wind-Electric, and Fuel-Cell Systems," *IEEE Transactions on Power Delivery*, vol. 10, no. 4, pp. 1920–1926, October 1995.
22. Yasuyuki Nishida, Mutsuo Nakaoka, Yukiko Ohgoe, and Akeshi Maeda, "A Simple Three-Phase Boost-Mode PFC Rectifier," *Industry Applications Conference, Thirty-First IAS Annual Meeting, IAS'96*, San Diego, CA, pp. 1056–1061, 1996.
23. Yasuyuki Nishida, "Historical Review of Passive PFC Rectifiers," *PCIM Europe 2003, Power Quality*, Nuremberg, pp. 219–224, May 2003.
24. Predrag Pejović, and Žarko Janda, "Low-Harmonic Three-Phase Rectifiers Applying Current Injection," *Power Electronics and Motion Control, PEMC'98*, Prague, pp. 2.157–2.162, September 1998.
25. Predrag Pejović, and Žarko Janda, "Optimal Current Programming in Three-Phase High Power Factor Rectifier Based on two Boost Converters," *IEEE Transactions on Power Electronics*, vol. 13, no. 6, pp. 1152–1163, November 1998.
26. Predrag Pejović, and Žarko Janda, "A Novel Harmonic-Free Three-Phase Diode Bridge Rectifier Applying Current Injection," *14th Annual Applied Power Electronics Conference, APEC'99*, Dallas, TX, pp. 241–247, March 1999.
27. Predrag Pejović, and Žarko Janda, "An Analysis of Three-Phase Low-Harmonic Rectifiers Applying the Third Harmonic Current Injection," *IEEE Transactions on Power Electronics*, vol. 14, no. 3, pp. 397–407, May 1999.
28. Predrag Pejović, "A Simple Control Circuit for Dual Boost Rectifier Providing Sinusoidal Input Currents," *8th European Conference on Power Electronics and Applications*, Lausanne, September 1999.
29. Predrag Pejović, and Žarko Janda, "Low-Harmonic Three-Phase Rectifier Applying Current Injection," *IEE Proceedings-Electric Power Applications*, vol. 146, no. 5, pp. 545–551, September 1999.

30. Predrag Pejović, and Žarko Janda, “An Improved Current Injection Network for Three-Phase High Power Factor Rectifiers that Apply the Third Harmonic Current Injection,” *IEEE Transactions on Industrial Electronics*, vol. 47, no. 2, pp. 497–499, April 2000.
31. Predrag Pejović, “Low-Harmonic Three-Phase Rectifier,” *Power Electronics Specialists Conference*, PESC’00, Galway, pp. 1029–1034, June 2000.
32. Predrag Pejović, “Three-Phase High Power Factor Rectifier Based on the Third Harmonic Current Injection with Passive Resistance Emulation,” *Power Electronics Specialists Conference*, PESC’00, Galway, pp. 1342–1347, June 2000.
33. Predrag Pejović, and Žarko Janda, “Three-Phase High Power Factor Rectifier Applying a Novel Current Injection Network,” *Power Electronics and Motion Control*, PEMC’00, Košice, pp. 2.40–2.44, September 2000.
34. Predrag Pejović, “Two Three-Phase High Power Factor Rectifiers that Apply the Third Harmonic Current Injection and Passive Resistance Emulation,” *IEEE Transactions on Power Electronics*, vol. 15, no. 6, pp. 1228–1240, November 2000.
35. Predrag Pejović, and Žarko Janda, “Three-Phase Rectifiers that Apply Optimal Current Injection,” *IEEE Transactions on Aerospace and Electronic Systems*, vol. 38, no. 1, pp. 163–173, January 2002.
36. Predrag Pejović, “A Novel Low-Harmonic Three-Phase Rectifier,” *IEEE Transactions on Circuits and Systems-I: Fundamental Theory and Applications*, vol. 49, no. 7, pp. 955–965, July 2002.
37. Predrag Pejović, and Doron Shmilovitz, “Application of the Third Harmonic Current Injection in Three-Phase Thyristor Rectifiers to Reduce the Input Current Harmonic Distortion,” *PCIM Europe 2003, Power Quality*, Nuremberg, pp. 225–230, May 2003.
38. Predrag Pejović, and Doron Shmilovitz, “Low-Harmonic Thyristor Rectifiers Applying Current Injection,” *IEEE Transactions on Aerospace and Electronic Systems*, vol. 39, no. 4, pp. 1365–1374, October 2003.
39. Predrag Pejović, Predrag Božović, and Doron Shmilovitz, “Low Harmonic Three Phase Rectifier that Applies Current Injection and Passive Resistance Emulator,” *PCIM Europe 2005*, pp. 63–68, June 2005.
40. Predrag Pejović, Predrag Božović, and Doron Shmilovitz, “Low-Harmonic, Three-Phase Rectifier that Applies Current Injection and a Passive Resistance Emulator”, *IEEE Power Electronics Letters*, vol. 3, no. 3, pp. 96–100, September 2005.
41. Mukul Rastogi, Rajendra Naik, and Ned Mohan, “Optimization of a Novel DC-Link Current Modulated Interface with 3-Phase Utility Systems to Minimize Line-Current Harmonics,” *23rd Annual Power Electronics Specialists Conference*, PESC’92, pp. 162–167, June/July 1992.
42. Mukul Rastogi, Ned Mohan, and Christopher P. Henze, “Three-Phase Sinusoidal Current Rectifier with Zero-Current Switching,” *9th Annual Applied Power Electronics Conference and Exposition*, APEC’94, Orlando, FL, pp. 718–724, February 1994.
43. Mukul Rastogi, Rajendra Naik, and Ned Mohan, “A Comparative Evaluation of Harmonic Reduction Techniques in Three-Phase Utility Interface of Power Electronic Loads,” *IEEE Transactions on Industry Applications*, vol. 30, no. 5, pp. 1149–1155, September/October 1994.
44. Mukul Rastogi, Ned Mohan, and Christopher P. Henze, “Three-Phase Sinusoidal Current Rectifier with Zero-Current Switching,” *IEEE Transactions on Power Electronics*, vol. 10, no. 6, pp. 753–759, November 1995.
45. Tiiu Sakkos, and Vello Sarv, “Power Factor Correction of Three-Phase Diode Rectifiers with Capacitive Smoothing Using a Diode-Switched-Transformer Active Filter,” *Power Electronics and Motion Control*, PEMC’96, Budapest, pp. 1.368–1.371, September 1996.

46. Tiiu Sakkos, and Vello Sarv, "Efficient Two-Stage Active Filters for Power Factor Correction of Diode Rectifiers," *Power Electronics and Motion Control*, PEMC'98, Prague, pp. 7.1–7.6, September 1998.
47. John C. Salmon, "Reliable 3-Phase PWM Boost Rectifiers Employing a Stacked Dual Boost Converter Subtopology," *IEEE Transactions on Industry Applications*, vol. 32, no. 3, pp. 542–551, May/June 1996.
48. John C. Salmon, "Operating a Three-Phase Diode Rectifier with a Low-Input Current Distortion Using a Series-Connected Dual Boost Converter," *IEEE Transactions on Power Electronics*, vol. 11, no. 4, pp. 592–603, July 1996.
49. Vello Sarv, "Switched-Inductor and Switched-Transformer Active Power Filters for Harmonic Reduction and Unsymmetry Compensation," *IEEE/KTH Stockholm Power Tech Conference*, Stockholm, Sweden, pp. 247–252, June 1995.
50. Bhim Singh, Brij N. Singh, Ambrish Chandra, Kamal Al-Haddad, Ashish Pandey, and Dwarka P. Kothari, "A Review of Three-Phase Improved Power Quality AC-DC Converters," *IEEE Transactions on Industrial Electronics*, vol. 51, no. 3, pp. 641–659, June 2004.
51. Marija Stojšavljević, and Predrag Pejović, "An Extrapolation Method for Accelerated Convergence to Steady State Solution of Power Electronics Circuits," *PCIM Europe 2005*, pp. 574–578, June 2005.

INDEX

- AC components, 112, 128, 239, 253, 268
capacitor voltage, 94, 134, 147, 158,
175, 221–23
generalized equivalent representation
of current injection systems, 183*f*,
184*f*
of output voltages, 110
- AC ripple, 27
- Amplitude spectrum, input current, 18,
88–89
- Amplitudes
 injected current, 73, 77–78
 normalization of, 223–25
 optimal, 201
- Autotransformer-based devices, 52–58
 design of, 57–58
- Auxiliary currents, waveforms for, 252
- Basic current injection network, 129*f*
- Basic topologies, 127–30
- Bidirectional switches, 266
- Boundary conditions, 149, 218, 221,
222–23, 287
 rectifier states and, 287*t*, 297*t*
- Capacitance, 186, 187
- Capacitors, 130*f*, 218
 choice of, 133–47
 C_S/2, 175, 182
 electrolytic, 94–95, 100, 178*f*
 voltage AC component, 96, 221–23
 voltage DC component, 94
- Closed-form solutions, 291
- Continuous conduction mode, 83, 138,
142, 152, 229
 discontinuous conduction mode and,
 141–43, 151–55
 of three-phase diode bridges, 180, 188
 upper boundary of, 208–9
 voltage-loaded resistance emulators in,
 193–98
- Core limbs
 fluxes of, 53–57
- magnetomotive forces on, 58
- C_P, electrolytic capacitors and, 178*f*
- C_S/2 capacitors, 175, 182
- Current injection, 305, 306. *See also*
 Optimal current injection
 simple, 91
 three-phase diode bridge and, 28–29
- Current injection devices, 31–71
 autotransformer-based, 52–58
 delta-wye connected transformer,
 67–71
 stages of switches in, 237*f*
 switching, 233–66
 test circuits, 47*f*
 three-phase inductors, 43–51
 three-phase transformers with
 unloaded delta-connected
 secondary winding, 36–37
 with two single-phase transformers,
 40–42
 volt-ampere rating of, 136–37
 wye-wye connected transformers,
 58–66
 with zigzag autotransformers, 37–40
- Current injection methods, 2–3, 21, 233,
236
 principles of, 23–29
 in three-phase diode bridge rectifiers,
 23*f*
- Current injection network A, 91–96
 comparisons of, 101–6
 equivalent circuits of, 96*f*
 input current THD and Q-factor in,
 103*f*
 waveforms in, 105*f*
- Current injection network B, 96–98
 comparisons of, 101–6
 equivalent circuits of, 98*f*
 at even triples of line frequency,
 95–98
 inductor volt-ampere rating for, 100–1
 input current THD and Q-factor in,
 103*f*

- at odd triples of line frequency, 97
waveforms in, 105*f*
- Current injection network C, 106–15,
166, 169, 193, 248
equivalent circuits in, 106–7
input current THD and Q-factor in,
108*f*
waveforms of, 109*f*
- Current injection networks, 91–96,
97–106, 107–15, 304
applying resistance distribution, 131*f*
basic topologies for, 127–30
capacitor choice in, 133–34
derived topologies for, 130–33
equivalent circuit of, 171*f*
with odd and even harmonics, 132*f*
for optimal current injection, 127–39
parts of, 181*f*
two-capacitor, 130*f*
waveforms of voltages at, 236*f*
- Current-loaded resistance emulators,
165–91
component choice, 174–80
current injection network power and,
193–98, 248–51
higher order harmonics, 180–91, 215
- DA, 146–47, 217–18, 269, 271, 281,
283–86, 295–97
- DB, 144–48, 151, 216–23, 269, 271,
281–87, 295–97
- DC components, 27, 128–30, 218, 253,
256
capacitor voltage, 94
- Delta-wye connected transformers,
67–71, 276, 281, 304
- Derived models, 185, 231
- Derived topologies, 133–33
- Diode bridge input current, waveforms
of, 241*f*, 254*f*
- Diode bridge input currents, waveforms
of, 84, 241*f*, 253, 254*f*
- Diode bridge load currents, 25–29,
117–19
- Diode bridge operation, 8–9, 180
- Diode bridge output terminals, 12, 27,
79–80, 85–86, 127, 142
load currents, 25, 28, 83, 305
power from, 80, 86, 87*f*, 168
- Diode bridge rectifiers, 17, 141–43, 165,
233
- Diode bridges, 198, 207, 210
choices of, 213–15
- Diode rectifier bridges, 28
- Diode state functions, 13*t*, 61, 75, 216
defining, 13
waveforms of, 14*f*
- Dirac impulse δ -function, 211–13
- Discontinuous conduction mode, 5, 16,
138, 141–4, 177, 185, 305–6
analysis of, 143
continuous conduction mode and,
141–43, 152–55, 160–61
with high filtering and negligible
losses, 155–58
with low filtering and negligible
losses, 151–54
rectifiers operating in, 141–48
special cases of, 151–58
switching current injection devices
and, 243–44
THD in, 210*f*
voltage-loaded resistance emulators in,
207–13
- Displacement power factor, 81*f*
- Dotted curves, 191
- DR1, 169, 184, 198, 217–23, 270–71,
282, 284–86, 295, 297*f*
- DR2, 217–23, 270–71, 282, 285, 286,
295–97
- Dynamic degeneration, 147–48, 184–85,
220–23
- Electrolytic capacitors, 50, 94–95, 100,
134, 159, 175–76,
 C_p and, 178*f*
- Emulated resistance, 123–25, 134, 260,
262
- Equivalence model of rectifiers, 145*f*
- Equivalent circuit
of rectifier with current-loaded
resistance emulator, 270*f*, 282*f*
states of, 217*t*, 226*t*
- Equivalent circuits, 169, 171, 181, 200,
237
of current injection network A, 96*f*
of current injection network at triple of
line frequency, 170*f*, 171*t*
of current injection network B, 98*f*
of current injection network C, 106–7
harmonics balancing, 213
at odd triples of line frequency, 93*f*
of rectifiers, 73*f*, 217*f*
- Equivalent resistance, 142, 154, 165,
204–5, 247–48
- Equivalents, idealized, 171*f*

- Even harmonics, odd harmonics applied simultaneously with, 132*f*
- Even triples of line frequency, 11, 74, 95–96, 98–101, 106–8, 122, 138, 170, 200, 234, 258
- Even-indexed diodes, 8, 25, 28
- Experimental curves, 191
- Experimental results, of voltage-loaded resistance emulators, 230–32
- Faraday's law, 33–34, 45–46
- Ferromagnetic core, 32, 43–44, 46, 52, 67
- Filtering
- high, 154–58, 209, 211
 - low, 152–54
 - in voltage-loaded resistance emulators, 194
- First conducting diode, 8
- First limb
- flux in, 57
 - forces, 38
- Flux components, at line frequency, 56
- Flux linkage, 99–101, 110, 111*t*, 293
- Fourier series expansion, 9–11, 110, 121, 156, 169–70, 213, 273
- of AC component of output voltage, 110
 - of input currents, 17–18
 - of output terminal voltages, 169
 - of output voltage, 11
 - of voltage at output terminal, 73–74
 - waveform representation of, 120–21
- Fundamental frequencies, 26
- Fundamental harmonics, 16, 174, 200
- input current, 80
 - of input currents, 16
 - RMS of, 76, 290
 - substituting expressions for, 200
- Generalized equivalent representations, of current injection systems AC side, 183*f*, 184*f*
- G_{OUT} , 138, 139*f*, 260–61
- η , input current THD dependence on, 280*f*, 301*f*
- Harmonic standards, 88
- Harmonics. *See* Even harmonics; Fundamental harmonics; Higher order harmonics; Odd harmonics; THD
- High filtering, 143, 154, 159–60, 209, 211, 244
- discontinuous conduction mode with, 155–58
- Higher order harmonics, 74, 89, 100, 108, 112, 114, 117, 143, 151, 155, 170, 173–74
- in current-loaded resistance emulators, 180–91
 - influence of, 101–2, 105
- Impedance, 19–20, 55, 93–95, 97–98, 107, 133, 155, 175–76
- Inductance matrix, 47
- Inductor cores, volt-ampere rating of, 98–101, 175–76
- Inductor currents, dynamically degenerated, 221–23
- Inductor volt-ampere rating, 100–1, 106, 111
- Injected current, amplitude, 77, 92, 94, 112, 142, 163, 166, 170–71, 201, 203–8, 211, 227, 239, 245, 249
- Injected currents, 24–26, 29, 40, 48, 56, 58, 64, 77 (188 instance)
- Input currents
- amplitude spectrum, 88
 - in current injection network A, 103*f*, 104*f*
 - in current injection network B, 103*f*, 104*f*
 - in current injection network C, 108*f*
 - expressions for, 24–25, 238*t*
 - of first phase in optimal third-harmonic current injection, 88
- Fourier series expansions of, 17–18
- fundamental harmonics of, 16, 80
- independent, 117–18
- of rectifier, 152*f*, 153*f*, 154*f*
- RMS of, 112
- sinusoidal, 71, 119
- spectrum of, 17–18
- THD of, 24, 77, 82, 101–2, 103*f*, 104*f*, 108, 134*f*, 139*f*, 153–54, 191*f*, 197–98, 203, 206*f*, 207*f*, 209–11, 228*f*, 229*f*, 230*f*, 232*f*, 260*f*, 261*f*, 262*f*, 271–73, 279*f*, 280*f*, 290–91
- THD of, as function of efficiency, 83*f*
- transformer, 60
- waveforms of, 15*f*, 18, 20*f*, 21*f*, 70, 70*f*, 76*f*, 197*f*, 239, 243*f*, 289
- Input power
- rectifier, 16, 80, 83, 110, 114, 135–37, 169, 274
 - rectifier output power and, 65

- Input transformers, volt-ampere ratings of, 64–65
- Input voltages, waveforms of, 9*f*, 20*f*
- I_{OUT}
 input current THD and, 232*f*
 V_{OUT} and, 232*f*
- J_{OUT} , 225, 228, 230–231
 M_{OUT} and, 162*f*
 rectifier efficiency and, 82*f*, 280*f*, 300*f*
 THD and, 139*f*
 variations in, 159–64
- Kirchoff's current law, 26–27, 47, 75, 284, 285, 298
- Kirchoff's voltage law, 146
- Limb flux, 49
 components of, 56–57
 maximum, 57
- Line frequency, 125, 127
 equivalent circuits at odd triples of, 93*f*
 even triples of, 97–98, 101, 107–8, 235 (38 instances)
 flux components of, 56
 higher order odd triples of, 171*f*
 odd triples of, 98, 171*f* (45 instances)
 phase resonance and, 93
- Line voltages, 47
- Load level parameters, 188, 190
- Logic functions, 264–65
- Low filtering, 151–54
- Magnetic circuit, 43, 46, 53
 of three-phase transformer current injection device, 44*f*
 of three-phase transformers core, 44*f*
- Magnetic current injection, 2–5, 235, 237–39, 241–43, 245, 249–50, 258–59, 263–64
- Magnetic flux, 32, 43, 46
- Magnetomotive force, 43, 46, 53
 on core limbs, 38, 52–53, 58–59
- Monotonous functions, 290
- MOSFET, 264
- M_{OUT}, J_{OUT} and, 162*f*
- NAND gates, 264–65
- Negative output terminal, 27, 74–75, 85, 195, 222–23, 244, 285
- voltage at, 49, 168, 171–72, 211, 235, 284
- Network power, current-loaded resistance emulators and, 248–51
- Neutral point, 41, 46, 48–49, 58, 68, 137
 inductance of, 48–49, 51–52, 55, 67, 268–69
- Neutral point inductivity, control of, 52–58
- Nonlinear elements, 144–45, 180, 216–18, 284, 295
- Nonlinear loads, 1
 n_{opt} , 203, 205, 273, 278, 279*f*, 291, 300*f*
- Normalization, 149–51, 187–88, 223–25, 298
 amplitude, 223
 base resistance for, 149, 224
 rectifier model equations and, 150*t*
 of variables, 5, 187, 223, 305
- Odd harmonics, even harmonics applied simultaneously with, 132*f*
- Odd triples of line frequency, 10–13, 74, 92–93, 95, 97–98, 101, 105–7, 122, 124, 131, 135, 152, 169–71, 200, 234, 237, 247, 258 (45 instances)
- Odd-indexed diodes, 8, 25, 28
- Ohm's law, 149, 224
- Optimal amplitudes, 77–78, 201, 204–6, 227, 245
- Optimal current injection, 2, 64–66, 117–25, 127–39, 251, 253–55, 256, 275, 292. *See also* Current injection
- current injection networks for, 24, 26–28, 49–52, 74–75, 79–82, 91–98, 101–2 (435 instances)
- first current injection network for, 256*f*
- output current ripple, 19, 21, 138–39
- second current injection network for, 96, 258–59
- switching current injection device and, 233–34, 238–48, 251–65
- Optimal third-harmonic current injection, 61–64, 73–89, 94–95, 107, 110–11, 142, 204, 167. *See also* Third harmonic current injection
- input current of first phase, 18, 88, 188, 195, 238, 289
- waveforms in, 86*f*, 105*f*
- Optimal values, 203–4
- Output currents
 ripple, 19, 21, 138, 194, 260–62
 waveforms of, 19, 20*f*
- Output power, 15, 83, 89, 172, 231, 274

- rectifier, 61, 64–65, 68, 231, 276, 292
 Output terminal
 diode bridge, 27, 83, 173, 196, 216
 negative, 27, 74–75, 195, 211,
 222–23, 244, 251, 284–85
 positive, 8–9, 27, 85, 195, 211, 22–23,
 268
 voltages between, 12, 27, 92, 107,
 169, 173, 237
 waveforms of, 9, 10/
 Output terminal voltages
 averages of, 12, 123, 128, 169, 237,
 269
 Fourier series expansion of, 9, 11, 110,
 121, 156, 169–70, 273–74, 292
 spectral components of, 75, 83, 94,
 114, 171, 176, 196, 209
 Output voltages, 11, 62, 110, 128, 152,
 154, 194, 274, 283, 292
 AC component of, 11, 50, 109–10,
 123, 138, 261
 Fourier series expansion of, 9–11, 110,
 169, 292
 waveforms of, 10/*f*, 11/*f*, 19, 20/*f*
 Parallel resonant circuits, 176–77, 179,
 187, 191/*f*, 250
 Parasitic effects, 46, 48
 Parasitic resistance, 92, 183, 201
 Passive resistance emulators, 5–6
 PF. *See* Power factor
 Phase displacement, 77–78
 constraints, 25–26
 efficiency and, 82
 of input current fundamental
 harmonics, 80–81
 Phase resonance, line frequency and, 93
 Phase voltage, waveforms, 19, 21/*f*
 Piecewise linear rectifier models, 148/*t*
 Positive output terminal, 27
 power from, 85
 voltage at, 73, 222–23, 268
 Positive terminal, of rectifier diode
 bridge, 75
 Power dissipation, 130–32, 165, 258–59
 Power factor (PF), 16
 displacement, 81/*f*
 rectifier, 80
 Power quality, 1
 Primary current
 RMS of, 65
 transformer model for, 33
 Primary windings, 68–69
Q-factor, 93, 101–3, 110–11, 118, 133,
 186–87, 247, 305
 in current injection network A, 103/*f*
 in current injection network B, 103/*f*
 in current injection network C, 108/*f*
 input current THD and, 103–4, 110
R, variations in, 159–64
 ρ
 dependence of input current THD on,
 161, 271/*f*, 299/*f*
 dependence of n_{opt} on, 279/*f*, 300/*f*
 rectifier efficiency dependence on,
 280/*f*, 300/*f*
 variations in, 159–64
 Rectifier(s), 243–44. *See also* Three-phase diode bridge rectifiers
 boundary conditions and, 287/*t*, 297/*t*
 in discontinuous conduction mode,
 141–45, 151–52
 input current of, 152/*f*, 153/*f*, 154/*f*
 waveforms, 157/*f*
 Rectifier currents, waveforms of, 174/*f*,
 202/*f*, 212/*f*
 Rectifier diode bridge, positive terminal
 of, 75
 Rectifier efficiency, 82/*f*
 input current THD as function of, 83/*f*
 J_{OUR} and, 153/*f*, 154/*f*
 ρ and, 280/*f*, 300/*f*
 Rectifier equivalent circuits, 73/*f*
 Rectifier input currents, 14–15
 Rectifier input power, 16, 135, 137
 Rectifier models, 143–49
 normalization and, 150/*t*
 piecewise linear, 148/*f*
 Rectifier operation neglecting losses,
 270–76
 Rectifier output power, 15–16, 61, 64–65,
 71, 125, 292
 input power and, 65, 80
 Rectifier parameters, 21/*t*
 Rectifier parasitic resistance, 149
 Rectifier power factor, 80
 Rectifier voltages, waveforms of, 13, 173,
 273
 Remaining voltage, waveform of, 12
 Resistance distribution parameter
 in current injection network A, 104/*f*
 current injection network applying,
 144/*f*
 in current injection network B, 104/*f*
 input current THD and, 108

- Resistance emulators, 97, 102
 current-loaded, 165–91
 currents and voltages at, 199/
 design for, 167
 transformer secondary current, 195
 waveforms of currents at, 179/
 Resistance R , 276
 Resistors $2aR$, 92
 Resistors R_2 , 131
 Resonance constraints, 267
 Resonance frequency, 186–87
 Resonance parameters, 150, 161, 187
 defining, 224–25
 THD and, 163/
 R_{EVEN} , 128, 138, 257
 RI_{OUT}
 input current THD and, 206/
 transformer optimal turns and, 205/
 RMS. *See* Root-mean-square values
 R_{ODD} resistors, 256–58
 Root-mean-square (RMS) values, 8, 15
 calculating, 128
 of fundamental harmonic of
 waveform, 76, 290
 of injected current, 136, 275
 of input currents, 112
 of primary currents, 63, 65
 of secondary currents, 67
 of winding currents, 135
 of winding voltages, 40
- Second conducting diode, 8
 Second limb forces, 38
 Secondary currents, 35, 64–65, 67, 287
 resistance emulator transformer, 195
 RMS of, 69–70
 Secondary windings, 68, 281
 74LS00, 265
 74LS138, 265
 Simple current injection networks, 91
 Simulation results, of voltage-loaded
 resistance emulators, 225–30
 Single-phase cores, volt-ampere rating of,
 32
 Single-phase transformers, 33/*f*, 33, 38,
 40–42, 281
 Spectral components, 10–11, 69, 74, 120,
 122, 124, 171, 235
 of output terminal voltages, 93–94,
 122
 of rectifier output terminal voltages, 98
 Square-wave current injection, 6,
 267–301, 306
 analysis of, considering losses,
 294–301
 analysis of, neglecting losses,
 281–94
 current-loaded resistance emulators
 and, 269–80
 voltage-loaded resistance emulators
 and, 281–301
 State-space models, 180, 184, 185,
 188–90, 215, 305
 normalization of variables in, 223–25
 state 1 in, 218
 state 2 in, 219
 state 3 in, 220–21
 state 4 in, 222
 state 5 in, 222–23
 of voltage-loaded resistance
 emulators, 215–25
 Switches, bidirectional, 266
 Switching current injection devices,
 233–66, 306
 discontinuous conduction mode and,
 243–44
 optimal current injection and, 251–55,
 256–63
 realization of, 264–66
 third harmonic current injection and,
 238–43, 245–58
 Symmetry, 95, 96, 289
 System matrix, 59–60, 119
 THD. *See* Total harmonic distortion
 Third harmonic current injection, 2, 3, 64,
 69, 166/*f*, 306. *See also* Optimal
 third-harmonic current injection
 applying switching current injection
 devices, 238–43
 switching current injection device and,
 245–48
 Third harmonic currents, 28
 flow of, 28/*f*
 Third limb forces, 38
 Third order system, 218
 Three-phase diode bridge rectifiers, 5,
 7–21, 303, 305
 applying current injection, 23/*f*
 continuous conduction of, 188
 current injection and, 28
 diagram of, 7/*f*
 Three-phase inductors, 43–51
 design of, 51
 Three-phase transformers
 magnetic circuit of, 44/*f*

- with unloaded delta-connected
 - secondary winding, 36–37
 - volt-ampere ratings for, 34–36
- Three-phase voltage systems, 167–68
 - undistorted symmetrical, 195
- Three-wire systems, 117, 303
- Time derivatives, 54, 56, 225
- Topologies
 - basic, 127–30
 - derived, 130–33
- Total harmonic distortion (THD), 7, 16, 17, 19, 23, 24, 29, 69, 73, 85, 91, 158–59, 105, 165, 189, 190, 192–93, 201, 227, 260, 267, 273, 278, 299, 303–5
 - in current injection network A, 103*f*, 104*f*
 - in current injection network B, 103*f*, 104*f*
 - in current injection network C, 108*f*
- determining, 76
- in discontinuous conduction mode, 211
- input current, 77, 82, 101–2, 105, 110, 134*f*, 139*f*, 191*f*, 196–97, 203, 206*f*, 207*f*, 209–10, 228*f*, 229, 230*f*, 261–62, 272–73, 279*f*, 280*f*, 291, 299
 - input current, as function of efficiency, 83*f*
 - J_{OUT} and, 160*f*
 - minimums of, 79*f*
 - resonance parameters and, 163*f*
- Transformer(s). *See also* Delta-wye
 - connected transformers; Three-phase transformers; Wye-delta
 - transformers; Wye-wye connected
 - transformers
 - single-phase, 33*f*, 40–42
 - volt-ampere rating of, 34–35, 63–65, 135
 - zigzag autotransformers, 4, 37–40
- Transformer core
 - flux in, 33–34
 - main limiting factors for, 99
- Transformer currents, waveforms of, 178*f*
- Transformer input currents, 60–61
- Transformer models, 33, 40, 169, 174, 183
- Transformer optimal turns, RJ_{OUT}/V_m and, 205*f*
- Transformer primary, 33, 60, 176, 177, 184
 - waveforms of, 61, 63*f*
- Transformer secondary, 33, 58, 64, 69, 137, 287
 - waveforms, 62*f*, 65, 66*f*
- Transformer T1, 40, 41
 - volt-ampere rating of, 42
- Transformer T2, 40, 41
 - volt-ampere rating of, 42
- Transformer turns ratios, 106, 197, 201, 205, 208, 210, 221, 229, 273, 289
 - choices of, 214
 - input current THD and, 203, 228*f*
- Transformer volt-ampere rating, 34–36, 61, 65, 71, 132, 135, 179, 233
- Transformer windings
 - voltage across, 182
 - waveforms of currents through, 113*f*
- Tripled line frequency, 10
- Two-capacitor current injection networks, 130*f*
- Unloaded delta-connected secondary winding, three-phase transformers with, 36–37
- Unloaded secondary, wye-delta transformer with, 36*f*
- V_A , 8, 145, 198, 216, 234, 235, 268
- V_B , 9, 145, 198, 216, 234, 235, 269
- V_C , 10*t*, 12–13, 134, 146, 218, 221–22, 234*f*, 235–36, 246, 249*f*, 256, 259*f*
- V_m
 - input current THD and, 206*f*
 - transformer optimal turns and, 205*f*
- Voltage(s). *See also* Input voltages; Output voltages; Three-phase voltage systems
 - line, 47
 - negative output power, 211–12, 268–69, 284
 - phase, 18–21
 - rectifier, 13, 173–74
 - remaining, 12
- Voltage equations, 39–40, 45
- Voltage-loaded resistance emulators, 193–232
 - component choices in, 213–15
 - in continuous conduction mode, 198–207
 - in discontinuous conduction mode, 207–13
 - experimental results of, 230–32
 - filters in, 194

- simulation results of, 225–30
 square-wave current injection and,
 281–301
 state-space model of, 215–25
- Volt-ampere ratings, 4, 31–36, 37, 40,
 45, 49–51, 58, 61, 63–64, 68–71,
 135, 247–48, 250–51, 259, 275,
 293–94
- of 1:1 transformer, 109–11
 application of, 36
 computing, 36
 concept of, 32
 of current injection devices, 136–37
 defined, 32
 dependence of, on a , 50*f*
 of inductor cores, 99–101, 176
 of input transformers, 66–67
 of single-phase cores, 32
 for three-phase transformers, 35–36
 of transformer, 35–36, 64, 65, 135
 of transformer T1, 40–42
 of transformer T2, 40–42
 of wye-wye transformers, 275–76
- V_{OUT} , 9*f*, 11–12, 20*f*, 94, 172, 173*f*, 232*f*,
 272*f*, 274, 288, 295
 I_{OUT} and, 232*f*
- Waveforms, 84*f*, 85*f*, 86*f*, 87*f*, 113*f*, 124*f*,
 173*f*, 272*f*, 283*f*, 288*f*
 for auxiliary currents, 252
 in current injection network A, 105*f*
 in current injection network B, 105*f*
 in current injection network C, 109*f*
 of currents at resistance emulator AC
 side, 179*f*
- of diode bridge input currents, 86,
 241*f*, 254*f*
 of diode bridge output terminal load
 currents, 84
- of diode state functions, 14*f*
- Fourier series expansions of, 120–21
 fundamental harmonics of, 76
 for ideal current injection, 120*f*, 122*f*
 ideal sinusoidal, 252*f*
 of injected currents, 242*f*
 of input currents, 15*f*, 17–18, 20*f*, 21*f*,
 71, 76*f*, 197*t*, 239, 243*f*, 287–89
 of input voltages, 9*f*, 20*f*
 in optimal third-harmonic current
 injection, 239–42
- of output current, 19, 20*f*
 of output terminal, 10*f*
 of output voltage, 11*f*, 21, 22*f*
 of phase voltage, 19, 21*f*
 of power from diode bridge output
 terminals, 87*f*
- rectifier, 157*f*
 rectifier currents, 174*f*, 202*f*, 212*f*
 rectifier voltages, 13, 173–74
 remaining voltage, 12
 sinusoidal, 127, 254–55
 of transformer currents, 178*f*
 transformer primary currents, 61, 63*f*
 transformer secondary currents, 62*f*,
 65, 66*f*
- in transformer windings, 110
 of voltages at network terminals, 236*f*
- Winding currents, RMS of, 135
 Winding voltages, 40, 111*f*
 RMS of, 40